The Role of *TWIST-1* in the Regulation of Mesenchymal Stem Cell Growth, Fracture Repair and Bone Loss

Lachlan Cooper

Mesenchymal Stem Cell Group
Division of Haematology
Hanson Institute
SA Pathology
&
Department of Medicine
Faculty of Health Science
University of Adelaide

A thesis submitted to the University of Adelaide
For the degree of Doctor of Philosophy
May 2013

Table of Content

Abstract

Mesenchymal stem cells (MSC) have the capacity to differentiate into osteoblasts, chondrocytes and adipocytes *in vivo*. It is well established that the basic Helix-Loop-Helix transcription factor *TWIST-1* plays an important regulatory role within the context of bone remodelling and formation in both developmental and adult settings by regulating the proliferation, differentiation and commitment of MSC. Recent studies have demonstrated that elevated levels of *TWIST-1* in MSC results in the maintenance of an immature population of cells with enhanced proliferative and adipogenic potential while simultaneously reducing the cells capacity to undergo osteogenesis and chondrogenesis.

The aim of this thesis was to define the role of *TWIST-1* in MSC commitment and differentiation within the context of bone fracture healing and bone loss during osteoporosis. Microarray results highlighted differential expression of Wnt pathway genes *WNT2* and *WNT2B* in MSC with enforced *TWIST-1* expression. Purified MSC isolated from bone marrow aspirates obtained from normal human donors were used to generate over-expressing *WNT2* and *WNT2B* MSC lines using established retroviral based systems. Genetically modified MSC were used to examine the effect of *WNT2* and *WNT2B* on osteogenesis, chondrogenesis, adipogenesis and proliferation of MSC *in vitro*. Results showed regulation of *WNT2* and *WNT2B* by *TWIST-1* through direct interactions between *TWIST-1* protein and the proximal promoter regions of *WNT2* and *WNT2B*. Furthermore, functional analysis demonstrated enhanced adipogenesis in MSC with enforced expression of *WNT2B*.

To assess the role of *TWIST-1* deficiency in fracture healing and the disease state of osteoporosis *in vivo,* a heterozygous *TWIST-1*$^{+/-}$ mutant mouse model was used. The role of *TWIST-1*

deficiency in fracture healing was assessed by induction of a femoral fracture followed by analysis at one, two four and eight weeks post fracture to examine the different stages of fracture healing. Analysis showed enhanced osteoblastic differentiation and accelerated fracture repair in heterozygous *TWIST-1*$^{+/-}$ mutant mice when compared to relevant wild type littermate control mice. The role of *TWIST-1* deficiency in osteoporosis was examined by induction of osteoporosis by ovariectomy. Results from this study showed heterozygous *TWIST-1*$^{+/-}$ mice maintained bone volume following ovariectomy induced osteoporosis.

Declaration

I certify that this work contains no material which has been accepted for the award of any other degree or diploma in any university or other tertiary institution and, to the best of my knowledge and belief, contains no material previously published or written by another person, except where due reference has been made in the text. I give consent to the copy of my thesis, when deposited at the University Library, being made available for loan and photocopying, subject to the provisions of the Copyright Act 1968. I also give permission for the digital version of my thesis to be made available on the web, via the University's digital research repository, the Library catalogue and also through web search engines, unless permission has been granted by the University to restrict access for a period of time.

Signed

Lachlan Cooper

Date:

Acknowledgements

First I would like to thank my supervisors Professor Stan Gronthos and Professor Andrew Zannettino. Thanks to Stan for always making time for me when I needed it and for knowing what to say to keep me motivated even when I didn't know I needed motivation. I very much appreciate Andrew's honesty, professionalism, wisdom and ability to connect with everyone on a personal level within a work setting. Thank you both for creating an environment that inspires personal growth and enables everyone in the laboratory to achieve and maintain a high standard of research.

I feel privileged to have worked with and learnt from Sandra Isenmann, one of the most passionate and technically talented scientists I will ever have the pleasure of working with. Thanks for believing in me, pushing me, gently reminding me, always being a great friend and passing on the reasons behind what works and what doesn't, in every protocol.

Thanks to everyone in the Bone and Cancer Laboratories for being such a great group of people who look out for one another and help each other succeed. Romana Panagopoulos, Mary Matthews, Dr Danijela Menicanin, Dr Agnes Arthur, Kris Mrozik, Catherine Gan, Sharon Paton, Kate Pilkington, Dr Peter Psaltis, Dr Peter Diamond, Dr Steve Fitter, Dr Sally Martin, Sarah Hemming, Dr Tony Cambareri, Jenny Drew, Dr Kate Vandyke, Dr Jim Cakouros, Thao Nguyen, Dr Kim Hynes, Dr Duncan Hewett, Dr Jacqueline Noll, Vicki Wilczek and Dr Sharon Hampton-Smith; I have received help and guidance from all of you and have developed friendships that I value greatly.

Stan and Agnes need to be singled out for their help teaching me the surgical techniques related to this project, Kate Vandyke for her amazing help and expertise with all of my histological and μCT analysis, Mary for teaching me how to scan bones using μCT, Steve, Peter and Sandra for help with all of my molecular cloning and infection techniques, Romana for keeping me sane while we were working long days together on fractures and ovariectomies, Kate Pilkington for early starts and the occasional all-nighter sorting, Sharon Paton for feeding my cells whenever I was sick, Sarah for helping out with population doubling assays when there weren't enough hours in the days and Jim for teaching me ChIP protocols.

Thanks to my partner Bec for making sure I was eating even if it meant bringing food into the lab at midnight, for picking me up in the rain, for dealing with my thesis getting the majority of my attention, and for being there for me through the journey that is a PhD.

Thanks to Mum and Dad for always encouraging, but never pressuring, me to do the things I love. Thanks to my little sister Jade for all of your chats and for being a great friend. Thanks to Grandma and Grandpa for always being proud of me and helping me want to be a good person.

I dedicate this thesis to my Grandpa who was always there for me, loved me unconditionally, and showed me what it is to be a good person.

Thank you.

Abbreviations

3D	Three dimentional
AGE	Agarose gel electrophoresis
ALK PHOS	Alkaline phosphatase
ATCC	American Type Culture Collection
ATP	adenosine triphosphate
bHLH	beta helix loop helix
BLAST	Basic Local Alignment Search Tool
BMD	Bone mineral density
BMMC	Bone marrow mononuclear cell
BMP	Bone morphogenetic protein
BMSC	Bone marrow stromal cell
BMSSC	Bone marrow stromal stem cell
Brdu	5-bromo-2-deoxyuridine
BSA	Bovine serum albumin
BSP	Bone sialoprotien
C/EBPα	CCAAT/Enhancer Binding Protein alpha
CBFA1	Core binding factor-1
cDNA	Complementary deoxyribonucleic acid
CDS	Coding DNA sequence
CFU	Colony forming unit
CFU-F	Colony forming unit-fibroblast
ChIP	chromatin immunoprecipitation
CoA	Coenzyme A
COL2a1	Collagen type II alpha 1
CSA	chondroitin sulphate A
DAVID	Database for Annotation, Visualization and Integrated Discovery
DEPC	Diethylpyrocarbonate
DERMO	Dermis-expressed protein 1
DLX5	Distal-Less homeobox 5
DMEM	Dulbecco's modified Eagle's medium
DMSO	Dimethyl sulfoxide

DNA	Deoxyribonucleic acid
DNAse	Deoxyribonuclease
dNTP	Deoxyribonucleotide triphosphate
DTT	dithiothreitol
E47	Immunoglobulin Enhancer Binding Factors
EB	Elution buffer
ECF	Enhanced chemifluorescence
EDTA	Ethylenediaminetetraacetic acid
EZH2	Enhancer of zeste homolog 2
FACS	Fluorescence activated cell sorting
FCS	Foetal calf serum
FGFR2	Fibroblast growth factor receptor 2
GAG	glycosaminoglycan
GFP	Green fluorescent protein
GM-CSF	Granulocyte/macrophage-CSF
HBSS	HANKS balanced salt solution
HEPES	4-(2-hydroxyethyl)-1-piperazineethanesulfonic acid
Het	Heterozygous
hMSC	Human mesenchymal stem cell
HSC	Haematopoietic stem cells
IgG	Immunoglobulin G
IgM	Immunoglobulin M
IP	Intraperitoneal
iPSC	Induced pluripotent stem cell
LB	Luria Broth
LDB2	Lim domain binding 2
MACS	Magnetic cell sorting
MAF	Musculoaponeurotic fibrosarcoma
M-CSF	Macrophage colony-stimulating factor
MEM	Minimum essential medium
MPP	Multipotent progenitor cells
mRNA	Messenger ribonucleic acid

MSC	Mesenchymal stem cell
MSX2	Muscle segment homeobox 2
NBF	Neutral buffered formalin
NK	Natural killer
NOD	Normal osteoblast donor
OCN	Osteocalcin
OPN	Osteopontin
OVX	Ovariectomised
PAGE	Polyacrylamide gel electrophoresis
PBND	PCR buffer with non-ionic detergents
PBS	Phosphate buffered saline
PCR	Polymerase chain reaction
PD	Population doublings
PGP	Pre-glycoprotein
PGP-2	Prostaglandin E2
PTH	Parathyroid hormone
PTHrP	Parathyroid hormone-related protein
PTTG1	Pituitary tumor-transforming 1
Q-PCR	Real-time polymerase chain reaction
RANK	Receptor activator of nuclear factor kappa-B
RANKL	Receptor activator of nuclear factor kappa-B ligand
RBC	Red blood cell
RNA	Ribonucleic acid
RO	Reverse osmosis
ROI	Region of interest
rpm	revolutions per minute
RT	Room temperature
RT-PCR	Real-time polymerase chain reaction
RUNX2	Run related transcription factor
SDF-1/CXCL12	Stromal cell dirived factor 1
SDS	Sodium dodecyl sulfate
SMAD	SMAD protein

SOC	Super optimal broth with cotabolite repression
STRO-1	Stromal precursor antigen - 1
TAE	Buffer containing Tris base, Acetic acid and EDTA
TAZ	Tafazzin protein
TBS	Tris buffered saline
TE	Buffer containing Tris and EDTA
TGF-β	Transforming growth factor beta
TRAP	tartrate-resistant acid phosphatase 5
Tris HCL	Tris Hydrochloride
Tween 20	Polyethylene glycol sorbitan monolaurate
TWIST-1	Transcription factor Twist-1
TWIST-2	Transcription factor Twist-2 (*DERMO-1*)
uCT	micro-computed tomography
UV	Ultra violet
VSVG	Vesicular stomatitis virus G-protein
Wnt	Wnt family of signalling molecules
WNT2	Wingless-type MMTV integration site family, member 2
WNT2B	Wingless-type MMTV integration site family, member 2B
WST-1	4-[3-(4-iodophenyl)-2-(4-nitrophenyl)-2H-5-tetrazolio]-1,3- benzene disulphonate
WT	Wild Type
α-MEM	α-modified Eagle's medium

Publications

Scientific Manuscripts

1. Arthur, A., R.A. Panagopoulos, **L. Cooper**, D. Menicanin, I.H. Parkinson, J.D. Codrington, K. Vandyke, A.C.W. Zannettino, S.A. Koblar, N.A. Sims, K. Matsuo, and S. Gronthos. (2012). EphB4 enhances the process of endochondral ossification and inhibits remodelling during bone fracture repair. *Journal of Bone and Mineral Research* n/a-n/a.

2. Cakouros, D., S. Isenmann, **L. Cooper**, A. Zannettino, P. Anderson, C. Glackin, and S. Gronthos. (2012). Twist-1 induces Ezh2 recruitment regulating histone methylation along the Ink4A/Arf locus in mesenchymal stem cells. *Mol Cell Biol* 32:1433-1441.

Conference Proceedings

1. **L. Cooper**, S. Isenmann, A. Arthur, D. Cakouros, A. C.W. Zannettino, S. E. Hemming, S. Gronthos. Enhanced fracture healing of heterozygous Twist-1 knockout mice. *The Australian Health and Medical Research Congress*, Adelaide, Australia, November 2012

2. **Lachlan Cooper**, Sandra Isenmann, Agnieszka Arthur, Dimitrios Cakouros, Kim Hynes, Andrew CW Zannettino, Stan Gronthos. *TWIST-1* Interactions Involved in Mediating Mesenchymal Stromal/Stem Cell Proliferation, Differentiation and Lineage Commitment. *International Society for Stem Cell Research,* Toronto, Canada, June 2011.

3. **Lachlan Cooper**, Sandra Isenmann, Agnieszka Arthur, Andrew CW Zannettino, Dimitrios Cakouros, Stan Gronthos. *TWIST-1* Mediated Maintenance of Mesenchymal Stromal/Stem Cells and Cell Fate Determination. *Australian & New*

Zealand Bone & Mineral Society 20th Annual Scientific Meeting, Adelaide, Australia, September 2010.

4. **Lachlan Cooper**, Sandra Isenmann, Agnieszka Arthur, Andrew CW Zannettino, Carlotta A. Glackin, Dimitrios Cakouros, Stan Gronthos. The TWIST Family of Basic-Helix-Loop-Helix Transcription Factors, *TWIST-1* and *-2*, Mediate Mesenchymal Stromal/Stem Cell Proliferation and Differentiation. *The Australian Health and Medical Research Congress*, Melbourne, Australia, November 2010.

5. **Lachlan Cooper**, Sandra Isenmann, Agnieszka Arthur, Andrew CW Zannettino, Carlotta A. Glackin, Dimitrios Cakouros, Stan Gronthos. The TWIST Family of Basic-Helix-Loop-Helix Transcription Factors, *TWIST-1* and *-2*, Mediate Mesenchymal Stromal/Stem Cell Proliferation and Differentiation, *Adelaide University Centre for Stem Cell Research Annual Meeting,* Adelaide, Australia, 2009.

6. Sandra Isenmann, Agnieszka Arthur, Andrew CW Zannettino, Jenna L. Turner, **Lachlan Cooper**, Songtao Shi, Carlotta A. Glackin, Stan Gronthos. The basic-helix-loop-helix transcription factors, *TWIST*-1 and-2, mediate mesenchymal stromal/stem cell growth and cell fate determination, **Presentation** - *Australian & New Zealand Orthopaedic Research Society Conference*, Adelaide, Australia, September, 2009.

1 Introduction

1.1 Overview

The transcription factor, *TWIST-1* has been shown to play important regulatory roles in the differentiation, proliferation, commitment and senescence of human mesenchymal stem cells (MSC) (Cakouros et al., 2012; Franco et al., 2011; Isenmann et al., 2009; Komaki et al., 2007; Menicanin et al., 2010; Miraoui and Marie, 2010; Ying Zhang, 2008). As allogeneic and autologous MSC-based cellular therapies are being assessed in various human trials worldwide for safety and efficacy, understanding the molecular mechanisms underlying the mode of action of MSC is becoming increasingly important (Arthur et al., 2009; Grassel and Anders, 2012; Kitada and Dezawa, 2012; Mabed and Shahin, 2012; Mundra et al., 2012).

Whilst pre-clinical and clinical studies utilising MSC are currently reporting exciting outcomes over traditional therapies, the mode of action is poorly understood with little consensus within the literature on the relative levels of contribution of paracrine effects stimulating host cells verses direct reconstitution of affected tissue by implanted MSC (An et al., 2012; Baglio et al., 2012; Kon et al., 2000; Millard and Fisk, 2012; Pierro et al., 2012). Understanding the mechanisms by which MSC mediate and contribute to basic bone biology is vital for the effective use of these cells and will enable the control of spontaneous malignant transformation and enable the standardization of specific biological properties of ex-vivo expanded MSC.

The following introduction describes basic bone biology and our understanding of the important role of MSC in these processes along with the molecular mechanisms that control the action of these cells. In particular it examines the functional role of *TWIST-1* on the processes of MSC

proliferation, differentiation, commitment and senescence as well as suggesting possible cellular processes regulated by *TWIST-1* that may determine the progression of bone loss during osteoporosis and rate of bone fracture healing following trauma.

1.1.1 Bone Structure and Composition

The structure and composition of bone make it an ideal tissue to perform the functions of support, protection and calcium storage. Bone is a composite material consisting of a protein phase (mainly type I collagen) and a mineral phase (carbonated hydroxyapatite) (Agna et al., 1958; Chen et al., 2011). To allow for the highest possible density of collagen in the bone, mature lamella bone is comprised of tightly packed bundles of collagen fibres that form in layers.

1.2 Bone Formation

Bone formation, or ossification, is the process by which bone tissue replaces connective tissue to form the skeleton. There are two methods of pre-natal bone formation; intramembranous ossification, resulting in the formation of flat bones (such as bones that form the cranium, the ilium, the sternum, the rib cage, the sacrum and the scapula), and endochondral ossification, resulting in the formation of long bones (such as the femora, tibiae, and fibulae of the legs; the humeri, radii, and ulnae of the arms; metacarpals and metatarsals of the hands and feet, the phalanges of the fingers and toes, and the clavicles) (figure 1.1).

During intramembranous ossification bone is generated on or within fibrous connective tissue membranes, where MSC differentiate into osteoblasts which secrete osteoid, an un-calcified bone matrix that is eventually mineralised, before the cell differentiates further to form osteocytes that

Figure 1.1 - Basic anatomy of long bones.

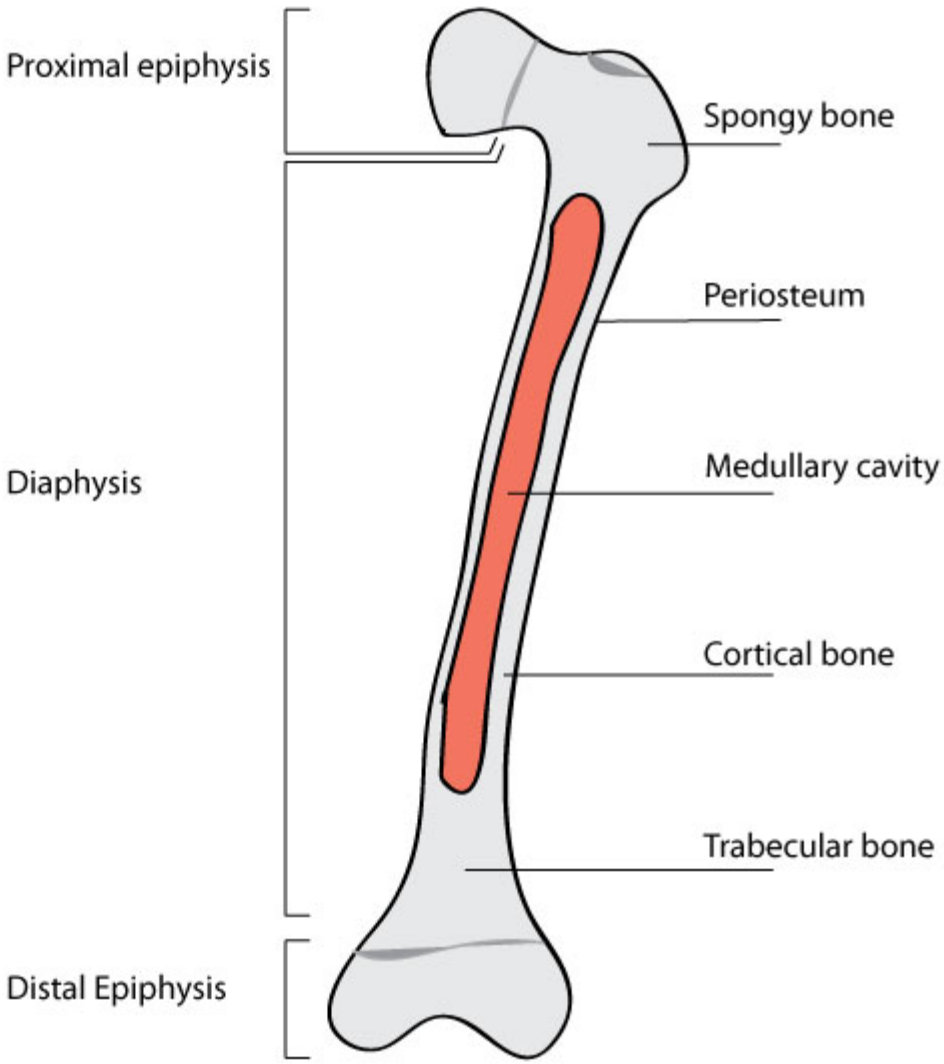
Proximal epiphysis
Diaphysis
Distal Epiphysis
Spongy bone
Periosteum
Medullary cavity
Cortical bone
Trabecular bone

are encapsulated within the hardened bone matrix (Clarke, 2008). The bone matrix develops into thin columns of bone called trabeculae which then fuse to form the lattice-like cancellous bone (Freemont, 1993). Blood and lymphatic vessels grow into the centre of the bone to develop the bone marrow cavity and a dense layer of connective tissue forms on the outside of the bone termed the periosteum (Owen, 1980). Most outer layers of cancellous bone are replaced by compact bone but the inner mass remains spongy.

Endochondral ossification, the replacement of cartilage with bone, begins when the embryonic mesenchyme condenses (Wuthier, 1982). During development, osteogenic progenitor cells differentiate into osteoblasts and secret matrix beneath the perichondrium which is termed the periosteum once bone is formed (Dwek, 2010). The newly formed bone collar restricts the availability of nutrients to the cartilage cells which atrophy. Capillaries grow into the disintegrating cartilage and act to deliver MSC which differentiate into osteoblasts to form primary ossification centres which eventually replaces most of the cartilage with bone (Martini, 2007). The newly formed cavity is filled with spongy bone and marrow. Blood vessels then penetrate the epiphysis to deliver osteoblasts and create secondary ossification centres (Olszta et al., 2007). Primary and secondary ossification, occur via distinct mechanisms. Primary ossification occurs at the locus of epiphysial cartilage and involves rapid mineralization to form unorganized woven bone microarchitecture (Cameron, 1963). Secondary bone formation follows and the primary woven bone is remodelled by bone resorbing osteoclasts, derived from haematopoietic progenitor cells, into a more organized bone comprising collagen fibrils secreted by osteoblasts that are assembled into a parallel lamellar structure.

1.2.1 Bone Remodelling

Bone is in a constant state of remodelling, first described by Frost in 1964 and outlined in (figure 1.2), which occurs as a stepwise process whereby mature bone is removed by osteoclasts and new bone tissue is formed by osteoblasts (H. M. Frost; Mundy GR, 1982). It is estimated that the adult human skeleton undergoes complete turnover approximately every 7-10 years (Manolagas, 2000). It is generally acknowledged that bone mineral density in humans peaks at around 30 years of age. As a person ages past 30 their bone mineral density declines and this leads to conditions related to low bone mass such as osteoporosis (Mundy, 1999). Using a rat bone defect model, Baron and colleagues demonstrated that the bone remodelling in rats was closely correlated with the bone remodelling process in humans (Baron R, 1984). These important studies helped develop a suitable model for studying the complex process of bone remodelling *in vivo* (Baron R, 1984).

Understanding the triggers responsible for promoting the different stages of this complex process will help us to control the process and mitigate the effects of bone loss due to age, trauma and disease. The regulation of osteoclatsogenesis occurs primarily through the action of hormonal changes and through factors produced by stromal cells and osteoblasts. Factors (such as 1,25-dihydroxyvitamin D3, *PTH*, *PTHrP* and interleukin-6, 1β and 11) stimulate osteoclastogenesis by regulating the production of receptor activator of nuclear factor kappa-B ligand (*RANKL*) and macrophage colony-stimulating factor (*M-CSF*) by MSC, reviewed in (Zaidi, 2007). There is both a membrane bound and soluble form of *RANKL* produced by osteoblasts to enable the recruitment and activation of osteoclasts by binding the osteoclast expressed cell surface protein *RANK* (Roodman, 1999). To prevent *RANKL* and *RANK* interacting, and thus regulate osteoclastogensis, osteoblasts produce osteoprotegerin (*OPG)* that acts as a decoy receptor by

Figure 1.2 - Bone remodelling cycle. Pre-osteoclasts are recruited to the bone surface by cytokines and factors released by cells within the bone matrix. The pre-osteoclasts differentiate into active osteoclasts and resorb the mineral matrix releasing factors that lead to the chemotaxis of osteoprogenitors to the site of the resorption pits. They differentiate into the osteoblasts that form the osteoid matrix that eventually undergoes mineralization. The osteoblasts trapped in the matrix from osteocytes and, under relevant stimulus, release factors that recruit pre-osteoclasts to start the process again. Adapted from (Michgan, 2005).

binding *RANKL*, preventing interactions between *RANKL* and *RANK* proteins. Once activated, multinucleated bone lining osteoclasts resorb bone by creating a sealed chamber that contains secretions of hydrogen and chloride ions to lower the pH which helps dissolve the mineral component of the bone (Silver et al., 1988). Tartrate-resistant acid phosphatase, cathepsin K, matrix metalloproteinase 9 and gelatinase are then secreted by multinucleated osteoclasts in order to breakdown the remaining organic extracellular matrix (Delaisse et al., 2003). Other factors secreted by osteoblasts such as *M-CSF* and SDF-1/*CXCL12* have also been shown to be important mediators of osteoclast migration, maturation and function (Gronthos and Zannettino, 2007; Zannettino et al., 2005)

Following resorption of the bone surfaces, osteoblasts migrate into the resorption pits and lay down an osteoid scaffold made predominately of collagen type I. Approximately 15% of osteoblasts remain trapped within the osteoid matrix lacunae to become osteocytes (Ducy et al., 1997). Mineral crystals of calcium and phosphate form along the collagen fibrils to generate hydroxyapatite which is the main inorganic constituent of bone.

1.3 Mesenchymal Stem Cells

The classification of stem cells is defined by certain criteria which include multilineage differentiation and extensive self-renewal capacity (Mayhall et al., 2004). Stem cells can be broadly divided into three main types, namely, embryonic stem cells, adult or postnatal stem cells and recently, induced pluripotent stem cells (iPSC). Embryonic stem cells are derived from blastocytes and have the capacity to generate cells from all three germ layers and to develop into any tissue that constitutes the mature organism (Daadi et al., 2008). Induced pluripotent stem cells are somatic cells that have been reprogrammed genetically in order to induce pluripotency

(Takahashi et al., 2007; Takahashi and Yamanaka, 2006). iPS cells are comparable to embryonic stem cells in terms of their high growth potential, pluripotency, morphology and gene expression profiles. Moreover, both cell types exhibit the potential for tumour formation. In contrast, adult stem cells are currently thought to be tissue specific, multi-potential cells with a limited growth capacity.

Adult human MSC, also called bone marrow stromal cells (BMSC), were first identified in the aspirates of rodent marrow by their ability to form adherent colonies of colony forming unit-fibroblastic (CFU-F) cells (Friedenstein et al., 1970; Friedenstein et al., 1976). Further studies showed that these adherent fibroblastic cells were also present in the bone marrow of a number of other species including humans (Castro-Malaspina et al., 1980; Gronthos et al., 2003a; Pittenger et al., 1999). In addition to the bone marrow, human MSC have been isolated from multiple tissues including adipose tissue, tendon, umbilical cord blood, dental pulp, periodontal ligament, circulating blood, lungs and synovial membrane (Barachini et al., 2009; De Bari et al., 2001; Gronthos et al., 2000; Kuznetsov et al., 2001; Miura et al., 2003; Salingcarnboriboon et al., 2003; Seo et al., 2004; Yongmin Yan, 2009; Zannettino et al., 2008; Zuk et al., 2001). Furthermore, bone marrow derived MSC give rise to bone marrow supportive stroma that regulate and maintain haematopoietic stem cells that give rise to blood cells and platelets via a process termed haematopoiesis (Sacchetti et al., 2008). The CFU-F population is a heterogeneous mix of both multipotential BMSC and committed progenitors, thought to be derived from a pool of self-renewing stem cells (Friedenstein et al., 1978; Gronthos et al., 2003b; Kuznetsov et al., 1997; Owen and Friedenstein, 1988; Pittenger et al., 1999) (figure 1.3). In 2005, the international society for cellular therapy suggested that fibroblast-like plastic-adherent cells be termed multipotent mesenchymal stromal cells and the term mesenchymal stem cells be reserved for

Figure 1.3. The STRO-1 bright cells in an MSC population are the most immature. This figure illustrates the advantage presented by identifying the STRO-1 bright population as a means of isolating the multipotential, self-replicating portion of MSCs over plastic adherence techniques. Known transcription factors that regulate specific lineages are shown. Adapted from (Gronthos and Simmons, 1996).

cells that meet specified stem cell criteria (Horwitz et al., 2005). To clarify further, in 2006 the minimal criteria for defining multipotent mesenchymal stromal cells was established and includes plastic-adherence in standard culture conditions and expression of CD105, CD73 and CD90 while lacking expression of CD45, CD34, CD14 or CD11b, CD79alpha or CD19 and HLA-DR surface molecules (Dominici et al., 2006). While this definition goes some way to ensuring accurate comparison between different groups, it is still limited due to the non-specific nature of the markers used and because of the lack of any assessment of multidifferentiation and self-renewal capacity *in vivo*. The population of cells that are the focus of this thesis are derived from the *STRO-1* positive fraction of bone marrow (Gronthos et al., 2003a), adhere to plastic, display the cell surface marker profile described above and are capable of differentiating into osteoblasts, chondrocytes, adipocytes, cardiomyocytes, myoblasts and neural cells (Gronthos et al., 2006; Gronthos et al., 2003a; Horwitz et al., 1999; Jiang et al., 2002; Shi and Gronthos, 2003; Zannettino et al., 2007).

Plastic adherence is used as a technique to enrich for CFU-F and takes advantage of the adherent properties of CFU-F/MSC populations (Pittenger et al., 1999). However, this property is not unique to MSC, where other cell populations demonstrate the ability to adhere to plastic including mature stroma cells, endothelial cells, smooth muscle cells and monocytes/macrophage. More recent studies have tried to identify cell surface antigens that are unique to MSC in order to distinguish MSC from committed stromal cells, vascular cells and haematopoietic cell populations (Gronthos et al., 1994). Using a combination of magnetic activated cell sorting (MACS) and fluorescence activated cell sorting (FACS), clonogenic MSC have been isolated from aspirates of human bone marrow based on their co-expression of the STRO-1 antigen and either STRO-3 (bone specific alkaline phosphatise), STRO-4 (heat shock

protein-90β), CD106 or CD146 (Gronthos et al., 2007; Gronthos et al., 2009; Gronthos and Zannettino, 2008a; Gronthos et al., 2003a; Shi and Gronthos, 2003; Simmons and Torok-Storb, 1991; Tanaka-Douzono et al., 2001). This approach has generated a highly enriched CFU-F population with a five-thousand-fold increase in colony forming cells over unfractionated bone marrow mononuclear cell preparations (BMMC) (Gronthos et al., 1994; Gronthos et al., 2003a) with a capacity to self-renewal in vivo (Sacchetti et al., 2007). Importantly, STRO-1/CD106/CD146 positive bone marrow fractions were devoid of any committed stromal elements, endothelial cells and haematopoietic stem/ progenitor/ myeloid/ erythroid cell populations (Zannettino et al., 2007). The use of this combined MACS/FACS protocol was a major breakthrough that allowed, for the first time, a detailed study of near pure populations of clonogenic MSC (Gronthos et al., 2003a). These prospectively isolated cells have an enhanced capacity to proliferate and display no detectable levels of mature osteogenic, adipogenic or chondrogenic markers (*RUNX2*, *PPARγ2* or collagen type II respectively) by RT-PCR. Furthermore, STRO-1 selected MSC exhibit higher multi-lineage potential, homing, support of HSC, induction of angiogenesis and immunomodulatory properties compared to plastic adherent derived MSC (Gronthos 2003a; Psaltis JCP 2010; Bensidhoumal Blood 2004; Gonclaves et al. Exp Hematol. 2006; Nasef et al. In J Lab Hematol. 2009). Together, these data demonstrate that prospective isolated MSC represent an immature and potent subset within the original heterogeneous CFU-F population.

Previous studies have focused on determining the unifying characteristics and developmental relationships between the different MSC populations isolated from a multitude of adult tissues (De Ugarte et al., 2003; Menicanin et al., 2010; Mrozik et al., 2010; Musina et al., 2005) with a common perivascular or pericyte phenotype (Doherty et al., 1998; Gronthos 2003; Shi and

Gronthos 2003; Farrington-Rock 2004; Sacchetti et al., 2007; Covas et al., 2008). Since enrichment protocols and isolation techniques are not standardized, different methodologies may give rise to subsets of cells of varying developmental potential from within a heterogeneous population (Rebelatto et al., 2008). Given that different techniques for procuring starting material for the isolation of MSC vary in invasiveness and the amount of available tissue for expansion, research into the varied properties of tissue-specific MSC populations has focused on the identification of cells with the best outcomes using standardised protocols involving their expansion potential, reconstitution of tissue or the modulation of immunity (Kern et al., 2006; Winter et al., 2003). As the properties of tissue specific MSC were identified, the analysis of gene expression of tissue specific populations of MSC was investigated using microarray technology (Jansen et al., 2010; Lee et al., 2004; Segawa et al., 2009; Wagner et al., 2005). To understand the genetics regulating the differentiation potential of tissue specific MSC some groups have focused on the epigenetic signatures of MSC isolated from different tissues while others have investigated the gene expression profile of MSC during differentiation events (Aranda et al., 2009; Kulterer et al., 2007). The most common signalling molecules and transcription factors involved in MSC differentiation are highlighted in figure 1.4 (Augello and De Bari, 2010).

The studies described above go some way to defining the MSC at the level of the genome, however, to successfully define these cells it is vital to isolate and characterize MSC from multiple tissues clonally as this is the only way to positively eliminate the variability associated with the heterogeneous cultures described above. Our laboratory has investigated the clonogenic potential of MSC-like cells from various tissues in order to identify common molecular markers and establish the stem cell portion of isolated heterozygous populations of cells (Menicanin et al., 2010). This work categorised clonal populations based on the capacity of the cells to differentiate into multiple lineages and the proliferative potential of the clones. Microarray analysis was

Figure 1.4 - Schematic overview of signalling molecules and transcription factors involved in the regulation of chondrogenic, adipogenic and osteogenic differentiation of MSCs. Adapted from (Andrea Augello and Cosimo De Bari, 2010)

conducted, comparing highly proliferative multipotent clones and short lived unipotent clones from multiple tissues (adult bone marrow, dental pulp and periodontal ligament), and uncovered transcription factors differentially regulated in all three tissue groups. The most significant genes identified as part of this study were the transcription factors *E2F2*, *PTTG1* and *TWIST-1* and the transcriptional cofactor, *LDB2* which were highly expressed by high proliferative multipotent clonal cells from three different tissues sources. This data shows that the *TWIST-1* gene may play similar roles in multiple human cell populations, including the regulation of differentiation and proliferation, and not just MSC.

1.3.1 The transcriptional regulation of adipogenic MSC differentiation

The functional role of adipocytes within the bone marrow cavity is poorly defined and characterisation of the differentiation pathways responsible for regulation of MSC will help to reveal the role of these cells. The CCAAT/enhancer binding protein alpha (C/EBPα) and the peroxisome proliferator-activated receptor gene (*PPAR-γ2*) are the two major components in the transcriptional regulation of MSC towards the adipogenic linage, where *PPAR-γ2* is commonly referred to as the master regulator of adipogenesis (Kawai et al., 2010). There is evidence to suggest that the action of *PPAR-γ* is two-fold, enhancing adipogenesis, by driving the expression of adipose-related genes and blocking osteoblastogenesis by downregulating the expression of osteogenic genes (Akune et al., 2004; Ali et al., 2005). Results from our laboratory have shown that the transcription factor *TWIST-1* acts to upregulate the expression of *PPAR-γ2* and related adipocyte markers, leptin and adipsin directing MSC towards the adipogenic lineage (Isenmann et al., 2009).

1.3.2 The transcriptional regulation of chondrogenic MSC differentiation

Transforming growth factor beta (*TGF-β*) is a potent stimulator of chondrogenic differentiation of MSC and is routinely used to induce chondrogenesis and assess the chondrogenic potential of pelletised MSC *in* vitro (Barry et al., 2001; Pittenger et al., 1999; Weiss et al., 2010). *TGF-β* acts by directly activating the members of the SMAD pathway, *SMAD2* and *3* leading to stabilisation of the Sox9 transcription complex (Furumatsu et al., 2005; Yang et al., 2001) and subsequent induction of chondrogenic differentiation. The nuclear transcription factor *SOX9* is the main component of the master regulatory axis of chondrogenesis comprised of *SOX9*, 5 and 6 (Ikeda et al., 2004). During chondrogenesis, *SMAD3*, a *TGF-β* signalling molecule stimulates *SOX9* transcriptional activation by modulating interactions between *SOX* genes and *CBO/p300* thus mediating transcriptional regulation of the *COL2a1* gene (Furumatsu et al., 2005). Our laboratory demonstrated a reduction in the capacity of *TWIST-1* overexpressing MSC stimulated with *TGF-β* to produce glycosaminoglycans and thus a reduction in the chondrogenic capacity of these cells (Isenmann et al., 2009). This result was correlated with a down regulation in the gene expression of *SOX9* and collagen type X. Recently *TWIST-1* has been shown to inhibit the trans activator function of *SOX9* providing insight into the way in which *TWIST-1* can down regulate chondrogenic differentiation of MSC (Gu et al., 2012).

1.3.3 The transcriptional regulation of osteogenic MSC differentiation

The differentiation of MSC into bone forming cells known as osteoblasts, has been shown to be mediated by a cascade of cellular signals driven by the transcription factor, *CBFA1/RUNX2*, that binds to, and regulates, the promoter regions of important bone associated genes including bone sialoprotein, osteopontin, osteocalcin, alkaline phosphatase and type I collagen (Ducy et al., 1997; Gronthos et al., 1994; Karsenty, 2000; Komori et al., 1997; Liu et al., 1999; Martin et al.,

1997; Nacamuli et al., 2003). The importance of *RUNX2* in bone development is highlighted by *RUNX2* null mice which display a complete absence of bone formation (Komori et al., 1997). The *TWIST-1* protein interacts with the *RUNX2* DNA binding domain to inhibit its function and block *RUNX2*-induced osteoblast gene expression (Bialek et al., 2004). Once *TWIST-1* protein levels have decreased, and MSC commit to the osteogenic lineage pathway, a number of other genes downstream of *RUNX2*, such as the zinc finger transcription factor osterix, play critical roles in maintaining and regulating the differentiation of pre-osteoblasts into osteoblasts (Nakashima et al., 2002). There are also numerous transcriptional regulators including, *DLX5, MAF, TAZ and MSX2,* that have been shown to act as co-activators that regulate the activity or expression of *RUNX2* and control osteoblast differentiation (Cui et al., 2003; Hong et al., 2005; Lee et al., 2005; Nishikawa et al., 2010; Robledo et al., 2002; Satokata et al., 2000).

1.4 TWIST-1

The twist family of genes consists of *TWIST-1* (*TWIST*) and *DERMO-1* (*TWIST-2*) map to chromosome 7p21 and 2q37.3 respectively (Bourgeois et al., 1996; Perrin-Schmitt et al., 1997). These genes encode basic helix-loop-helix (bHLH) transcription factors that are involved in the transcriptional regulation of various genes involved in mesodermal tissue development (Chen and Behringer, 1995). The bHLH transcription factor family are characterised by the presence of two alpha helices joined by a loop and act by forming heterodimers (the dimerization of two contrasting proteins) or homodimers (the dimerization of two identical proteins) (Castanon and Baylies, 2002). Once dimerized, these transcription factors are able to bind to a conserved motif within the promoter region known as the E-box (CANNTG) which leads to transcriptional regulation of the gene (Murre et al., 1989). The preferential E-box sequence for *TWIST-1* binding is CATATG (Castanon et al., 2001; Ip et al., 1992). bHLH transcription factors are able to

activate transcription, or in the case of forming heterodimers, completely silence gene transcription. The functional role of the Twist genes was first hypothesized when observing patient outcomes related to loss of function mutations in the bHLH motif of the protein (Kress et al., 2005).

1.4.1 The effect of *TWIST-1* mutations on humans and mice

TWIST-1 mutations commonly occur in the bHLH binding domain of the protein. The translation of *TWIST-1* determines the onset of osteoblast differentiation and the absence of the *TWIST-1 gene*, or mutations leading to loss of function, lead to the premature differentiation of osteoblasts and a condition known as Saethre-Chotzen syndrome (Bialek et al., 2004). This condition is characterized by craniosynostosis; a condition in which the fibrous sutures of the skull are prematurely fused during development which leads to complications with normal brain and skull formation. The locus for Saethre-Chotzen syndrome maps to chromosome 7p21-p22. *TWIST-1* was originally chosen as a candidate gene for Saethre-Chotzen syndrome as mouse amino acid residues are 100% conserved and the phenotype resulting from mutations leading to loss of function is similar to that of Saethre-Chotzen syndrome in humans (Howard et al., 1997). Mutations in the binding domain of *TWIST-1* lead to loss of function and illustrate the importance of *TWIST-1* in the regulation of osteogenesis. The importance of *TWIST-1* in development has been demonstrated in mice as homozygous loss of function leads to embryonic lethality after 11.5 days of development due to the failure of fusion of the cranial neural folds (Chen and Behringer, 1995). Heterozygous *TWIST-1* mice display a distinct phenotype that presents as an additional toe on either or both hindlegs (polydactyly), malocclusion and changes in the rate of ossification of some bones in the skull that leads to nasal septum deviation and asymmetry of the skull (Bourgeois et al., 1998).

While *TWIST-1* appears to be important in mesodermal tissue and craniofacial bone formation during development, its role in MSC maintenance and differentiation in postnatal tissues has only recently been described by our laboratory (Isenmann et al., 2009). Its potential role in osteoporosis has recently been predicted by association of *TWIST-1* polymorphisms and bone mineral density in post-menopausal women (J.-Y. Hwang, 2010), whereas its role in fracture repair is largely unknown.

1.4.2 *TWIST-1* regulation of osteogenic differentiation

The association of *TWIST-1* mutations and aberrant bone formation in patients with Saethre-Chotzen syndrome led to further studies aimed at identifying potential molecular targets of *TWIST-1* and their role in bone formation (Jabs, 2001). Using human osteosarcoma cell lines, work conducted by Lee and colleagues demonstrated that expression levels of human *TWIST-1* can alter osteoblastic differentiation patterns in bone formation (Lee et al., 1999). Cells overexpressing *TWIST-1* were found to be more progenitor-like, while cells in which *TWIST-1* expression was silenced with anti-sense RNA were found to be more representative of more differentiated osteoblast cells (Lee et al., 1999) (figure 1.5). This study indicates that overexpression of a single transcription factor can block osteoblast differentiation and can also revert osteoblastic cells to a more progenitor or stem cell like state. Therefore, the level of *TWIST-1* can influence osteogenic gene expression and may act as a master switch in initiating bone cell differentiation by regulating the osteogenic cell lineage.

The correlation of *TWIST-1* mutations linked to causing aberrant bone formation in patients with Saethre-Chotzen syndrome has led to further investigations examining potential molecular targets

Figure 1.5 - *TWIST-1* overexpressing HSaOS-2 cells can maintain the immature stem cell phenotype. Cells infected with *TWIST-1* antisense, demonstrate decreased levels of *TWIST-1* and display a more differentiated osteoblast phenotype. Adapted from (Lee et al., 1999).

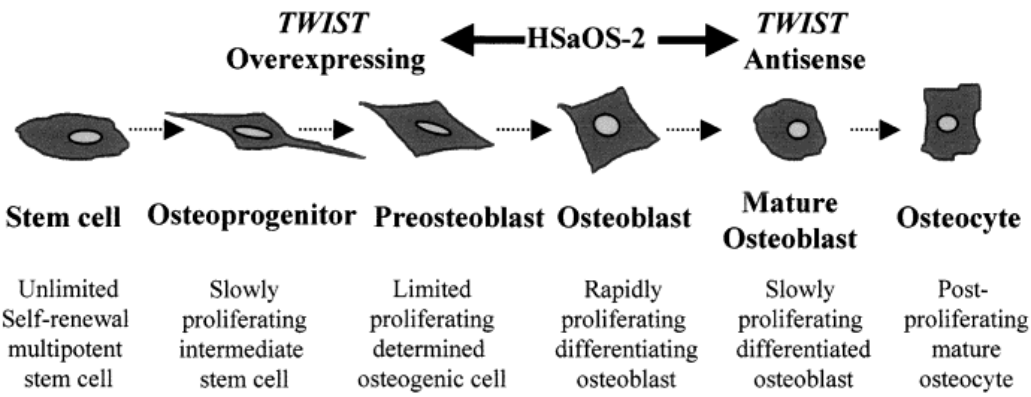
TWIST
Overexpressing
HSaOS-2
TWIST
Antisense
Stem cell
Osteoprogenitor
Preosteoblast
Osteoblast
Mature Osteoblast
Osteocyte
Unlimited Self-renewal multipotent stem cell
Slowly proliferating intermediate stem cell
Limited proliferating determined osteogenic cell
Rapidly proliferating differentiating osteoblast
Slowly proliferating differentiated osteoblast
Post-proliferating mature osteocyte

of *TWIST-1* and the role of these interactions on bone formation (Jabs, 2001). Studies performed in our laboratory have demonstrated that *TWIST-1* overexpression in human MSC maintained an immature cell phenotype (figure 1.6) and dramatically increased the lifespan of these cells (figure 1.7), while inhibiting the capacity of MSC to differentiate into functional osteoblasts (figure 1.8) (Isenmann et al., 2009). Furthermore, this study showed elevated levels of *RUNX2* and *MSX2* transcripts and reduced levels of *BMP2*, *OPN* and *OCN* transcripts in MSC with enforced *TWIST-1* expression suggesting a mechanism for the observed inhibition of osteoblastic differentiation as described in previous reports (Komori, 2002; Liu et al., 2001).

The *TWIST-1* protein has been shown to be a target of Wnt pathway genes as it has been demonstrated that *WNT1* inhibits chondrogenesis through the upregulation of *TWIST-1* (Dong et al., 2007; Howe et al., 2003). Others have demonstrated the involvement of *TWIST-1* in BMP signalling by showing that *BMP2* stimulates the expression of *TWIST-1* (Inai et al., 2008; Ma et al., 2005). While other groups have shown that *TWIST-1* can act as an inhibitor of BMP signalling and *Id1* can regulate BMP signalling through a positive feedback loop repressing *TWIST-1* (Hayashi et al., 2007). Induction of *TWIST-1* expression by *TGF-β* has also been established by groups investigating signals that regulate chondrocyte differentiation (Dong et al., 2007). Conversely, *TGF-β2* has been shown to be selectively upregulated upon *TWIST-1* phosphorylation (Xue et al., 2012).

Knockout models have been developed to examine the role of *TWIST-1* on osteoblastic differentiation. It has been shown that the periodontium contains a MSC-like population that express stem cell markers such as *STRO-1* and CD146/MUC18 and have the potential to generate cementum, bone- and periodontal ligament-like tissue *in vivo* (Seo et al., 2004). Studies

Figure 1.6 - Enforced expression of *TWIST-1* or *DERMO-1* maintains immature MSC *in vitro*. (A) Flow cytometric analysis of single cell suspensions of ex vivo expanded *TWIST-1* (Twist), *DERMO-1* (Dermo) or vector control (GFP) MSC lines, grown under standard culture conditions, based on the cell surface expression of the mesenchymal precursor marker, *STRO-1* or the osteoblast associated marker, alkaline phosphatase (ALK PHOS) antigens. (B) Real-time PCR analysis of the relative expression of the transcription factors, *CBFA1* and bone associated genes, bone sialoprotien (BSP), osteopontin (OPN), osteocalcin (OCN). The data represent the mean values ± standard errors of triplicate experiments normalized to the house keeping gene b-actin. Statistical differences (*) ($p < 0.05$, unpaired t-test). Adapted from (Isenmann, 2009)

Figure 1.7 - Enforced expression of *TWIST-1* or *DERMO-1* promotes cellular proliferation. (A-C) Representative micrographs are shown depicting the cellular morphology of ex vivo expanded *TWIST-1* (Twist), *DERMO-1* (Dermo) and vector control (GFP) MSC lines at different population doublings (PD) post transduction and stable selection. (D) Serial subculture and expansion of different transduced cell lines was performed until exhausting cellular growth. The data represent the mean values ± S.E. of the total population doublings for multiple *TWIST-1*, *DERMO-1* and corresponding control MSC lines generated from five different marrow samples. Statistical differences (*) ($p < 0.05$, unpaired t-test). Adapted from (Isenmann, 2009)

Figure 1.8 - Enforced expression of *TWIST-1* or *DERMO-1* inhibits osteogenesis. (A) Representative micrographs depicting Alizarin red staining of mineralized nodules in cultures of stable multi-colony derived high expressing *TWIST-1* (Twist), *DERMO-1* (Dermo) MSC lines and corresponding controls (GFP) cultured under osteogenic inductive conditions. (B) Calcium levels within the extracellular matrix were measured and normalized to DNA content per well. The data represents the mean values ± standard errors generated from different *TWIST-1, DERMO-1* and vector control MSC lines generated from three different bone marrow samples. Statistical differences (*) ($p < 0.05$, unpaired t-test). Adapted from (Isenmann, 2009)

conducted by Komaki and colleagues (Komaki et al., 2007) in which *TWIST-1* mRNA expression was 'knocked down' in periodontal ligament cells using an *TWIST-1* siRNA expression vector showed that suppression of the *TWIST-1* gene results in early differentiation of cemento/osteoblasts when compared to the untreated control cells. The overexpression of *TWIST-1* in murine bone cells has also been investigated where it was found that *TWIST-1* overexpression inhibited osteoblast differentiation (Bialek et al., 2004). More recently, Cakouros et al demonstrated that *TWIST-1* overexpressing cells have elevated levels of *EZH2* and reduced levels of E47 which, in turn, represses the Ink4A/Arf locus, by regulation of methylation, and leads to a repression of cellular senescence and subsequent increases in the lifespan of MSC (Cakouros et al., 2012). Overall, these studies support our hypothesis that *TWIST-1* plays a role in MSC proliferation, differentiation, commitment and senescence.

1.5 Concluding Remarks

Current literature provides strong support for the critical role of different stromal populations in skeletal tissue development and maintenance. Whilst the role of *TWIST-1* in the context of development has been investigated extensively, little is known about its role in fracture healing and osteoporosis. Studies investigating the role of *TWIST-1* on MSC populations *in vitro* have prompted further investigation into the role of this gene on adult populations in the context of non-developmental processes including fracture repair and osteoporosis. Preliminary linkage studies have been performed regarding a possible correlation between *TWIST-1* and osteoporosis with encouraging outcomes. However, limited investigations have been performed to show causation or mechanisms regarding these observations and several questions remain unanswered. Questions to be addressed include (i) what are the targets of *TWIST-1* affecting differentiation

and proliferation of MSC in vitro and in vivo? (ii) what is the role of *TWIST-1* in fracture repair and osteoporosis?

1.6 Hypotheses

Hypothesis 1 - *TWIST-1* directly regulates key molecules that promote MSC self-renewal and maintenance.

Hypothesis 2 - *TWIST-1* regulates the transcription of critical genes associated with fracture healing where functional *TWIST-1* mutations lead to abnormal bone formation following fracture.

Hypothesis 3 - *TWIST-1* regulates the transcription of critical genes associated with the disease state of osteoporosis, where *TWIST-1* expression is required for the normal progression of osteopososis.

1.7 Aim

Aim 1 - To identify putative *TWIST-1* gene targets using cDNA microarray analysis and determine the role of these targets in MSC self-renewal, maintenance and commitment.

Aim2 - To assess the *in vivo* role of *TWIST-1* in the process of long bone repair using a murine femoral fracture model comparing *TWIST-1*$^{+/-}$ heterozygous mutant and wild-type mice.

Aim 3 - To assess the *in vivo* role of *TWIST-1* in the process of the pathological disease state of bone loss due to osteoporosis using a murine model comparing *TWIST-1*$^{+/-}$ heterozygous mutant and wild-type mice.

2 Materials and Methods

2.1 Cell Culture

2.1.1 Table 2.1. Culture Media

Cell type	**Abbreviation**	Supplements
MG63 NOD Infected MSC MSC	**α-MEM + additives**	α-MEM (JRH, 51451-500M) 10% FCS (Thermo Electron, Melbourne, 15-011-0500V) 50U/mL, 5µg/mL Penicillin, Streptomycin (CSL, 85101) 1mM Sodium Pyruvate (SAFC, 59203C-100ML) 100µM L-ascorbate-2-phosphate (Novachem, Melbourne, Aust) 2mM L-Glutamine (JRH, 59202-100M)
HEK293-T	**DMEM + additives**	DMEM (JRH, 5144-500M) 10% Hyclone FCS (SH30396.03, Lot. KPJ22093) 50U/mL, 5µg/mL Penicillin, Streptomycin 10mM HEPES 1mM Sodium Pyruvate 2mM L-Glutamine
JM 109	**LB media**	10g / L Tryptone Peptone (Becton Dickinson, Sparks, MD, USA) 5g / L Yeast Extract (Becton Dickinson, Sparks, MD, USA) 10g / L NaCl (Sigma Aldrich, Castle Hill, Australia)
NOD	**Mineralisation Media**	α-MEM (Sigma-Aldrich, St. Louis, MO, USA) 5% FCS (Therm. Electron, Melbourne, VIC, Australia) 50U/mL, 5µg/mL Penicillin, Streptomycin (CSL, 85101) 1 mM Sodium Pyruvate (SAFC, Lenexa, KS, USA) 100µM L-ascorbate-2-phosphate (Novachem, Melbourne, Aust) 2 mM L-Glutamine (SAFC, Lenexa, KS, USA) 10^{-7} M dexamethasone phosphate (Hospira Australia) 1.8 mM inorganic phosphate, KH2PO4, (BDH Chemicals, UK)
NOD	**Adipogenic Media**	α-MEM (Sigma-Aldrich, St. Louis, MO, USA) 5% FCS (Thermo Electron, Melbourne, 15-011-0500V) 50U/mL, 5µg/mL Penicillin, Streptomycin (CSL, 85101) 1 mM Sodium Pyruvate (SAFC, Lenexa, KS, USA) 100µM L-ascorbate-2-phosphate (Novachem, Melbourne, Aust) 2 mM L-Glutamine (SAFC, Lenexa, KS, USA) 0.5 µM hydrocortisone (Sigma-Aldrich, St. Louis, MO, USA) 60 µM indomethacin (Sigma-Aldrich, St. Louis, MO, USA) 0.5 mM IBMX (3-Isobutyl-1-methyl-xanthine) (Sigma, USA)

	Cell type	**Abbreviation** Supplements
NOD	**Chondrogenic Media**	DMEM (JRH Biosciences, Lenexa, KS, USA) 50U/mL, 5µg/mL Penicillin, Streptomycin (CSL, 85101) 1 mM Sodium Pyruvate (SAFC, Lenexa, KS, USA) 100µM L-ascorbate-2-phosphate (Novachem, Melbourne, Aust) 2 mM L-Glutamine (SAFC, Lenexa, KS, USA) 10 ng/ml TGF-β3 (Peprotech, Rocky Hill, NJ, USA)
JM 109	**SOC media**	2.0% Tryptone Peptone (Becton Dickinson, Sparks, MD, USA) 0.5% Yeast Extract (Becton Dickinson, Sparks, MD, USA) 10 mM NaCl (Sigma-Aldrich, St. Louis, MO, USA) 2.5 mM KCl (BDH Chemicals, Australia) 10 mM $MgCl_2$-$6H_2O$ (Merck, Kilsyth, VIC, Australia) 10 mM Glucose (Merck, Kilsyth, VIC, Australia) rhTGFβ3 (PeproTech, Rocky Hill, NJ, USA)

2.1.2 Table 2.2 Cell Culture Buffers

Buffer Name	**Components**
HBSS	Hanks balanced salt solution (JRH Biosciences, Lenexa, KS, USA)
1xPBS	MilliQ water (Media production unit, IMVS) 10% Phosphate Buffered Saline, Ca+/Mg+ free (Sigma-Aldrich, USA)
HHF Buffer	HBSS 5% FCS (Thermo Electron, Melbourne, VIC, Australia) 50 U/mL, 5 µg/mL Penicillin, Streptomycin (Sigma-Aldrich, USA)
Blocking Buffer	HHF Buffer 5% normal human serum (Red Cross, SA, Australia)
MACS Buffer	1xPBS 1% BSA (SAFC, Lenexa, KS, USA) 5 mM EDTA (Merck, Kilsyth, VIC, Australia) 0.01% sodium azide

2.1.3 Cell Culture Conditions

All cell culture procedures were conducted in a Class II laminar flow hood (Top Safe 1.2, Bio Air, Siziano, Italy). Cells cultured for expansion were maintained in MCO-18AIC Sanyo CO_2

incubators (Sanyo Oceania, North Ryde, NSW, Australia), at 37^{o}C, 5% CO_2 in a humidified environment. Eppendorf 5810 centrifuge (Eppendorf South Pacific, North Ryde, NSW, Australia) was used for centrifugation of cell suspensions during expansion. The use of cells obtained from human subjects was approved by the Royal Adelaide Hospital ethics committee under protocol # 940911a.

2.1.4 Isolation of mesenchymal stem cells using Magnetic Activated Cell Sorting

This MSC isolation method was based on the protocol described previously (Gronthos and Zannettino, 2008b). Following informed consent, approximately 40mL of human bone marrow was aspirated from the posterior iliac crest of healthy young volunteers (18-35yrs). The samples were then diluted with an equal volume of blocking buffer (HHF supplemented with 5% (v/v) normal human serum), mixed well and strained through a 70µm cell strainer (Becton Dickinson Biosciences, San Jose, CA, USA). Lymphoprep density gradient separation was performed to isolate the mononuclear cells as described in section 2.1.5. Cells were then pooled and enumerated using a haemocytometer as described in 2.1.12. Following enumeration, cells were resuspended in 500µL of *STRO-1* supernatant per 5 x 10^7 cells and incubated on ice for one hour with occasional agitation. Cells were then washed twice in HHF wash buffer and resuspended in 0.5mL HHF containing biotinylated goat anti-mouse IgM (Southern Biotechnology Associates, Birmingham, UK) and incubated at 4^{o}C for 45 minutes. The cells were then washed three times in MACS buffer (Ca^{2+} and Mn^{2+} free PBS was supplemented with 1% BSA in PBS, 5mM EDTA and 0.01% sodium azide) before being resuspended in 450µL of MACS buffer to which 50µL of streptavidin microbeads (Miltenyi Biotec; Bergisch Gladbach, Germany) were added (10µL of microbeads/10^7 cells in 90µL MACS buffer). The mixture was incubated on ice for 15 minutes before being washed once in ice-cold MACS buffer and loaded onto the mini MACS column

(Miltenyi Biotec, MS column). Cells reactive to the *STRO-1* antibody were bound to the magnetised matrix of the column. The column was washed three times with 500µL MACS buffer to remove any non-specifically bound *STRO-1*$^-$ cells. The column was removed from the magnetic field and the *STRO-1*$^+$ cells were collected by flushing the column with 1mL of MACS buffer. The *STRO-1*$^+$ cells were then culture expanded as described in section 2.1.6.

2.1.5 Isolating mononuclear cells

Approximately 40mL of bone marrow was collected from healthy donors and mononuclear cells were isolated using Lymphoprep density gradient separation (Nycomed Pharma AS, Oslo, Norway). Marrow (~20mL)/HHF (~15mL) mixture was underlayed with 12.5mL lymphoprep and centrifuged at 800*g* for 30 minutes with no brake. This was sufficient to separate out the mononuclear layer which was then transferred to a fresh 14mL centrifuge tube, washed in 10mL hanks HHF twice followed by centrifugation at 800*g* for 7minutes at 4^{o}C. The cells were resuspended in α-MEM + additives.

2.1.6 Culture of human MSC

Following immunoselection with *STRO-1,* bone marrow cells were cultured in 75cm^2 tissue culture flasks at 30 x 10^3 cells per cm^2 in α-MEM + additives, at 37^{o}C in a humidified environment supplemented with 5% CO_2. Cells were cultured to 80-90% confluence at which time; cells were harvested by enzymatic digestion with 0.05% trypsin (2.1.7) (SAFC, Lenexa, KS, USA) then used for experiments or reseeded (8 x 10^3 cells per cm^2) for further expansion.

2.1.7 Trypsin Digestion

Trypsin was used to detach adherent cells from the surface of tissue culture flasks. Briefly, culture media was aspirated and cells were washed once with PBS or HANKS to remove any remaining protein. Enough 0.05% trypsin solution (SAFC, Lenexa, KS, USA) was added to cover the cells. Cells were incubated at 37^{o}C for 3-5minutes to enable enzymatic digestion of proteins bonding the cultured cells to the tissue culture flask.

2.1.8 Human osteosarcoma cell line MG63s

Cells were cultured in T^{75} tissue culture flasks at 8 x 10^3 cells per cm^2 in α-MEM + additives, at 37^{o}C in a humidified environment supplemented with 5% CO_2. Cells were cultured to 80-90% confluence at which time cells were harvested by enzymatic digestion with 0.05% trypsin (2.1.7) (SAFC, Lenexa, KS, USA) then used for experiments or reseeded (8 x 10^3 cells per cm^2) for further expansion.

2.1.9 Adherent retroviral HEK 293T packaging cell line

Cells were cultured in T^{75} tissue culture flasks in DMEM + additives. These cells were cultured at a density of 80-90% confluence. When cells reached required confluence they were harvested by enzymatic digestion with 0.05% trypsin (2.1.7) (SAFC, Lenexa, KS, USA) then used for experiments or reseeded (5 x 10^3 cells per cm^2) for further expansion.

2.1.10 Cryopreservation of cells

Cells were cryopreserved in FCS containing 10% (v/v) of dimethyl sulfoxide (DMSO; BDH AnalaR® Merck, Kilsynth, Victoria, Australia). Immediately prior to freezing, 1mL of pre-

prepared, cold FCS 20% DMSO solution was added drop wise to ~1 x 10^6 cells in 1ml of FCS on ice. Cell suspensions were then transferred to 2mL ampoules and cryopreserved in a Mr Frosty (C1562 Freezing Container, Nalgene, USA) placed into a -80^{o}C freezer for at least four hours. The Mr Frosty freezing container ensures the cells are cooled at the appropriate rate of 1^{o}C per minute. Once at -80^{o}C the ampoules were then transferred to the vapour phase of liquid nitrogen for extended storage at -196°C.

2.1.11 Thawing of cryopreserved cells

Cells were removed from liquid nitrogen (-196^{o}C) and immediately thawed in a 37^{o}C bath. Once thawed, cell suspensions in FCS 10% (v/v) of DMSO were immediately transferred to a 14mL polypropylene tube containing 11mL of appropriate growth media. This preparation was centrifuged at 800*g* for 7 minutes at 4^{o}C. Cell pellets were then resuspended in 10mL of appropriate growth media and plated at a density of 8 x 10^3 cells / cm^2.

2.1.12 Counting Cells

Washed cells were resuspended in 1mL of appropriate media. From this cell suspension, 10µL was removed for counting. Depending on the estimated cell number, a dilution factor between two and ten was used to count cells. Mononuclear cells were counted in white cell fluid (2% acetic acid in distilled H_2O) which preferentially lyses erythrocytes. All other cells were counted using trypan blue (Sigma Aldrich, Castle Hill, Australia). Trypan blue enters the cell membranes of dead cells and all cells that are not blue can be counted as live cells. To obtain an accurate cell number at least 100 cells were counted using a haemocytometer.

2.2 Functional Analysis of *WNT2* and *WNT2B* overexpressing MSC

2.2.1 Assessment of Population Doublings

Overexpressing MSC were seeded at $8x10^3$ cells/cm^2 and allowed to expand to approximately 90% confluence before being harvested by trypsin/EDTA (JRH Biosciences, Lenexa, KS, USA) treatment. Cells were passaged at a seeding density of $8x10^3$ cells/cm^2 into 24 well plates until they had reached *in vitro*-cellular senescence (section 2.2.2). Cell counts were performed at each passage and population doublings were calculated using the formula (log^2 final cell number / log^2 seeding cell number). The final population doubling value for each colony was represented as the sum of population doubling values obtained at each passage. The population doubling times per cell passage were calculated using the formula: Generation time = (log^2 x days in culture) / (log final cell number – log seeding cell number).

2.2.2 Senescence Assay

A Cell Signalling Technology's Senescence Assay Kit was used to measure the presence of senescence-associated β-galactosidase (Cell Signaling Technology, Boston, MA, USA). Growth media was removed and cells were rinsed once with 1x PBS. Rinsed cells were fixed with 1mL of 1x Fixative Solution and incubated at room temperature for 15 minutes. Following fixation, cells were rinsed twice with 1x PBS before 1mL of β-galactosidase staining solution was added to each well and plates incubated at 37^{o}C overnight in a dry-air incubator. Once stained, cells were enumerated manually.

2.2.3 Assessment of Osteogenic Differentiation Potential

In vitro mineralization assays were performed as previously described (Gronthos et al., 1994; Gronthos et al., 2003a). Briefly, MSC were seeded at $8x10^3$ cells per cm^2 in 24 well plates and cultured in mineralization media for 28 days with media changes twice weekly. At 28 days the wells were washed in 1xPBS and fixed with 10% Neutral Buffered Formalin (Fronine Laboratory Supplies, Lomb Scientific, Taren Point, NSW, Australia) for 1 hour. Mineralized cultures were stained with 2% Alizarin Red S (Sigma-Aldrich Inc., St. Louis, MO, USA) in RO water. For quantitative assessment of mineral deposition, cells were seeded at $8x10^3$ cells per cm^2 in 96 well plates and cultured in mineralization induction media for 28 days with media changes twice weekly. At 28 days the wells were washed three times with 1x PBS and the mineralised matrix dissolved in 100µL of 0.6 M HCl (Merck, Kilsyth, VIC, Australia) for 1 hour at room temperature. The dissolved mineral solution was then transferred to 96-well microtitre plates and calcium levels were quantitated by the Cresolphthalein Complexone assay (Thermo Electron Corporation, Melbourne, VIC, Australia). Briefly, 5µL of each supernatant was transferred to a single well of a fresh microtitre plate. A calcium chloride (calcium/phosphorous combined standard (Sigma Aldrich, St. Louis, MO, USA) standard curve was also established in triplicate. Equal volumes of reagent A (cresolphthalein complexone 0.10mmol/L, 8-hydroxyquinoline 5.2mmol/L, polyvinylpyrrolidine 0.07 mmol/L) and reagent B (2-amino-1-methylpropanol 260mmol/L) were mixed and 200µL was added per well. The plates were incubated at room temperature for 2 minutes and the absorbance was read at 540nm on a microplate reader (EL808 Ultra, BIO-TEK Instruments, Winooski, VT, US).

Following dissolution of the mineral with HCl, the wells were washed with 1x PBS and the cells were digested with 100µL of proteinase K (100µg/mL) (Invitrogen, Carlsbad, Canada) for 2

hours at room temperature or overnight at 4°C. The cells were then triturated thoroughly to ensure complete disruption, 50µL volumes were transferred to a white 96-well microtitre plate (Costar, Corning, New York, NY, USA). DNA content per well was then quantified using the Picogreen assay as described in section 2.2.4.

2.2.4 Picogreen DNA Assay

Following digestion (section 2.2.3) 50µL of DNA standards (table 2.3) were added to appropriate wells and 50µL of sample digests to appropriate wells. Picogreen stock was diluted 1:300 into 1 x TE buffer. Diluted Pico Green (150µL) was added to all wells and the plate gently agitated to mix and protected from light (Quant-iT dsDNA Assay kit cat#P11496, Invitrogen, Mulgrave, Victoria, Australia). The plate was then read on the Polar Star Optima Microplate Reader under florescence settings with the following paramaters;

Table 2.3 - Microplate picogreen settings and high molecular weight DNA standards

Excitation filter:	485P
Emission filter:	520P
Gain:	1300
Optics:	3 mm liquid light guides
Number of cycles:	1
Number of flashes:	10
Shake time:	60 s before reading cycle

Standards - High molecular weight DNA (Sigma, cat.# D4522, 5mg)

Prepare 10mg/mL stocks in sterile RO water and dilute standards to 5mg/mL, 2.5mg/mL, 1.25mg/mL, 0.625mg/mL, 0.312mg/mL and 0mg/mL.

.

2.2.5 Assessment of Adipogenic Differentiation Potential

Adipogenesis assays were performed as previously described (Gronthos et al., 2003a; Pittenger et al., 1999). MSC were seeded at $8x10^3$ per cm^2 in 24 well plates and cultured for 28 days in the presence of adipogenic media with media changes twice a week. At 28 days, the wells were washed three times with 1xPBS and cells fixed in 10% Neutral Buffered Formalin (NBF) for 1 hour at room temperature. Oil Red O staining solution was prepared by dissolving 0.5g of Oil Red O stain (MP Biomedicals, Solon, OH) in 100 mL of isopropanol (Ajax Finechem, Taren Point, NSW, Australia) and further diluted 1.5:1 in RO water. Formation of lipid-laden fat cells was determined by Oil Red O staining. For quantitative assessment, overexpressing MSC were seeded at $8x10^3$ per cm^2 in 96 well plates and were cultured for 28 days in the presence of adipogenic media with media changes twice a week. At the conclusion of the assay, wells were washed three times with 1xPBS, fixed in 10% Neutral Buffered Formalin for 1 hour at room temperature and stained with nile red and DAPI (4µg/mL) (Sigma-aldrich, Sydney, Australia #N3013 and #D9542) before being imaged using an Olympus iX70 multi-wavelength inverted florescent microscope (Olympus, Tokyo, Japan) and enumerated manually.

2.2.6 Assessment of Chondrogenic Differentiation Potential

Chondrogenesis assays were performed as previously described (Isenmann et al., 2009). Briefly, $1x10^6$ MSC were resuspended in DMEM media, centrifuged at 600*g*, at 4^oC for 5 minutes to

form cell pellets. The cell pellets were cultured for 28 days in chondrogenic induction media ± TGFβ3 with media changes twice weekly. At the conclusion of the assay, pellet cultures were fixed in 10% Neutral Buffered Formalin at 4^{o}C overnight. Pellet cultures designated for RT-PCR analysis were washed 3 times in 1x PBS and RNA extraction and cDNA synthesis were performed as described as described in Section 2.4.2.1. RT-PCR analysis was performed, as described as described in 2.4.2.4.

For quantitative assessment of glycosaminoglycan (GAG) production, MSC were seeded at 5x10^4 per well of 96-well plates in αMEM + additives as previously described (Gronthos et al., 2003b). Following overnight adhesion 10ng/mL TGFβ3 was added to cultures. After 48 hours, TGFβ3-containing media was replaced with 100μL of media containing 1μCi $^{35}SO_4$ (sulphur-35 radionuclide) (ParkinElmer Life Sciences, Boston, MA, USA) and the plates were incubated at 37°C in 5% CO_2 overnight. To prepare papain digest solution at the final concentration of 20 U/mL, 62.1mg of papain (Papain from Carica Papaya, 3.1 U/mg) (Sigma-Aldrich, St. Louis, MO, USA) was dissolved in 333μL of 3 M sodium acetate (Sigma-Aldrich, St. Louis, MO, USA), 48μL of 0.5 M EDTA (Ethylenediamenetetraacetic acid) (Chem Supply, Gilman, SA, Australia), 1mL of 200 mM of N-acetyl-L-cysteine (Sigma-Aldrich, St. Louis, MO, USA) and 8.619 mL of RO water. The matrix was then digested at 65°C for 2 h with 100μL of 20 U/mL papain digest solution. Cetylpyridinium chloride solution was made by dissolving 1 g of cetylpyridinium chloride monohydrate (Sigma-Aldrich, St. Louis, MO, USA) in 16mL of ethanol and further diluting this solution in 24mL of RO water. Glycosaminoglycans were precipitated by the addition of 40μL of cetylpyridinium chloride solution followed by 5 minutes of mixing at 50 rpm at room temperature. CSA solution was made by dissolving 50mg of Chondroitin sulfate A (Sigma-Aldrich, St. Louis, MO, USA) in 10mL of RO water. CSA solution (10μL) was then added and the plate was mixed for a further 5 minutes at 50 rpm at room temperature. The

precipitated proteins were then transferred to a glass fibre filter (Packard Bioscience Company, Meriden, CT, USA) using a cell harvester (Packard Filtermate Harvester, Packard Bioscience Company, Meriden, CT, USA). The membranes were dried for 2 hours at 37^{o}C before adding 25µL MicroscintTM (PerkinElmer Life and Analytical Sciences, Boston, MA, USA) per well where the amount of $^{35}SO_4$-labelled GAG per well was measured using a TopCount NXT Microplate Scinitillation & Luminescence counter (Perkin Elmer Life and Analytical Sciences, Downers Grove, IL, USA). In order to normalize to DNA concentration, replicate cultured cells were digested in 100µL papain digest solution (100 U/mL) at 65°C for 6 hours. 50µL of the cell lysate suspension was then transferred to a white microtitre plate and DNA content was measured using Picogreen as described in Section 2.2.4. Glycosaminoglycan levels were then normalised to DNA content to determine relative GAG production per cell.

2.2.7 Histological Assessment

Fixed chondrocyte pellets were processed, embedded and 5µm sections prepared by Mr J. Manavis (Department of Neuroscience, Hanson Institute, Adelaide, SA, Australia). Sections were de-paraffinised through incubations in 2 changes of xylene (Ajax Finechem, Taren Point, NSW, Australia), 3 changes of absolute ethanol (Merck, Kilsyth, VIC, Austrlia) and a final wash in RO water. To neutralise endogenous peroxidase activity the sections were incubated in 0.5% H_2O_2 (Ajax Finechem, Taren Point, NSW, Australia) (v/v) in methanol (Chem Supply, Gillman, SA, Australia) for 30 minutes and non-specific binding was blocked by incubating sections with 3% (v/v) normal goat serum in 1xPBS for 1 hour at RT. Sections were then incubated overnight with either an isotype-matched, nonbinding control monoclonal antibody (1B5, IgG1) or the anti-collagen II monoclonal antibody type II, (MAB1330) (Chemicon International, Temecula, CA) used at 1 in 100 dilution in 3% (v/v) normal goat serum in 1XPBS. Wash buffer was made by

adding 50 mM Tris-HCl (Sigma-Aldrich, St. Louis, MO, USA) and 0.1% Tween-20 (Sigma-Aldrich, St. Louis, MO, USA) in RO water. Slides were then washed three times with wash buffer and bound antibody was revealed using the Dako EnVision+® Kit (Dako, Glostrup, Denmark). The sections were incubated with the Peroxidise-Labelled Polymer (Dako, Glostrup, Denmark) for 30 minutes, then washed with wash buffer and incubated with the DAB Substrate-Chromogen (Dako, Glostrup, Denmark) solution for 5-10 minutes. Sections were counterstained briefly with haematoxylin (ProSciTech, Turingowa Central, QLD, Australia) and mounted in DePex mounting media (BDH Chemicals, Poole, UK).

2.2.8 CFUF

Mice were humanely euthanized using CO_2 gas followed by cervical dislocation. The fractured and non-fractured contralateral femora were surgically removed and cleared of soft tissue in a Class II laminar flow hood (Top Safe 1.2, Bio Air, Siziano, Italy), using sterile instruments. The distal and proximal ends of each femur were removed using sterile forceps and a surgical blade (#22). A 10mL syringe attached to a 21 gauge needle was then inserted into either end of the bone with a screwing motion. The bone marrow was then flushed with complete α-MEM media (table 2.1) until the femur appeared colourless. The femur was then rotated so that the needle was positioned in the other end and flushed with media once more. The flushed bone marrow was then stored on ice in a 50mL Falcon tube and the flushed femur stored in a 6cm culture dish with enough complete α-MEM media to cover femur (~500µL).

The femur was then crushed into small pieces with a sterile scalpel blade and transferred to a 10mL yellow capped tube with 1mL CollagenaseI/DNAseI solution (table 2.4). The crushed bone was then incubated for 45minutes - 1hour at 37^{o}C with shaking at 200rpm. Once digested, 10mL

complete α-MEM media was added to the bone chips. The digested bone chips were then strained through a 70μm cell strainer and combined with the flushed bone marrow. The remaining bone chips were transferred as explants to a T^{75} flask containing 10mL complete media and cultured until confluent. The filtered bone chip / marrow solution was then centrifuged at 800*g* at 4°C for 10 minutes. Once centrifuged, cells were counted in white cell fluid and diluted to concentrations of 9, 18 and 36 x 10^5 cells per well (3mL per well) and plated in duplicate in 6 well plates.

The plated cells were then incubated for 1 hour at 37°C. After 1 hour the supernatant from the plated wells was transferred to a fresh 6 well plate and complete α-MEM was added to the original plate. Both plates were then incubated for 14 days before staining for CFU-F colonies.

Table 2.4. CollagenaseI/DNAseI solution

5mL CollagenaseI 6mg/mL
5mL sterile 1x PBS
2.6μL DNAse 1 (12800 units/67 μL stock)

2.2.9 Staining CFU-F Colonies

After 2 weeks of incubation media was tipped off gently and cells were fixed in ~1mL of fixative solution / well for approximately one minute. Wells were then washed with RO water three times before being stained with 1mL Alkaline Phosphatase Stain (table 2.5) / well and incubated at room temp with agitation for 30 minutes. The stain was then tipped off and wells were washed with RO water before being counter stained with Toluidine Blue for one minute. Wells were then

rinsed with RO water until the water ran clear. Stained wells were then enumerated using an inverted microscope according to the conditions illustrated in figure 2.1.

Table 2.5. CFU-F Staining Reagents

Fixative solution;
20mL RO water
400 µL Citrate Concentrate
30mL Acetone
Alkaline Phosphatase Stain
48mL RO water
One Fast Violet B capsule (Leukocyte Alkaline Phosphatase kit, Sigma, Sydney, Australia)
2mL Napthol AS-MS Phosphate Alkaline Solution
Toluidine Blue Stain
30mL 40% formaldehyde
480mL PBS 1x
0.51g Toluidine Blue

2.2.10 Flow-Cytometric Analysis

To characterise the immunophenotype of *ex vivo* expanded MSC, flow cytometric analysis was used to assess the expression of mesenchymal and non-mesenchymal stem-cell associated surface markers. Adherent *ex vivo* expanded MSC were washed once with HBSS and liberated by enzymatic digestion by the addition of 3 mL of 0.05% Trypsin/EDTA solution per T^{75} culture

Figure 2.1 – Stained CFU-F Colonies (A) A 100% colony represents a colony with 100% of cells stained positive for alkaline phosphatase (pink staining). This is the most committed cell type. (B) A 75% colony represents a colony with ~75% of cells stained positive for alkaline phosphatase. (C) A 50% colony represents a colony with ~50% of cells stained positive for alkaline phosphatase. (D) A 25% colony represents a colony with ~25% of cells stained positive for alkaline phosphatase (E) A nill colony represents a colony with no cells stained positive for alkaline phosphatase (blue staining). This is the most immature cell type.

(A)

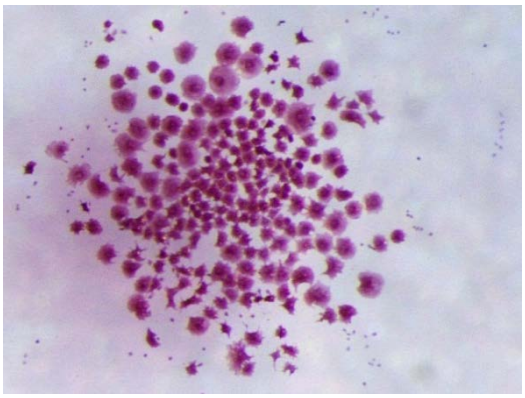

(B)

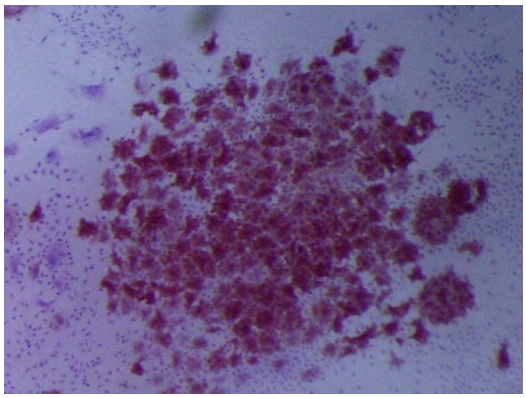

(C)

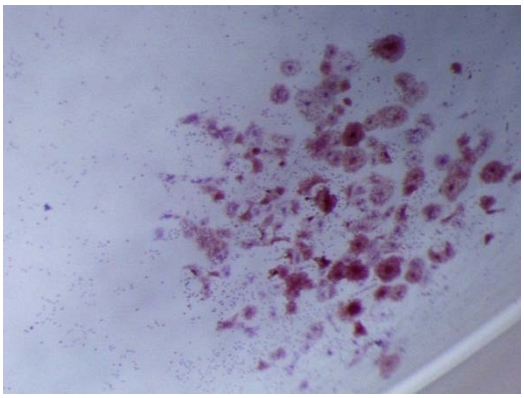

(D)

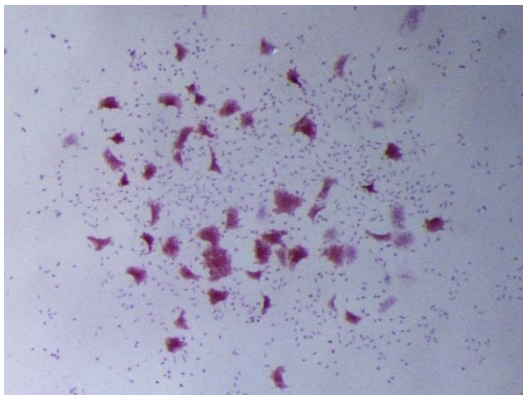

(E)

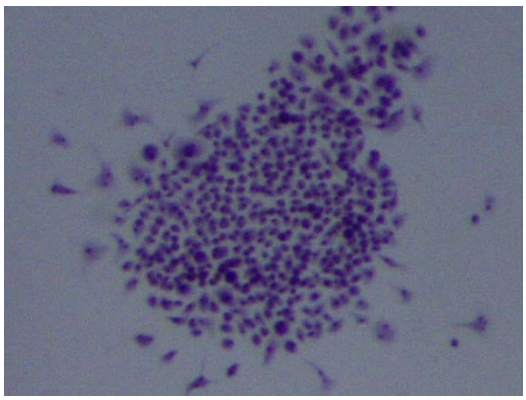

flask for 5 minutes at 37ºC. The single cell suspension was then washed twice in HHF buffer. Cell count and assessment of viability was performed as described in Section 2.1.12. MSC were resuspended for immunolabeling in 500 μL blocking buffer and incubated on ice for approximately 30 minutes to minimize Fc receptor-mediated binding of antibodies. Individual FACS tubes containing 2 x 10^5 cells were incubated with appropriate primary murine monoclonal antibodies specific to mesenchymal stem cell associated markers, haemopoietic, non-mesenchymal stem cell-associated markers and isotype-matched controls at a concentration of 20μg/mL for 1 hour on ice. The list of these antibodies is detailed in table 2.6. The cells were washed twice in 1 mL of HHF and incubated with secondary detection reagent; goat anti-mouse IgG- or goat anti-mouse IgM-PE (PE) (Phycoerythrin) conjugated antibody (1:50, Southern Biotechnology, Birmingham, AL, USA) for 45 minutes on ice. The cells were then washed in 1mL of HHF and fixed in 500μL of FACS Fix solution. Analysis was performed on a fluorescence-activated cell sorter fitted with a 250 MW argon laser (Beckman Coulter Cytomics FC500, using CXP Cytometry List Mode Data Acquisition and Analysis Software version 2.2, Beckman Coulter, Miami, FL, USA).

Table 2.6. List of Antibodies

Name	Isotype	Source
1B5	IgG1	Prof. L.K Ashman (University of Newcastle, Australia)
1D4.5	IgG2a	Prof. L.K Ashman (University of Newcastle, Australia)
1A6.12	IgM	Prof. L.K Ashman (University of Newcastle, Australia)
B478	IgG1	ATCC
CD14	IgG2	Beckman Coulter
CD34	IgG1	Beckman Coulter
CD45	IgG1	Beckman Coulter
CD73	IgG1	Becton Dickinson
CD90	IgG1	Becton Dickinson
CD105	IgG1	Becton Dickinson
CD146	IgG2a	(Filshie et al., 1998; Shi and Gronthos, 2003)
CD166	IgG1	Becton Dickinson
STRO-1	IgM	(Gronthos et al., 2003a; Simmons and Torok-Storb, 1991)
Goat anti Mouse	IgG PE	Southern Biotech
Goat anti Mouse	IgM PE	Southern Biotech
Streptavidin	PE	Caltag Laboratories

All primary antibodies and isotype matched controls were used at a concentration of 20µg/mL with the exception of STRO-1 and 1A6.12 which were used as neat supernatants. Fluorescent conjugated secondary detection antibodies were used at a concentration of 10µg/mL.

2.3 Cell Imaging

Fluorescence images were taken using an Olympus CKX41 microscope with attached Olympus U-RFLT50 UV light and DP20 camera (Olympus, Tokyo, Japan). Cells were placed on microscope stage and microscope was manually adjusted to correct focal point. All photos were then taken using automatic camera settings.

2.4 Molecular Techniques

2.4.1 Microarray Analysis

An Illumina V8 microarray analysis (Illumina, Scoresby, Victoria, Australia) comparing *TWIST-1* overexpressing MSC with empty vector control MSC was conducted to identify *TWIST-1* gene targets involved in self-renewal, maintenance and differentiation of MSC. This microarray returned approximately 350 differentially expressed genes with confidence of 95% or greater. Genes were manually sorted into categories based on their properties such as; transcription factors, cell adhesion molecules, structural molecules, DNA binding molecules, cell signalling molecules, and genes related to adipogenesis, osteogenesis, chondrogenesis and proliferation. Analysis utilising the Database for Annotation, Visualization and Integrated Discovery (DAVID) (SAIC-Frederick, Inc., Frederic, MD, USA) was conducted to identify patterns related to input genes and known functional pathways. Protocols; as described by Huang and colleagues (Huang et al., 2008; Huang et al., 2009) were used to identify 12 genes which were researched manually based on current literature.

2.4.2 Analysis of Gene Expression - PCR

The following methods of gene analysis were based on reports by Gronthos et al. (Isenmann et al., 2007; Schwarz, 1968)

2.4.2.1 Preparation of total RNA

The collection and preparation of total cellular RNA was accomplished using TRIzol (Life Technologies, City, Carlsbad, Canada). Up to 1 x 10^6 MSC were lysed in 1mL TRIzol, directly in wells or, if grown in a flask, removed from flask using trypsin prior to being lysed in TRIzol. Chloroform (200µL per mL) was added to this solution and tubes were shaken vigorously for 15 seconds before a 30^{o}C incubation of approximately 3 minutes. Centrifugation of this mixture at 12,000*g* for 15 minutes at 2^{o}C resulted in phase separation. The lower two layers contained protein and DNA while RNA remained in the upper aqueous phase. This aqueous phase was transferred to a fresh tube and total RNA was precipitated using isopropanol (500µL per mL) and glycogen (1µL per mL; Sigma Aldrich, Castle Hill, Australia). This preparation was incubated for one hour on ice to ensure maximum RNA precipitation. To pellet RNA, cells were centrifuged at 12,000*g* for 10 minutes at room temperature. Supernatant was removed and the pellets washed in 1mL of 75% ethanol before being centrifuged at 7,500*g* for 5 minutes at 4^{o}C. Ethanol was removed and the RNA was allowed to air dry for approximately 10 minutes. The dried RNA was then dissolved in RNAse free water at room temperature for 10 minutes before being quantitated using a NanoDrop Mass spectrometer (NanoDrop ND-1000 Spectrophotometer, Biolabgroup, Clayton, Victoria, Australia) and stored at -20^{o}C.

2.4.2.2 Quantification and purity analysis of RNA

The NanoDrop mass spectrometer was used for quantification and purity analysis of RNA samples. Samples were diluted 1:1 with buffer TE before 1.5uL was added to the stage of the NanoDrop. Absorbance at 260nm was measured to determine the quantity of RNA and purity was measured by the ratio of A_{260}:A_{280}. Ratios between 1.85 and 1.95 were commonly obtained. Samples with values within this range were considered to be of high purity and were either used immediately to generate cDNA or stored at -20^{o}C for future use.

2.4.2.3 Complementary DNA (cDNA) synthesis

Complementary cDNA was generated using the SuperScript III Reverse Transcriptase kit (Invitrogen, Carlsbad Canada). Briefly, 1µL oligo(dT), 1-5µg total RNA, 1µL dNTP mix and distilled water to a total volume of 13µL was added to each microcentrifuge tube. This mixture was heated to 70^{o}C for 5 minutes and then incubated on ice for at least 1 minute in order to denature the RNA. The tube was then briefly centrifuged before 4µL 5x first-strand buffer, 2µL 0.1M DTT and 1µL of SuperScript III RT (200 units / µL) was added. This solution was mixed with gentle pipetting before being incubated at 42^{o}C for one hour to allow for primer extension and first strand synthesis. The reaction was stopped by incubation at 70^{o}C for 15 minutes leading to deactivation of the reverse transcriptase enzyme. RNAse free water was then added to a volume of 50x the number of µg template RNA added originally. The resulting cDNA was used as a template for PCR reactions and stored at -20^{o}C.

2.4.2.4 Real-time PCR

Using cDNA generated by the above methods (2.4.2.3) PCR was conducted to assess the levels of RNA expression. Beta-actin (β-actin) was used as a housekeeping control gene and samples were normalized against this control. A reaction mixture containing 2µL of sample cDNA, 7.5µL cyber green (Jomar Diagnostics, Adelaide, South Australia, Australia), 0.75µL (10µM) mixed primer pairs and 4.75µL DEPC water was mixed to generate a 15µL reaction for each tube of a 72 tube rotor of a Rotor Gene RG-6000 Realtime PCR machine (Corbett Research, Sydney, Australia). The primer pairs and cycling parameters used in this thesis are outlined below in tables 2.7 to 2.12.

Table 2.7. Real time PCR Primers

Gene - Realtime	Forward Primer	Reverse Primer
β- Actin	5` GAT CAT TGC TCC TCC TGA GC 3`	5` GTC ATA GTC CGC CTA GAA GCA T 3`
TWIST-1	5` CCG GAG ACC TAG ATG TCA TTG 3`	5` GGC CTG TCT CGC TTT CTC TT 3`
TGFβ2	5′ TTG ACG TCT CAG CAA TGG AG 3′	5′ TCG CCT TCT GCT CTT GTT TT 3′
ACVR2A	5′ ACA AGA TGG CCT ACC CTC CT 3′	5′ CGT TAA GCA ACT GGG CTT TC 3′
AXIN2	5′ CTG GCT ATG TCT TTG CAC CA 3′	5′ CTT CAC ACT GCG ATG CAT TT 3′
BMP4	5′ GGA GGA GGA AGA GCA GAT CC 3′	5′ GGG ATG CTG CTG AGG TTA AA 3′
WNT2	5′ AGA TGT GAT GCG TGC CAT TA 3′	5′ TAA ACA AAG GCA GAT TCC CG 3′
WNT2B	5′ AAG ATG GTG CCA ACT TCA CC 3′	5′ ATT TCT GCA TTC CTT GCA CC 3′
RUNX2	5′ GTG GAC GAG GCA AGA GTT CA 3′	5′ CAT CAA GCT TCT GTC TGT GCC 3′
Osteopontin	5′ ACA TCC AGT ACC CTG ATG CTA CAG 3′	5′ GTG GGT TTC AGC ACT CTG GT 3′
PPARγ2	5′ CTC CTA TTG ACC CAG AAA GC 3′	5′ TCA AAG GAG TGG GAG TGG TC 3′
Adipsin	5′ GAC ACC ATC GAC CAC GAC 3′	5′ CCA CGT CGC AGA GAG TTC 3′
SOX9	5′ AGG TGC TCA AAG GCT ACG AC 3′	5′ GCT TCT CGC TCT CGT TCA GA 3′
COL2	5′ GCC TGG TGT CAT GGG TTT 3′	5′ GTC CCT TCT CAC CAG CTT TG 3′

Table 2.8. Genotyping PCR Primers

Gene - Genotyping	Primer Sequence
Twist 114 (Het)	5′ CCG GAT CTA TTT GCA TTT TAC CAT GGG TCA TC 3′
Twist 115 (Het)	5′ CCT CTA CCT GAC CGT TAG ATG GAC TCG G 3′

Table 2.9. Cloning PCR Primers

Gene - Cloning	Primer Sequence
WNT2B R.	5’ AAT TAA CTC GAG GAC GCC CTA GGT GTA GCA G 3’
WNT2B F. (646bp)	5’ AAT TAA GGT ACC GAG GAC CGA GGC ACA GAG 3’
WNT2B F. (1213bp)	5’ AAT TAA GGT ACC CTC GGG AGG CAC CTC TAA C 3’
WNT2B F. (2246bp)	5’ AAT TAA GGT ACC CTG GGT TGG GAG GAG GTA A 3’
WNT2B F. (3568bp)	5’ AAT TAA GGT ACC CCC TTG AAC TTC AGC AGA GC 3’
WNT2 R.	5’ AAT TAA CTC GAG CGC TGA TAA AGT TTC AAA CGA 3’
WNT2 F. (535bp)	5’ AAT TAA GAG CTC CTC TTC ATC CCA GCT TCA GG 3’
WNT2 F. (1016bp)	5’ AAT TAA GAG CTC CCT GGT CTT CCT TCC TTT CC 3’
WNT2 F. (1961bp)	5’ AAT TAA GAG CTC GAG GAC ACG ATG TGC TGA GA 3’
WNT2 F. (2939bp)	5’ AAT TAA GAG CTC GGT GGA GAT GGC TCA GTT GT 3’

Table 2.10. Sequencing PCR Primers

Gene - Sequencing	Primer Sequence
Twist Seq. 347	5′ GAG AGA TGA TGC AGG ACG TGT 3′
Twist Seq. 644	5′ GGA GTC CGC AGT CTT ACG AG 3′
Twist Seq. 998	5′ CCT AGA TGT CAT TGT TTC CAG AGA 3′
Twist Seq. 1348	5′ AAG GCA TCA CTA TGG ACT TTC TCT 3′
WNT2 F. (535bp)	5′ AAT TAA GAG CTC CTC TTC ATC CCA GCT TCA GG 3′
WNT2 F. (1016bp)	5′ AAT TAA GAG CTC CCT GGT CTT CCT TCC TTT CC 3′
WNT2 F. (1961bp)	5′ AAT TAA GAG CTC GAG GAC ACG ATG TGC TGA GA 3′
WNT2 F. (2939bp)	5′ AAT TAA GAG CTC GGT GGA GAT GGC TCA GTT GT 3′
Wnt2b2 pro1213 seq	5′ GTT AGA GGT GCC TCC CGA G 3′
Wnt2b2pro2246 seq	5′ TTA CCT CCT CCC AAC CCA G 3′
Wnt2b2pro646 seq	5′ CTC TGT GCC TCG GTC CTC 3′
RVprimer3 (PGL3)	5′ CTA GCA AAA TAG GCT GTC CC 3′
GLprimer2 (PGL3)	5′ CTT TAT GTT TTT GGC GTC TTC CA 3′
RCF-1 (iG2)	5′ TTG GGG GAC TCT GCT GAC CAC 3′
IRES rev (iG2)	5′ ACA CCG GCC TTA TTC CAA G 3′

Table 2.11. ChIP PCR Primers

Gene - ChIP	Forward Primer	Reverse Primer
FGFR2	5′ CCT TGT CTG GCG GTT CTT T 3′	5′ CAC ACC ACT GAG GCT TCT GA 3′
GAPDH	5′ GAA GGT GAA GGT CGG AGT CA 3′	5′ CCC ATA CGA CTG CAA AGA CC 3′
WNT2 - 001	5′ AAA GCC AAC AGG TCA TTT CG 3′	5′ CCT GAA GCT GGG ATG AAG AG 3′
WNT2 - 002	5′ ATT CCA TTG GCC TCA CCA T 3′	5′ TCC GAG GAA CCA GAA ACA TT 3′
WNT2 - 003	5′ GAA TGG GAG GGA AAT GGA AT 3′	5′ TTA AAT CCA CGC CAG AGG AC 3′
WNT2 - 004	5′ TCC AGA AAG AGA ATT GGG TTC 3′	5′ GGA GGA AAG AAG GTT ACA GCA A 3′
WNT2 - 005	5′ GGA GTC ATT GCC TGA GGA AG 3′	5′ CAG AAC CCA ATT CTC TTT CTG G 3′
WNT2B - 001	5′ TAG AAG TGG GGC TGC TGA GT 3′	5′ GAC GCC CTA GGT GTA GCA G 3′
WNT2B - 002	5′ AGA CGA AGG AGG GAA AAA GC 3′	5′ TTA GAC CTG GCT CCT GCT TG 3′
WNT2B - 003	5′ ACC CCA TCT GCT TAC ACT CG 3′	5′ TCC TGG GCT TAA CTT CGA GA 3′
WNT2B - 004	5′ CGG TGG GGA GAG AGG TTA AA 3′	5′ GTT AGA GGT GCC TCC CGA GT 3′

Table 2.12. PCR cycling parameters

Activation	Hold 1 – 15 minutes - 95^{o}C
Cycling (40 cycles)	15 seconds - 95^{o}C 25 seconds - 60^{o}C 10 seconds - 72^{o}C
Final extension	Hold 2 – 3 minutes - 72^{o}C
Melt Curve	90 second pre melt, 5 second steps 1 degree per step, 72^{o}C - 99^{o}C

2.4.2.5 Sequencing

A PCR reaction using the conditions described below (table 2.13) was used to amplify target DNA with fluorescent nucleotides. Following PCR, samples were transferred to a 1.5mL eppendorf tube containing 80µL 75% isoprobanol and 1µL Glycogen (29mg/mL). These samples

were incubated for 15 minutes at room temperature away from light before DNA was pelleted by centrifugation at 16,000*g* for 15 minutes at room temperature. Supernatant was then aspirated and DNA pellets washed with 200µL 75% ethanol before being centrifuged at 16,000*g* for 2 minutes. Ethanol was aspirated and pellets allowed to dry for 10 minutes away from light. Samples were then delivered to IMVS sequencing centre and stored at -20^{o}C until analysed.

Table 2.13. DNA Sequencing

Sequencing - PCR Reaction Concentrations

Mix	final	for 1 reaction
Big Dye V3	0.125 x buffer	1.0µL
5 x sequencing buffer	0.875 x buffer	3.5µL
Sequencing primer (3.2 µM)	3.2pM	1.0µL
Plasmid DNA	200ng	200ng
H2O		To 20µL
		20 µl total

Sequencing - PCR Cycling Conditions

PCR condition	Temperature	Time	
Initial denature	96 °C	2 min	
Denaturing	96 °C	10 sec	**25 cycles**
Annealing	50 °C	5 sec	
Elongation	60 °C	4 min	
Hold	4 °C	∞	

2.4.2.6 Isolation of DNA from agarose

Isolation of DNA from agarose gels was conducted using the UltraClean™ GelSpin™ DNA Extraction Kit (Geneworks, SA, Australia). Briefly, the desired DNA band was excised from a TAE agarose gel using a scalpel and a 1:1 print out of the imaged gel. The excised agarose fragment was then weighed and 3 volumes of GelBind were added to the gel slice. This solution was incubated for 2 minutes at 55°C to allow gel to melt. Once fully melted the tube was inverted to mix. The homogenous solution was added to a spin filter and centrifuged at 10,000*g* for 10 seconds to bind DNA to the membrane. The spin column was removed from the collection tube and the collection tube was vortexed for 5 seconds to mix the flow-through. The flow through was reloaded back into the spin filter to allow any unbound DNA to bind and subsequently increase DNA yield. The spin column was centrifuged at 10,000*g* for 10 seconds and flow-through discarded. The spin column was washed with 300µL GelWash buffer was added to wash away residual salt and agarose. This solution was centrifuged at 10,000*g* for 10 seconds and flow-through discarded before being centrifuged again for 30 seconds at 10,000*g*. The spin column was transferred to a clean 2mL collection tube and 50µL of Elution Buffer was added directly to the centre of the spin filter. The spin column was allowed to stand for 1 minute before being centrifuged at 10,000*g* for 30 seconds. The collection tube containing DNA was stored at -20°C until required.

2.4.2.7 PCR Product Purification

Purified PCR products were prepared using the QIAquick PCR Purification Kit (QIAGEN, Chadstone, Victoria, Australia). Briefly, 5 volumes of Buffer PB were mixed with one volume of the PCR sample. This solution was applied to a QIAquick spin column in a 2mL collection tube and centrifuged at max speed for 1 minute. Flow-through was discarded and spin column was

washed with 0.75mL Buffer PE and centrifuged for 1 minute at max speed. Flow-through was discarded and column was centrifuged for an additional 1 minute to remove any residual Buffer PE. The spin column was placed in a clean 1.5mL microcentrifuge tube and 30uL of elution buffer was added to the centre of the spin column membrane and allowed to stand for 1 minute before being centrifuged at max speed for 1 minute. Purified DNA was stored at -20^{o}C until required.

2.4.2.8 Heat Shock Transformation

The pRUF-iG2-Gateway vector was engineered in house by Dr. Peter Diamond. Retroviral vectors pRUF-iG2-Gateway, pRUF-iG2-Gateway-*WNT2*, pRUF-iG2-Gateway-*WNT2B*, VSVG and pGp (System Biosciences, Mountain View, CA, USA) were transformed into chemically competent JM109 (ATCC reference number - 53323) cells for amplification. Ampoules of JM109 cells cryopreserved at -80^{o}C were removed from the freezer and thawed on ice for 10 minutes. Transformation involved incubating the cells on ice for 30 minutes after the addition of 500ng – 1000ng DNA of one of the plasmids to be amplified. Cells were then incubated at 42^{o}C for 90 seconds before being cooled on ice for a further 2 minutes. At this time, 200µL of SOC media was added and the mixture was incubated for 45 minutes at 37^{o}C. Following this incubation, 5µL of cell suspension was plated onto ampicillin (50µg/ml) agar plates in order to generate single colonies. SOC media was used as it contains protein precursors essential for the rapid repair of cell walls damaged by heat shock transformation.

2.4.2.9 FastPlasmid™ Mini Kit (5 PRIME)

Isolation of DNA from 3mL (mini prep) cultures was achieved using the FastPlasmid™ Mini Kit (5 Prime, Hamburg, Germany). Complete lysis solution was chilled on ice prior to use. A 3mL bacteria culture was incubated overnight at 37°C with shaking at 200rpm. From the culture, 2mL was pelleted at 12,000*g* for 1 minute in a 2mL culture tube. The media was removed from the pellet using aspiration and replaced with 400µL of ice cold complete lysis solution. This mixture was then vortexed at the highest setting for a full 30 seconds to achieve homogeneity before being incubated at room temperature for three minutes. The lysate was transferred to a spin column assembly and centrifuged at max speed for one minute. Following centrifugation the column was washed with 400µL of wash buffer and centrifuged at max speed for one minute. The filtrate in the waste tube was discarded and the column centrifuged once more to ensure removal of all remaining liquids. The column was then transferred to a collection tube and 50µL of elution buffer added directly to the centre of the spin column. The column was centrifuged for a final time to allow the DNA to be eluted from the column and remain in solution in the collection tube. The column was then discarded and DNA stored at -20°C or used immediately for future experiments.

2.4.2.10 Maxiprep plasmid preparation

As described above (Section 2.4.2.8), transformed JM109 cells were cultured on ampicillin agar plates and incubated overnight at 37°C. Single colonies were selected and starter cultures were generated in 5mL of LB media and cultured overnight at 37°C. Starter culture (1mL) was then transferred to 500mL LB media and amplified overnight at 37°C. The remaining 4mL of starter culture was stored at 4°C. The starter culture of the colony that produced the highest yield was diluted 1:1 into 80% glycerol and preserved at -80°C for future plasmid amplification. A

maxiprep of each culture was then prepared using the QIAGEN® Midi or Maxi column (Qiagen, Doncaster, Victoria, Australia). Briefly; cultures were centrifuged at 6,000*g* for 15 minutes at 4°C to harvest the bacterial cells. The bacterial pellet was resuspended in Buffer P1 and once resuspended; buffers P2 and P3 were added and mixed thoroughly. This mixture was incubated on ice for 20 minutes. Following incubation, the mixture was centrifuged at 20,000*g* for 30 minutes at 4°C, after which supernatant (containing the DNA) was promptly removed. The pellet was re-centrifuged at 20,000*g* for 15 minutes and supernatant was removed promptly. This supernatant was then applied to a QIAGEN-tip and allowed to enter the resin by gravity flow. The QIAGEN-tip was then washed with 2 x 30mL of Buffer QF. Room temperature isopropanol (UniVar, Seven Hills, Australia) was then added to this mixture, mixed immediately and spun at 15,000*g* for 30 minutes at 4°C to precipitate the DNA. As the DNA had been precipitated, the supernatant was discarded and the DNA pellet was then resuspended using a combination of 400µL TE buffer (10mM Tris-HCL pH7.4, 1mM EDTA), 25µL 3M sodium acetate (Sigma Aldrich, St Louis, MO, USA) and 1mL of 100% ethanol (this is an in house modification to the original Qiagen protocol). The mixture was inverted and centrifuged at 15,000*g* for 5 minutes in a 1.7mL Eppendorf tube. This yielded a pellet that was washed two times in 75% ethanol for 2 minutes each time and then allowed to air dry in a cell culture laminar flow hood. Once almost dry, 50-250µL, depending on the size of the pellet, of EB buffer (Qiagen, Doncaster, Victoria, Australia) was added to resuspend the DNA. Each sample was then analysed using a NanoDrop Mass spectrometer (NanoDrop ND-1000 Spectrophotometer, Biolabgroup, Clayton, Victoria, Australia) to determine the concentration and purity of DNA (described in 2.4.2.2).

2.4.2.11 Agarose Gel Electrophoresis (AGE)

Agrose gel electrophoresis is used to determine the size of samples of DNA or RNA based on the distance travelled through a gel. This method was used to verify the size of DNA plasmids generated via the above Maxiprep plasmid amplification and isolation protocol (2.4.2.10). Agarose gels were prepared using agarose (Sigma Aldrich, Castle Hill Australia, USA) in TAE buffer (0.8M Tris, 0.4M Sodium Acetate, 0.02M EDTA Na_2, pH ~ 8.2) on a glass plate. Using a BioRad electrophoresis apparatus, 1.5µg of DNA was analysed in 0.7% agarose and run at 95V for 30 minutes. The gel was then soaked in ethidium bromide (0.5µg/mL) (Sigma Aldrich, Castle Hill, Australia, G8751) for 10 minutes and scanned using a Typhoon 9410 variable mode imager (GE Healthcare Lifesciences, Uppsala, Sweden).

2.4.3 Cloning

2.4.3.1 Gateway™ Cloning

Outlined in figure 2.2, commercial shuttle clones for *WNT2* (#GC-G0265) and *WNT2B* (GC-Z7523) CDS were purchased from GeneCopoeia™ (GeneCopoeia, Rockville, MD, USA). Both CDS were in the Gateway compatible pDONR™ vectors. Vector DNA arrived on Whatman paper which was soaked for 30 minutes in 20µL TE buffer at room temperature. This DNA solution was then transformed into chemically competent DH5α (2.4.2.8) and plated on Kanomycin 50µg/mL agar plates overnight at 37°C. The following day colonies were picked and amplified in 3mL LB/Kanomycin 50µg/mL media overnight at 37°C with rotation at 200rpm. DNA was prepared from overnight 3mL cultures the 5 Prime kit described in section 2.4.2.9. DNA was quantitated using the NanoDrop (2.4.2.2) and the volume required for 150ng was calculated for a LR clonase reaction.

Figure 2.2 - Gateway cloning system. Gateway cloning was used for all overexpression constructs generated. BP clonase recombination was used to generate an entry vector. LR clonase recombination was then used to generate the final expression construct.

Gateway® Cloning

Original Vector

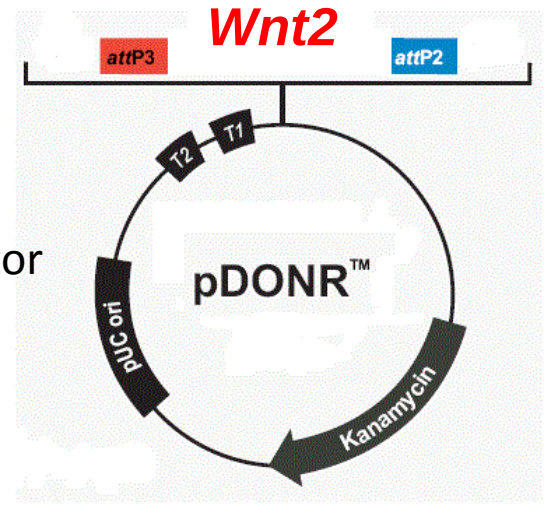

BP Clonase Recombination

Entry Vector

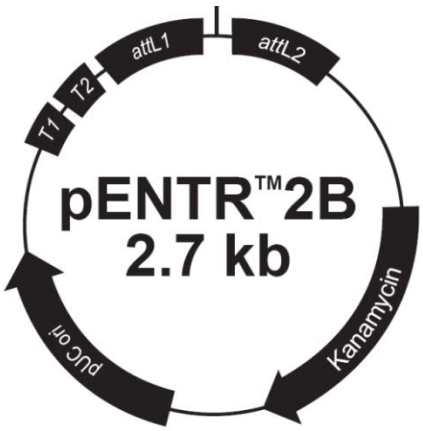

LR Clonase Recombination

Expression Construct

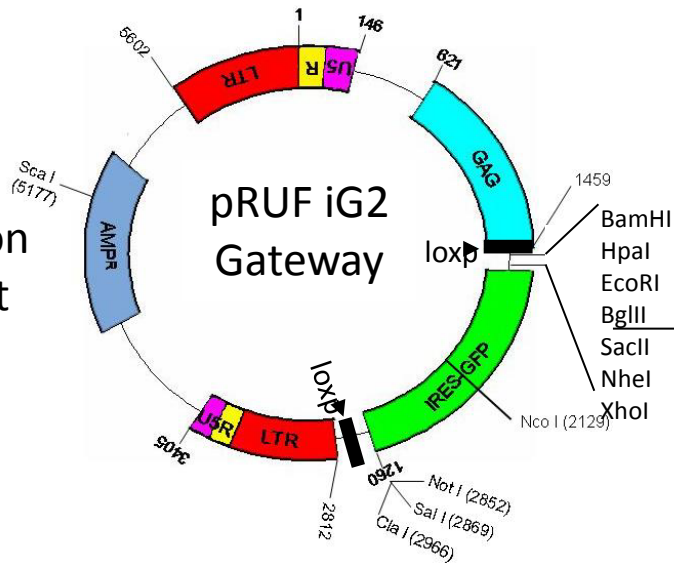

To complete the LR clonase reaction the following reagents were added to a 200µL PCR tube; 150ng of the pDONR vector (containing either *WNT2* or *WNT2B*), 1µL pRUF-iG2-Gateway vector, TE buffer to bring volume to 8µL and 2µL LR clonase enzyme (thawed on ice for 2 minutes). This reaction mixture was then incubated overnight at 25^{o}C. The following morning 1µL proteinase K (section 2.6.2) was added and samples incubated for 10 minutes at 37^{o}C before 5µL was transformed into DH5α (2.4.2.8) and plated on 100µg/mL Ampicillin agar plates and incubated overnight at 37^{o}C. Colonies were picked the following day, transferred to 3mL 100µg/mL Ampicillin LB broth mini cultures and incubated overnight at 37^{o}C with rotation at 200rpm. DNA was prepared from overnight 3mL cultures using the 5 Prime kit described in section 2.4.2.9. At this stage DNA was sequenced (section 2.4.2.5) to confirm correct orientation and identify any sequence mutations. Once sequence was confirmed to be correct, DNA was further expanded and used for infection of MSC cells as described in section 2.5.3.

2.4.3.2 Isolation of genomic DNA

Isolation of genomic DNA from whole blood was performed using the Aquapure genomic DNA Blood kit (Bio-Rad, Hercules, CA, USA). Briefly, 300µL whole blood was added to a 1.5mL microfuge tube containing 900µL RBC Lysis Solution. This solution was then inverted to mix and incubated for 10 minutes at room temperature before being centrifuged for 20 seconds at 14,000*g*. The supernatant was then removed with a pipette leaving behind a visible white cell pellet and a small amount of residual liquid. The tube was vortexed to resuspend the cells in the remaining liquid and 300µL of Genomic DNA Lysis solution was added. This solution was carefully pipetted to resuspend and lyse the cells. Samples were then RNase treated by addition of 1.5µL RNase A solution (Qiagen, Doncaster, Victoria, Australia) and incubated at 37^{o}C for 30

minutes. The sample was cooled to room temperature and 100µL Protein Precipitation Buffer was added to the cell lysate. This solution was vortexed vigorously for 20 seconds to mix uniformly and then centrifuged at 14,000*g* for 3 minutes. The supernatant was poured into a clean microfuge tube containing 300µL isopropanol / 1µL glycogen and mixed by inverting gently 50 times. The solution was centrifuged at 14,000*g* for 1 minute and supernatant was poured off and the tube drained briefly on paper towel. The DNA pellet was washed with 300µL of 70% ethanol and centrifuged at 14,000*g* for 1 minute. The ethanol was removed by aspiration and the washed pellet was allowed to air dry for 10 minutes. The air dried DNA pellet was dissolved in 100µL of DNA Hydration Buffer and incubated at room temperature overnight. Once resuspended, DNA was stored at -20^{o}C until required.

2.4.3.3 Cloning Promoter Fragments into PGL3 Basic

As illustrated in figure 2.3, promoter fragments from *WNT2* and *WNT2B* were identified and cloned into PGL3 basic vector to further confirm microarray results which showed that enforced expression of *TWIST-1* in MSC lead to an upregulation of *WNT2* and *WNT2B* gene expression. Briefly, a 5kb region of the DNA from *WNT2* and *WNT2B* promoters was analysed for the presence of *TWIST-1* binding sites, CANNTG, and, after confirmation of binding sites, primers were designed to amplify fragments of approximately 500bp, 1000bp, 2000bp and 3000bp as described in (section 2.4.3.2). The following PCR conditions were used as a starting point for all fragments with small adjustments necessary for successful amplification of all fragments;

Figure 2.3 - Cloning into PGL3 Basic. (A) Purified PCR product of 0.5kb Wnt2 promoter fragment before cloning. 1.5% agarose gel, 80V, 90minutes (B) The location of the cloned promoter fragment after ligation is shown. (C) Digestion products to show the presence of both vector and insert after cloning. 0.7% agarose gel, 80V, 90minutes. This process was repeated for all promoter fragments.

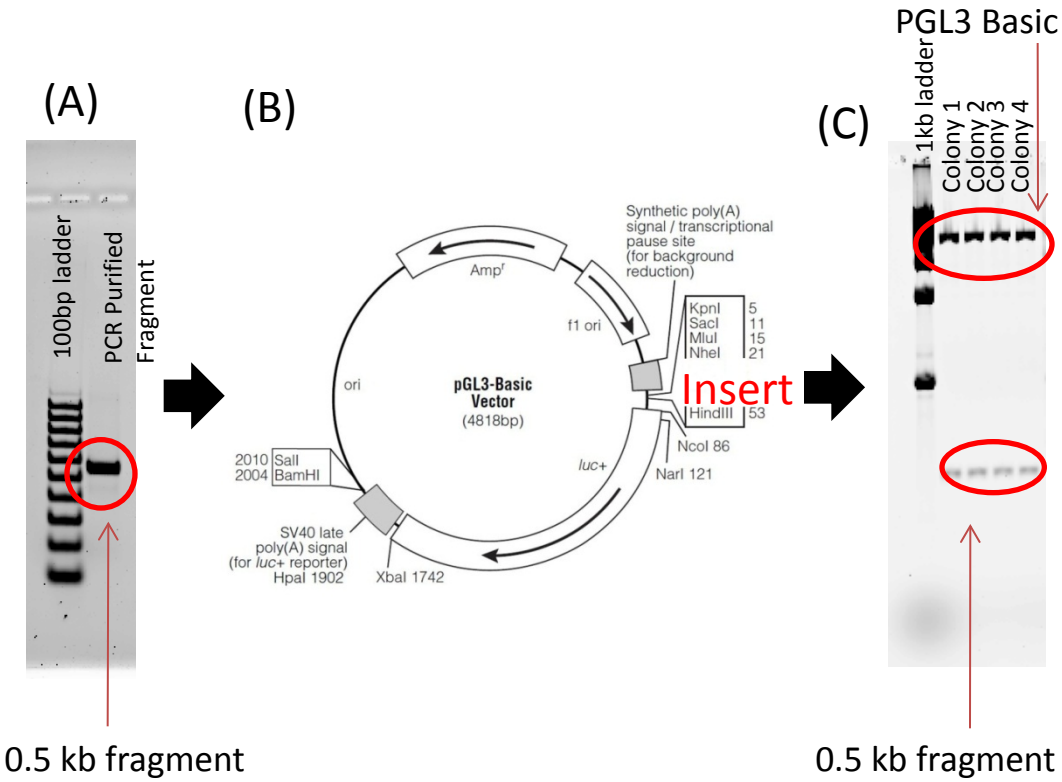
(A)
100bp ladder
PCR Purified Fragment
0.5 kb fragment
(B)
Synthetic poly(A) signal / transcriptional pause site (for background reduction)
Amp^r
f1 ori
ori
pGL3-Basic Vector (4818bp)
KpnI 5
SacI 11
MluI 15
NheI 21
Insert
HindIII 53
NcoI 86
NarI 121
luc+
2010 SalI
2004 BamHI
SV40 late poly(A) signal (for luc+ reporter)
HpaI 1902
XbaI 1742
(C)
PGL3 Basic
1kb ladder
Colony 1
Colony 2
Colony 3
Colony 4
0.5 kb fragment

Table 2.14. Cloning Paramaters

PCR Reaction Concentrations

Mix	final	for 1 reaction
Pfu Turbo	2.5U	1.0µL
10 x Buffer	1 x	2.5µL
Forward Primer	0.4µM	1.0µL
Reverse Primer	0.4µM	1.0µL
dNTPs	0.2 mM	1.0µL
Genomic DNA	-	1.0µL
H_2O		17.5µL
		25 µl total

PCR Cycling Conditions

PCR condition	Temperature	Time	
Initial denature	98 °C	2 min	
Denaturing	98 °C	30 sec	**30 cycles**
Annealing	50 °C	30 sec	
Elongation	72 °C	1 min	
Final Elongation	72 °C	10 min	
Hold	4 °C	∞	

PCR products were run on an agarose gel (section 2.4.2.11) to determine the size of amplified fragments. Amplified products were excised and gel purified as described in section 2.4.2.6. Purified DNA was used as the template for a second amplification reaction using the same PCR conditions for the fragment when amplified from genomic DNA. The DNA generated from this

reaction was purified using the QIAquick PCR purification kit (section 2.4.2.7) and stored at -20°C until required. Purified DNA was digested at 37°C for 3 hours in the following reaction mix before being heat inactivated at 65°C for 30 minutes;

Table 2.15. Double Digest Reaction Concentrations

Mix	final	for 1 reaction
DNA	1µg	2.5µL
10 x Buffer	1µL	1.0µL
SacI	10 Units	0.5µL
XhoI	10 Units	0.5µL
H_2O		to 10µL

The PGL3 basic vector was digested and heat inactivated using the same reaction conditions above. Once digested both vector and insert were dephosphorylated using antartic phosphatase (New England Biolabs, #M0289S) at 37°C for 30 minutes. Dephosphorylated samples were gel purified (section 2.4.2.6) before being combined for ligation in the following concentrations for 4°C overnight. To calculate the required volume of insert the following formula was used;

(50ng (vector) x Insert size (kb) / Vector Size (kb)) x 3

Table 2.16. Ligation Reaction Concentrations

Mix	final	for 1 reaction
Insert	varies with size	
PGL3 Vector	50ng	0.6µL
Ligation Buffer	1 x	1.0µL
T4 DNA ligase	1 Unit	1.0µL
H_2O		to 10µL

After overnight incubation samples were heat inactivated at 70oC for 10 minutes. Ligated samples were transformed into chemically competent bacteria (section 2.4.2.8), and plated on ampicillin plates overnight. Approximately 5 colonies were isolated and mini preps cultured overnight. Mini preps were processed the following day (section 2.4.2.9) and DNA sequenced (section 2.4.2.5). Once the sequence was confirmed, samples were amplified to midi prep size, processed (section 2.4.2.10), stored at -20oC and used for transfection reactions in the luciferase assays described below in section 2.5.4.

2.5 Protein analysis

2.5.1 Preparation of protein lysates

Whole cell lysates were prepared on ice from 3 x 10^6 MSC. Cells were washed once with 10mL of ice cold PBS before 300µL of Lysis buffer (table 2.17) was added and cells were scraped off the dish using a cell scraper.

Table 2.17. Lysis Buffer Solution

Reagent	[Stock]	[Final]	volume (5mL final)
Tris-HCl pH 7.4	1M	20mM	100µL
EDTA	0.5M	2mM	20µL
NaCl	2M	150mM	375µL
Triton-X100	100%	1%	50µL
Sodium Vanadate	200mM	2mM	50µL
Sodium Fluoride	500mM	2mM	20µL
SDS	10%	0.1%	50µL
PMSF	100mM	2mM	100µL
Sodium Pyrophosphate	250mM	10mM	200µL
Glycerol	100%	10%	500µL
water			3535µL

Cells were transferred to an eppendorf tube and vortexed. This preparation was incubated on ice for approximately 30 minutes and cells were lysed by sonication for 10 seconds at 3 watts using a probe sonicator (XL2007, Misonix Inc., Farmingdale, NY, USA). Cell lysate was then centrifuged for 30 minutes at 16,000*g* at 4^{o}C. Centrifugation was sufficient to separate the out the nuclear proteins and other cellular debris which formed a pellet at the bottom of the tube. The supernatant was transferred to a new tube from which an aliquot was taken and protein concentration quantitated using the RC/DC protein assay kit (Bio-Rad Laboratories, Hercules, CA, USA) according to the manufacturer's instructions.

2.5.2 Western blot analysis

Once protein concentrations were determined, 50µg of protein per lane was loaded onto a 12% polyacrylamide gel and electrophoresed at 15mA while proteins migrated through the stacking

layer and 30mA to separate protein through the separating layer. Gels were transferred to a Hybond-P 0.45µm PVDF membrane (Amesham Bioscience UK Limited, Little Chalfont, UK) using the SEMI-PHOR^{TM} Hoefer Semi Dry blotter (Hoefer Scientific Instruments, San Fransisco, USA). The membranes were washed three times with TBS / 0.1% Tween 20 (Sigma Aldrich, St Louis, MO, USA) and blocked with 50mL blocking buffer overnight at 4^{o}C. Blocking buffer was comprised of 5% Amersham block (Amersham Biosciences UK Limited, Little Chalfont, UK) in TBS / 0.1% Tween 20. After blocking, membranes were washed three times using TBS / 0.1% Tween 20 to remove any residual blocking buffer solids.

The membrane was then ready to be probed with primary antibodies. For the purpose of identification of *TWIST-1* overexpression at the protein level, the mouse monoclonal *TWIST-1* antibody (Twist2C1a, IgG1; sc81417, Santa Cruz Biotechnology Inc., California, USA) was used. This antibody was diluted 1 in 200 into 5% BSA / TBS / Tween 20. The membrane was submerged in this solution and probed overnight at 4^{o}C on a rocker. The membrane was washed three times in TBS / 0.1% Tween 20. Following the final wash, the membrane was probed with a secondary antibody (goat anti-mouse Ig affinity isolated alkaline phosphatase conjugated, P326A, Chemicon Australia Pty. Ltd., Melbourne, Australia) diluted 1 in 2000 into % BSA / TBS / Tween 20. The secondary antibody was incubated with the membrane for 1 hour at room temperature on a rocker. The membrane was washed a further three times with TBS / Tween 20, rinsed three times with TBS, developed using 1mL ECF substrate and visualized using a Typhoon 9410 variable mode imager (GE Healthcare, Europa Bio Products, RPN5785).

2.5.3 Retroviral Techniques

The retroviral packaging plasmids PGP and VSVG were required to generate *TWIST-1*, *WNT2*, *WNT2B* and control hMSC lines. These plasmids contain the viral genes for Gag, Pol and Env which encode the structure of the viral core, reverse transcriptase and viral envelope proteins, respectively. Overexpression constructs were generated using techniques described in Section 2.4.3.1. The expression plasmids required for the overexpression studies included; pRUF-iG2-Gateway (control), pRUF-iG2-Gateway-Wnt2 and pRUF-iG2-Gateway-Wnt2B. Before any transduction studies could be performed, considerable amounts of DNA were required in order to transiently transfect the retroviral packaging cell line, HEK-293-T.

2.5.3.1 Retroviral supernatant preparation

HEK293-T cells were grown to confluence in a T^{75} culture flask before being plated to 6cm dishes at a density of ~9 x 10^5 cells per dish. Cells were incubated overnight at 37^{o}C to ensure adherence. On the following day, mixtures of 5µg retroviral GFP plasmid, 4µg pGP plasmid, 4µg of VSV-G plasmid and 500µl of DMEM + additives were incubated for 5 minutes at room temperature before being added to 20µL of Lipofectamine 2000 (Invitrogen, CA, USA) in 500uL DMEM + additives. The combined mixtures were then incubated at room temperature for 20 minutes before being added drop wise to HEK 293-T cells. Cells were allowed to incubate for 48 hours at 37^{o}C in 5% CO_2. Successful transfection was assessed by examining the cells for green fluorescence protein expression using a UV fluorescent microscope (Olympus, Tokyo, Japan) (figure 2.4).

Figure 2.4 - GFP positive expressing cells. (A) A representative field of view showing greater than 75% GFP positive transfected cells when excited by UV light (400X). (B) GFP positive expressing MSCs infected with PRUF-iG2-Gateway-Wnt2, (400x), following 48 hours transduction.

A

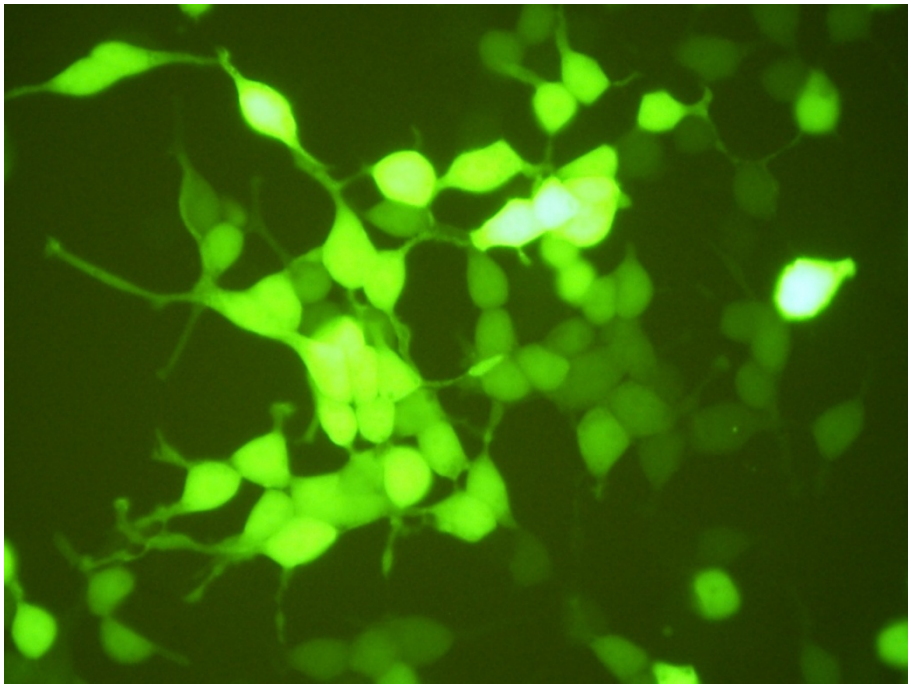

B

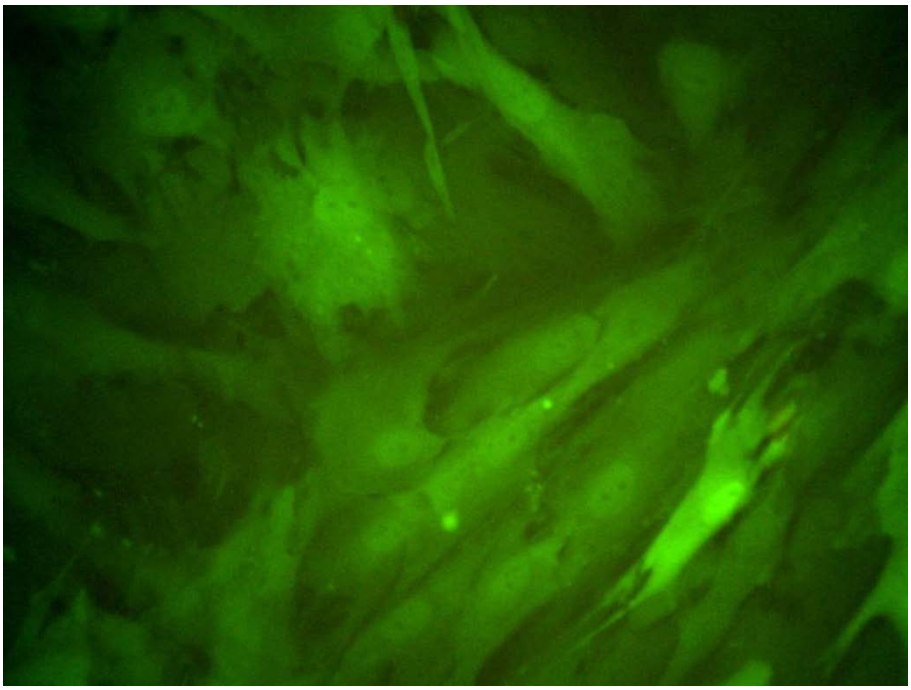

2.5.3.2 Retroviral infection

Once transfection was verified using a fluorescent microscope, supernatant containing viral particles was removed from HEK293-T cells using a cannula attached to a 20mL syringe. This solution was filtered through a 0.45µm low binding NALGENE 25mm surfactant free cellulose acetate membrane (Nalgene, Interpath, Heidelberg West, Victoria, Australia) to remove any cellular debris or cells. Viral supernatant was used immediately to transduce cells as freezing the supernatant resulted in a loss of infection efficiency. Freshly harvested supernatant was diluted 1:1 with α-MEM + additives supplemented with Polybrene (4µg/mL; Sigma Aldrich, Castle Hill, Australia). This mixture was added drop wise to the target MSC which were incubated for 48 hours. After infection, GFP expression was verified using a UV microscope (figure 2.4). Cells were reinfected in the same manner described above to increase the number of infected cells. After a further 48 hours the viral supernatant was removed and replaced with appropriate growth media, α-MEM + additives.

2.5.3.3 FACS sorting of infected cells based on GFP expression

Infected MSCs were cell sorted based on GFP expression. To prepare samples for sorting, cells (not more than 75% confluent) were washed with HANKS and liberated from the surface of a T^{75} culture flask using 1 x Trypsin (Section 2.1.7). Trypsin was then inactivated by the addition of 10mL 3% FCS in HANKS media. The detached cells in solution were transferred to a 14mL polypropylene tube and centrifuged at 800*g* for 5minutes at 4^{o}C. The resulting pellet was resuspended in 10mL of 3% FCS and filtered through a 70µm cell strainer to remove cell clumps and duplets. This single cell solution was centrifuged once more at 800*g* for 5minutes at 4^{o}C. The cell pellet was resuspended in ~800µL of 3% FCS, depending on cell number, and transferred to a 5mL polypropylene round bottom tube (Becton Dickinson, Franklin Lakes, NJ, USA). The cells

were sorted using an Epics Altra HyPer Sort FACS machine (Beckman Coulter, Miami, Florida, USA). The brightest 30% of cells in the positive fraction of the population were selected using Expo 32 Multi-comp software (Software version 1.2B). This selected portion of the population was collected in pre-prepared 5mL polypropylene collection tubes containing 2mL of α-MEM + additives (20% FCS). These cells were centrifuged at 1600*g* for 2 minutes at room temperature, resuspended in α-MEM + additives and plated at 8 x 10^3 cells/cm^2. Following infection, overexpression was verified using RT-PCR (section 2.1.2.1) and western blot analysis (section 2.5.3 figure 2.5).

2.5.3.4 Assessment of overexpression

After selection of each transduced cell line by FACS, the populations were expanded to approximately 6 x 10^6 cells and cryopreserved in liquid nitrogen using the method described in section 2.1.10. At the time of storage a sample of cells from each cell line (approximately 5 x 10^5) was used to isolate total RNA. From this total RNA, cDNA was generated and used to verify the upregulation of genes at the mRNA level.

2.5.4 Luciferase assays

Approximately 3x10^5 MG63 cells per well were plated in 6 well plates and allowed to adhere for a minimum of 4 hours. The PGL3 vector containing a, *WNT2* or *WNT2B,* promoter region plus a PRUF-iG2-Gateway-GFP (control) or PRUF-iG2-Gateway-GFP-TWIST-1 (*TWIST-1* overexpression) vector was used in a dual transfection protocol to assess the effect of enforced *TWIST-1* expression on the regulation of *WNT2* and *WNT2B* promoters. The transfection protocol used was identical to that used in Section 2.5.3.1 but scaled for the smaller volume of a 6 well

Figure 2.5 - Verification of *TWIST-1* gene expression following transduction. (A) Real-time PCR results indicate that the upregulation of *TWIST-1* transcripts in *TWIST-1* overexpressing cells is statistically significant to GFP-control lines. (B) Western blot using a *TWIST-1* specific monoclonal antibody demonstrates confirmation of a 28kD protein in MG63 cells transduced with the pruf-IRES-GFP-TWIST-1 construct (TWIST) in comparison to the Mock, pruf-IRES-GFP control (GFP). (C) The blots were stripped and re-probed with α-tubulin as the loading control. Statistically significant ($p < 0.05$, paired t-test) results when compared to GFP control cell line denoted by (*).

A

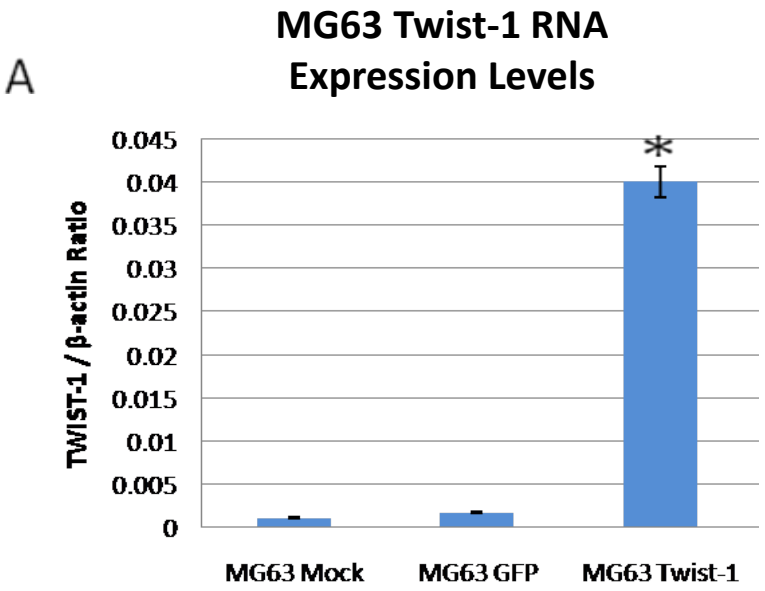
MG63 Twist-1 RNA Expression Levels
TWIST-1 / β-actin Ratio
0.045
0.04
0.035
0.03
0.025
0.02
0.015
0.01
0.005
0
*
MG63 Mock
MG63 GFP
MG63 Twist-1

B

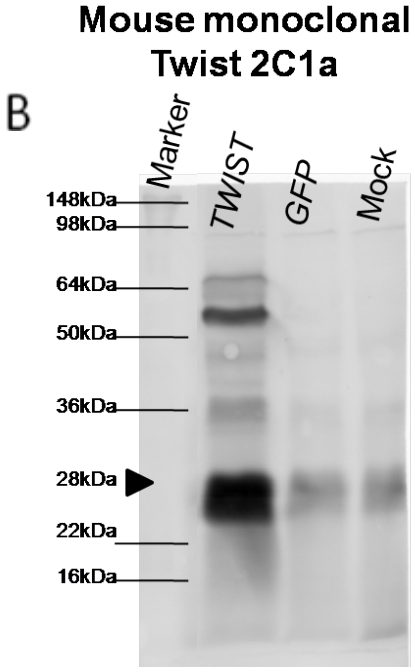
Mouse monoclonal Twist 2C1a
Marker
TWIST
GFP
Mock
148kDa
98kDa
64kDa
50kDa
36kDa
28kDa
22kDa
16kDa

C

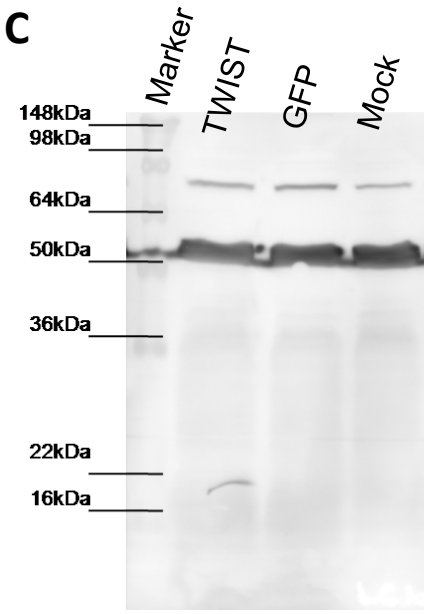
Marker
TWIST
GFP
Mock
148kDa
98kDa
64kDa
50kDa
36kDa
22kDa
16kDa

plate. Cells were allowed to incubate for 48 hours at which time GFP expression was checked using a UV fluorescent microscope. After GFP expression was confirmed cells were incubated for a further 24 hours. At this time, protein lysates were collected using the Promega - Dual-Luciferase® Reporter Assay Kit (Promega, Alexandria, NSW, Australia). Briefly, cells were trypsonised, 10% were collected for FACS analysis and stored in FACS fix. The remaining 90% were transferred to eppendorf tubes and washed using 1 x PBS before being placed on ice. Four volumes of water were added to 5X reporter lysis buffer. Washed samples were centrifuged at 800*g* for 5 minutes at 4^{o}C before supernatant was aspirated and 250µL of diluted lysis buffer was added to each sample tube. Samples were vortexed for 15 seconds and centrifuged at 12,000*g* for 15 seconds at room temperature. Supernatant was transferred to a new tube and stored at -80^{o}C until required. The protein concentration of each sample was determined using the RC/DC protein assay kit (Bio-Rad Laboratories, Hercules, CA, USA). Luciferase activity was determined by addition of 20µg of each sample to wells of a flat bottom 96 well plate. Immediately after the addition of protein, 200µL of luciferase assay reaction buffer (table 2.18) was added and the reaction started by injection of 40µL of luciferin solution to each well. The plate was then read immediately using luminescence settings on the Topcount NXT Microplate Scinitillation & Luminescence counter (Perkin Elmer Life and Analytical Sciences, Downers Grove, IL, USA).

Table 2.18. – Luciferase Assay Reagents

Luciferin Solution

	Final Concentration	Amount
Luciferin	0.28 mg/mL	10mg
H_2O		35.7mL

Luciferin Assay Phosphate Buffer ($K_2H_2PO_4$)

1 Part	KH_2PO_4 1M
4 Parts	K_2HPO_4 1M

Luciferase Assay Buffer

	Final Concentration	Amount
1M $K_2H_2PO_4$	100mM	1 mL
1M $MgSO_4$	8mM	80µL
1M DTT	2mM	20µL
100 mM ATP	7.5mM	75µL
5mM CoA	0.175mM	80µL
H_2O		8.5 mL

2.5.5 Chromatin Immunoprecipitation

Chromatin isolation and Immunoprecipitation (ChIP) was carried out using the Magna ChIP™ G one day chromatin immunoprecipitation kit (Millipore, Billerica, MA, USA). Approximately 1 x 10^7 cells were cultured in T^{175} culture flasks with α-MEM complete media. When cells reached 80-90% confluence, 550µL of 37% formaldehyde was added (final concentration 1%) for 10 minutes at 37°C to crosslink protein and DNA within the cells. After 10 minutes, cells were washed twice with 1 x PBS and 2mL cold PBS containing 1 x protease inhibitor cocktail (Roche, Basel, Switzerland) was added to each flask. Cells were then scraped from each dish, transferred to microcentrifuge tubes and centrifuged (800*g*, 4°C, 5 minutes) to pellet cells. Supernatant was

removed and cells resuspended in 0.5mL of cell lysis buffer containing 2.5µL of protease inhibitor cocktail. Resuspended cells were then incubated on ice for 15 minutes and vortexed every 5 minutes before being centrifuged (800*g*, 4^{o}C, 5 minutes) to pellet lysed cells. Supernatant was removed and cells resuspended in 0.5mL nuclear lysis buffer containing 2.5µL of protease inhibitor cocktail.

Resuspended lysed cells were sonicated using a Bioruptor bath sonicator (Diagenode, Liège, Belgium) at 3 watts for two 15 minute cycles in an ice bath to obtain croslinked DNA from ~300-600bp in length. Sonicated samples were centrifuged (12,000*g*, 4^{o}C, 10 minutes) to remove any insoluble material, transferred to fresh microcentrifuge tubes in 50µL aliquots and stored at -80^{o}C.

When required, sheared crosslinked chromatin was thawed on ice and diluted 10x in 450µL of dilution buffer containing 2.25µL protease inhibitor cocktail. At this stage, a 5µL sample was removed to be used as an input control and stored at 4^{o}C. Positive (anti-RNA Polymerase, 1µg), negative isotype control (Normal Mouse IgG, 1µg) and *TWIST-1* (Twist2c1a, 1µg) antibodies (table 2.6) were added to respective samples along with 20µL of fully suspended protein G-conjugated magnetic beads (Millipore, Billerica, MA, USA). Samples were incubated overnight at 4^{o}C with constant rotation. A magnetic rack was used to separate magnetic bead/antibody/chromatin complex out of solution and supernatant removed completely. Magnetic bead/antibody/chromatin complex was resuspended in 0.5mL each of Low Salt Immune Complex Wash Buffer, High Salt Immune Complex Wash Buffer, LiCl Immune Complex Wash Buffer and Finally TE Buffer for 5 minutes at 4^{o}C with rotation followed by magnetic clearance and supernatant removal between each buffer.

Washed Protein/DNA complexes were incubated at 62°C in 100µL ChIP elution buffer / 1µL Proteinase K for 2 hours with shaking to reverse Protein/DNA crosslinks and bonds between antibodies and magnetic beads. Proteinase K was heat inactivated by heating samples to 95°C for 10 minutes with no shaking. Samples were cooled to room temperature, magnetic beads were isolated with a magnetic rack and supernatant containing DNA transferred to a fresh microcentrifuge tube. DNA was purified by addition of 500µL Bind Reagent A to each 100µL DNA sample (and Input controls). This solution was transferred to a Spin Filter in a Collection Tube and centrifuged (30 seconds, 12,000*g*, 4°C). The resulting supernatant was discarded and collection tube reused for washing with 500µL of Wash Reagent B by centrifugation (30 seconds, 12,000*g*, 4°C). The supernatant was discarded and tubes re centrifuged to remove any remaining wash buffer (30 seconds, 12,000*g*, 4°C). The Spin Filter was transferred to a new collection tube and 50µL of Elution Buffer C was added directly to the centre of the membrane. The Spin Filter was centrifuged (30 seconds, 12,000*g*, 4°C) and the resulting eluent, purified DNA ready to be analysed, was stored at -20°C until it was used for Real Time Q-PCR.

2.6 Animal Techniques

2.6.1 *TWIST-1* mouse colony

The *TWIST-1* mutant mice were originally generated by Chen and Behringer by replacing the protein coding region of the gene with a neomycin resistance cassette, resulting in a "loss of function" mutation (Chen and Behringer, 1995). This group demonstrated the importance of *TWIST-1* in development by showing that *TWIST-1* null mouse embryos died at day 11.5 with defects in head mesenchyme, somites and limb buds. We received the *TWIST-1*$^{+/-}$ mice as a kind donation from A/Prof. Barry Powell (CHRI, Adelaide). When received the colony was housed in the containment facility of the Veterinary Services Division, SA Pathology. In order to eradicate

pathogens from potentially infected mouse colonies, and as a precaution when receiving mice from an outside facility, the colony was rederived before being housed in the conventional Veterinary Services Division, SA Pathology. Once rederived, standard breeding protocols were followed as the mice were considered free of pathogens. The mice were on a mixed background and did not display any of the phenotypic traits described by Chen and Behringer (Chen and Behringer, 1995). It wasn't until the fourth generation of back crossing the strain with pure C57BL/6 mice that phenotypic variations were noted (section 4.3.1.1). After a further two backcrosses the phenotype was predictable and occurred in every litter. The mice used in fracture and ovariectomy experiments were backcrossed to pure C57BL/6 mice for seven generations.

2.6.2 Genotyping

Approximately 5mm was cut from the end of the tail of 3 week old mice and placed in a 1.7mL eppendorf tube at -20^{o}C. To each tube, 300µl PBND lysis buffer (table 2.20) and 4µl Proteinase K (Invitrogen, Mulgrave, Victoria, Australia) (10mg/ml stock) was added and tubes were incubated at 56^{o}C overnight in a thermomixer rotating at 650rpm. Proteinase K was inactivated by incubating samples at 95^{o}C for 10 minutes. Samples were centrifuged at 16,000*g* for 10 minutes at room temperature before supernatant was transferred to a fresh tube and stored at -20^{o}C until required.

Table 2.19. – Genotyping PCR

PCR Reaction Concentrations

Mix	final	for 1 reaction
10x PCR buffer	1x	2.5 µl
MgCl2 (25mM)	2mM	2.0 µl
primer 1 (10 µM)	0.4µM	1.0 µl
primer 2 (10 µM)	0.4µM	1.0 µl
dNTPs (5mM)	0.2 mM	1.0 µl
Taq-Polymerase (Amplitaq, 5U/ul)	1U	0.2 µl
H2O		16.3 µl
Template DNA		1.0 µl
		25 µl total

PCR Cycling Conditions

PCR condition	Temperature	Time	
Initial denature	95 °C	10 min	
Denaturing	95 °C	30 sec	**35 cycles**
Annealing	64 °C	30 sec	
Elongation	72 °C	1 min	
Final elongation	72 °C	5 min	
Hold	4 °C	∞	

Table 2.20. – Genotyping Reagents

LYSIS BUFFER (PBND PCR Buffer with Non-Ionic Detergents)

Final conc.	Stock Solution	for 500ml
50mM KCl	-	1.87 g
10mMTrisHCl (pH 8.3)	1.0 M	5 ml
2.5mM MgCl2-6H2O	-	255mg
0.1mg/ml gelatin	-	50mg
0.45% NP40	100%	2.25ml
0.45% Tween20	100%	2.25ml

Make up to 500 ml with milliQ water and autoclave.

Aliquot into 5ml tubes and store at -20°C

PROTEINASE K

Final conc.	Stock Solution	for 10ml
10mMTrisHCl (pH 8.3)	1.0 M	100ul
20mM CaCl2	100mM	2ml
50% glycerol	100%	5ml

Make up to 10 ml with milliQ water.

Dissolve 5mg (0.005g) Proteinase K in 500ul buffer.

Aliquot (20ul) and store at -20^{o}C.

2.6.3 Fracture Surgery

The role of *TWIST-1* was assessed in a mouse fracture model using seven week old *TWIST-1* heterozygous knockout mice (*TWIST-1*$^{+/-}$) compared to that of homozygous littermate controls

(*TWIST-1*$^{+/+}$) as previously described (Arthur et al., 2012). The surgical procedure involved anesthetising the animal for the duration of surgery by administering 80mg/kg Ketamine and 10mg/kg Xylazine by intraperitoneal injection. The area of the leg in which the surgery was performed was shaved and cleaned using ethanol swabs and Betadine. A 1-2 cm incision was made through the skin parallel to the femur. This incision was followed by a blunt end dissection to separate the two muscles covering the femur, exposing the femur. A curved pin was placed under the femur to lift it up slightly, away from the muscle. The femur was cut using bone scissors to create a fracture. The cartilage covering the knee was moved to one side to allow a 25 gauge needle to be inserted through the knee joint into the intramedullary cavity of the femur in order to create an access point for the carbon rod. The needle was withdrawn and a, 0.5mm diameter, carbon rod inserted to stabilise the fracture, by connecting both sides of the fractured femur. The remainder of the carbon rod protruding from the knee joint was cut off to allow the knee cap to be repositioned correctly. Additionally, the muscle exposing the femur and the skin was closed separately using sutures. Following surgery, the mouse was administered butorphanol (2.5 mg/kg) subcutaneously for pain relief. This analgesic was readministered in the afternoon of the surgery and the morning following surgery. An X-ray of the fractured femur and the positioning of the needle was taken immediately after the surgery and periodically throughout the time course of the project to determine the stability of the bone fracture; additionally mice underwent live μCT imaging at 2 weekly intervals starting with the day following surgery. The animal recovered on a heated pad until it was conscious, after which time it was transferred to a cage, containing a heating pad. The animal was monitored continuously for the first 30 minutes once conscious.

This study was approved by the SA pathology ethics committee (study 56/09) and The University of Adelaide ethics committee (study M-2008-078).

2.6.4 Ovariectomy Surgery

Twelve week old heterozygous *TWIST-1*$^{+/-}$ mutant female mice were randomly assigned to either ovariectomy (OVX) or Sham-OVX operation group. The operation involves a 0.5cm incision made in the skin of mid back region of the animal. A small cut was then made in the muscle layer approximately 5mm either side of the spinal cord. The ovaries were located through these holes. Using a haemostat the ovaries were clamped at the fallopian tube and removed with a surgical blade (#11). The haemostat, which seals the capillaries, was then removed; the skin was closed over, sutured and held together using an auto-clip.

The mice were monitored regularly for the remainder of the project. At eight weeks the mice were humanely euthanized by carbon dioxide overdose and cervical dislocation. The mice were analysed using 3-dimensional micro-computed tomography (μCT) prior to histological analysis (described in section 2.6.5). For biomechanical testing, femora recovered from the OVX and sham-OVX groups were removed and tested for maximum load at breaking and flexural rigidity using the TestResources Inc., testing system (Section 2.6.9).

This study was approved by the SA pathology ethics committee (study 23/11) and The University of Adelaide ethics committee (study M-2013-37).

2.6.5 μCT – Skyscan 1174 Scanning

All μCT scanning of fixed tissue was conducted using the Skyscan 1174 compact micro-CT machine (Bruker Micro-CT, Kartuizersweg, Kontich, Belgium). A config file was loaded and flat field correction run at the required magnification (6.5μm for ovariectomy study and 7.8μm for fracture study). The sample, wrapped in PBS soaked tissue to avoid over-heating and movement,

was loaded in the specimen holder and the door closed. Field of view was determined manually by moving sample stage up or down to include the region of interest and sample rotated to make sure it remained within the field of view for a full 180^{o} rotation. The sample was scanned using the following settings; small camera pixels, rotation step of 0.5, averaging at 2, and random movement selected. Images were reconstructed using NRecon (Software version (local) V1.6.4.0, Bruker Micro-CT, Kartuizersweg, Kontich, Belgium) by loading the dataset generated above, generating a preview and using the following output settings; Reconstruct ROI, Inverse selected, threshold of 0 min and 0.075 max, smoothing at 2, ring artefact reduction at 15 and beam hardening correction at 30%.

2.6.6 µCT – Analysis

2.6.6.1 Fracture

Fractured femurs were analysed by µCT as previously described (Arthur et al., 2012). Reconstructed image files were loaded in cTAN (software version 1.10.9.0, Bruker Micro-CT, Kartuizersweg, Kontich, Belgium) and a region of interest was selected by identifying 450 slices each side of the fracture and tracing the perimeter of the bone. The region of interest dataset was then loaded in DataViewer (software version 1.4.3.2, Bruker Micro-CT, Kartuizersweg, Kontich, Belgium) and orientated with the knee towards the top of the screen (x-axis) and flattest portion of the femur parallel to the y axis and towards the bottom of the screen. Orientated images were then loaded in cTAN and batch analysed using batman with manual thresholding and the following analysis criteria; images were shrink-wrapped and de-speckled before Tissue Volume, Bone Volume, Percentage bone Volume, Tissue Surface, Bone Surface, Intersection Surface, Bone Surface to Volume Ratio, Bone Surface Density, Trabecular Pattern Factor and Centroid (x, y and z) were calculated and 3D images generated in .p3g and .stl formats. Statistical analysis

was carried out using GraphPad PRISM (version 6, GraphPad Software, La Jolla, USA) and 3D images were generated using Paraview (software version 3.98, Kitware, Clifton Park, New York, USA).

2.6.6.2 Ovariectomy

Excised femurs were analysed by μCT as previously described (Robertson et al., 2006). Reconstructed image files were loaded in DataViewer and orientated with the knee towards the top of the screen (x-axis) and flattest portion of the femur parallel to the y axis and towards the bottom of the screen. Orientated image files were loaded in cTAN and a region of interest was selected by identifying the growth plate and calculating the slice 0.05mm proximal to the growth plate as the first slice and extending 0.8mm towards the diaphysis of the femur. All cortical bone was excluded from the analyses by manual segmentation and saved as a ROI file, not a data set. Orientated images were then loaded in cTAN and batch analysed using the batch manager function with manual thresholding, separately loaded ROI files to eliminate cortical bone and the following analysis criteria; images were de-speckled before Tissue Volume, Bone Volume, Percent bone Volume, Tissue Surface, Bone Surface, Intersection Surface, Bone Surface to Volume Ratio, Bone Surface Density, Trabecular Pattern Factor, Centroid (x, y and z), Structural Model Index, Trabecular Thickness, Trabecular Number and Trabecular Separation were calculated and 3D images generated in .p3g and .stl formats. Statistical analysis was carried out using GraphPad PRISM (version 6, GraphPad Software, La Jolla, USA) and 3D images were generated using Paraview (software version 3.98, Kitware, Clifton Park, New York, USA).

2.6.7 Histology

2.6.7.1 Methacrylate Processing

Samples were fixed in 10% neutral buffered formalin (NBF) for four days at -20^{o}C before being transferred to phosphate buffered saline (PBS) and stored at -20^{o}C. Tissue was trimmed from one side of excised femora to ensure correct orientation. Samples were transferred to 25mL polypropylene tubes half filled with 70% acetone at 4^{o}C for dehydration. Following one hour acetone was changed to 90% for one hour, 100% for one hour and 100% for one hour a second time. At this stage samples were fully dehydrated and acetone was replaced with 10mL plastic embedding mixture.

Table 2.21. Plastic Embedding Mixture – 11mL per sample

10mL Methylmethacrylate
1mL PEG 400

Samples, with lids loosened, were transferred to a vacuum for one week to allow for complete infiltration of the plastic embedding mixture. Following complete infiltration, embedding mixture was transferred to a waste container and replaced with 10mL plastic embedding mixture + Perkadox 16 (0.04g / 10mL). With lids tightened, samples were placed into a glass tray containing ~3cm water and kept in an incubator at 37^{o}C until completely polymerised. Tubes were cut open with a bandsaw to remove the plastic block, which was sanded and attached to an aluminium block using araldite epoxy resin. Sectioning was carried out Dr Paul Anderson (Musculoskeletal Biology Research Laboratory, SA Pathology).

2.6.7.2 Paraffin Processing

Excised femora were fixed in 10% neutral buffered formalin (NBF) for four days at 4°C before being transferred to phosphate buffered saline (PBS) and stored at 4°C. Samples were transferred to decalcification solution (table 2.22) and decalcified at 4°C. Samples were classed as decalcified by the absence of bone detected using X-Ray. Once completely decalcified, samples were processed overnight for paraffin infiltration in the Neuropathology Laboratory (Hanson Institute, South Australia). Infiltrated samples were embedded into paraffin blocks using an Leica embedding station (Leica, North Ryde, NSW, Australia) and embedding cassettes (Techno-Plas, St Marys, SA, Australia). Embedded samples were sectioned in the Neuropathology Laboratory (Hanson Institute, South Australia).

Table 2.22. Decalcification Solution (pH 8.0)

20x PBS	200mL
NaOH	75g
EDTA	744.4g
H_2O	To 4L

2.6.7.3 Trap Staining

Acetate-Tartrate buffer was made up, divided evenly into two 50mL falcon tubes (A and B) and warmed to 37°C. To this solution was added; 20 mg napthol AS-BI phosphate dissolved in 1 mL N,N-dimethylformamide (Tube A). Sections were dewaxed through xylene and rehydrated through ethanol and H_2O (paraffin) or deplasticised in 100% acetone (methacrylate). Tube A was transferred to a coplin jar and slides were inserted and incubated in this solution for 30 minutes at 37°C. In a 5mL tube, 80mg sodium nitrate was dissolved in 2mL dH2O and, five minutes before

the end of the 30 minute incubation, 2mL pararosaniline stock solution was added to the 2mL sodium nitrate solution. Once dissolved, 2.5mL of this solution was added to Tube B before being transferred to a coplin jar. Sections were transferred to the pararosanaline solution and incubated for 15 minutes at 37^{o}C. After 15 minutes samples were checked for pink staining. If no pink staining was present, samples were incubated for a further 5 minutes or until pink staining was visible. Once pink staining was observed samples were counterstained in methyl green. Samples were rinsed in tap water and dipped in methyl green (0.05%) for 5 seconds (paraffin) or 60 seconds (methacrylate) before being rinsed in running water. Counterstained samples were then washed in alcohol and dehydrated in alcohol and xylene before a coverslip was applied.

Table 2.23. Acetate-Tartrate Buffer

H_2O	100mL
Sodium acetate	2.72g
1.2% acetic acid	pH to 5.2 with
Sodium tartrate	2.3g

2.6.7.4 Haematoxylin and Eosin Staining

Sections were dewaxed through xylene and rehydrated through ethanol and H_2O before being stained in haematoxylin for 5 minutes. Once stained, slides were rinsed in running tap water, immersed in bicarbonate solution for 10 seconds, differentiated in 0.3% acid alcohol for 5 seconds, rinsed in running tap water, immersed in bicarbonate solution for 10 seconds and rinsed in running tap water. Slides were then counterstained with eosin for two minutes before being dehydrated in three alcohol washes and two zylene washes. Slides were then ready to coverslip.

Table 2.24. - Haematoxylin and Eosin Staining Reagents

Haematoxylin	
dH_2O	1400 mL
Aluminium ammonium sulphate	100g
Haematoxylin (CI 75290)	5 g
100% ethanol	20 mL
Sodium iodate	2 g
Acetic acid	40 mL
Glycerol	600 mL

Bicarbonate Solution	
Bicarbonate	10g
H_2O	400mL

Acid Alcohol	
H2O	300mL
Concentrated HCl (36%)	3mL
100% Ethanol	700mL

Eosin	
Distilled water	44 mL
100% Ethanol	841 mL
1% eosin Y (CI 45380; Sigma P2759-100G)	114 mL
1 % aqueous phloxine (CI 45410; cyanosine)	11.4 mL
Glacial acetic acid	4.6 mL

2.6.7.5 Von Kossa Staining

Slides were deplasticised in acetone for 15 minutes before being rinsed with RO water twice in a coplin jar. Once deplaticised, slides were bathed in a 1% sodium nitrate solution and placed under UV light in a Class II laminar flow hood (Top Safe 1.2, Bio Air, Siziano, Italy) for 45 minutes. Following 45 minute incubation, silver nitrate solution was poured off and dH_2O was gently added to the coplin jar twice to rinse slides before being immersed in 4% sodium carbonate 10% formaldehyde solution for 5 minutes. Slides were then rinsed in dH_2O before being immersed in 2.5% sodium thiosulphate for 5 minutes. Slides were rinsed in dH_2O, transferred to a metal rack and incubated in haematoxylin and eosin as described in section 2.6.7.4.

2.6.7.6 Safranin O Staining

Slides were deplasticised in acetone for 15 minutes or dewaxed as described above (Section 2.6.7.4) before being rinsed twice in dH_2O and stained in Fast Green for 5 minutes. Following staining, slides were dipped once in 1% acetic acid before being counterstained in Safranin O stain for 3 minutes. Slides were dipped in 1% acetic acid and thoroughly blotted on both sides before being differentiated and dehydrated by transferring quickly through three changes of ethanol of 3-5 seconds each and two changes of zylene.

Table 2.25. Safranin O Staining Reagents

Fast Green Solution	
Fast Green FCF (cat # F-7252-25G)	0.1 g
dH_2O	50 mL

Safranin O Solution	
Safranin O (cat # S8884-25G)	0.05 g
dH_2O	50 mL

2.6.7.7 Imaging Slides

Digital images of stained slides were generated using the NanoZoomer 2.0-HT scanner (Hamamatsu, Shizuoka, Japan). Briefly, slides were whipped clean with 70% ethanol and loaded into NanoZoomer trays. Focal points were selected manually for each slide and each slide was imaged with 20x magnification.

2.6.7.8 Histoporphometric Analysis

Histomorphometric analysis was carried out using ImageJ open source software version 1.46r (Wayne Rasband, NIH, USA). Haematoxylin and eosin stained sections were used to enumerate bone area and bone surface. Safranin O sections were used to enumerate the fibrous and cartilage tissue area and tissue surface. Manual counting of osteoclasts and osteoblasts was carried out using NDP.view digital pathology software (Hamamatsu, Shizuoka, Japan). Sample slides are shown in figure 2.6.

Figure 2.6 – Annotated Histological Sections

(A) Tri nucleated bone lining osteoclast

(B) Bone lining osteoblast

(C) Osteocyte

(D) Bone

(E) Hematopoietic cells

(F) Trap positive tri nucleated bone lining osteoclast

Scale bar: 100µm

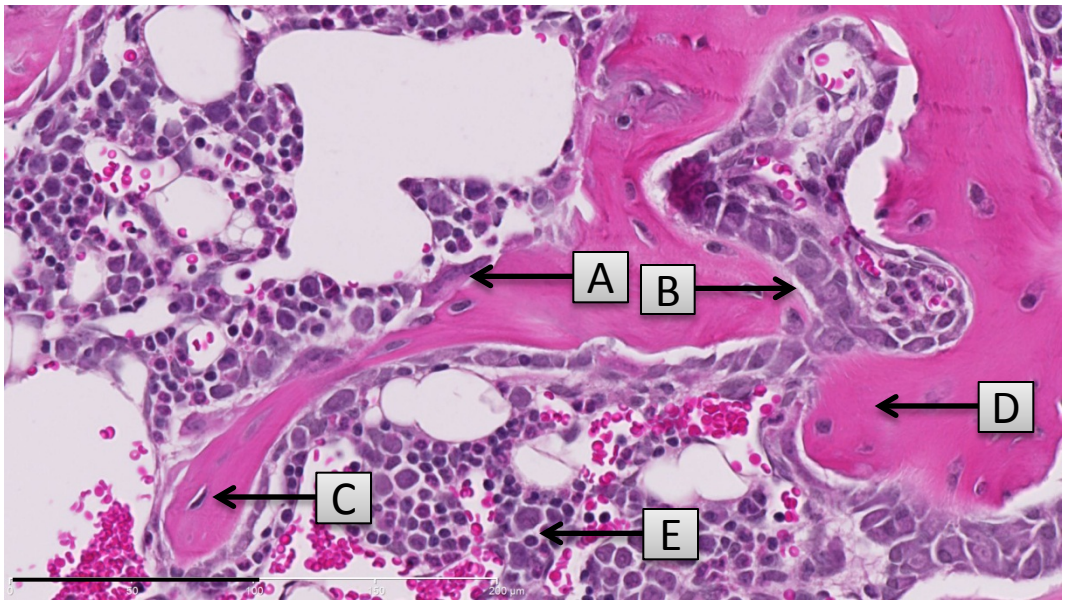
A
B
D
C
E

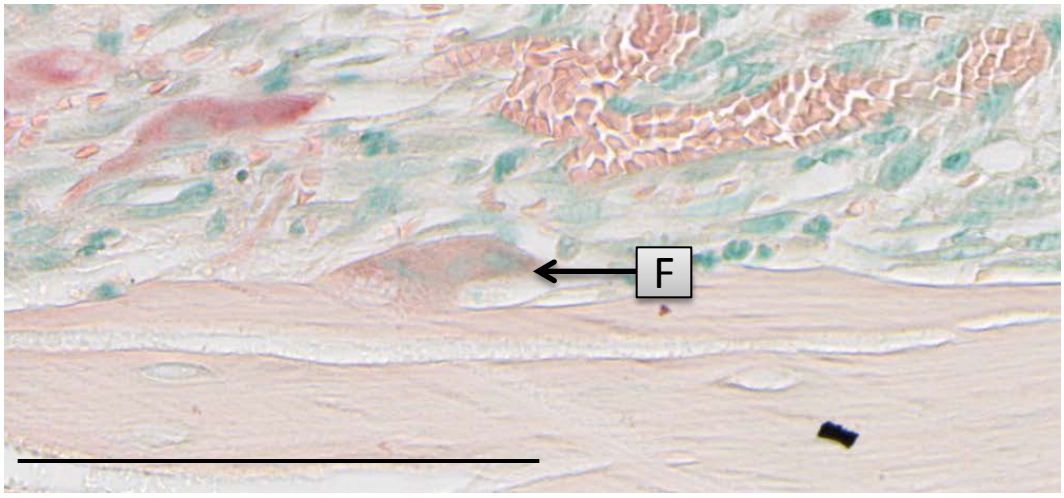
F

2.6.8 X-Ray

All x-ray images were taken using the Faxitron MX-20 X-Ray unit (Faxitron Bioptics, Tuscon, Arizona, USA) and automatic exposure settings in Faxitron software (Software version DX 1.0 Faxitron Bioptics, Tuscon, Arizona, USA).

2.6.9 Mechanical Testing

Mechanical testing was undertaken to compare the structural properties of the control and fracture groups of the fracture study or the sham and OVX groups of the ovariectomy study. Four-point bend tests (fracture study) or three-point bend tests (ovariectomy study) were conducted to failure using a materials testing machine (Model 800LE4; TestResources Inc, Shakopee MN, USA) based on previously published protocols (Schriefer et al., 2005; Silva et al., 2002). The upper span (loading) width was 3.0 mm and the lower span (support) width was 7.0 mm. Both the upper and lower contact anvils had a radius of 1.0 mm. Femurs were positioned posterior side down on the support anvils to cause bending about the medial-lateral axis (posterior side in tension). The bones were centred on the supports to ideally induce failure at the mid-point along the diaphysis on the tension (posterior) side. A pre-load of 1 N was applied and then a constant cross-head displacement rate of 0.017 mm/s for the bend tests to failure. Compliance in the load-line and bend fixtures was removed from the displacement measurement by using a correction factor obtained from tests with an aluminium calibration specimen. The bend tests were conducted in air (22-24 °C) and before testing the bones were kept in PBS soaked gauze at room temperature for 1 hr.

Load-displacement curves were analysed using standard Euler-Bernoulli theory for linear-elastic beams to obtain the bending stiffness and the ultimate bending moment. The bending stiffness, or

flexural rigidity, was calculated by multiplying the measured displacement by $6/(3aL-4a^2)$ where L is the lower span width and a is half the difference between the lower and upper span widths. The bending moment was calculated by multiplying the ultimate force by the value a. No correction for shear deformation was made. Post analysis normalization was carried out by orientating μCT images posterior side down and calculating the midpoint. Once the midpoint was determined the centroid value was calculated and distance from the centroid to the external surface of the posterior side of the bone measured. These values were then used to normalize data by multiplying the ultimate load by the distance value and dividing by the moment of inertia. As the distance value and moment of inertia were measured only for contralateral non fractured limbs and used to normalize both fractured and non-fractured limbs of the animal, this normalization also corrected for the size differences between the WT mice and the *TWIST-1*$^{+/-}$ mice.

2.7 Statistical Analysis

Data analysis was carried out using Microsoft Excel 2010 (software version 14.0.6129.5000), to arrange data and statistical analysis. Paired students t-tests were used to evaluate statistically significant differences in *in vitro* assays. Analysis of all other data was performed using GraphPad PRISM (version 6, GraphPad Software, La Jolla, USA). For *in vivo* fracture experiments, samples were compared using two-way analysis of variance (ANOVA) with Bonferroni's post-tests. For *in vivo* ovariectomy experiments, samples were compared using one-way analysis of variance (ANOVA) with Tukey's post-tests. Differences were considered to be statistically significant when the P value was less than 0.05.

3 Identification of *TWIST-1* target genes involved in MSC proliferation and differentiation.

3.1 Introduction

Studies investigating murine foetal bone development have shown *TWIST-1* expression is highest in immature bone cells and is down regulated in mature bone cell populations (Alborzi et al., 1996; Connerney et al., 2006; Rice et al., 2000). Our laboratory has shown that *TWIST-1* is highly expressed in freshly isolated *STRO-1*$^{+}$ MSC but is rapidly down regulated following ex vivo expansion (Isenmann et al 2009). Furthermore, enforced expression of *TWIST-1* in cultured human MSC results in enhanced proliferative capacity and increased adipogenic differentiation while simultaneously reducing the capacity of MSC to undergo chondrogensis and osteogenesis (Isenmann et al., 2009). These studies also demonstrated that enforced expression of *TWIST-1* in MSC is positively correlated to an increase in *STRO-1* expression and elevated transcript levels of the transcription factors Id-1 and Id-2, factors that have been associated with cellular proliferation (Norton and Atherton, 1998). Findings demonstrating enhanced adipogenic differentiation capacity in *TWIST-1* overexpressing MSC was associated with an increase in gene expression of the adipogenic master regulatory factor *PPARγ2* (Isenmann et al., 2009). Furthermore, our laboratory demonstrated that enforced expression of *TWIST-1* resulted in upregulation of *RUNX2* and *MSX2* while simultaneously downregulating the expression of *BMP2*, as well as committed osteogenic markers *BSP*, *OPN* and *OCN*. These findings correlate with previous studies reporting that increased *RUNX2* expression is associated with a reduction in the expression of target genes resulting in inhibition of bone cell differentiation (Geoffroy et al., 2002; Komori, 2006; Liu et al., 2001). The observation of a reduction in the capacity of MSC to produce glycosaminoglycans and a reduction in their capacity to undergo chondrogenesis correlated with a down regulation of *SOX9* and collagen type X (Isenmann et al., 2009).

Other groups investigating the differentiation, proliferation and commitment of human MSC have described interactions between *TWIST-1,* the Wnt pathway and the TGF-β superfamily of molecules. The involvement of *TWIST-1* in BMP signalling has been demonstrated by showing that *BMP2* stimulates the expression of *TWIST-1* (Inai et al., 2008; Ma et al., 2005). Contrary to these findings, other groups have shown that *TWIST-1* can act as an inhibitor of BMP signalling and Id1 can regulate BMP signalling through a positive feedback loop repressing *TWIST-1* (Hayashi et al., 2007). Induction of *TWIST-1* expression by transforming growth factor beta (*TGF-β)* has also been established by groups investigating signals that regulate chondrocyte differentiation (Dong et al., 2007). Conversely, *TGF-β2* has been shown to be selectively upregulated upon *TWIST-1* phosphorylation (Xue et al., 2012). *TGF-β* can potently stimulate the differentiation of MSC toward the chondrogenic lineage and is routinely used to induce chondrogenesis and assess the chondrogenic potential of pelletised MSC *in vitro* (Barry et al., 2001; Pittenger et al., 1999; Weiss et al., 2010). *TGF-β* acts by directly activating the SMAD pathway, *SMAD 2/3* leading to stabilisation of the *SOX9* transcription complex (Furumatsu et al., 2005; Yang et al., 2001) and subsequent induction of chondrogenic differentiation. Bone morphogenetic proteins (BMP) are members of the TGF-β family and act as potent stimulators of osteoblast differentiation (Wozney, 2002). They act locally as signalling molecules by binding to cell surface receptors to transduce signals via SMAD proteins, *SMAD1*, 5 and 8, that then form stable complexes with *SMAD4* to translocate into the nucleus and activate genes involved in osteoblastic differentiation (Augello and De Bari, 2010; Ebara and Nakayama, 2002). The action of BMPs is unique as they induce the differentiation of MSC towards the osteoblastic lineage but also enhance the differentiated function of the resulting osteoblast (Canalis et al., 2003).

The *TWIST-1* protein has been shown to be involved in the Wnt pathway as it has been demonstrated that *WNT1* inhibits chondrogenesis through the upregulation of *TWIST-1* (Dong et

al., 2007; Howe et al., 2003). As shown in figure 3.1, the Wnt family is made up of 19 genes that code for signalling molecules that play important roles in bone formation by regulating the expression of genes that mediate osteoblastogenesis (Logan and Nusse, 2004; Pandur et al., 2002). Similar to *TWIST-1*, the Wnt pathway has been implicated in the pathogenesis of craniosynostosis with high levels of canonical Wnt signalling associated with cranial suture patency and low levels are associated with suture fusion (Behr et al., 2010a; Liu et al., 2007; Yu et al., 2005). Mammalian MSC populations have been shown to express Wnt proteins as well as other components of both the canonical and non-canonical Wnt pathways, indicating that these cells have the necessary machinery to participate in cellular events mediated by this family of proteins (Bodine et al., 2006; Rawadi and Roman-Roman, 2005; Westendorf et al., 2004). It has been shown that mice deficient in *LRP5* have a reduction in peak vertebral trabecular bone volume of approximately 40% (Kato et al., 2002). Conversely, an activating mutation has been identified in *LRP5* that results in an increase in bone density in affected individuals (Boyden, 2002; Little et al., 2002b). To illustrate the critical role of Wnt signalling in osteoblast development, Hongliang and colleagues generated a *Dermo-1* cre-mediated β-catenin knockout mouse model (Hu et al., 2005). This group was able to demonstrate the total abolition of Wnt signalling in this animal model leading to an absence of bone in both the endochondral and intramembranous skeleton. The canonical Wnt signalling pathway has also been demonstrated to be involved in the regulation of MSC, through regulation of *RUNX2* (Behr et al., 2010b; Bodine and Komm, 2006; Bodine et al., 2006; Etheridge et al., 2004; Gaur et al., 2005; Glass and Karsenty, 2007; Glass Ii and Karsenty, 2006; Gregory et al., 2005; Hartmann, 2006; Hill et al., 2005; Krishnan et al., 2006; Liu et al., 2008; Piters et al., 2008; Westendorf et al., 2004; Williams and Insogna, 2009). Further studies demonstrated that β-catenin is required for early stage osteoblast differentiation and deletion of β-catenin forces cells to differentiate into chondrocytes (Hill et al., 2005).

Figure 3.1 - The Wnt pathway Left - The Wnt pathway in the inactive state. In the absence of Wnt binding LRP5/6 is bound by repressor proteins Sclerostin or Dickkopf and its function inhibited. This leaves the APC/GSK/Axin complex in its active state and leads to phosphorylation and proteosomal degradation of β-Catenin. Right - The active state of the Wnt pathway. A wnt protein binds LRP5/6 and Axin is sequestered to the cell surface. This leads to the destabilisation of the APC/GSK/Axin complex and subsequent stabilization of β-Catenin allowing translocation to the nucleus and activation of gene transcription. Adapted from (Miller, 2002; T. J. Martin, 2008)

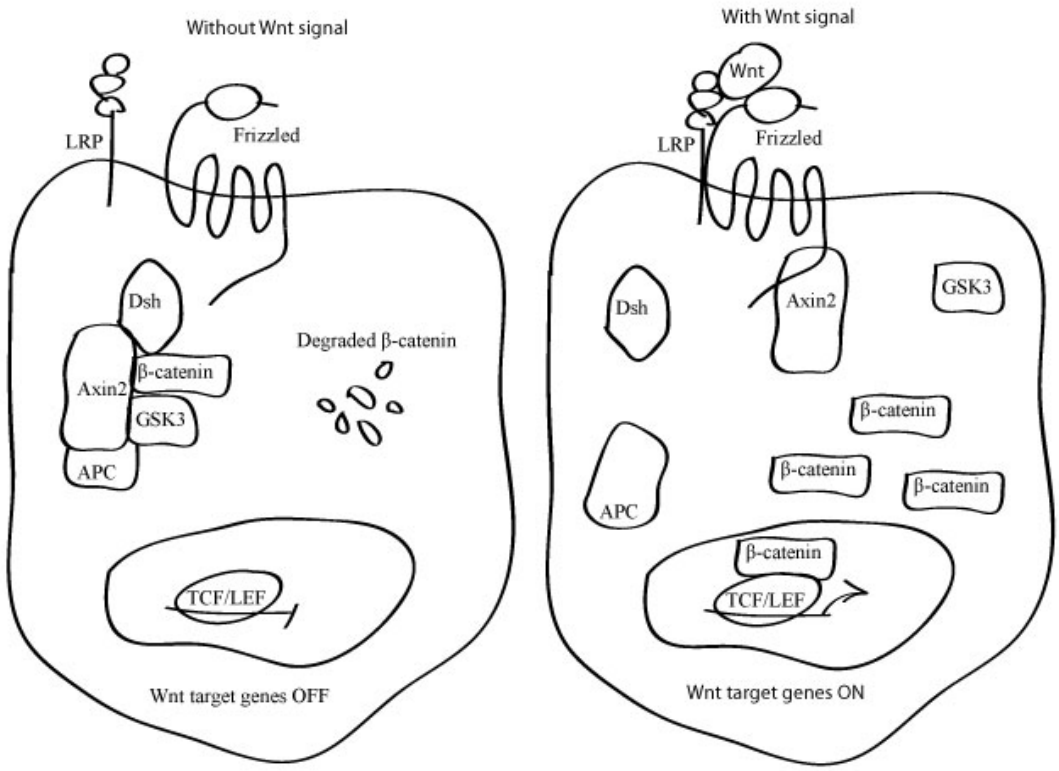
Without Wnt signal
LRP
Frizzled
Dsh
Axin2
β-catenin
GSK3
APC
Degraded β-catenin
TCF/LEF
Wnt target genes OFF
With Wnt signal
Wnt
LRP
Frizzled
Dsh
Axin2
GSK3
β-catenin
β-catenin
β-catenin
APC
β-catenin
TCF/LEF
Wnt target genes ON

The aim of this study was to identify the functional role of *TWIST-1* binding targets in the processes of proliferation, differentiation and commitment of human MSC. Microarray data will be used to identify possible gene targets and these targets will be assessed for interactions with *TWIST-1*. In addition, MSC overexpressing *TWIST-1* targets will be generated using retroviral infection techniques and their role in adipogenesis, osteogenesis, chondrogenesis, proliferation and senescence determined using functional assays.

3.2 Results

3.2.1 Microarray analysis identified differentially expressed *TWIST-1* targets

An Illumina V8 microarray analysis comparing gene expression levels of cultured human MSC engineered to overexpress human *TWIST-1* (retrovirally infected using a pruf-IRES-GFP-TWIST-1 expression construct) and corresponding control MSC (retrovirally infected with empty vector control; pruf-IRES-GFP) was conducted in our laboratory (unpublished observations) to identify *TWIST-1* target genes involved in the proliferation, differentiation and commitment of MSC. This microarray returned approximately 350 differentially expressed genes with confidence of 95% or greater (>1.5 fold change, p value <0.05). Patterns based on gene expression were analysed using the DAVID bioinformatics database (section 2.4.1) to provide a means to reduce the large list of genes identified by microarray into functionally related groups of genes (Huang et al., 2008; Huang et al., 2009).

Preliminary analysis of microarray data returned genes involved in the *TGFβ* and BMP signalling pathways, previously demonstrated to have a critical role in the regulation of commitment and differentiation of human MSC (Feng and Derynck, 2005; Guiqian Chen1, 2012; Zhou, 2011; Zhou et al., 2004). Molecules identified within these pathways include *BMP4*, *TGFβ2*, *SMAD6*, *ACVR2A*, *ID1*, *2* and *3* (figure 3.2). Furthermore, Wingless-type MMTV integration site family, member 2 (*WNT2*) and Wingless-type MMTV integration site family, member 2b (*WNT2B*), both known activators of canonical Wnt signalling were also identified as a potential *TWIST-1* targets (Figure 3.3). The genes *WNT2* and *WNT2B* were both upregulated in the presence of *TWIST-1* overexpression with fold changes of 3.7 and 1.6 respectively.

Figure 3.2 - *TWIST-1* regulates genes involved in the *TGF-β* signaling pathway. DAVID analysis of microarray showing *TWIST-1* regulated genes involved in the *TGF-β* signalling pathway. *BMP4* and *TGF-β2* have both been implicated in osteogenesis. These two genes are downregulated in the presence of enforced *TWIST-1* expression.

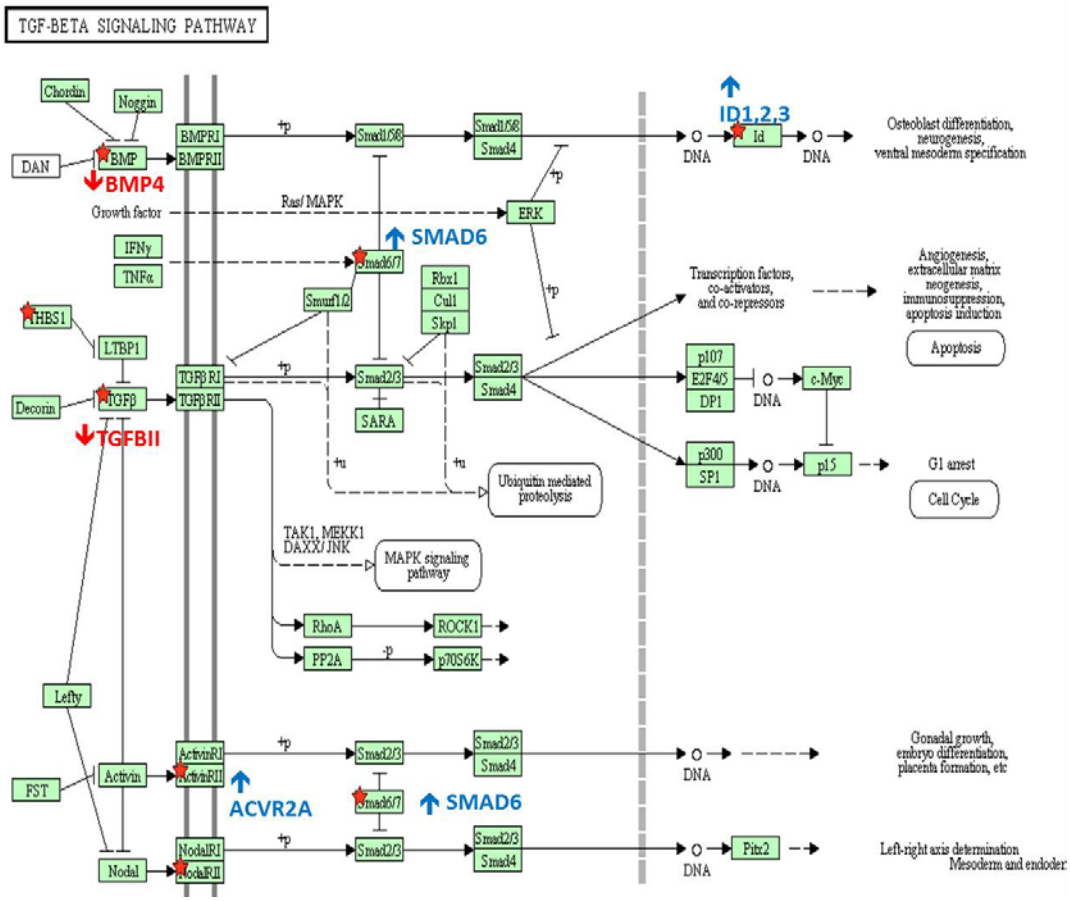
TGF-BETA SIGNALING PATHWAY
Chordin
Noggin
DAN
BMP
BMPRI
BMPRII
BMP4
Smad1/5/8
Smad1/5/8
Smad4
ID1,2,3
Id
DNA
DNA
Osteoblast differentiation,
neurogenesis,
ventral mesoderm specification
Growth factor
Ras/ MAPK
ERK
SMAD6
IFNγ
TNFα
Smad6/7
Rbx1
Cul1
Skp1
Smurf1/2
Transcription factors,
co-activators,
and co-repressors
Angiogenesis,
extracellular matrix
neogenesis,
immunosuppression,
apoptosis induction
Apoptosis
THBS1
LTBP1
TGFβ
Decorin
TGFBII
TGFβRI
TGFβRII
Smad2/3
Smad4
SARA
p107
E2F4/5
DP1
DNA
c-Myc
p300
SP1
DNA
p15
G1 arrest
Cell Cycle
Ubiquitin mediated
proteolysis
TAK1, MEKK1
DAXX/ JNK
MAPK signaling
pathway
RhoA
ROCK1
PP2A
p70S6K
Lefty
FST
Activin
ActivinRI
ActivinRII
ACVR2A
Smad2/3
Smad4
Smad6/7
SMAD6
DNA
Gonadal growth,
embryo differentiation,
placenta formation, etc
Nodal
NodalRI
NodalRII
Smad2/3
Smad4
Pitx2
DNA
Left-right axis determination
Mesoderm and endoderm

Figure 3.3 - *TWIST-1* regulates genes involved in the Wnt signaling pathway. DAVID analysis of microarray showing *TWIST-1* regulated genes involved in the Wnt pathway. *WNT2* and *WNT2B* promote Wnt signalling and *AXIN2* inhibits Wnt signalling. All three genes are upregulated in the presence of enforced *TWIST-1* expression.

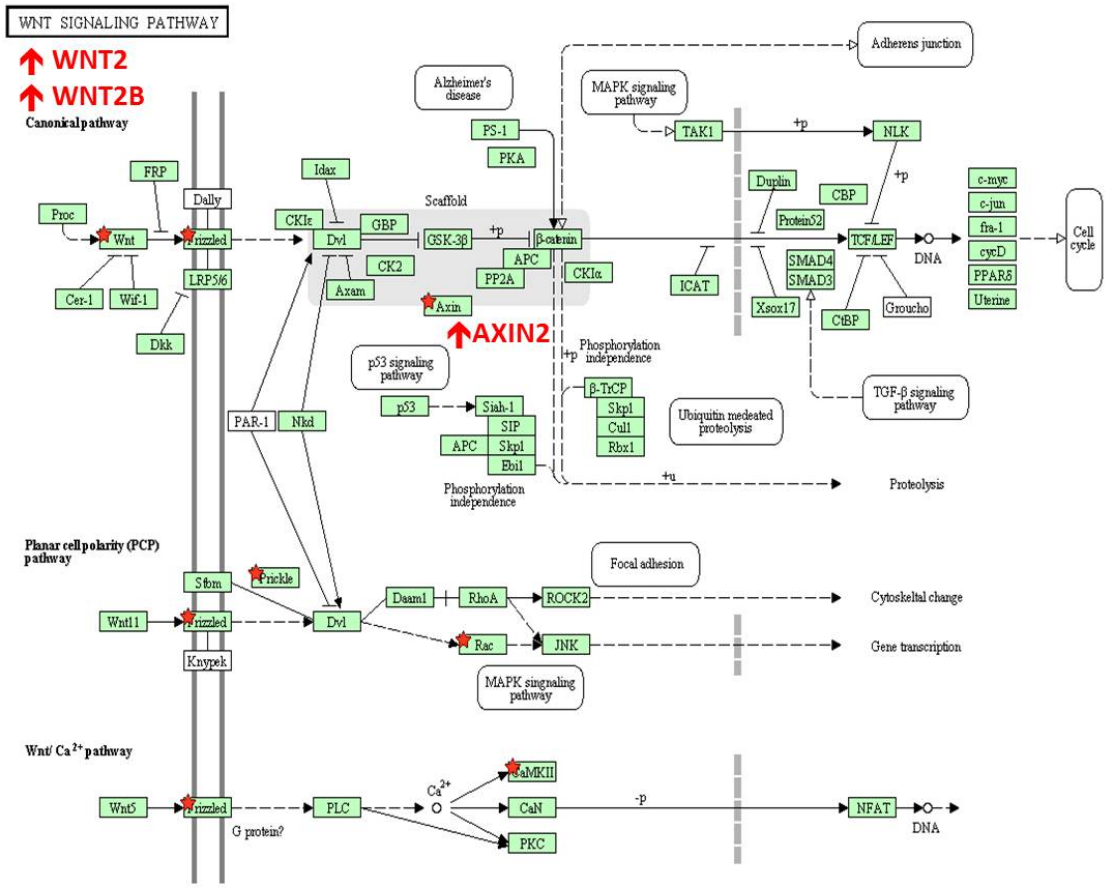
WNT SIGNALING PATHWAY
↑ WNT2
↑ WNT2B
Canonical pathway
FRP
Dally
Proc
Wnt
Frizzled
LRP5/6
Cer-1
Wif-1
Dkk
Idax
CKIε
GBP
Dvl
GSK-3β
+p
β-catenin
Scaffold
APC
CK2
PP2A
CKIα
Axam
Axin
↑AXIN2
Alzheimer's disease
PS-1
PKA
MAPK signaling pathway
TAK1
+p
NLK
Adherens junction
Duplin
CBP
Protein52
TCF/LEF
DNA
c-myc
c-jun
fra-1
cycD
PPARδ
Uterine
Cell cycle
ICAT
SMAD4
SMAD3
Xsox17
CtBP
Groucho
TGF-β signaling pathway
p53 signaling pathway
p53
Siah-1
SIP
Skp1
Ebi1
Phosphorylation independence
β-TrCP
Skp1
Cul1
Rbx1
Ubiquitin medeated proteolysis
+u
Proteolysis
PAR-1
Nkd
Planar cell polarity (PCP) pathway
Stbm
Prickle
Wnt11
Frizzled
Knypek
Dvl
Daam1
RhoA
ROCK2
Cytoskeltal change
Rac
JNK
Gene transcription
Focal adhesion
MAPK singnaling pathway
Wnt/ Ca 2+ pathway
Wnt5
Frizzled
G protein?
PLC
Ca2+
CaMKII
CaN
PKC
-p
NFAT
DNA

3.2.2 Confirmation of differential gene expression by RT-PCR

RT-PCR (section 2.4.2) analysis demonstrated a statistically significant ($p<0.05$, paired students t-test) down regulation of *BMP4* and upregulation of *ACVR2A*, *TWIST-1*, *AXIN2*, *WNT2* and *WNT2B* in MSC with enforced *TWIST-1* expression (figures 3.4 and 3.5). Of greatest significance, *WNT2* and *WNT2B* were statistically significantly ($p<0.05$, paired students t-test) upregulated with enforced *TWIST-1* expression with fold changes of >10 and >3 respectively. While not significant, *TGFβ-2* showed a trend of downregulation, while *SMAD6* was upregulated in MSC with enforced *TWIST-1* expression. Together, these results confirmed and further validated the microarray data discussed in section 3.2.1.

3.2.3 Canonical Wnt signalling pathway is activated by *TWIST-1*

Using western blot analysis (section 2.5.2) protein levels of activated β-catenin in MSC with enforced *TWIST-1* were demonstrated to be elevated > 7 fold when compared to GFP control cells cultured under the same conditions (figure 3.6). This result illustrates the potent effect of *TWIST-1* overexpression on Wnt pathway stimulation coupled with enhanced *AXIN2* activation, a known downstream target of Wnt signalling (Dao et al., 2007).

3.2.4 *TWIST-1* expression enhances *WNT2* and *WNT2B* promoter activity

Following verification of differential expression by real time PCR, 3kb of the proximal promoter regions of *WNT2* and *WNT2B* were analysed for *TWIST-1* binding sites (CANNTG). Consensus binding sites were identified in both promoters. Cloning primers were designed to amplify 0.5, 1, 2, and 3kb fragments of the promoter regions of *WNT2* and *WNT2B* and clone into the luciferase reporter vector PGL3 Basic (section 2.4.3.3 and figure 2.3). Following amplification, cloning and

Figure 3.4 – Regulation of TGF-β pathway genes confirmed by real-time PCR. RNA expression levels of genes identified by microarray as being differentially regulated in the presence of *TWIST-1* overexpression. P-vales; *ACVR2A* 0.043, *BMP4* 0.018, *TGF-β2* 0.07. *Smad6* 0.525. Statistically significant (n = 3) ($p < 0.05$, unpaired t-test) results when compared to GFP control cell line denoted by (*).

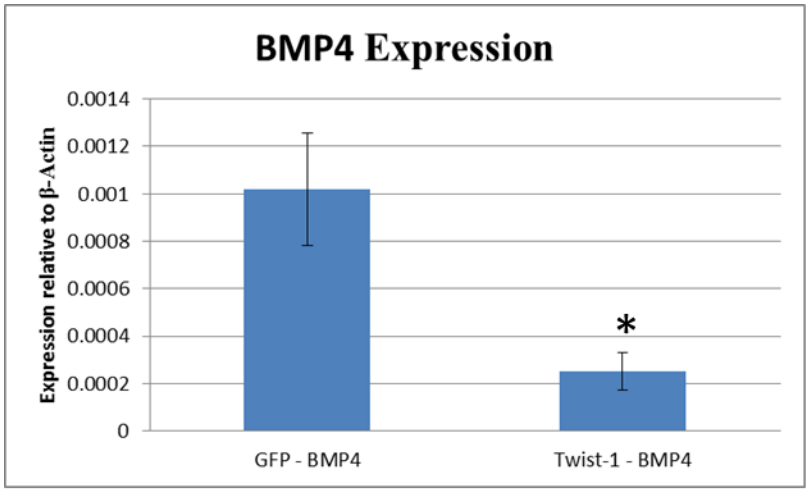
BMP4 Expression
Expression relative to β-Actin
0.0014
0.0012
0.001
0.0008
0.0006
0.0004
0.0002
0
*
GFP - BMP4
Twist-1 - BMP4

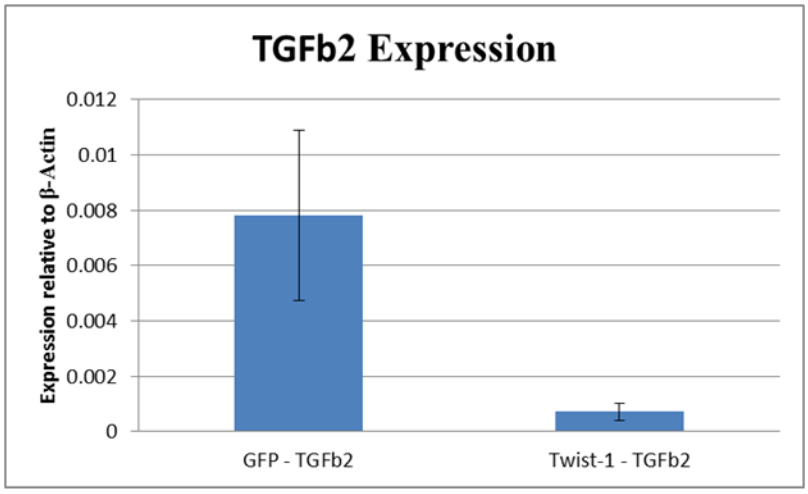
TGFb2 Expression
Expression relative to β-Actin
0.012
0.01
0.008
0.006
0.004
0.002
0
GFP - TGFb2
Twist-1 - TGFb2

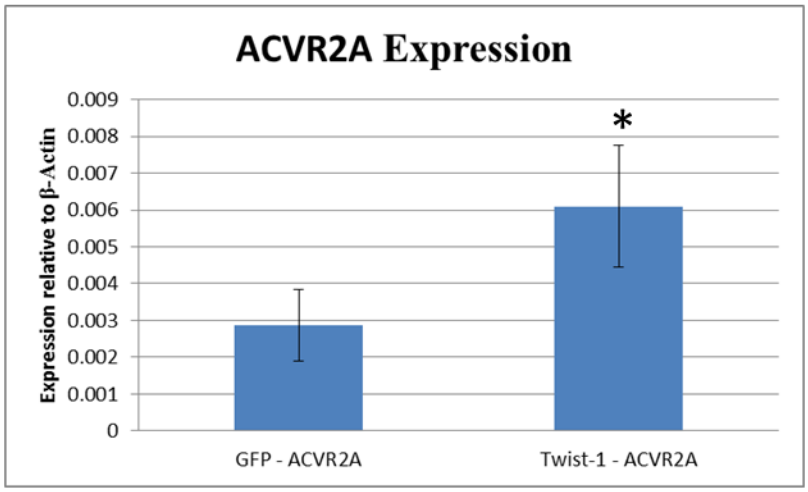
ACVR2A Expression
Expression relative to β-Actin
0.009
0.008
0.007
0.006
0.005
0.004
0.003
0.002
0.001
0
*
GFP - ACVR2A
Twist-1 - ACVR2A

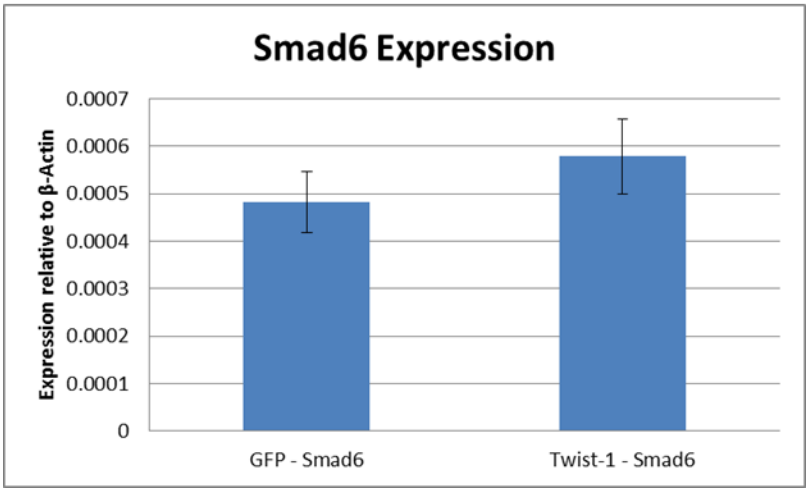
Smad6 Expression
Expression relative to β-Actin
0.0007
0.0006
0.0005
0.0004
0.0003
0.0002
0.0001
0
GFP - Smad6
Twist-1 - Smad6

Figure 3.5 - Regulation of Wnt pathway genes confirmed by real-time PCR. RNA expression levels of genes identified by microarray as being differentially regulated in the presence of *TWIST-1* overexpression. P-vales; *TWIST-1* 0.007, *AXIN2* 0.025, *WNT2* 0.028. *WNT2B* 0.022. Statistically significant ($n = 3$) ($p < 0.05$, unpaired t-test) results when compared to GFP control cell line denoted by (*).

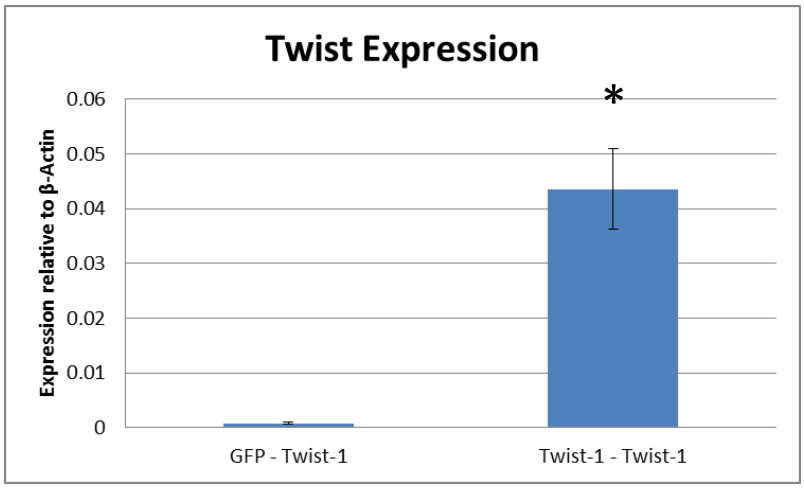
Twist Expression
Expression relative to β-Actin
0.06
0.05
0.04
0.03
0.02
0.01
0
*
GFP - Twist-1
Twist-1 - Twist-1

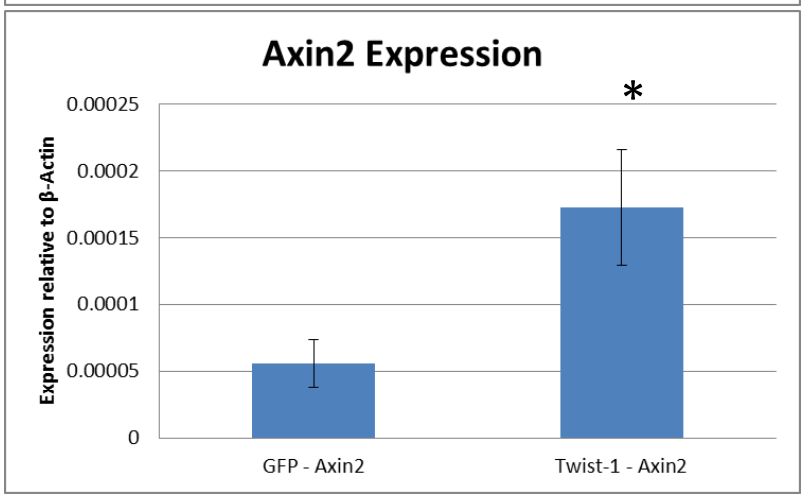
Axin2 Expression
Expression relative to β-Actin
0.00025
0.0002
0.00015
0.0001
0.00005
0
*
GFP - Axin2
Twist-1 - Axin2

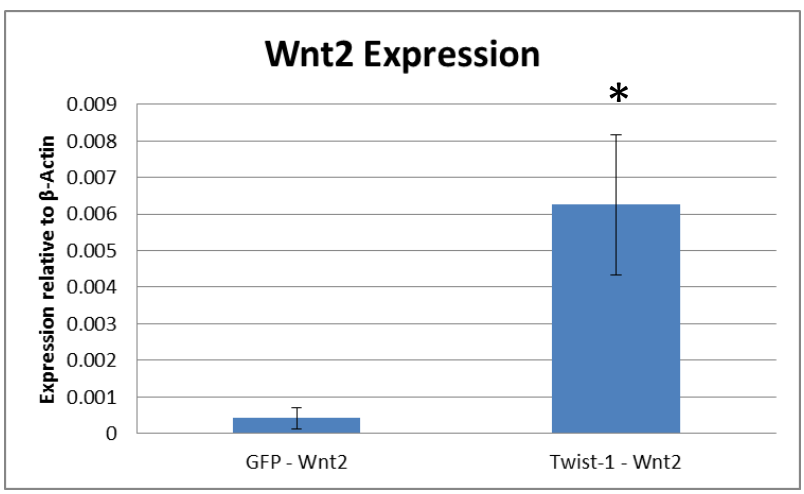
Wnt2 Expression
Expression relative to β-Actin
0.009
0.008
0.007
0.006
0.005
0.004
0.003
0.002
0.001
0
*
GFP - Wnt2
Twist-1 - Wnt2

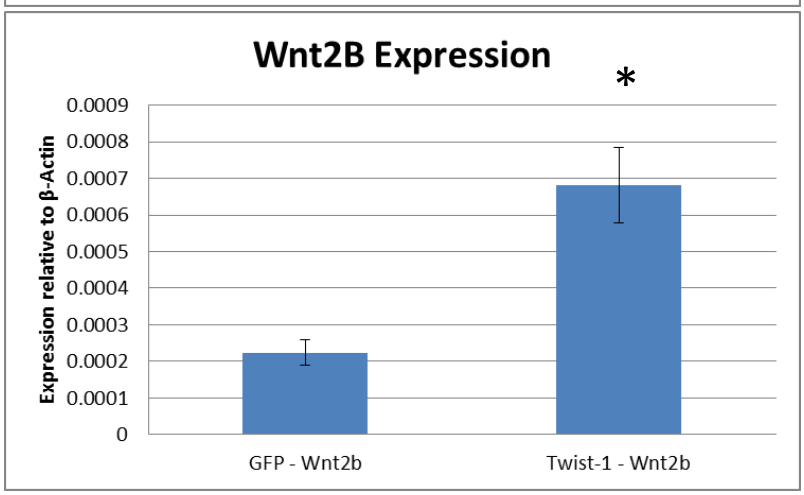
Wnt2B Expression
Expression relative to β-Actin
0.0009
0.0008
0.0007
0.0006
0.0005
0.0004
0.0003
0.0002
0.0001
0
*
GFP - Wnt2b
Twist-1 - Wnt2b

Figure 3.6 – Elevated activated β-catenin levels in *TWIST-1* overexpressing MSC. Western blot demonstrating elevated β-catenin levels in *TWIST-1* overexpressing MSC compared to GFP controls using normal media but not osteoinductive media. Representative images from three replicates.

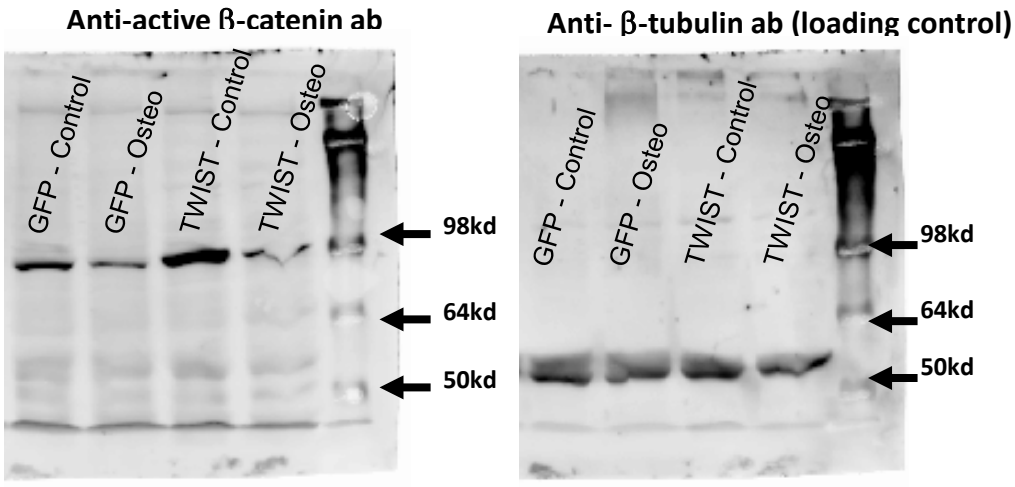
Anti-active β-catenin ab
GFP - Control
GFP - Osteo
TWIST - Control
TWIST - Osteo
98kd
64kd
50kd
Anti- β-tubulin ab (loading control)
GFP - Control
GFP - Osteo
TWIST - Control
TWIST - Osteo
98kd
64kd
50kd

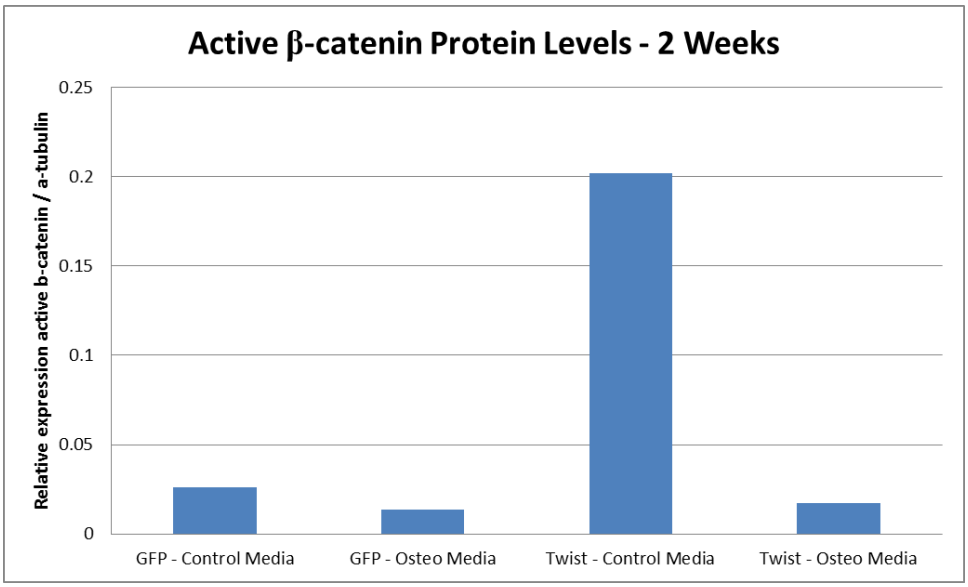
Active β-catenin Protein Levels - 2 Weeks
Relative expression active b-catenin / a-tubulin
0.25
0.2
0.15
0.1
0.05
0
GFP - Control Media
GFP - Osteo Media
Twist - Control Media
Twist - Osteo Media

sequence verification (results not shown) the luciferase reporter vectors were transiently transfected into MG63 cells along with either a Pruf-IRES-GFP (control) or Pruf-IRES-GFP-TWIST-1 construct to enforce *TWIST-1* expression. The expression of luciferase was quantified to measure the effect of *TWIST-1* overexpression upon the promoter regions of *WNT2* and *WNT2B*. It was demonstrated that overexpression of *TWIST-1* caused statistically significant ($p<0.05$, paired students t-test) upregulation of luciferase expression through the 1kb and 3kb promoter fragments of *WNT2* (figure 3.7). The 1kb *WNT2* promoter fragment contained the *TWIST-1* binding site with closest proximity to the transcriptional start site of *WNT2* identified *in silico,* providing further evidence for *TWIST-1* mediated promoter transcriptional regulation of *WNT2*. A preferential *TWIST-1* binding site (CATATG) was identified within the proximal 1kb *WNT2B* promoter fragment *in silico*, however, statistically significant ($p<0.05$, paired students t-test) upregulation of luciferase expression was observed using the 2kb and 3kb promoter fragments of *WNT2B* in conjunction with enforced *TWIST-1* expression (figure 3.8). These experiments provided further confirmation of the action of *TWIST-1* on the promoter regions of interest and hence, the regulation of expression of *WNT2* and *WNT2B*.

3.2.5 TWIST-1 binds directly to *WNT2* and *WNT2B* promoters

ChIP was used to confirm direct interactions between *TWIST-1* protein and the promoter regions of *WNT2* and *WNT2B* using either the IgG control antibody or *TWIST-1* specific antibody (Twist2c1a) as described in section 2.5.5. Enriched genomic DNA was used to amplify *WNT2* and *WNT2B* promoter regions containing *TWIST-1* E-box binding sites (CANNTG) identified *in silico* (section 2.4.3.3). Fold enrichment was calculated by measuring the levels of enriched genomic DNA using real-time PCR and comparing the levels to input genomic DNA. The results from this experiment revealed statistically significant ($p<0.05$, paired students t-test) *TWIST-1*

Figure 3.7 - Elevated *TWIST-1* expression enhances *WNT2* promoter activity. Luciferase reporter assays show the expression levels of luciferase driven by the cloned promoter fragments of *WNT2*. Statistically significant upregulation of luciferase expression is shown within the 1kb promoter fragment of the *WNT2* promoter. Statistically significant ($p < 0.05$, paired t-test) results when compared to GFP control construct denoted by (*).

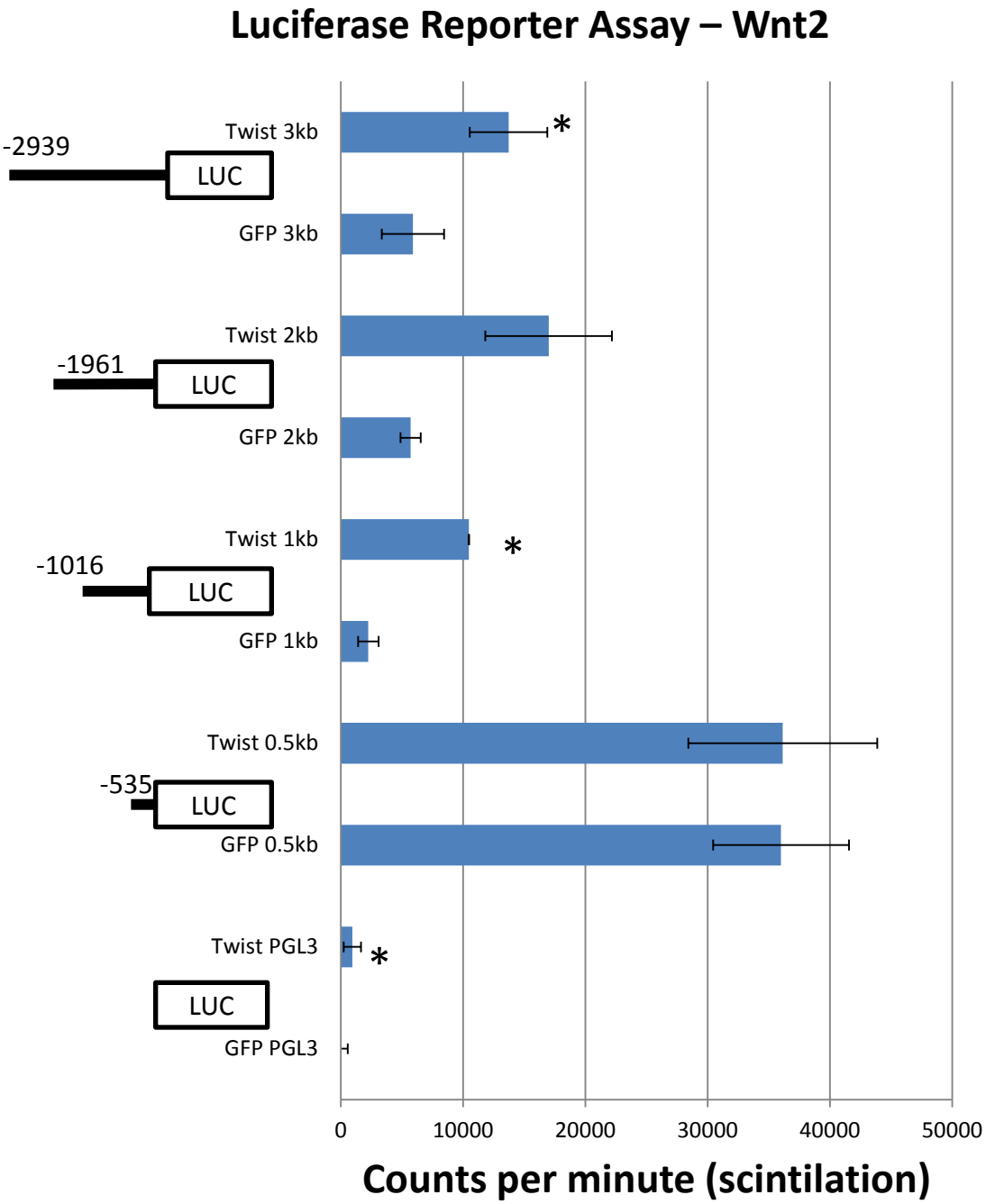
Luciferase Reporter Assay – Wnt2
Twist 3kb
-2939
LUC
GFP 3kb
Twist 2kb
-1961
LUC
GFP 2kb
Twist 1kb
-1016
LUC
GFP 1kb
Twist 0.5kb
-535
LUC
GFP 0.5kb
Twist PGL3
LUC
GFP PGL3
*
*
*
0
10000
20000
30000
40000
50000
Counts per minute (scintilation)

Figure 3.8 - Elevated *TWIST-1* expression enhances *WNT2B* promoter activity. Luciferase reporter assays show the expression levels of luciferase driven by the cloned promoter fragments of *WNT2B*. Statistically significant upregulation of luciferase expression is shown within the 2 and 3kb promoter fragments of the *WNT2B* promoter. Statistically significant ($p < 0.05$, paired t-test) results when compared to GFP control cell line denoted by (*).

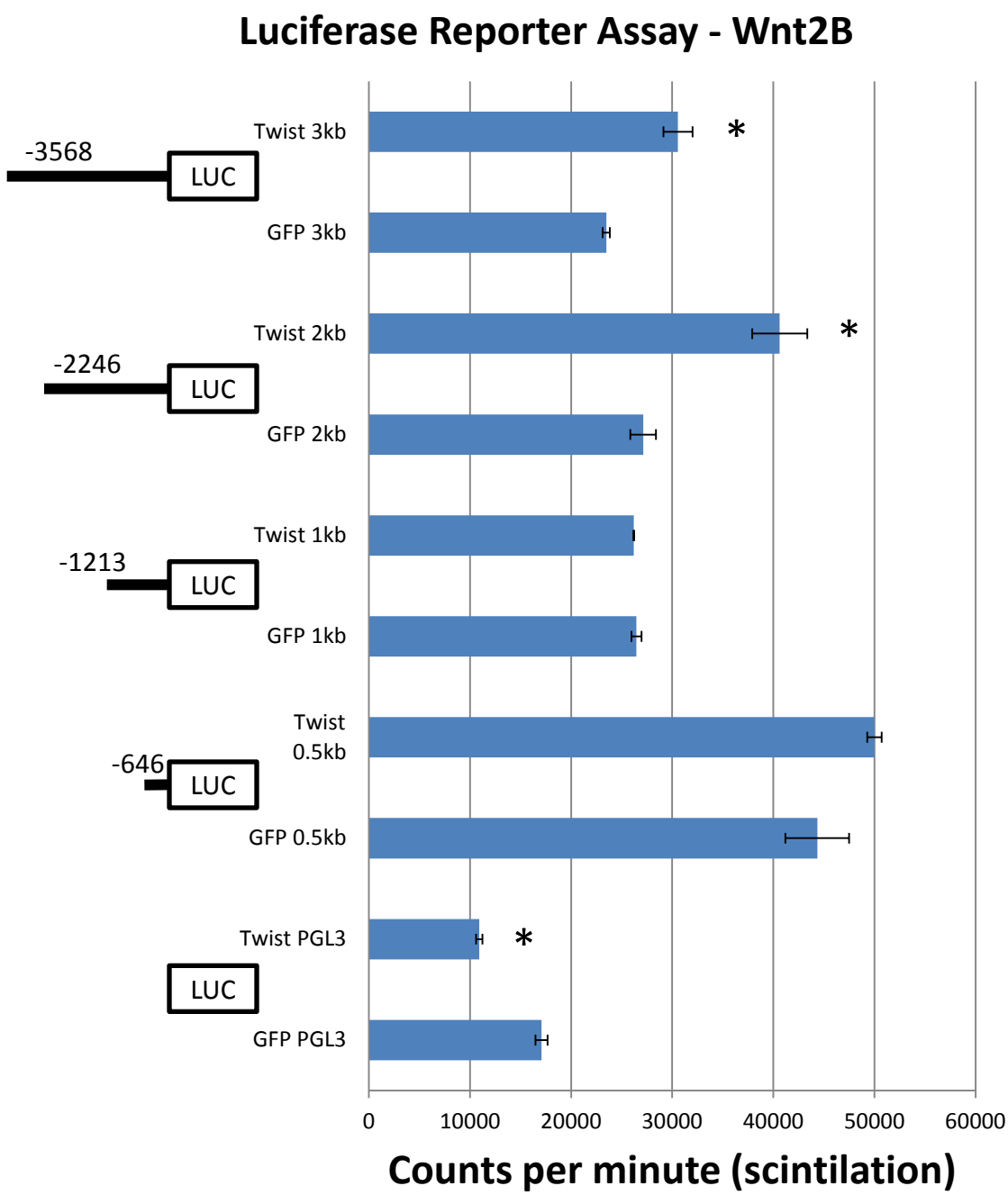
Luciferase Reporter Assay - Wnt2B
Twist 3kb
-3568
LUC
GFP 3kb
Twist 2kb
-2246
LUC
GFP 2kb
Twist 1kb
-1213
LUC
GFP 1kb
Twist
0.5kb
-646
LUC
GFP 0.5kb
Twist PGL3
LUC
GFP PGL3
*
*
*
0
10000
20000
30000
40000
50000
60000
Counts per minute (scintilation)

recruitment to the E-box binding site within the first 1kb of the proximal *WNT2* promoter (figure 3.9) as well as four other E-box binding sites further upstream. This data correlates with the luciferase data in section 3.2.4, as well as predictions based on *in silico* promoter analysis, demonstrating a direct interaction between *TWIST-1* protein and the promoter of *WNT2*.

A preferential binding site (CATATG) was identified, *in silico,* within the proximal 1kb of the *WNT2B* promoter. ChIP analysis demonstrated statistically significant ($p<0.05$, paired students t-test) *TWIST-1* recruitment to the preferential E-box binding site within the first 1kb of the proximal *WNT2B* promoter (figure 3.10) along with another E-box binding site upstream. This data correlated with *in silico* promoter analysis, however, luciferase data in section 3.2.4 showed no increases in luciferase levels within 1kb of the proximal *WNT2B* promoter.

3.2.6 Generation of *WNT2* and *WNT2B* overexpressing MSC by Retroviral Transduction

As described above, it is possible for *TWIST-1* to regulate the transcription of *WNT2* and *WNT2B* through direct interaction with their respective proximal promoters (section 3.2.5). To determine the effect of *WNT2* and *WNT2B* on MSC proliferation, differentiation and commitment, overexpressing lines were generated by retroviral transduction of cultured passage two MSC as described in (section 2.5.3.3). Once selected (section 2.5.3.3), overexpression of *WNT2* and *WNT2B* was confirmed in all cell lines, using RT-PCR, prior to their use in phenotypic and functional analysis (figure 3.11).

Figure 3.9 - *TWIST-1* binds directly to the *WNT2* promoter. ChIP assay shows percentage enrichment using *TWIST-1* antibody (*TWIST-1* 2c1a) compared to IgG control antibody. The differences between these two groups are statistically significant at every E-box within the *WNT2* promoter. Statistically significant ($p < 0.05$, paired t-test) results when compared to IgG control antibody denoted by (*).

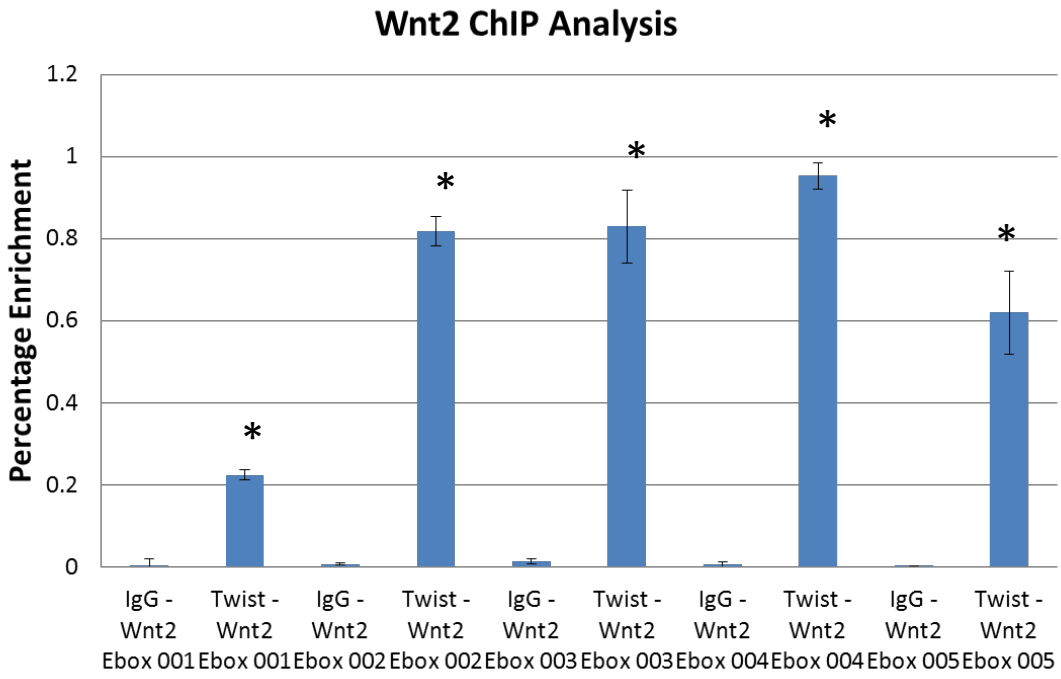
Wnt2 ChIP Analysis
Percentage Enrichment
1.2
1
0.8
0.6
0.4
0.2
0
*
*
*
*
*
IgG - Wnt2 Ebox 001
Twist - Wnt2 Ebox 001
IgG - Wnt2 Ebox 002
Twist - Wnt2 Ebox 002
IgG - Wnt2 Ebox 003
Twist - Wnt2 Ebox 003
IgG - Wnt2 Ebox 004
Twist - Wnt2 Ebox 004
IgG - Wnt2 Ebox 005
Twist - Wnt2 Ebox 005

Figure 3.10 - *TWIST-1* binds directly to the *WNT2B* promoter. ChIP assay shows percentage enrichment using *TWIST-1* antibody (*TWIST-1* 2c1a) compared to IgG control antibody. The differences between these two groups are statistically significant at E-box 3 and 4 within the *WNT2B* promoter. Statistically significant ($p < 0.05$, paired t-test) results when compared to IgG control antibody denoted by (*).

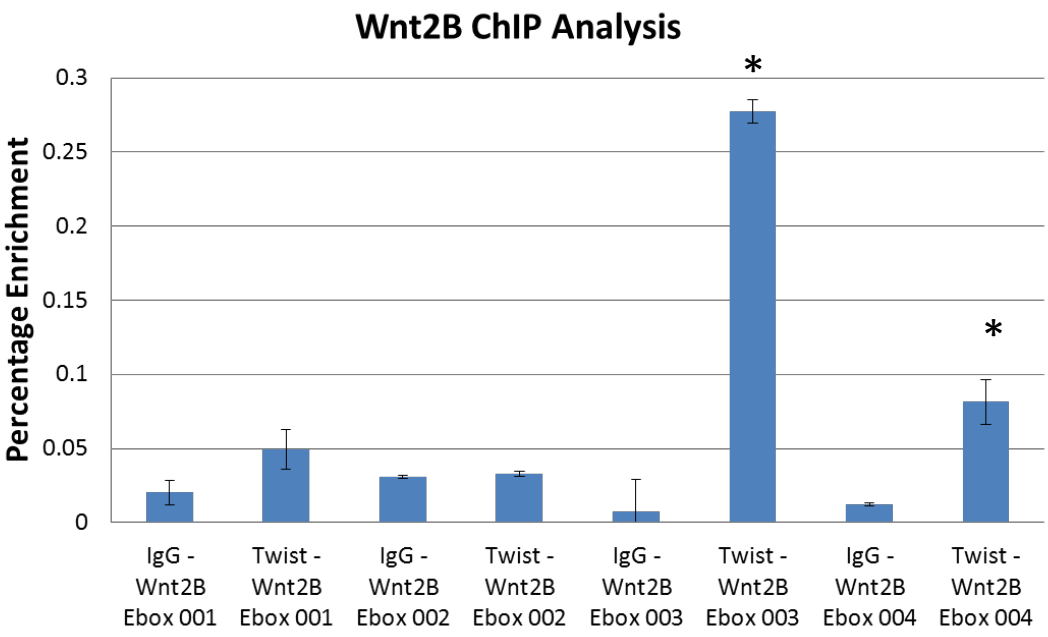
Wnt2B ChIP Analysis
Percentage Enrichment
0.3
0.25
0.2
0.15
0.1
0.05
0
*
*
IgG - Wnt2B Ebox 001
Twist - Wnt2B Ebox 001
IgG - Wnt2B Ebox 002
Twist - Wnt2B Ebox 002
IgG - Wnt2B Ebox 003
Twist - Wnt2B Ebox 003
IgG - Wnt2B Ebox 004
Twist - Wnt2B Ebox 004

Figure 3.11 - Verification of gene expression following transduction. Real-time PCR results indicate that the upregulation of *WNT2* and *WNT2B* transcripts in overexpressing cells is statistically significant when compared to iG2 control cells. Statistically significant ($n = 3$) ($p < 0.05$, unpaired t-test) results when compared to GFP control cell line denoted by (*).

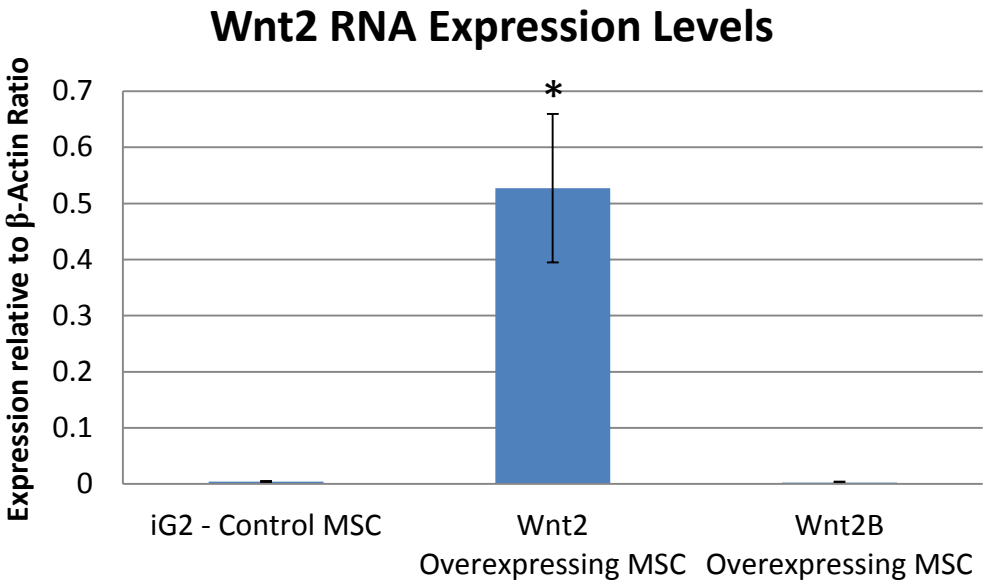
Wnt2 RNA Expression Levels
Expression relative to β-Actin Ratio
0.7
0.6
0.5
0.4
0.3
0.2
0.1
0
*
iG2 - Control MSC
Wnt2 Overexpressing MSC
Wnt2B Overexpressing MSC

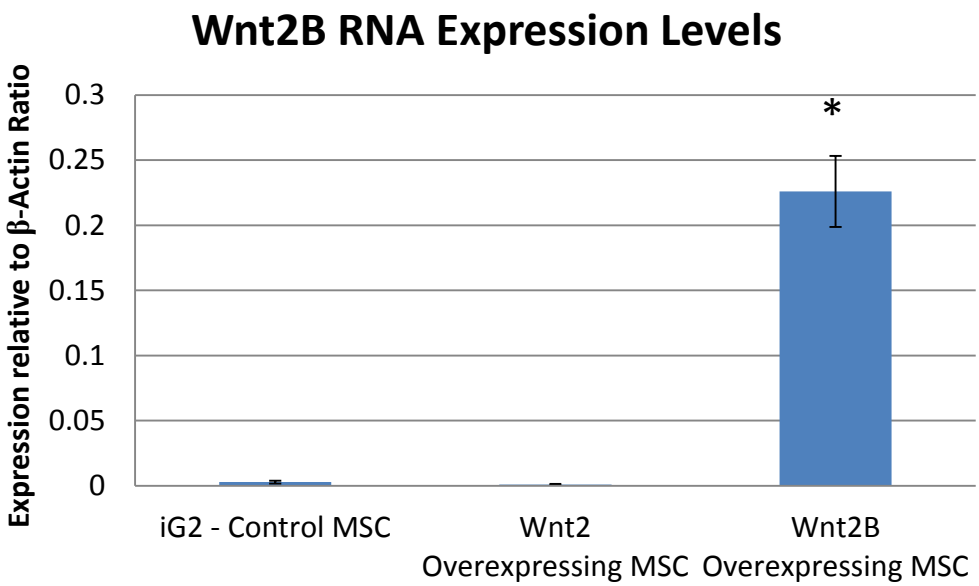
Wnt2B RNA Expression Levels
Expression relative to β-Actin Ratio
0.3
0.25
0.2
0.15
0.1
0.05
0
*
iG2 - Control MSC
Wnt2 Overexpressing MSC
Wnt2B Overexpressing MSC

3.2.7 Flow cytometric analysis of *WNT2* and *WNT2B* overexpressing MSC

The expression profile of cell surface antigens was assessed using flow cytometric analysis of known MSC and haematopoietic associated markers (figures 3.12 and 3.13). All MSC populations expressed mesenchymal stem cell associated markers CD146, B478, CD166, CD105, CD90 and CD73, and lacked the expression of monocyte/macrophage marker CD14, haematopoietic stem/progenitor cell marker CD34, and the leukocyte marker CD45. Furthermore, the cell surface expression of immature MSC marker STRO-1 was detected in 9.3% of iG2 control MSC compared to 15.2% of *WNT2* overexpressing and 15.7% of *WNT2B* overexpressing MSC indicating that *WNT2* and *WNT2B* populations contain a higher percentage of immature MSC when compared to relevant controls.

3.2.8 Effects of *WNT2* and *WNT2B* on known differentiation markers

Genes known to be involved in the commitment of human MSC were analysed in MSC with enforced expression of *WNT2* and *WNT2B*, cultured under standard MSC cell culture conditions (section 2.1.6), using real-time PCR (figures 3.14 and 3.15). Interestingly, the expression profiles of MSC with enforced *WNT2* and *WNT2B* were very similar. Transcript levels of *TWIST-1*, osteopontin and *PPARγ2*, a potent stimulator of adipogenesis, were all statistically significantly ($p<0.05$, paired students t-test) downregulated > 2 fold in MSC with enforced expression of *WNT2* or *WNT2B* while adipsin was statistically significantly upregulated. As it acts as part of a tightly controlled negative feedback loop, *AXIN2* is commonly used as conformation that the canonical Wnt pathway is activated (Dao et al., 2007; Lustig et al., 2002). *AXIN2* expression was statistically significantly ($p<0.05$, paired students t-test) upregulated > 2 fold in MSC with enforced expression of *WNT2* but not *WNT2B* thus confirming canonical Wnt pathway stimulation in *WNT2* overexpressing MSC. While the expression of *COL2* remained unchanged

Figure 3.12 - Flow Cytometric Analysis of *WNT2* overexpressing MSC (A) Representative histograms of cell surface marker *STRO-1* expression in iG2 control MSC verses *WNT2* overexpressing MSC. Solid histograms represent the expression of test markers and open histograms show the expression of negative isotype controls. **(B)** Cell surface expression of MSC and non-MSC markers iG2 control MSC verses *WNT2* overexpressing MSC. The data is presented as the median value of percentage of cells positive for the selected markers for the four cell ines tested.

(A)

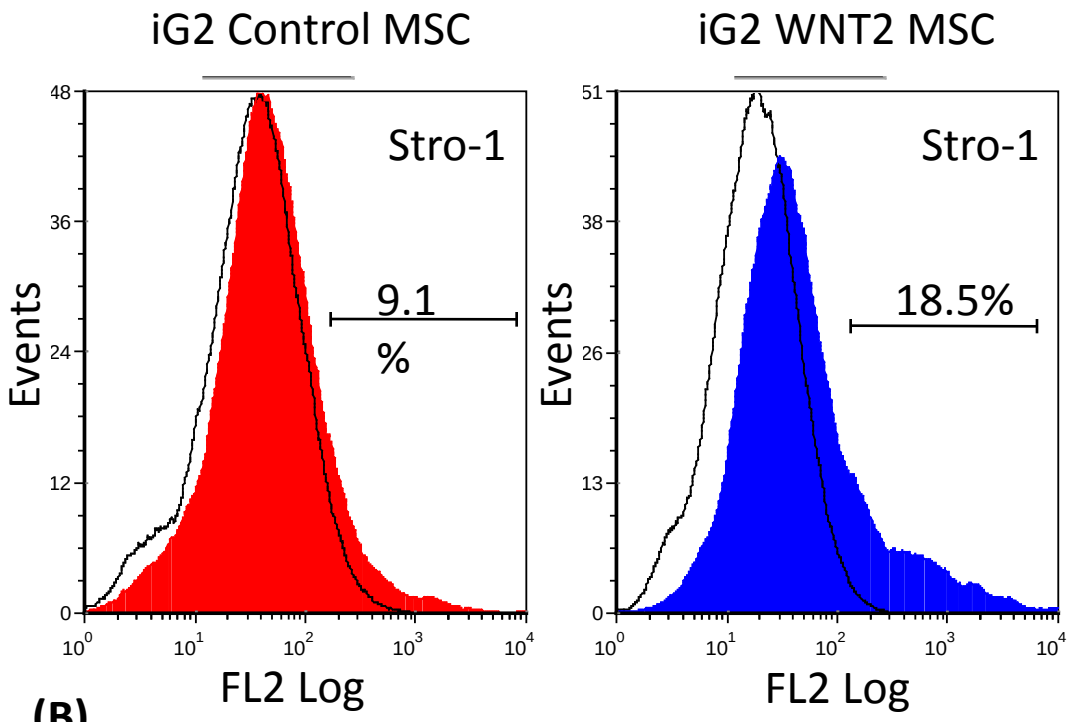

(B)

	iG2		Wnt2	
Antibody	Median (%)	Range (%)	Median (%)	Range (%)
STRO-1	9.3	± 3.1	15.1	± 5.7
CD146	16.4	± 7.7	32.8	± 13.0
B478	5.9	± 2.7	3.1	± 1.6
CD166	77.1	± 7.8	92.4	± 3.9
CD105	88.5	± 3.6	94.8	± 1.5
CD90	98.9	± 0.3	99.5	± 0.2
CD73	82.3	± 9.7	95.8	± 1.7
CD45	0.7	± 0.2	0.7	± 0.3
CD34	0.7	± 0.1	0.7	± 0.4
CD14	0.9	± 0.3	0.8	± 0.5

Figure 3.13 – Flow Cytometric Analysis of *WNT2B* overexpressing MSC **(A)** Representative histograms of cell surface marker STRO-1 expression in iG2 control MSC verses *WNT2B* overexpressing MSC. Solid histograms represent the expression of test markers and open histograms show the expression of negative isotype controls. **(B)** Cell surface expression of MSC and non-MSC markers iG2 control MSC verses *WNT2B* overexpressing MSC. The data is presented as the median value of percentage of cells positive for the selected markers for the four cell lines tested.

(A)

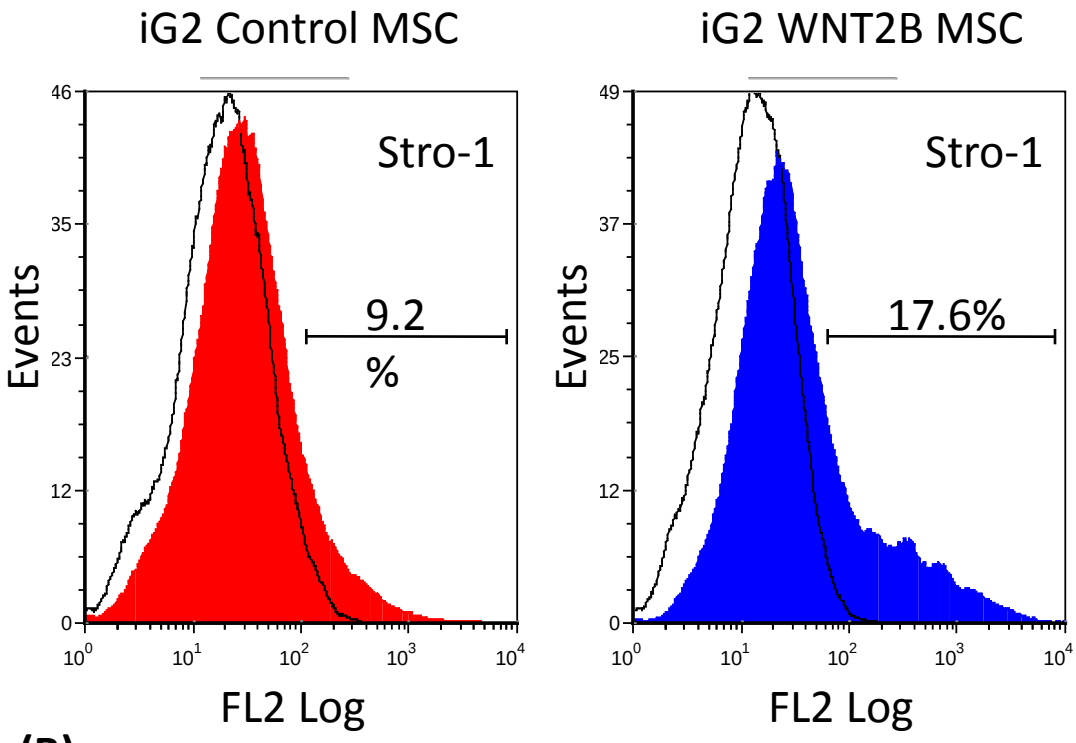

(B)

	iG2		Wnt2B	
Antibody	Median (%)	Range (%)	Median (%)	Range (%)
STRO-1	9.3	± 3.1	15.7	± 4.2
CD146	16.4	± 7.7	39.7	± 14.8
B478	5.9	± 2.7	7.2	± 3.3
CD166	77.1	± 7.8	93.7	± 2.8
CD105	88.5	± 3.6	94.8	± 2.1
CD90	98.9	± 0.3	99.0	± 0.4
CD73	82.3	± 9.7	95.4	± 2.2
CD45	0.7	± 0.2	1.0	± 0.6
CD34	0.7	± 0.1	1.0	± 0.5
CD14	0.9	± 0.3	1.1	± 0.6

Figure 3.14 – RNA expression profile of *WNT2* overexpressing MSC in normal media. Real-time PCR analysis of genes involved in adipogenssis, osteogenseis and chondrogenesis. Statistically significant ($n = 3$) ($p < 0.05$, unpaired t-test) results when compared to GFP control cell line denoted by (*).

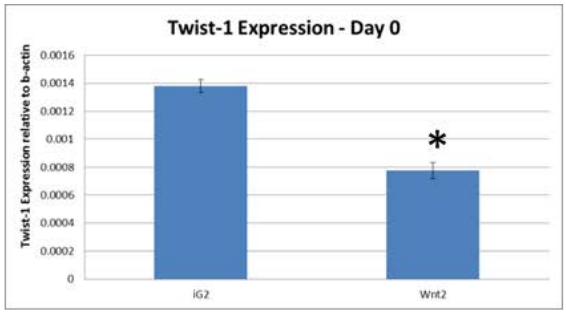
Twist-1 Expression - Day 0
Twist-1 Expression relative to b-actin
0.0016
0.0014
0.0012
0.001
0.0008
0.0006
0.0004
0.0002
0
*
iG2
Wnt2

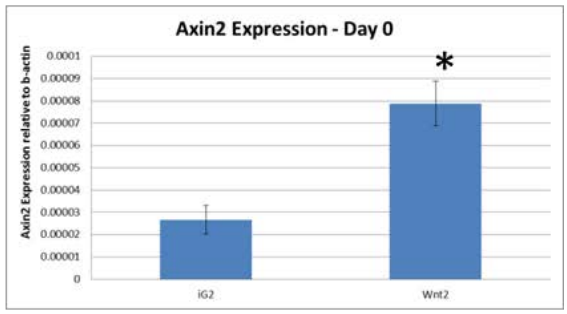
Axin2 Expression - Day 0
Axin2 Expression relative to b-actin
0.0001
0.00009
0.00008
0.00007
0.00006
0.00005
0.00004
0.00003
0.00002
0.00001
0
*
iG2
Wnt2


Runx2 Expression - Day 0
Runx2 Expression relative to b-actin
0.0016
0.0014
0.0012
0.001
0.0008
0.0006
0.0004
0.0002
0
iG2
Wnt2

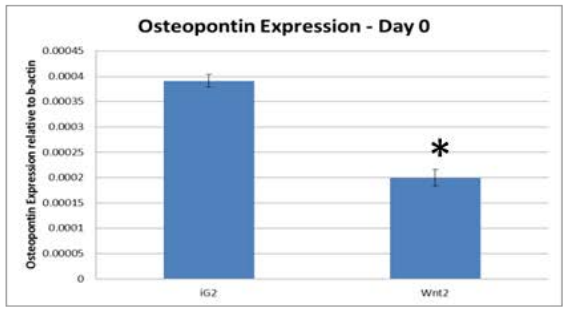
Osteopontin Expression - Day 0
Osteopontin Expression relative to b-actin
0.00045
0.0004
0.00035
0.0003
0.00025
0.0002
0.00015
0.0001
0.00005
0
*
iG2
Wnt2

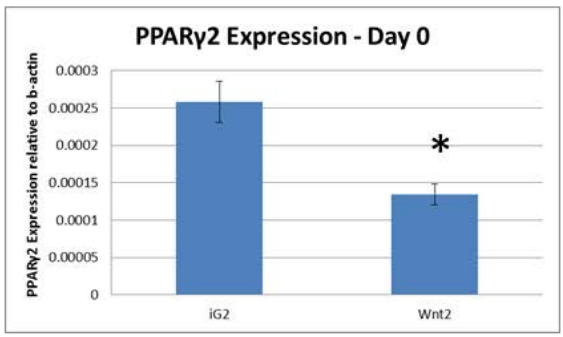
PPARγ2 Expression - Day 0
PPARγ2 Expression relative to b-actin
0.0003
0.00025
0.0002
0.00015
0.0001
0.00005
0
*
iG2
Wnt2

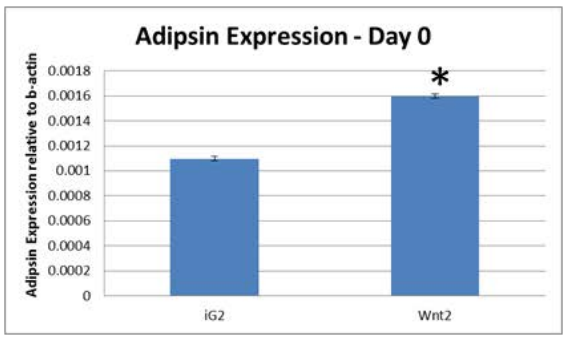
Adipsin Expression - Day 0
Adipsin Expression relative to b-actin
0.0018
0.0016
0.0014
0.0012
0.001
0.0008
0.0006
0.0004
0.0002
0
*
iG2
Wnt2

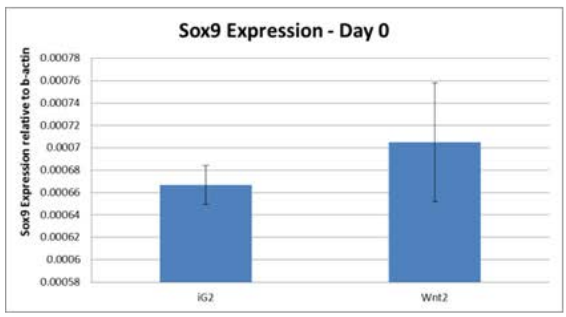
Sox9 Expression - Day 0
Sox9 Expression relative to b-actin
0.00078
0.00076
0.00074
0.00072
0.0007
0.00068
0.00066
0.00064
0.00062
0.0006
0.00058
iG2
Wnt2

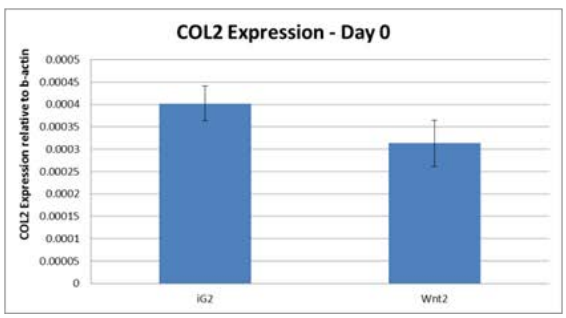
COL2 Expression - Day 0
COL2 Expression relative to b-actin
0.0005
0.00045
0.0004
0.00035
0.0003
0.00025
0.0002
0.00015
0.0001
0.00005
0
iG2
Wnt2

Figure 3.15 – RNA expression profile of *WNT2B* overexpressing MSC in normal media. Real-time PCR analysis of genes involved in adipogenssis, osteogenseis and chondrogenesis. Statistically significant ($n = 3$) ($p < 0.05$, unpaired t-test) results when compared to GFP control cell line denoted by (*).

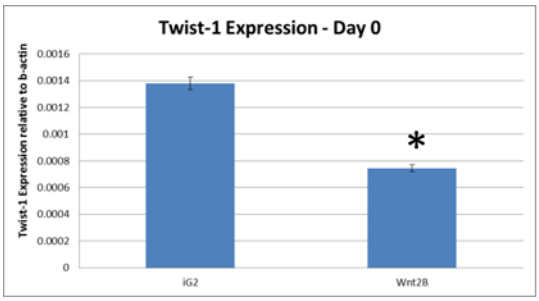
Twist-1 Expression - Day 0
Twist-1 Expression relative to b-actin
0.0016
0.0014
0.0012
0.001
0.0008
0.0006
0.0004
0.0002
0
*
iG2
Wnt2B

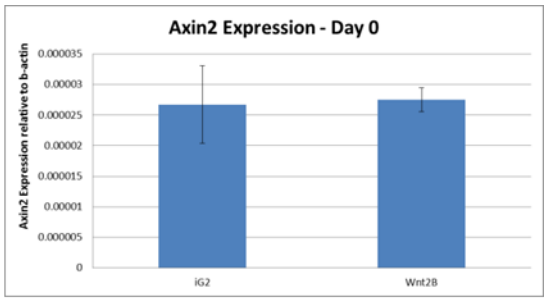
Axin2 Expression - Day 0
Axin2 Expression relative to b-actin
0.000035
0.00003
0.000025
0.00002
0.000015
0.00001
0.000005
0
iG2
Wnt2B


Runx2 Expression - Day 0
Runx2 Expression relative to b-actin
0.0014
0.0012
0.001
0.0008
0.0006
0.0004
0.0002
0
iG2
Wnt2B

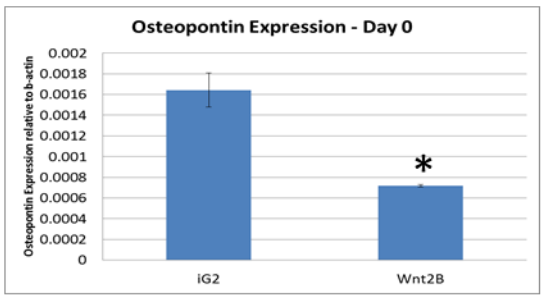
Osteopontin Expression - Day 0
Osteopontin Expression relative to b-actin
0.002
0.0018
0.0016
0.0014
0.0012
0.001
0.0008
0.0006
0.0004
0.0002
0
*
iG2
Wnt2B

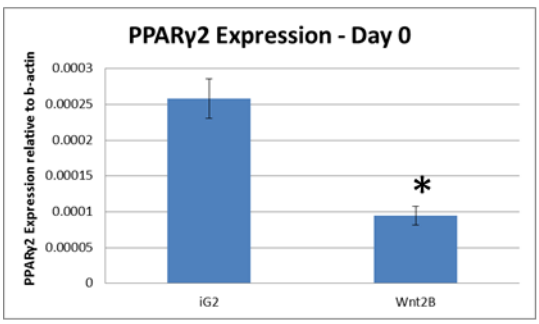
PPARγ2 Expression - Day 0
PPARγ2 Expression relative to b-actin
0.0003
0.00025
0.0002
0.00015
0.0001
0.00005
0
*
iG2
Wnt2B

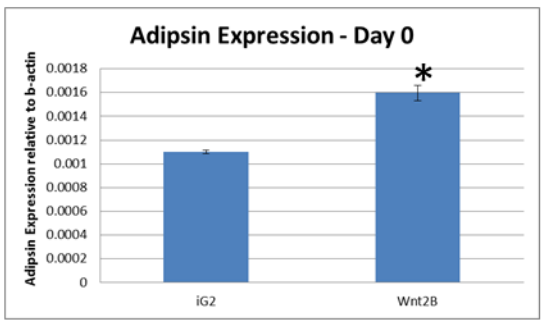
Adipsin Expression - Day 0
Adipsin Expression relative to b-actin
0.0018
0.0016
0.0014
0.0012
0.001
0.0008
0.0006
0.0004
0.0002
0
*
iG2
Wnt2B

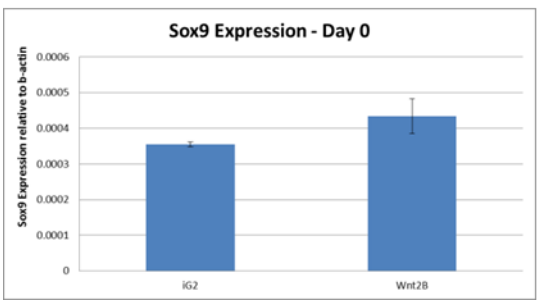
Sox9 Expression - Day 0
Sox9 Expression relative to b-actin
0.0006
0.0005
0.0004
0.0003
0.0002
0.0001
0
iG2
Wnt2B

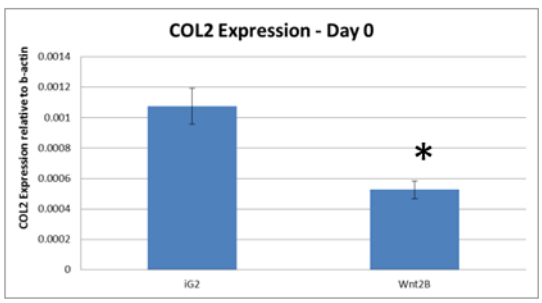
COL2 Expression - Day 0
COL2 Expression relative to b-actin
0.0014
0.0012
0.001
0.0008
0.0006
0.0004
0.0002
0
*
iG2
Wnt2B

in MSC overexpressing *WNT2,* it was statistically significantly ($p < 0.05$, paired students t-test) downregulated > 2 fold in *WNT2B* overexpressing MSC. The expression of master regulators *RUNX2,* osteogenesis, and *SOX9,* chondrogenesis, remained unchanged when comparing *WNT2* and *WNT2B* overexpressing MSC to control MSC.

3.2.9 *WNT2* overexpression had no effect on MSC multi-differentiation

The osteogenic, adipogenic and chondrogenic potential of *WNT2* overexpressing MSC were examined using methods described in section 2.2. The purpose of these studies was to elucidate the mechanisms utilised by *TWIST-1* to block the osteogenic and chondrogenic differentiation potential and enhance the adipogenic differentiation potential of MSC. Expression of osteogenic related gene *RUNX2* was statistically significantly ($p<0.05$, paired students t-test) upregulated in MSC with enforced expression of *WNT2,* after 28 days of cell culture in osteoinductive media, while osteogenic related gene osteopontin was statistically significantly downregulated (figure 3.16). As measured by calcium concentration relative to DNA concentration, the level of mineralization did not change between *WNT2* overexpressing and control MSC after 28 days of cell culture in osteoinductive media. Expression of adipogenic related genes adipsin and *PPARγ2* were both statistically significantly ($p<0.05$, paired students t-test) downregulated, fold change > 3, in MSC with enforced expression of *WNT2* after 28 days of cell culture in adipogenic induction media (figure 3.17). However, adipogenesis, measured by enumerating the relative number of nile red positive adipocytes per 10000 cells, remained unchanged between *WNT2* overexpressing and control MSC after 28 days of cell culture in adipogenic induction media. Histological analysis (figure 3.18) of pelletised MSC cultured in chondrogenic induction media showed that both MSC overexpressing *WNT2* and control MSC had the capacity to undergo chondrogenesis *in vitro*. After 28 days of cell culture in chondrogenic induction media the

Figure 3.16 - *WNT2* overexpression does not affect osteogenesis in hMSC **(A)** Alizarin Red staining of Control and *WNT2* populations cultured under inductive osteogenic conditions identified the presence of mineral nodules at 21 days. **(B)** Real-time PCR analysis of osteogenic markers *RUNX2* and osteopontin. **(C)** Calcium levels normalized to DNA concentration at 21 and 28 days post addition of inductive media. Comparing *WNT2* to control cell lines. Statistically significant ($n = 3$) ($p < 0.05$, unpaired t-test) results when compared to GFP control cell line denoted by (*).

(A)

21 Days

IG2

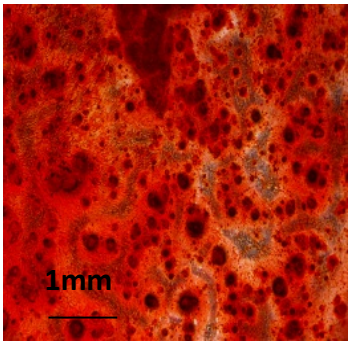

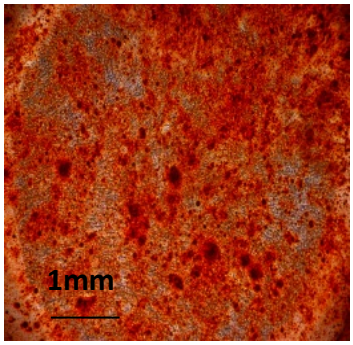

Wnt2

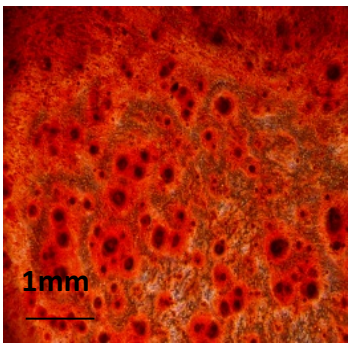

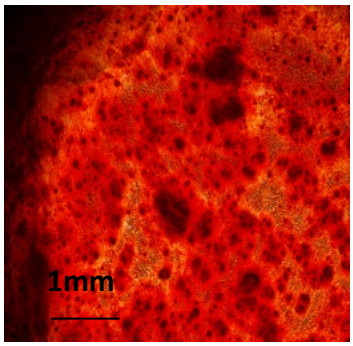

Donor 1 Donor 2

(B)

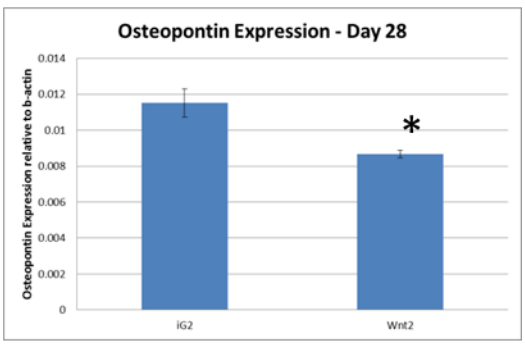

(C)

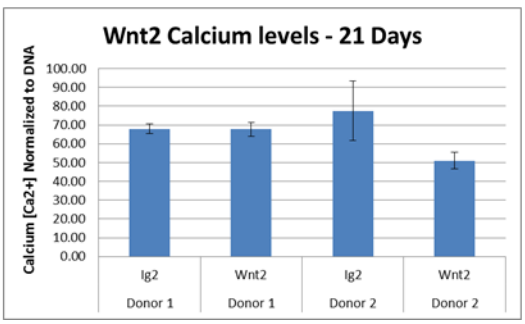

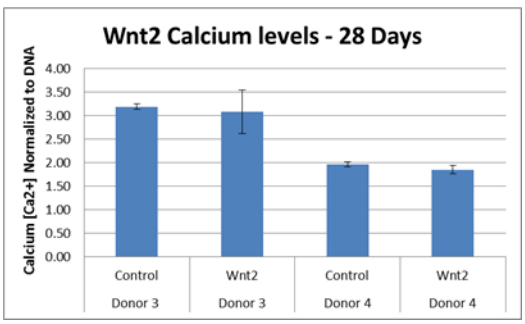

Figure 3.17 - *WNT2* overexpression does not affect adipogenesis in hMSC **(A)** Oil Red O staining of Control and *WNT2* populations cultured under inductive adipogenic conditions identified the presence of lipid globules at 28 days. **(B)** Real time PCR analysis of adipogenic markers adipsin and *PPRγ2*. **(C)** Adipocytes per 10000 cells at 28 days post addition of adipogenic inductive media comparing *WNT2* to control cell lines. Enumerated using Nile Red and Dapi Staining. Statistically significant ($n = 3$) ($p < 0.05$, unpaired t-test) results when compared to GFP control cell line denoted by (*).

(A)

IG2

Wnt2

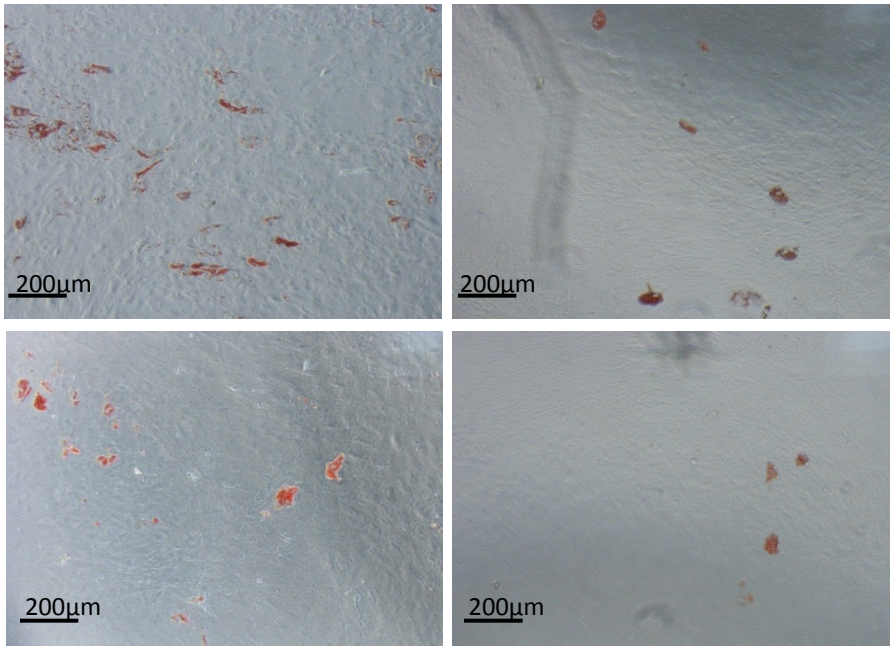

Donor 1 Donor 2

(B)

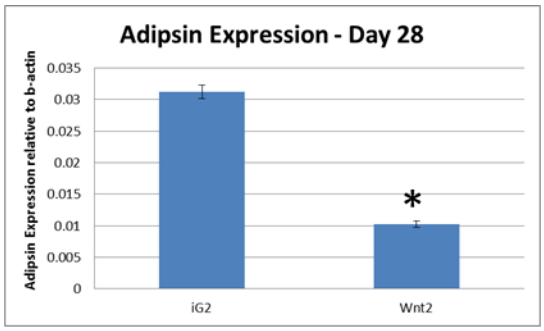

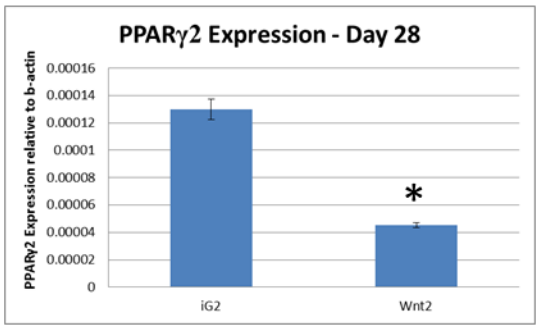

(C)

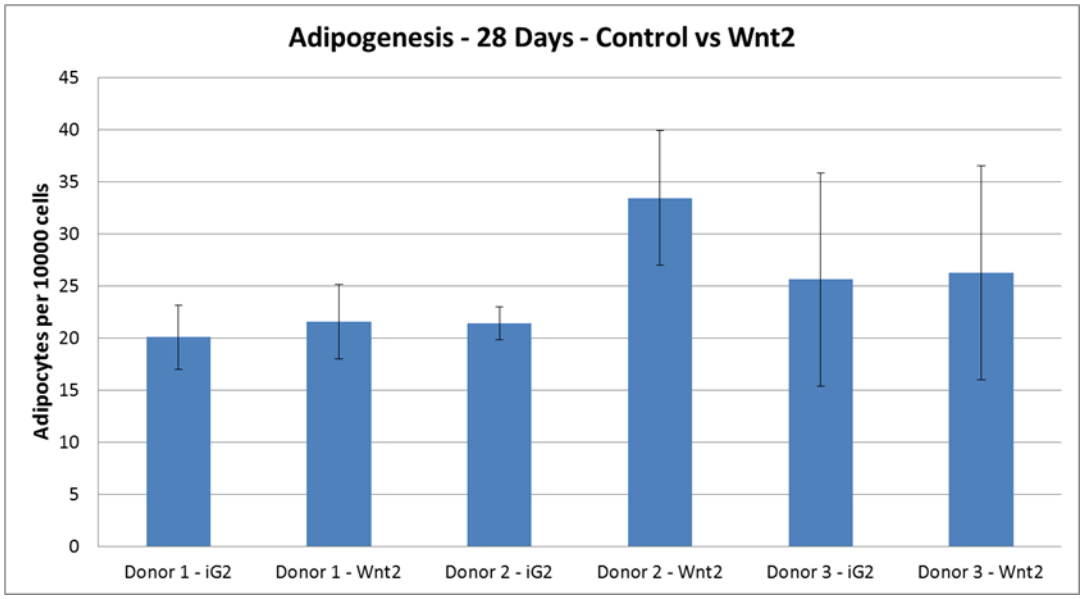

Figure 3.18 - *WNT2* overexpression does not affect adipogenesis in hMSC **(A)** Oil Red O staining of Control and *WNT2* populations cultured under inductive adipogenic conditions identified the presence of lipid globules at 28 days. **(B)** Real time PCR analysis of adipogenic markers adipsin and *PPRγ2*. **(C)** Adipocytes per 10000 cells at 28 days post addition of adipogenic inductive media comparing *WNT2* to control cell lines. Donor 3 not statistically significant. Enumerated using Nile Red and Dapi Staining. Statistically significant ($n = 3$) ($p < 0.05$, unpaired t-test) results when compared to GFP control cell line denoted by (*).

(A)

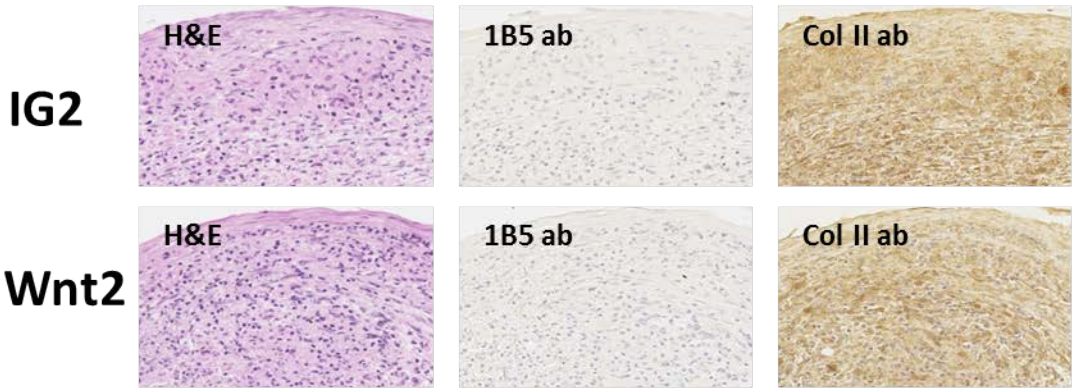
IG2
H&E
1B5 ab
Col II ab
Wnt2
H&E
1B5 ab
Col II ab

(B)

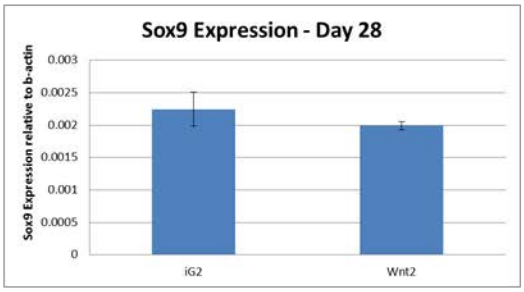
Sox9 Expression - Day 28
Sox9 Expression relative to b-actin
0.003
0.0025
0.002
0.0015
0.001
0.0005
0
iG2
Wnt2

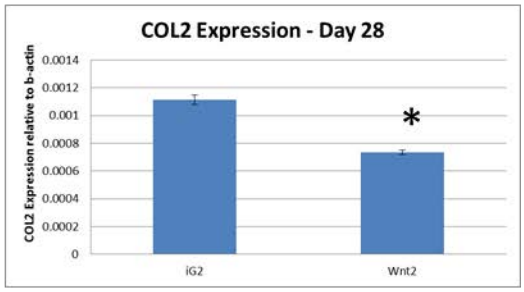
COL2 Expression - Day 28
COL2 Expression relative to b-actin
0.0014
0.0012
0.001
0.0008
0.0006
0.0004
0.0002
0
*
iG2
Wnt2

(C)

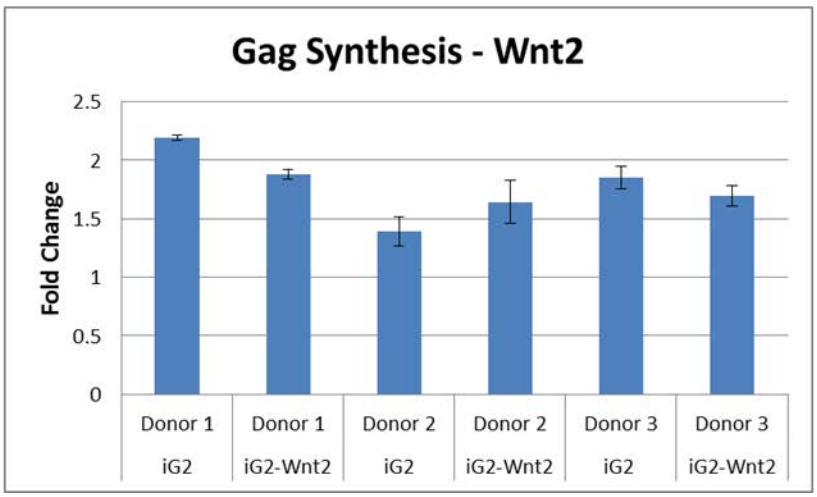
Gag Synthesis - Wnt2
Fold Change
2.5
2
1.5
1
0.5
0
Donor 1 iG2
Donor 1 iG2-Wnt2
Donor 2 iG2
Donor 2 iG2-Wnt2
Donor 3 iG2
Donor 3 iG2-Wnt2

expression of chondrogenic related gene *SOX9* remained unchanged between *WNT2* overexpressing MSC and control MSC while *COL2* expression was statistically significantly ($p<0.05$, paired students t-test) decreased in *WNT2* overexpressing MSC. The chondrogenic potential of *WNT2* overexpressing MSC and control MSC was quantitated, by measuring glycosaminoglycan synthesis following stimulation with chondrogenic inductive media for 28 days, and no differences were observed between *WNT2* overexpressing MSC and control MSC. Together, these results demonstrated that overexpression of *WNT2* did not significantly affect the differentiation of MSC towards the osteogenic, chondrogenic or adipogenic lineage.

3.2.10 *WNT2B* overexpression enhanced adipogenesis of MSC but did not affect osteogenesis or chondrogenesis

Using methods described in section 2.2, the osteogenic, adipogenic and chondrogenic potential of *WNT2B* overexpressing MSCs were examined. Expression of osteogenic related gene *RUNX2* was unchanged in MSC with enforced expression of *WNT2B* after 28 days of cell culture in osteoinductive media, while osteogenic related gene osteopontin was statistically significantly downregulated (figure 3.19). The level of mineralization was measured by quantitating calcium concentration relative to DNA concentration. There was no change in relative calcium levels between *WNT2B* overexpressing and control MSC after 28 days of cell culture in osteoinductive media. Expression of adipogenic related gene adipsin (figure 3.20) was not significantly different after 28 days of cell culture in adipogenic induction media while the expression of *PPARγ2* was statistically significantly ($p<0.05$, paired students t-test) upregulated in MSC with enforced expression of *WNT2B*. Adipogenesis was measured by enumerating the relative number of nile red positive adipocytes per 10000 cells and statistically significant ($p<0.05$, paired students t-test) stimulation of adipogenesis was observed in two of three donors overexpressing *WNT2B* after 28

Figure 3.19 - *WNT2B* overexpression does not affect osteogenesis in hMSC **(A)** Alizarin Red staining of Control and *WNT2B* populations cultured under inductive osteogenic conditions identified the presence of mineral nodules at 21 days. **(B)** Real-time PCR analysis of osteogenic markers *RUNX2* and osteopontin. **(C)** Calcium levels normalized to DNA concentration at 21 and 28 days post addition of inductive media. Comparing *WNT2B* to control cell lines. Statistically significant ($n = 3$) ($p < 0.05$, unpaired t-test) results when compared to GFP control cell line denoted by (*).

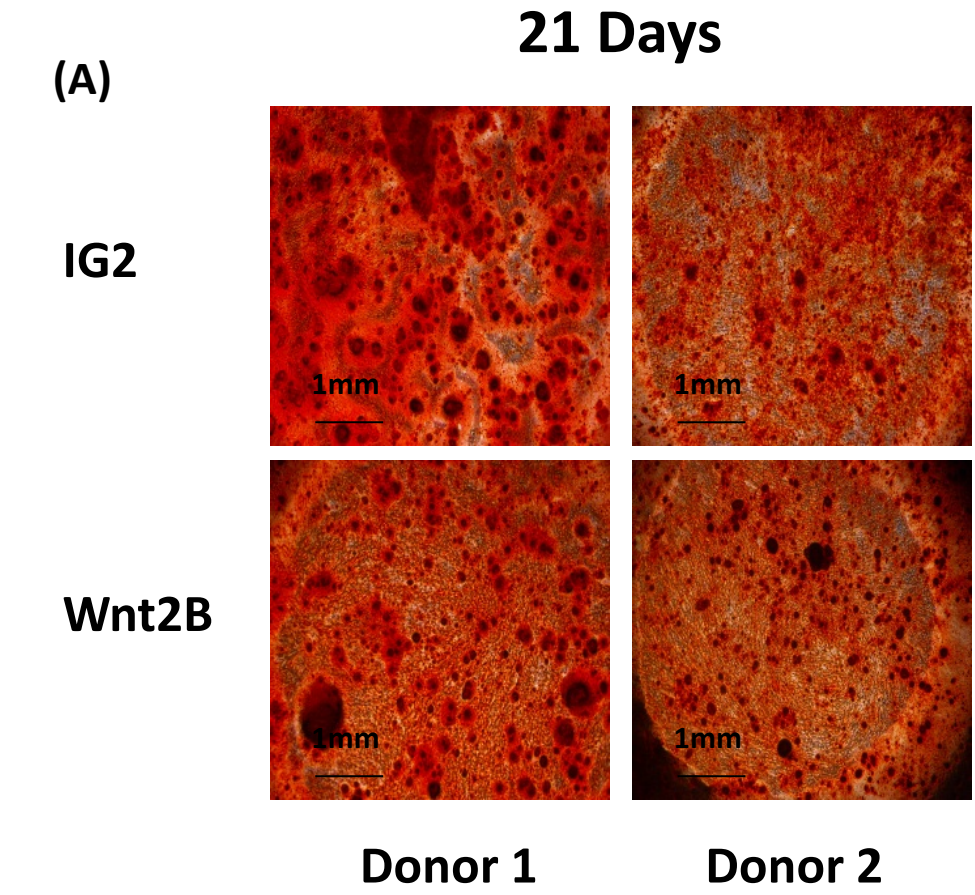
21 Days
(A)
IG2
Wnt2B
1mm
1mm
1mm
1mm
Donor 1
Donor 2

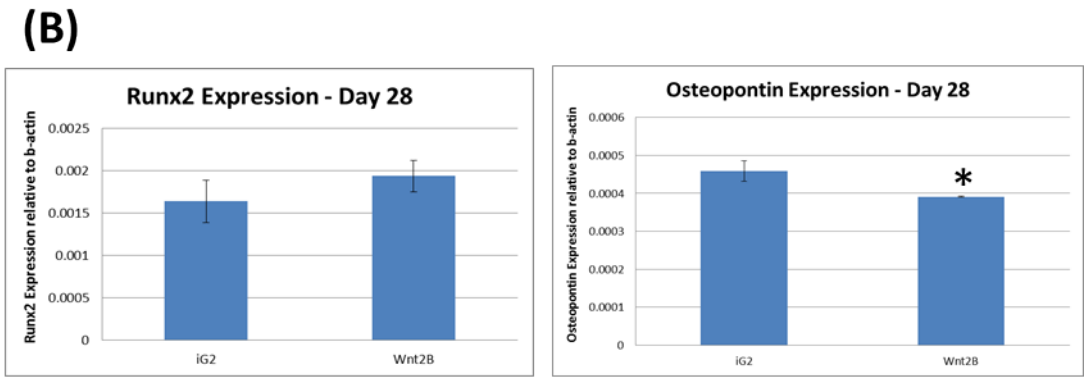
(B)
Runx2 Expression - Day 28
Runx2 Expression relative to b-actin
0.0025
0.002
0.0015
0.001
0.0005
0
iG2
Wnt2B
Osteopontin Expression - Day 28
Osteopontin Expression relative to b-actin
0.0006
0.0005
0.0004
0.0003
0.0002
0.0001
0
*
iG2
Wnt2B

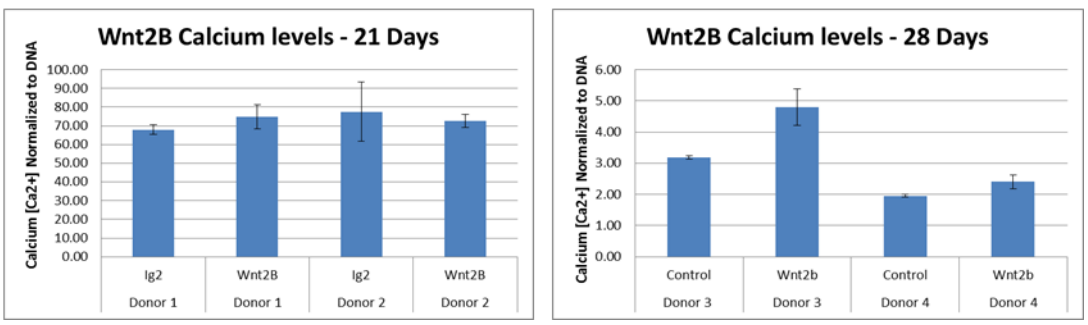
(C)
Wnt2B Calcium levels - 21 Days
Calcium [Ca2+] Normalized to DNA
100.00
90.00
80.00
70.00
60.00
50.00
40.00
30.00
20.00
10.00
0.00
Ig2 Donor 1
Wnt2B Donor 1
Ig2 Donor 2
Wnt2B Donor 2
Wnt2B Calcium levels - 28 Days
Calcium [Ca2+] Normalized to DNA
6.00
5.00
4.00
3.00
2.00
1.00
0.00
Control Donor 3
Wnt2b Donor 3
Control Donor 4
Wnt2b Donor 4

Figure 3.20 - *WNT2B* overexpression increases the adipogenic potential of MSC (A) Oil Red O staining of Control and *WNT2B* populations cultured under inductive adipogenic conditions identified the presence of lipid globules at 28 days. **(B)** Real time PCR analysis of adipogenic markers adipsin and *PPRγ2*. **(C)** Adipocytes per 10000 cells at 28 days post addition of adipogenic inductive media comparing *WNT2B* to control cell lines. Enumerated using Nile Red and Dapi Staining. Donors 1 and 2 showed statistically significant increases in the relative number of adipocytes. Donor 3 followed the same trend but with larger error between samples. Statistically significant ($n = 3$) ($p < 0.05$, unpaired t-test) results when compared to GFP control cell line denoted by (*).

(A)

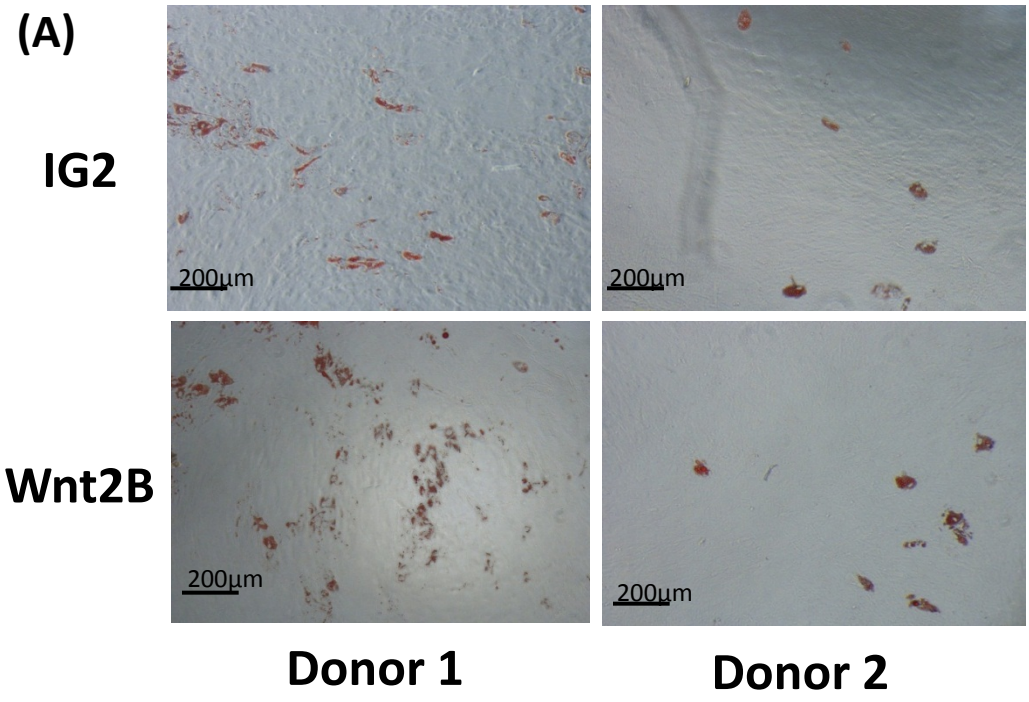
IG2
Wnt2B
200µm
200µm
200µm
200µm
Donor 1
Donor 2

(B)

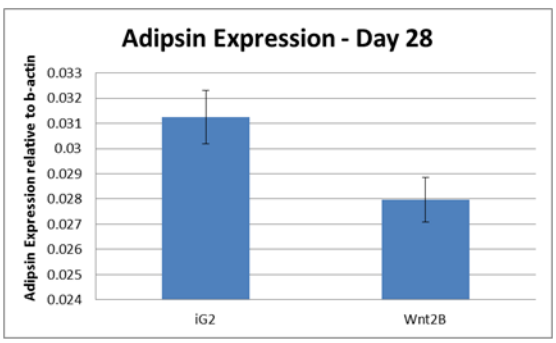
Adipsin Expression - Day 28
Adipsin Expression relative to b-actin
0.033
0.032
0.031
0.03
0.029
0.028
0.027
0.026
0.025
0.024
iG2
Wnt2B

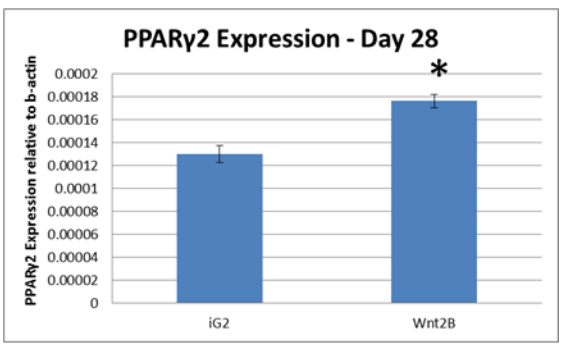
PPARγ2 Expression - Day 28
PPARγ2 Expression relative to b-actin
0.0002
0.00018
0.00016
0.00014
0.00012
0.0001
0.00008
0.00006
0.00004
0.00002
0
*
iG2
Wnt2B

(C)

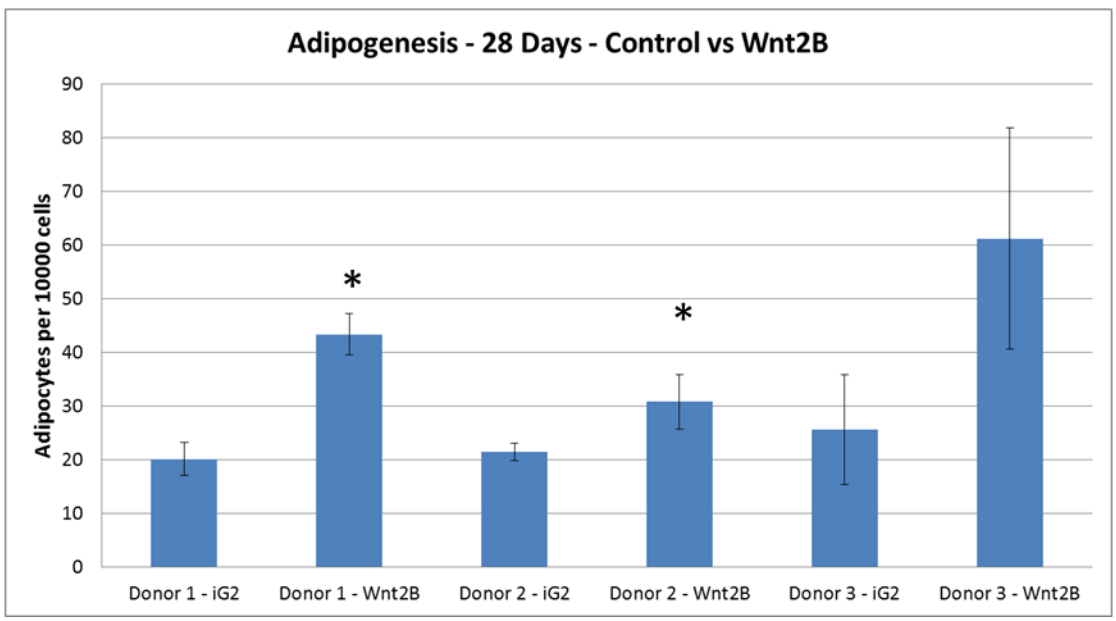
Adipogenesis - 28 Days - Control vs Wnt2B
Adipocytes per 10000 cells
90
80
70
60
50
40
30
20
10
0
*
*
Donor 1 - iG2
Donor 1 - Wnt2B
Donor 2 - iG2
Donor 2 - Wnt2B
Donor 3 - iG2
Donor 3 - Wnt2B

days of cell culture in adipogenic induction media. The third donor, although not statistically significant ($p = 0.1$, paired students t-test), followed the same trend of enhanced adipogenesis in MSC with enforced *WNT2B* expression. Histological analysis (figure 3.21) of pelletised MSC cultured in chondrogenic induction media for 28 days showed that both MSC overexpressing *WNT2B* and control MSC had the capacity to undergo chondrogenesis *in vitro*. After 28 days of cell culture in chondrogenic induction media the expression of chondrogenic related genes *SOX9* and *COL2* was statistically significantly ($p<0.05$, paired students t-test) upregulated (> 4 fold and > 2 fold respectively) in *WNT2B* overexpressing MSC. By measuring glycosaminoglycan synthesis following stimulation with chondrogenic inductive media for 28 days, the chondrogenic potential of *WNT2B* overexpressing MSC and control MSC was quantitated and compared. There were no statistically significant ($p<0.05$, paired students t-test) differences in the chondrogenic potential of *WNT2B* overexpressing MSC and control MSC. Together, these results demonstrated that overexpression of *WNT2B* did not significantly affect the differentiation of MSC towards the osteogenic or chondrogenic lineage but enhanced the adipogenic potential of MSC.

3.2.11 MSC proliferation and senescence are not impacted by enforced expression of *WNT2* or *WNT2B*

Examination of the proliferative potential of MSC overexpressing *WNT2* or *WNT2B* was assessed by enumerating population doublings as described in section 2.2.1. Population doubling data was generated from four *WNT2* and *WNT2B* overexpressing MSC lines and averaged. There were no statistically significant ($p<0.05$, paired students t-test) differences between the proliferation of control MSC when compared to MSC overexpressing *WNT2* or *WNT2B* (figures 3.22 and 3.23). As *TWIST-1* plays a significant role in prolonging the in vitro lifespan of MSC, cellular senescence of MSC overexpressing *WNT2* or *WNT2B* was quantified using the the β-

Figure 3.21 – *WNT2B* overexpression does not affect chondrogenesis in hMSC (A) Chondrogenic differentiation potential was assessed by immunohistochemical staining of chondrocyte pellets with anti-collagen type II antibody. All cell lines showed the capacity to differentiate into cells of chondrogenic lineage under inductive conditions. Images at 40x magnification. **(B)** Real time PCR analysis of chondrogenic markers *SOX9* and *COL2*. **(C)** Glycosaminoglycan synthesis was measured and normalized to DNA content per well following induction with chondrogenic inductive media. The data represents the chondrogenic potential of overexpressing MSC compared to their relative controls. Statistically significant ($n = 3$) ($p < 0.05$, unpaired t-test) results when compared to GFP control cell line denoted by (*).

(A)

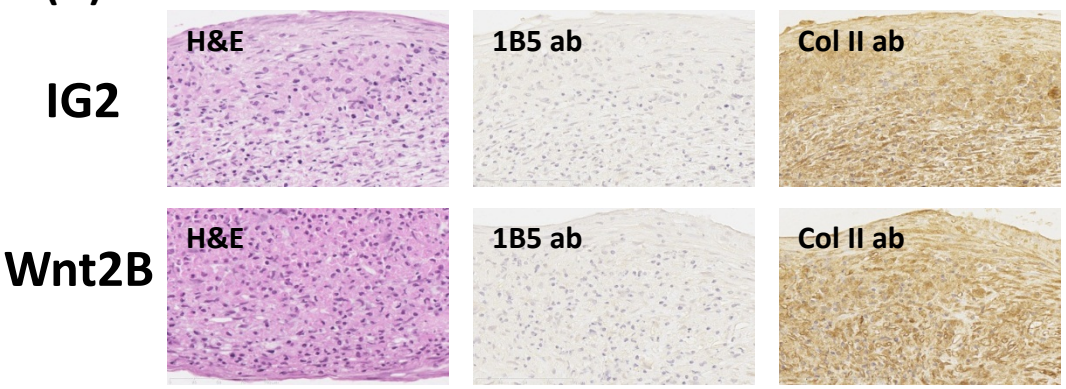
IG2
H&E
1B5 ab
Col II ab
Wnt2B
H&E
1B5 ab
Col II ab

(B)

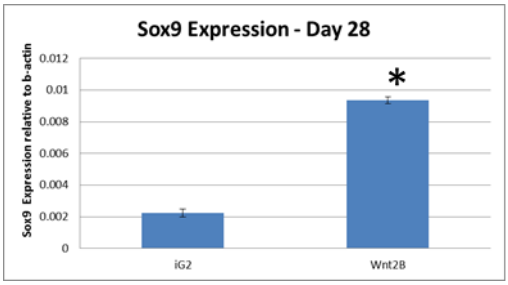
Sox9 Expression - Day 28
Sox9 Expression relative to b-actin
0.012
0.01
0.008
0.006
0.004
0.002
0
*
iG2
Wnt2B

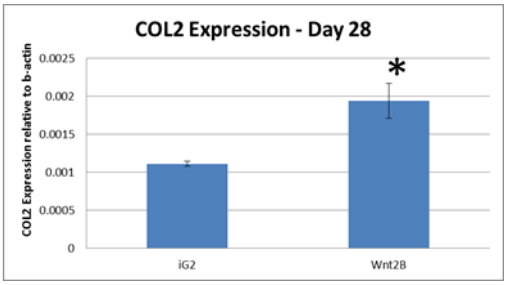
COL2 Expression - Day 28
COL2 Expression relative to b-actin
0.0025
0.002
0.0015
0.001
0.0005
0
*
iG2
Wnt2B

(C)

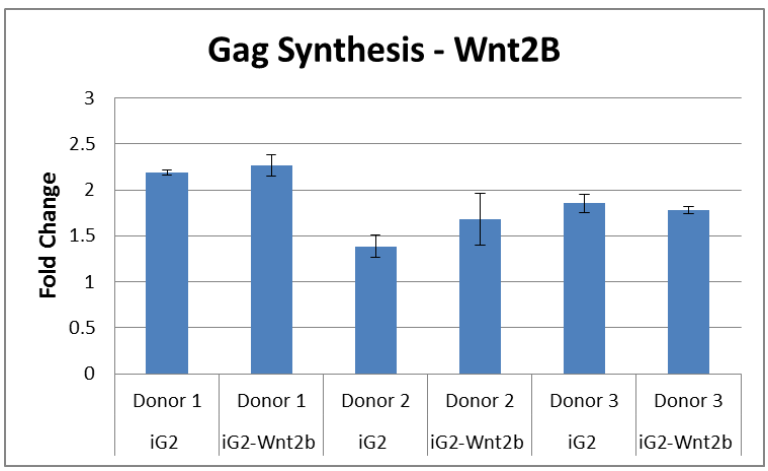
Gag Synthesis - Wnt2B
Fold Change
3
2.5
2
1.5
1
0.5
0
Donor 1 iG2
Donor 1 iG2-Wnt2b
Donor 2 iG2
Donor 2 iG2-Wnt2b
Donor 3 iG2
Donor 3 iG2-Wnt2b

Figure 3.22 – *WNT2* overexpression does not affect proliferation or senescence in hMSC (A) Population doublings demonstrated no change in the proliferation potential of *WNT2* overexpressing MSC compared to control cells. **(B)** Cellular senescence, measured by the percentage of x gal positive cells. Statistically significant ($n = 3$) ($p < 0.05$, unpaired t-test) results when compared to GFP control cell line denoted by (*).

(A)

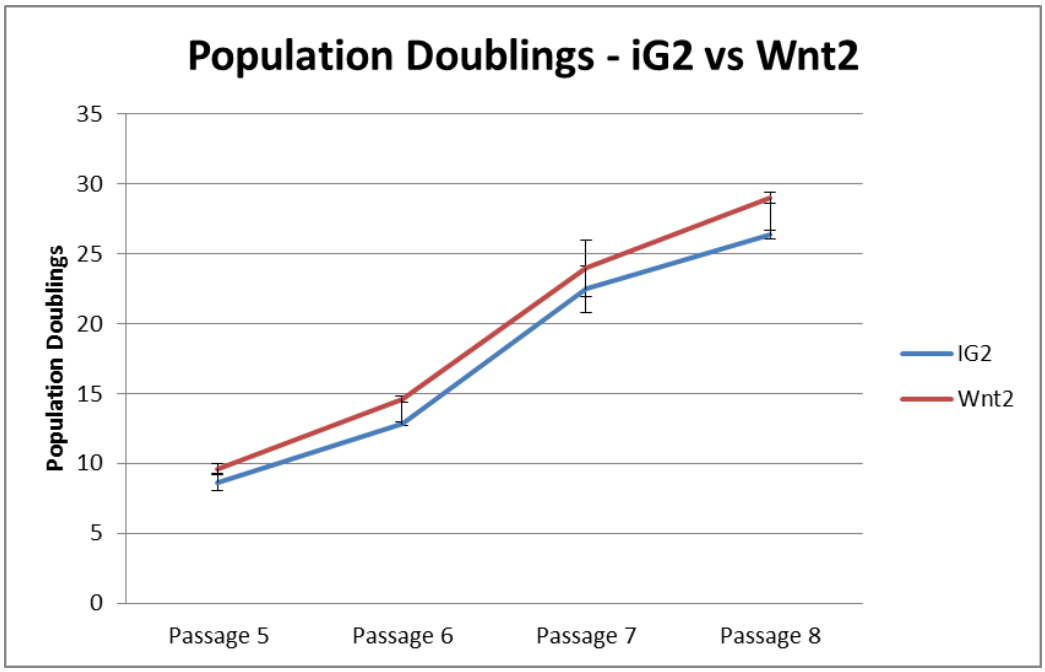
Population Doublings - iG2 vs Wnt2
Population Doublings
35
30
25
20
15
10
5
0
Passage 5
Passage 6
Passage 7
Passage 8
IG2
Wnt2

(B)

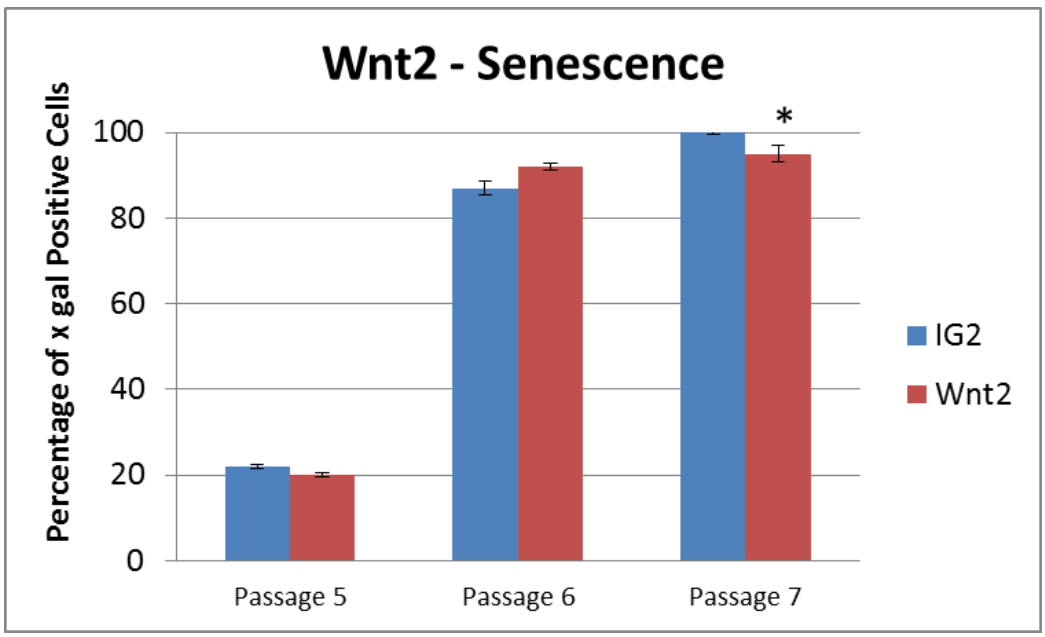
Wnt2 - Senescence
Percentage of x gal Positive Cells
100
80
60
40
20
0
*
Passage 5
Passage 6
Passage 7
IG2
Wnt2

Figure 3.23 – *WNT2B* overexpression does not affect proliferation or senescence in hMSC (A) Population doublings demonstrated no change in the proliferation potential of *WNT2B* overexpressing MSC compared to control cells. **(B)** Cellular senescence, measured by the percentage of x gal positive cells. Statistically significant Statistically significant ($n = 3$) ($p < 0.05$, unpaired t-test) results when compared to GFP control cell line denoted by (*).

(A)

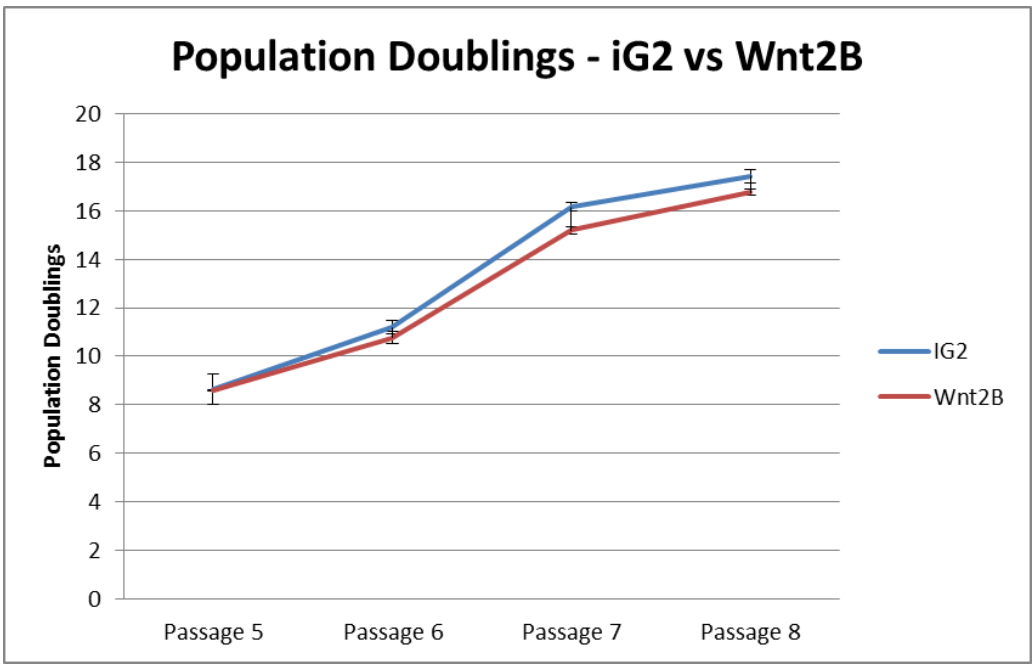
Population Doublings - iG2 vs Wnt2B
Population Doublings
20
18
16
14
12
10
8
6
4
2
0
Passage 5
Passage 6
Passage 7
Passage 8
IG2
Wnt2B

(B)

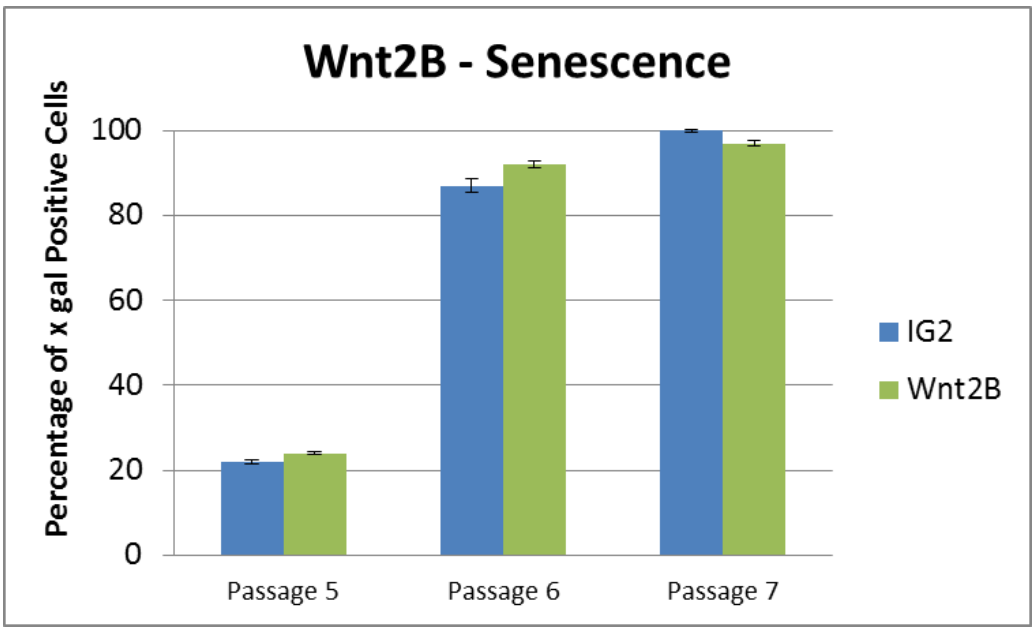
Wnt2B - Senescence
Percentage of x gal Positive Cells
100
80
60
40
20
0
Passage 5
Passage 6
Passage 7
IG2
Wnt2B

galactosidase staining kit described in section 2.2.2. Results showed that *WNT2* and *WNT2B* do not play a significant role in the senescence of MSCs (figures 3.22 and 3.23).

3.3 Discussion

Identified by the analysis of microarray data comparing *TWIST-1* overexpressing MSC to control MSC (Section 3.2.1), Wnt pathway genes, *WNT2* and *WNT2B* were shown to be upregulated in the presence of enforced *TWIST-1* expression. *WNT2* and *WNT2B* have been shown to be stimulators of canonical Wnt signalling and redundancy between the two molecules has been demonstrated in animal models (Goss et al., 2009; Tsukiyama and Yamaguchi, 2012). Using western blot analysis of protein lysates from *TWIST-1* overexpressing MSC we were able to demonstrate that enforced expression of *TWIST-1* led to elevated levels of activated β-catenin indicating canonical Wnt pathway stimulation, which was supported by elevated levels of *AXIN2* gene expression, a known target of Wnt signalling (Dao et al., 2007) (section 3.2.3).

Previous studies have highlighted the importance of the canonical Wnt pathway on the regulation of MSC differentiation providing evidence for pro-osteoblastic and chondrogenic activity with enhanced Wnt pathway signalling while negatively regulating adipogenesis (Gaur et al., 2005; Kawai et al., 2007; Ross et al., 2000; Zhou et al., 2008; Zhou et al., 2004). In contrast to these findings other groups have suggested that Wnt signalling inhibits osteogenic differentiation of MSC (de Boer et al., 2004). More recently investigators have proposed that Wnt signalling can both stimulate and repress MSC osteogenic differentiation and that there is a canonical Wnt signalling gradient involved in regulating the osteogenic differentiation of MSC *in vivo* (Liu et al., 2009). Supporting studies that demonstrated repression of osteogenic differentiation, MSC overexpressing *TWIST-1* generated in our laboratory were restricted in their capacity to differentiate towards the osteoblastic and chondrogenic lineages while pro-adipogenic properties were noted in the presence of enhanced Wnt pathway stimulation verified by elevated levels of β-catenin (Isenmann et al., 2009) and (section 3.2.3).

While there is less known about *WNT2* and *WNT2B* specifically, with regards to their role in the fate of human MSC, previous reports have demonstrated that purified *WNT2* recombinant protein stimulates the canonical Wnt pathway (Sousa et al., 2010). Our findings provide evidence for the regulation of both *WNT2* and *WNT2B* by *TWIST-1* through direct interactions (Section 3.2.5), and hence, show that *TWIST-1* is involved directly in the regulation of the canonical Wnt pathway. A negative regulator of the canonical Wnt signalling pathway, *AXIN2*, has been shown to regulate Wnt signalling through binding to *LRP5* and is itself controlled by a negative feedback loop mediated by Wnt/β-catenin/Tcf signalling (Jho et al., 2002; Mao et al., 2001). By analysis of *AXIN2* upregulation to confirm Wnt pathway stimulation, our findings show that enforced *WNT2* expression resulted in stimulation of the canonical Wnt pathway, while enforced *WNT2B* expression did not (Section 3.2.8).

Our results show no change in the function of *WNT2* overexpressing MSC when assessed in differentiation and proliferation assays (Sections 3.2.9 and 3.2.11). *WNT2* expression has been shown to be involved in the regulation of proliferation of neuronal progenitors and fibroblasts and in the differentiation of cardiac myocytes (Onizuka et al., 2012; Salazar et al., 2009; Sousa et al., 2010). The role of *WNT2* in human MSC has been investigated and Matushansky et al. treated MSC with PoAb-WNT2 to show that early markers of mesenchymal differentiation were not expressed in treated cells (Matushansky et al., 2007). This was correlated with data showing that *DKK1* inhibits the commitment to differentiation of MSC via *WNT2*. By investigating the expression level of *WNT2* during adipogenesis, Shen et al. were able to show that canonical Wnt signalling inhibits adipogenesis in adult human MSC derived from the bone marrow (Shen et al., 2011). Together these data illustrate the complex nature of the regulation of MSC through canonical Wnt signalling. It is clear that Wnt signalling does play some role in the proliferation and commitment of certain cellular populations, however, in contrast to others who have

investigated the effect of canonical Wnt pathway stimulation on MSC populations, our findings, assessing the role of *WNT2* specifically, show no statistically significant differences in the proliferation, differentiation or commitment of MSC. These results support the view that the role of the Wnt pathway in MSC regulation is due to a gradient effect, most likely involving different specific elements of the pathway (Dao et al., 2007).

Using ChIP analysis of the proximal promoter of *WNT2B*, our results provide evidence for direct binding of *TWIST-1* within the first 1kb of this promoter correlating with *in silico* analysis that identified a preferential *TWIST-1* binding site within the first 1kb of the *WNT2B* promoter (Section 3.2.5). However, statistically significant upregulation of luciferase expression was not observed when using the 1kb proximal promoter fragment (Section 3.2.4). This could be due to a second binding site within the 2kb fragment that is required for correct folding of promoter DNA and subsequent transcriptional activation. To demonstrate this, mutation studies directed towards the CANNTG sites within the *WNT2B* 2kb promoter fragment would need to be conducted. I would expect mutations directed towards the CATATG site within this 2kb fragment to result in suppressed activation of the luciferase reporter. When assessing the effect of *WNT2B* overexpression in MSC our results show no changes in the proliferation or chondrogenic / osteogenic differentiation of MSC, but provide evidence for enhanced adipogenesis. These findings are in contrast to those providing evidence for pro-osteoblastic and chondrogenic activity with enhanced Wnt pathway signalling while negatively regulating adipogenesis (Gaur et al., 2005; Kawai et al., 2007; Ross et al., 2000; Zhou et al., 2008; Zhou et al., 2004). However, these studies were investigating the function of MSC based on canonical Wnt pathway regulation and our results did not show elevated levels of *AXIN2* in *WNT2B* overexpressing MSC indicating that the Wnt pathway was not stimulated via the same mechanism as observed in *WNT2* overexpressing MSC. To investigate this further it would be interesting to target *WNT2B*

mediated signalling in *TWIST-1* overexpressing cells. Since there are currently no chemical methods to target *WNT2B* specifically, it may be necessary to inhibit *WNT2B* using siRNA/shRNA mediated knockdown methodologies in control and *TWIST-1* overexpressing MSC lines described above.

Our results provide evidence for the role of *WNT2B* in the stimulation of adipogenesis in MSC but do not further explain the role of *TWIST-1* within the context of MSC proliferation or osteogenic / chondrogenic differentiation. Several other genes identified in the microarray analysis described in section 3.2.1 and in a previous report (Isenmann et al., 2009) have been implicated in the regulation of MSC, including BMP2, *BMP4*, *TGFβ2*, *SMAD6*, and *AXIN2*. It has been demonstrated that the bone morphogenetic protein *BMP2* acts as a regulatory signal required for osteoblast differentiation (Piek et al., 2010; Young et al., 2005). The bone morphogenetic protein *BMP4* has been demonstrated to be important in the commitment of MSC to the adipogenic lineage (Ahrens et al., 1993; Bowers et al., 2006). Conversely, other studies have shown *BMP4* to be osteoinductive when present at elevated levels in MSC (Lavery et al., 2008). This data correlates with our previous investigations demonstrating downregulation of *BMP2* (Isenmann et al., 2009) and, more recently, *BMP4* (section 3.2.1) with enforced *TWIST-1* expression resulting in a reduced capacity of MSC to undergo osteogenesis. Furthermore, our group has demonstrated that enforced expression of *TWIST-1* in MSC forces the cells to preferentially favour adipogenic differentiation (Isenmann et al., 2009). The phenotype of *TGFβ2* knockout mice has been described and includes a number of non-craniofacial skeletal abnormalities including limb, rib and spinal defects (Sanford et al., 1997). Demonstrating the importance of *SMAD6*, Wang et al. were able to show *BMP2* mediated *SMAD6* gene activation through the transcription factor *RUNX2 (Wang et al., 2007)*. Further to this, *SMAD6* has been implicated directly in the regulation of osteogenic differentiation of MSC by mediating down

regulation of *RUNX2* (Fan et al., 2012). These results support the findings of our microarray study which revealed *TWIST-1* mediated upregulation of *SMAD6*, where Fan et al. demonstrate recovery of *RUNX2* expression and the osteoblastic potential of MSC with silencing of *SMAD6*. Together this data correlates with pathways identified by previous work from our laboratory investigating the effect of *TWIST-1* overexpression on MSC (Isenmann et al., 2009).

Transcription of *AXIN2* was demonstrated to be upregulated in the presence of *TWIST-1* overexpression in MSC (section 3.2.2) and, as direct interactions between *TWIST-1* and *AXIN2* have not been investigated, studies investigating these interactions could provide insight into the mechanism of action of *TWIST-1* within the Wnt pathway as the elevated levels observed could be the result of negative feedback or direct interactions with *TWIST-1* (Kikuchi, 1999). Further investigations determining whether *TWIST-1* has a direct role in *BMP2*, *BMP4*, *TGFβ2* and *SMAD6* gene regulation using similar methods to those used in this chapter, could provide important insights into the mechanism of action of *TWIST-1* on the proliferation, differentiation and commitment of MSC.

4 Heterozygous *TWIST-1*$^{+/-}$ mutant mice display enhanced osteoblastic differentiation and accelerated long bone fracture repair

4.1 Introduction

Fracture repair is a complex process involving a number of cellular interactions and biochemical reactions. This process is described in detail below and outlined in figure 4.1. By gaining an understanding of the molecular elements of fracture healing it may be possible to provide targeted treatment, decreased healing times and improved clinical outcomes.

At the time of injury, bleeding from the periosteum and soft tissues surrounding the fracture site results in the formation of a localized haematoma (Michael L. Voight, 2006). This causes an acute inflammatory response that acts as a source of haematopoietic cells to help clear the site of damaged tissue and cellular debris (Ozaki et al., 2000). Cytokines (GM-CFS, M-CFS, and VEGF), chemokines (CCL-2, CXCL-12 and CXCL-8) and interleukin molecules (IL-4, IL-6 and IL-10), are secreted at the fracture site and these factors regulate the migration, proliferation and differentiation of haematopoietic and mesenchymal stem cells (Alblowi et al., 2012; Einhorn et al., 1995; Keramaris et al., 2008). Furthermore, many of these factors have angiogenic and vasculogenic properties and ensure the maintenance of an appropriate blood supply to facilitate the ingress of haematopoietic cells and MSC to the injury site (Webb and Tricker, 2000).

The next major step in the fracture healing process is callus formation which occurs via two different processes at two distinct sites. The first involves woven bone being deposited distally in relation to the fracture site, beneath the periosteum. This bone is produced by osteoprogenitor cells via a process termed intramembranous ossification (Marsh, 1998). The second area of callus formation occurs directly over the fracture site, via a process termed endochondral ossification.

Figure 4.1 - Fracture healing. (A) Haematoma (tissue damage and bleeding followed by inflammation, weeks 1-2 (B) Callus (removal of dead bone by osteoclasts and infiltration of chondroblasts to form cartilage that eventually unites the fracture (C) This is slowly replaced by woven bone, weeks 2-6 (D) Consolidation (transformation of woven bone into solid lamellar bone bridging the fracture, 6-12 weeks (E) Remodelling (new lamellar bone formed is remodelled to resemble normal structure, >12weeks). Adapted from (Apley A.G., 1997).

This process forms a soft cartilaginous callus which bridges the fracture. The cartilage matrix forms following recruitment of skeletal progenitors attracted to the fracture site from the surrounding bone marrow and periosteum, which develop into committed cartilage producing cells, chondrocytes. Recently, these cells have been identified as being alpha-smooth muscle actin (*α-SMA*) positive cells that reside in the bone marrow, perivascular niche and periosteum (Grcevic et al., 2012; Kalajzic et al., 2008), this marker is also associated with MSC (Gronthos et al JCS 2003; Shi and Gronthos JBMR 2003). These studies identified an immature $\alpha\text{-}SMA^{+}$ cell population that developed into mature osteoblasts, providing direct evidence for terminal differentiation *in vivo.* They were also able to demonstrate the cells capacity to undergo osteogenesis, adipogenesis and chondrogenesis *in vitro*.

The next stage of the fracture healing process is remodelling. Following repair at the fracture site the calcified cartilage matrix is remodelled after being degraded by chondroclasts, providing an area in which the site for bone forming osteoblasts can synthesise a collagen based extracellular matrix (osteoid) which is then mineralised to form woven bone structures (Einhorn, 1998; Sherwood, 2004). Over time, the immature woven bone is remodelled by bone resorbing osteoclasts and bone forming osteoblasts which form mature lamellar bone capable of supporting mechanical loading (SONG and TUAN, 2004).

Fracture healing is one of the most complete repair processes in the human body as it occurs via mechanisms that allow for reconstitution of the injured tissue without scaring (McKibbin, 1978). However, over 20% of fractures are associated with healing difficulties whereby the natural repair processes are inadequate and result in a fracture that is not completely repaired (Lopez, 2009). In these cases surgical intervention using plates, nails, screws, pins and bone grafts is necessary (Linda J. Vorvick, 2010). It is for these reasons that fracture repair has been of major

interest as a candidate for cellular based therapies. A pioneering study in 2000 demonstrated a significant improvement in the repair of critical-size tibial defects in a sheep model using culture-expanded osteoprogenitor cells in conjunction with a hydroxyapatite carrier (Kon et al., 2000). More recently, studies investigating the safety and efficacy of allogeneic mesenchymal precursor cells in the repair of critical-size segmental defects in sheep, using a hydroxyapatite-tricalcium phosphate-collagen matrix as the carrier, have demonstrated enhanced healing related to early bone formation in treatment groups (Field et al., 2011; Zannettino, 2006). Together these results demonstrate the efficacy of new protocols combining traditional surgical intervention techniques with a bioscaffold seeded with MSC. The use of MSC is now a clinical reality with the Australian Therapeutic Goods Administration (TGA) recently issuing a licence to Mesoblast Pty Ltd to commercially manufacture and distribute patient specific or autologous adult stem cell products making these products available to hospitals and clinicians across Australia. The purpose of the following research is to better understand the molecular mechanisms that regulate MSC to allow for genetic manipulation of autologous cells for cellular based therapies or chemical targeting in order to regulate specific genes to influence the behaviour of cells and aid the natural process of fracture repair.

The fracture healing process in *TWIST-1*$^{+/-}$ mice was compared to that of homozygous littermate controls (Twist $^{+/+}$). Analysis of process of fracture healing was assessed by μCT imaging, X-ray analyses and mechanical testing. Analysis at the cellular level was performed using histological methods including; Safranin O, haematoxylin and eosin, tartrate-resistant acid phosphatase (TRAP) and Von Kossa staining to examine cartilage, fibrous and bone tissue as well as enumeration of osteoblasts and osteoclasts within samples. Furthermore, the incidence and osteogenic commitment of CFU-F populations was assessed for both fractured and contralateral non-fractured limbs.

4.2 Results

4.3 Pilot Study assessing the viability of internal fracture stabilization with a carbon rod

A pilot study was performed to assess the viability of using carbon rods for internal fixation of fractured femora using normal C57BL/6 mice. It was proposed that the advantage of using carbon over steel fixation was to enable imaging of live mice without interfering with the X-ray signal or having to sacrifice the animals to remove the internal fixation device prior to imaging. The use of a carbon rod for fixation also allowed histological analysis using methyl methacrylate as, an advantage over the current protocol which only allows for the use of paraffin embedding limbs for histological analysis.

4.3.1 Carbon rod does not interfere with X-ray imaging

Two of the principal methods of analysis for a fracture model are X-ray and micro CT analysis. Therefore, a major issue concerning the use of steel rod based internal fixation devices concerns the refractory properties of X-rays. Specifically, the use of steel as an internal fixation device prevents the use of mice in live imaging as the device must be removed prior to imaging due to interference (figure 4.2). This poses implications for animal usage as replicate animals at each time point of the longitudinal study need to be included and each animal must be sacrificed to remove the steel internal fixation from the femora before imaging. To address this issue, an alternate carbon material with the same diameter (0.5mm) as the steel pin was inserted into the bone cavity and assessed in parallel studies. We found that when carbon was used as the internal fixation device its density was sufficiently low to prevent the diffraction of X-rays resulting in clear imaging of the bone fracture site during live scanning (figure 4.2), reducing the number of mice required for analysis. Of note, no mice out of the 18 animals that received carbon rod

Figure 4.2 – Internal carbon rod does not interfere with X-Ray image. (A) An X-ray of a mouse at the time of surgery (left) and the same mouse two weeks post-surgery. The internal fixation device (steel needle) has dislodged and the fracture is no longer supported. **(B)** Shows the difference between the X-ray image generated using a steel needle (left) verses a carbon rod (right). Both images are taken directly after surgery. **(C)** Shows a mouse at the time of surgery with a visible fracture in the right femur (left) and the same mouse at 8 weeks post surgery where fracture healing can be seen clearly (right). Using a carbon rod as the internal fixation device gives a much clearer image using X-ray.

(A)

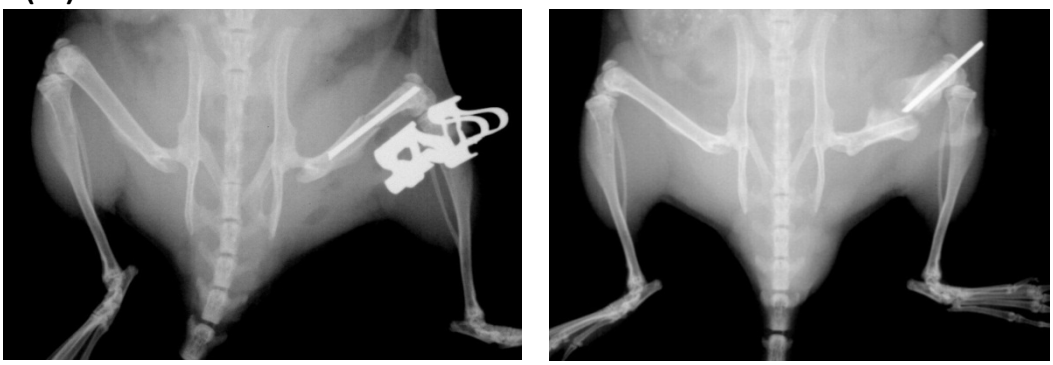

(B)

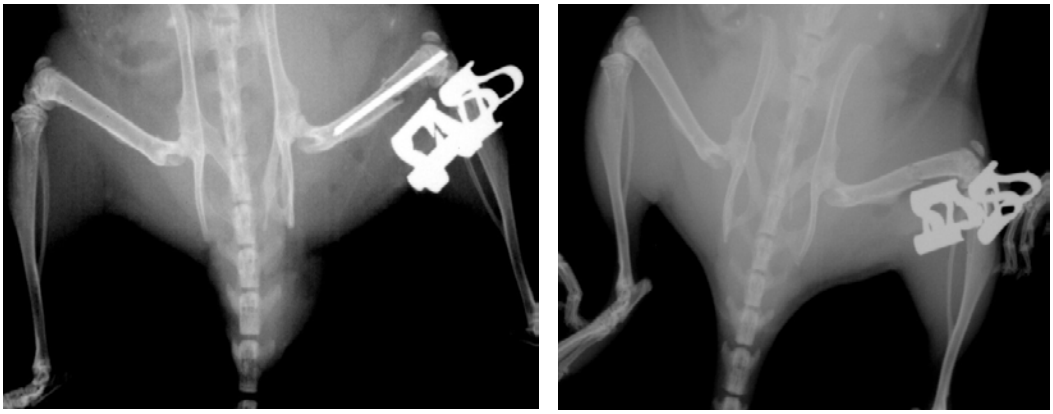

(C)

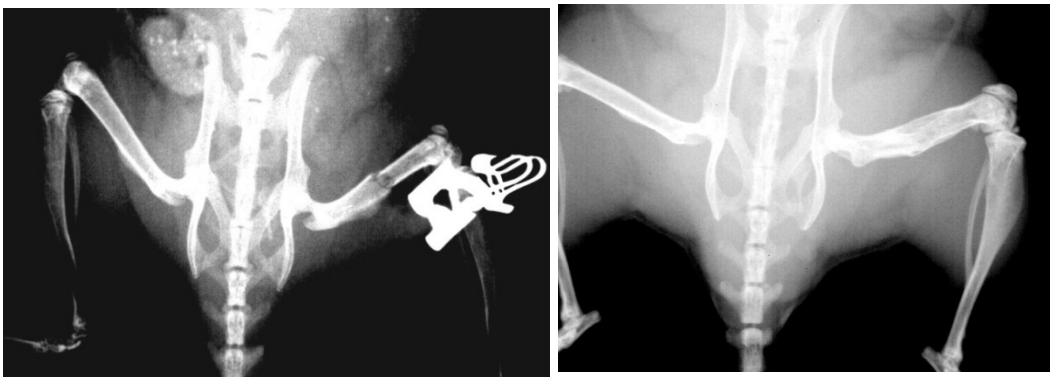

internal fixation exhibited any post-surgery complications. In contrast, the steel internal fixation device was found to dislodge back through the knee cap in 4 out of 18 mice. Importantly, bone gene expression levels that are known to increase during fracture healing compared to the normal contralateral limbs were unaffected by the presence of carbon rods compared to steel pins (figure 4.3). Therefore, the use of carbon rods was found to be a superior alternative to steel pins for stabilizing femoral fractures in mice and allowing for live imaging.

4.3.1.1 . Analysis of the Heterozygous Twist$^{+/-}$ Phenotype

The mice used in the following studies were back crossed to seven generations onto a pure C57BL/6 background until mice displayed the phenotype reported by Bourgeois et al. (Bourgeois et al., 1998). The following images generated by μCT imaging demonstrate the differences between the skull of a wild type C57BL/6 mouse and a heterozygous *TWIST*$^{+/-}$ mouse. Increases in bone volume of the skulls of *TWIST*$^{+/-}$ mice when compared to WT littermate controls was observed as well as fusion of coronal sutures (figure 4.4 and 4.5). The *TWIST-1*$^{+/-}$ mice were polydactyl which presented as an extra digit on one or both hind feet (figure 4.6). A small percentage of *TWIST-1*$^{+/-}$ mice had malocclusion and smaller in overall body size when compared to their WT littermate controls (data not shown). Using μCT and histomorphometric analysis there were no differences between the non-fractured femora of WT and *TWIST-1*$^{+/-}$ mice at one week post fracture (figure 4.7).

Figure 4.3 – Gene expression is comparable between fractures stabilized with carbon or steel. Bone Gene Expression for early bone transcription factor (*RUNX2*) and osteoblast markers (bone sialoprotein and alkaline phosphatase) in normal limbs left (L) and corresponding fractured limbs right (R) after four weeks post fracture n=3 animals. No statistically significant differences were observed when comparing steel fracture / carbon fracture ($n = 4$) ($p < 0.05$, ANOVA with Tukey's post test).


RUNX2 Expression
Expression relative to β-actin
0
1
2
3
4
5
6
Left - Runx2 - Carbon
Right - Runx2 - Carbon
Left - Runx2 - Steel
Right - Runx2 - Steel

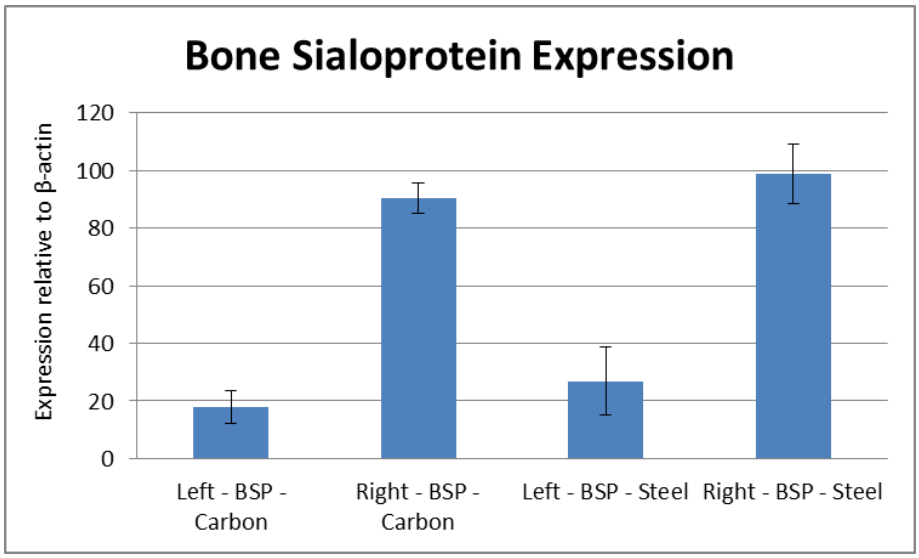
Bone Sialoprotein Expression
Expression relative to β-actin
0
20
40
60
80
100
120
Left - BSP - Carbon
Right - BSP - Carbon
Left - BSP - Steel
Right - BSP - Steel

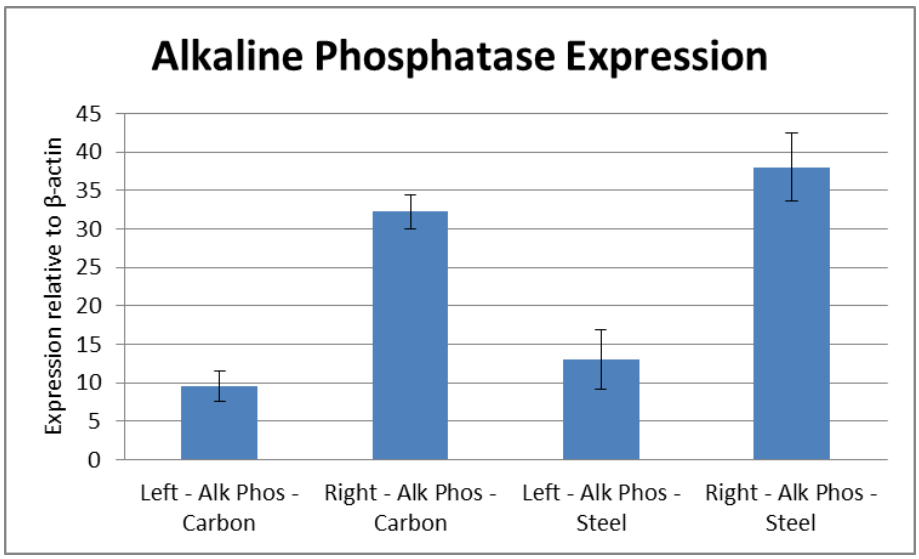
Alkaline Phosphatase Expression
Expression relative to β-actin
0
5
10
15
20
25
30
35
40
45
Left - Alk Phos - Carbon
Right - Alk Phos - Carbon
Left - Alk Phos - Steel
Right - Alk Phos - Steel

Figure 4.4 – *TWIST-1*$^{+/-}$ animals display a skull phenotype of increased bone density and rounded skulls. This lateral view of the mouse skull demonstrates the differences between WT mice (top) and *TWIST-1*$^{+/-}$ Het mice (bottom). The *TWIST-1*$^{+/-}$ Het mice have increased bone density and a slightly rounded skull when compared to the flat skull of the WT. This can be attributed to pre-fusion of cranial sutures reminiscent of craniosynostosis observed in humans with *TWIST-1* mutations.

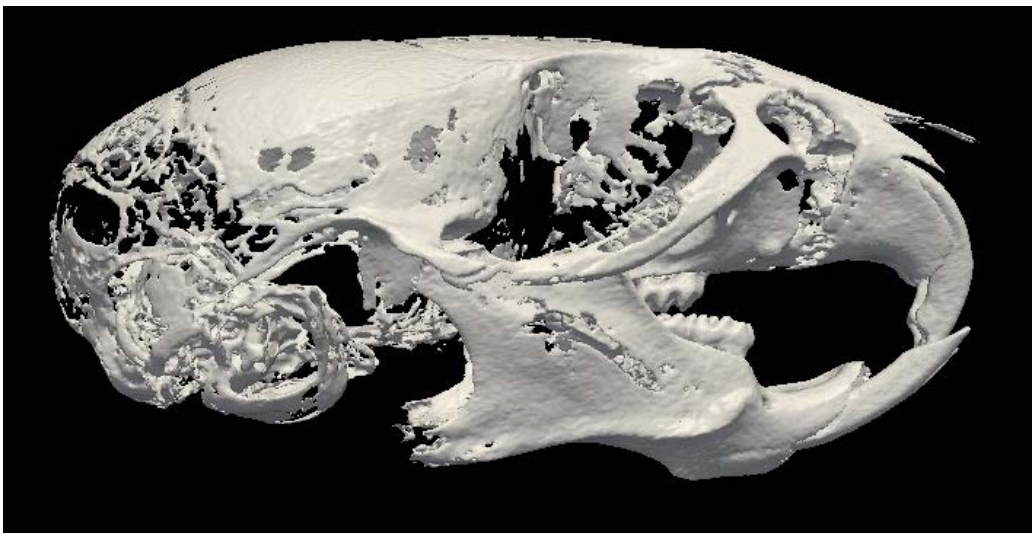

Figure 4.5 – *TWIST-1*$^{+/-}$ animals display a phenotype of fusion of coronal sutures. Looking at the skull from the top down the increase in bone density from WT (top) to *TWIST-1*$^{+/-}$ Het (bottom) is evident. The most important aspect of the above images is the apparent pre-fusion of the cranial sutures in the Het animals and the "Twisting" that this causes.

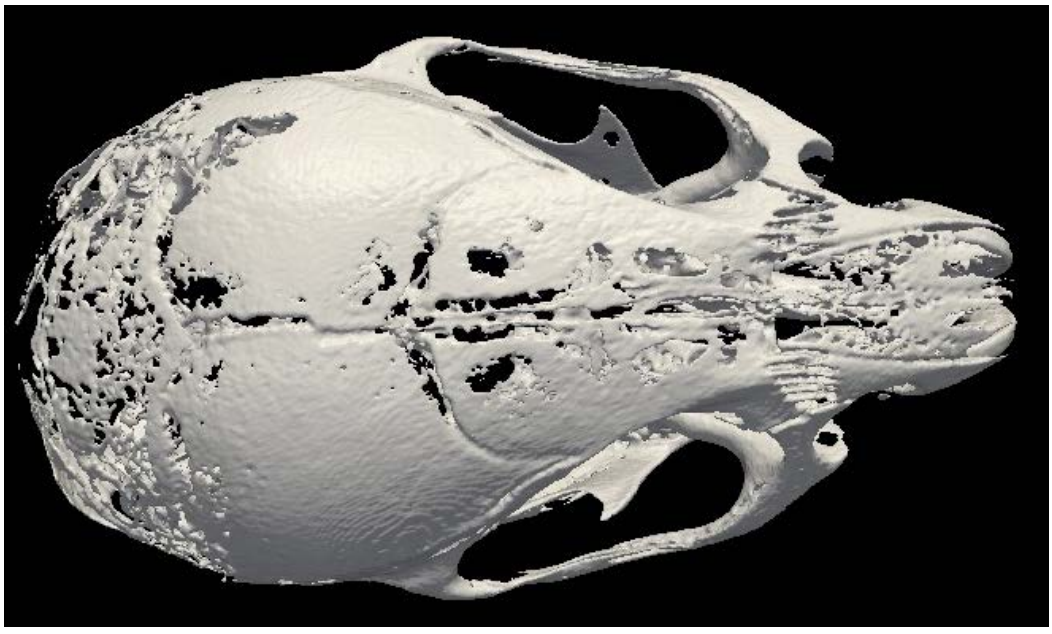

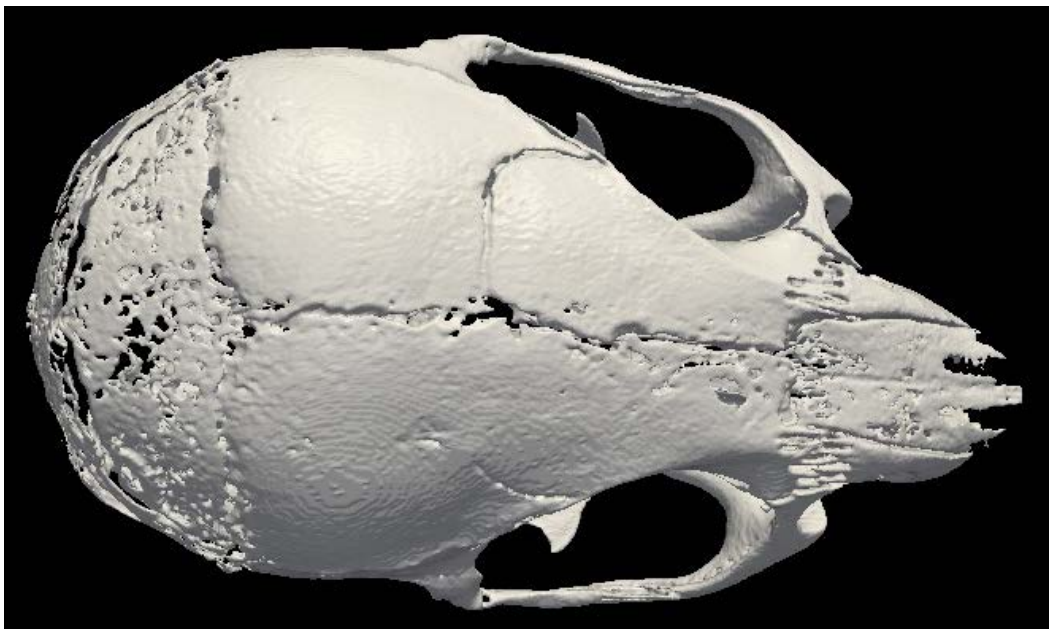

Figure 4.6 - *TWIST-1*$^{+/-}$ animals display a phenotype of polydactyl hind limbs. This X-ray shows a polydactyl hind foot of a *TWIST-1*$^{+/-}$ Het mouse (right) and a normal hind foot (left).

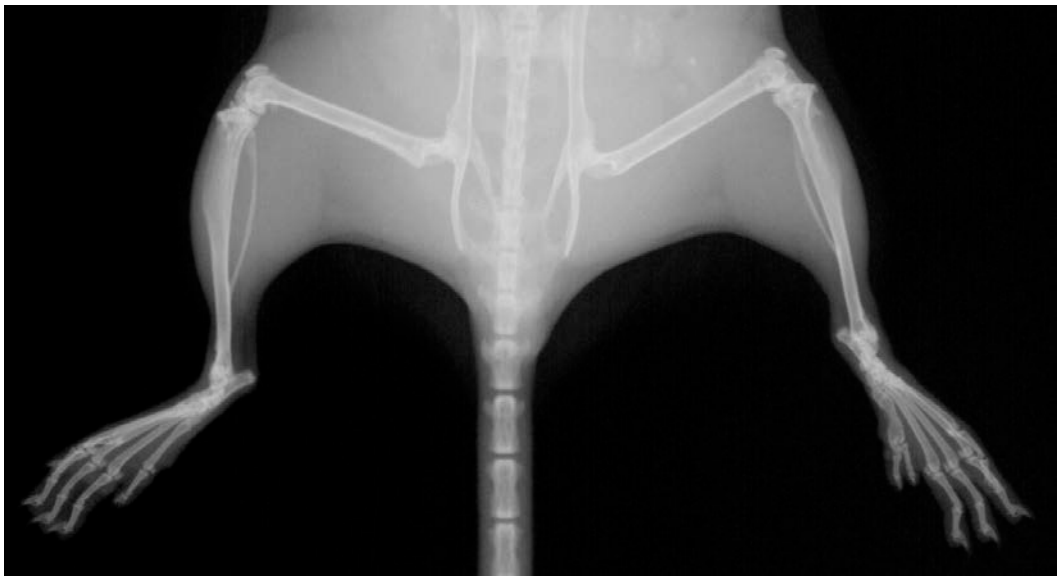

Figure 4.7 – No visible differences between non-fractured limbs of *TWIST-1*$^{+/-}$ and WT animals. 3D reconstructed images of non fractured femora at 1 week post fracture. (A) Longitudinal wild type non fractured femur. (B) Longitudinal heterozygous non fractured femur. (C) Longitudinal section of H&E stained non fractured femur from wild type mouse with normal histology at 1 week post fracture. (D) Longitudinal section of H&E stained non fractured femur from *TWIST-1*$^{+/-}$ mouse with normal histology at 1 week post fracture. (E) Longitudinal section of Safranin O stained non fractured femur from wild type mouse with normal histology at 1 week post fracture. (F) Longitudinal section of Safranin O stained non fractured femur from *TWIST-1*$^{+/-}$ mouse with normal histology at 1 week post fracture. Scale bar: 1mm

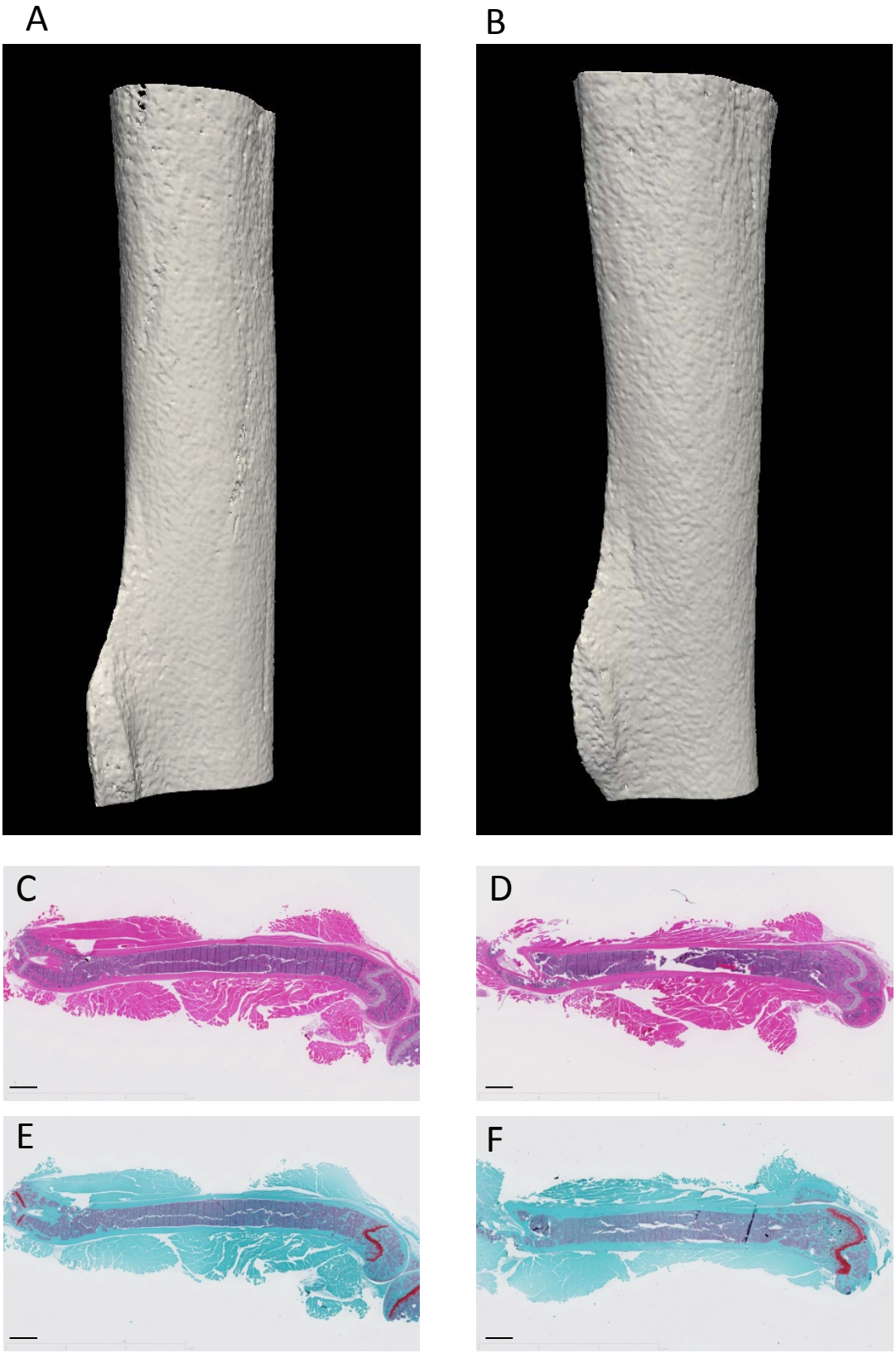
A
B
C
D
E
F

4.4 Fracture Experimental Plan and Analysis

The aim of the experiments detailed below in figure 4.8, was to investigate the role of *TWIST-1* in fracture repair. This process was assessed using quantitative histological analysis, enumeration of CFU-F number, μCT analysis and mechanical load testing.

4.4.1 *TWIST-1*$^{+/-}$ mice have reduced callus size at two four and eight weeks post fracture

Histomorphometric analysis was used to assess differences in the total area of the callus between WT and *TWIST-1*$^{+/-}$ mice (figure 4.9). Although *TWIST-1*$^{+/-}$ mice had smaller calluses at every time point there were no statistically significant differences observed ($p < 0.05$, 2 way ANOVA with Bonferroni's post test). However, the fractured limbs of *TWIST-1*$^{+/-}$ mice had statistically significantly ($p < 0.05$, 2 way ANOVA with Bonferroni's post test) smaller calluses at two, four and eight weeks post fracture when compared to WT littermate controls as shown by μCT analysis of tissue volume. This was also observed at four weeks using μCT generated 3D images and haematoxalin and eosin staining (figure 4.10) and at eight weeks in figure 4.11.

4.4.2 *TWIST-1*$^{+/-}$ mice display increased callus mineralization at one and two weeks post fracture

As a percentage of the total size of the fractured callus, bone volume was shown to be statistically significantly ($p < 0.05$, 2 way ANOVA with Bonferroni's post test) higher in *TWIST-1*$^{+/-}$ mice compared to WT mice at one and two weeks post fracture using histomorphometric analysis (figure 4.12). However, at four weeks post fracture, bone volume was shown to be statistically significantly ($p < 0.05$, 2 way ANOVA with Bonferroni's post test) lower in *TWIST-1*$^{+/-}$ mice compared to WT mice. There were no statistically significant ($p < 0.05$, 2 way ANOVA with

Figure 4.8 – Fracture experimental plan.

Experimental Overview

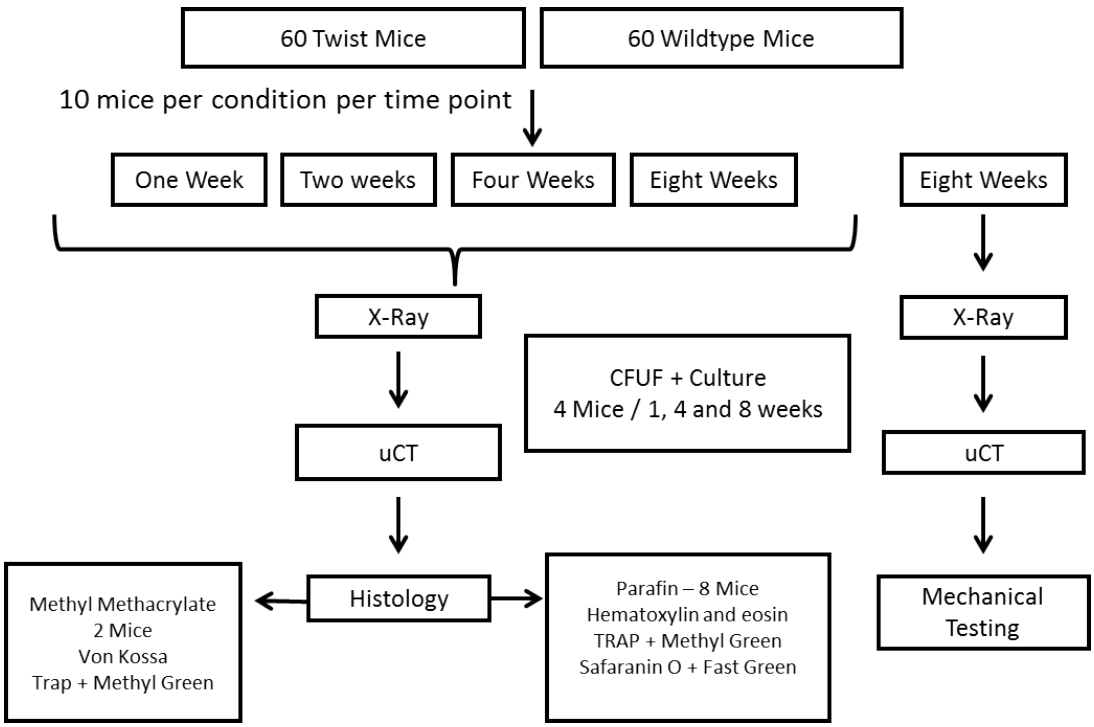

Figure 4.9 - *TWIST-1*$^{+/-}$ animals have a smaller callus at all time points. (A) Histomorphometric analysis showing Callus area **(B)** μCT data showing Tissue volume of callus. Statistically significant (n = 5) (2 way ANOVA, Bonferroni test, $p < 0.05$) WT fracture verses *TWIST-1*$^{+/-}$ fracture denoted by (*) and WT non-fracture verses *TWIST-1*$^{+/-}$ non-fracture denoted by (+).

(A)

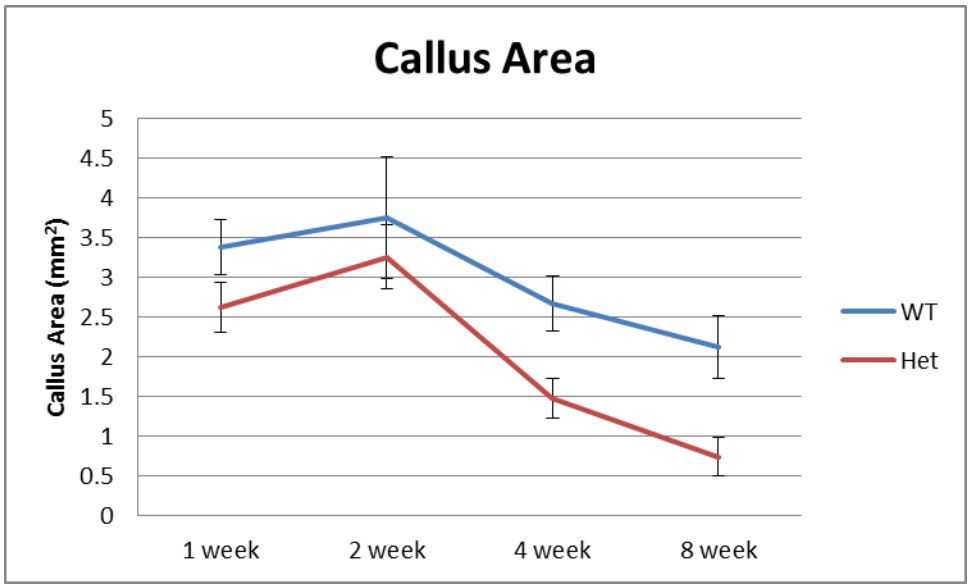
Callus Area
Callus Area (mm²)
5
4.5
4
3.5
3
2.5
2
1.5
1
0.5
0
1 week
2 week
4 week
8 week
WT
Het

(B)

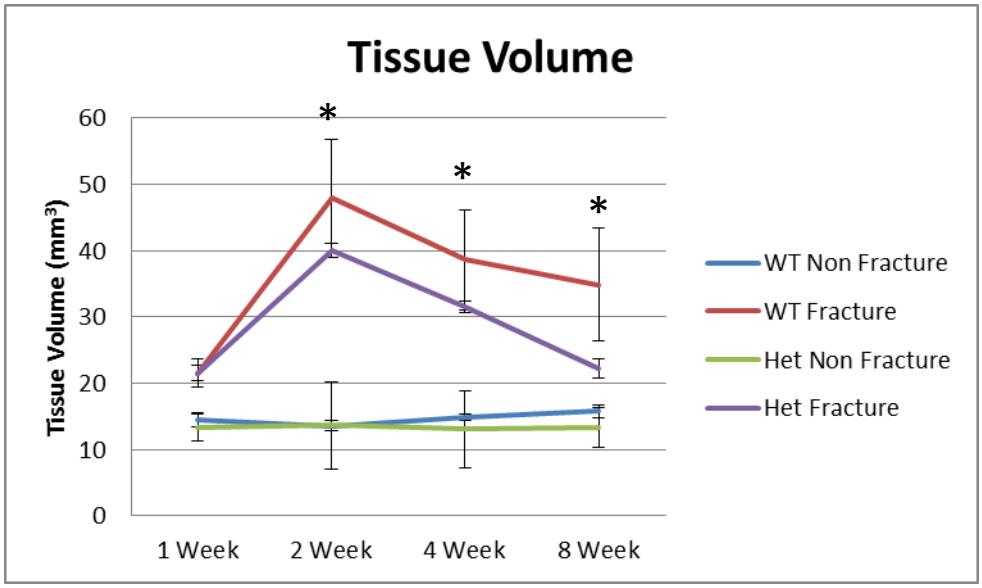
Tissue Volume
Tissue Volume (mm³)
60
50
40
30
20
10
0
*
*
*
1 Week
2 Week
4 Week
8 Week
WT Non Fracture
WT Fracture
Het Non Fracture
Het Fracture

Figure 4.10 - *TWIST-1*$^{+/-}$ mice have a more remodelled callus at 4 weeks post fracture. 3D reconstructed images of fractured femurs at 4 weeks post fracture. (A) Wild Type fractured femur. (B) Heterozygous fractured femur. (C) Section of H&E stained callus from the fractured femur of a wild type mouse at 4 weeks post fracture. (D) Section of H&E stained callus from the fractured femur of a *TWIST-1*$^{+/-}$ mouse at 4 weeks post fracture. Scale bar: 1mm

A

B

C

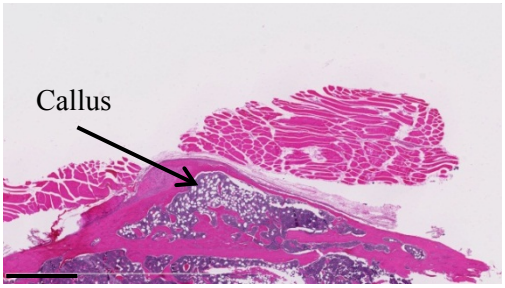

D

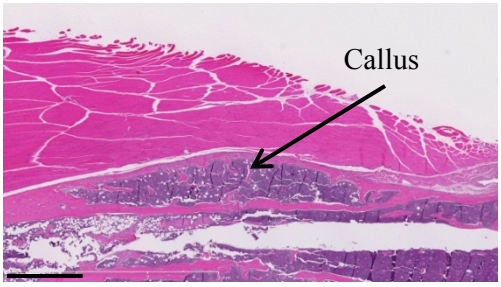

Figure 4.11 - *TWIST-1*$^{+/-}$ mice have a more remodelled callus at 8 weeks post fracture. 3D reconstructed images of fractured femurs at 8 weeks post fracture. (A) Wild Type fractured femur. (B) Heterozygous fractured femur. (C) Section of H&E stained callus from the fractured femur of a wild type mouse at 8 weeks post fracture. (D) Section of H&E stained callus from the fractured femur of a *TWIST-1*$^{+/-}$ mouse at 8 weeks post fracture. Scale bar: 1mm

A

B

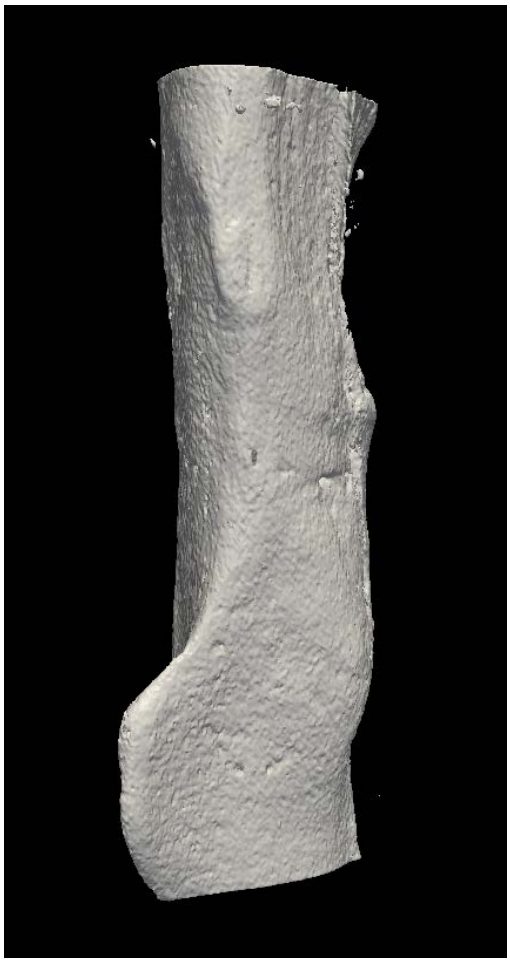

C

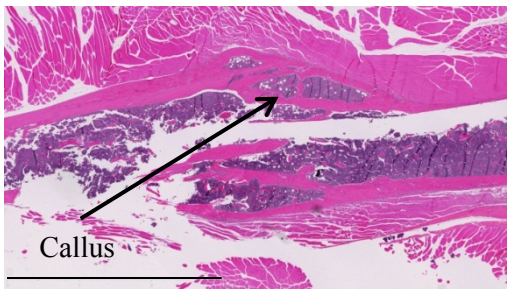

D

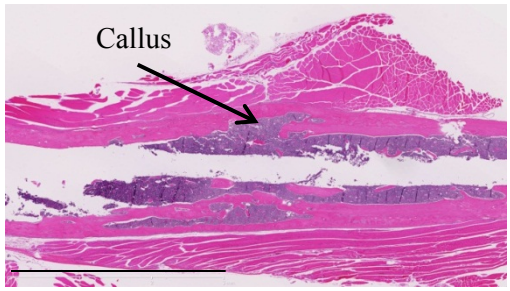

Figure 4.12 - *TWIST-1*$^{+/-}$ animals fractures show increased bone volume at one and two weeks post fracture. Histomorphometric data showing **(A)** Bone volume **(B)** Bone surface. Statistically significant (n = 5) (2 way ANOVA, Bonferroni test, $p < 0.05$) WT fracture verses *TWIST-1*$^{+/-}$ fracture denoted by (*) and WT non-fracture verses *TWIST-1*$^{+/-}$ non-fracture denoted by (+).

(A)

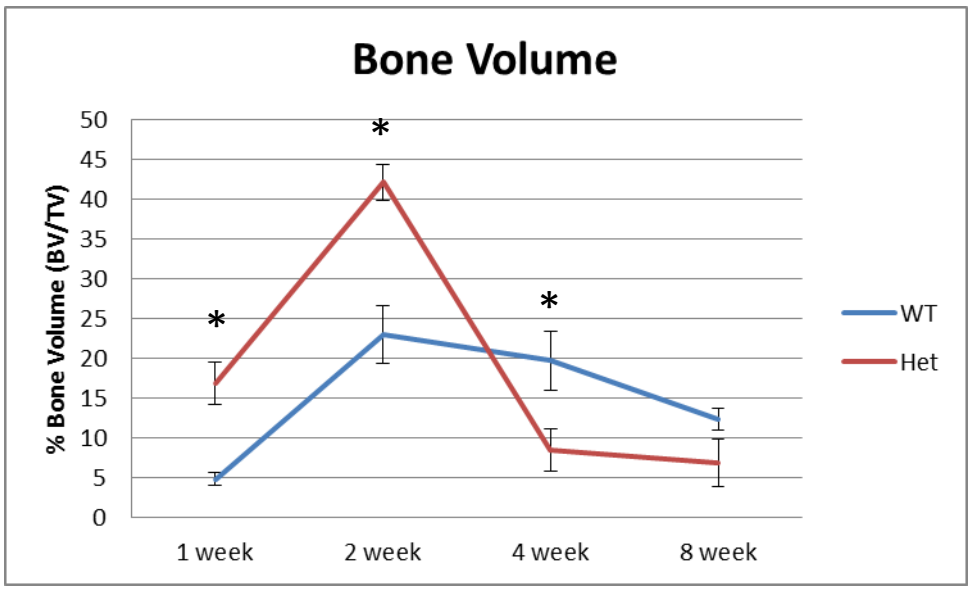
Bone Volume
% Bone Volume (BV/TV)
50
45
40
35
30
25
20
15
10
5
0
*
*
1 week
2 week
4 week
8 week
WT
Het

(B)

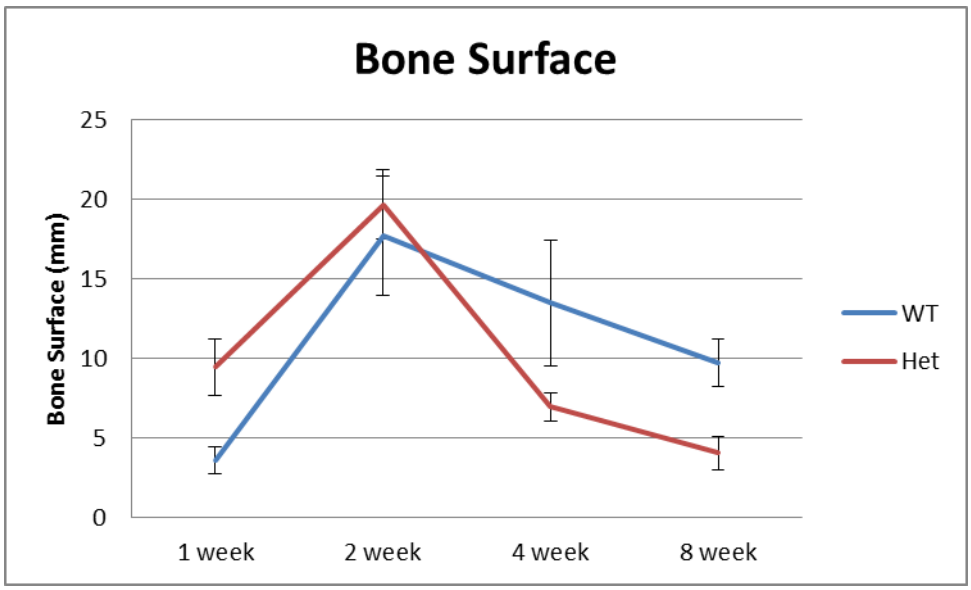
Bone Surface
Bone Surface (mm)
25
20
15
10
5
0
1 week
2 week
4 week
8 week
WT
Het

Bonferroni's post test) differences observed between the bone surface of WT and *TWIST-1*$^{+/-}$ mice at any time point. The amount of mineral at the distal and proximal ephiphysis of fractured limbs of *TWIST-1*$^{+/-}$ mice was greater than WT littermate controls at one week post fracture, assessed by μCT and histological examination (figure 4.13). Complete bone bridging in *TWIST-1*$^{+/-}$ mice resulted in early stabilisation of the fracture at two weeks post fracture, shown by μCT, haematoxalin and eosin and von Kossa staining in figure 4.14.

4.4.3 *TWIST-1*$^{+/-}$ and WT mice display comparable cartilage and fibrous tissue formation

No statistically significant ($p < 0.05$, 2 way ANOVA with Bonferroni's post test) differences were observed in cartilage area or fibrous area (figure 4.15) measured by histomorphometric analysis. However, WT mice demonstrated a non-significant trend towards a larger cartilage area as a percentage of the total area of the callus at one and two weeks post fracture. Further to this, *TWIST-1*$^{+/-}$ mice displayed a non-significant trend towards elevated fibrous tissue area as a percentage of the total area of the callus.

4.4.4 Mechanical properties restored to baseline in fractured limbs of *TWIST-1*$^{+/-}$ mice at eight weeks post fracture

At eight weeks post fracture the non-fractured contralateral limbs of WT and *TWIST-1*$^{+/-}$mice were able to support almost identical loads before mechanical failure measured by four point bending described in section 2.6.9 (figure 4.16). However, the fractured limbs of *TWIST-1*$^{+/-}$mice were able to support less load when compared to their WT controls. When analysing the differences between fractured and non-fractured limbs the WT cohort was statistically significantly ($p < 0.05$, ANOVA with Tukey's post test) different. However, there was no

Figure 4.13 - *TWIST-1*$^{+/-}$ mice have enhanced callus mineralization at 1 week post fracture. (A) Wild Type 3D reconstructed femur at 1 week post fracture. (B) *TWIST-1*$^{+/-}$ 3D reconstructed femur at 1 week post fracture. (C) Section of H&E stained callus from the fractured femur of a wild type mouse at 1 week post fracture. (D) Section of H&E stained callus from the fractured femur of a *TWIST-1*$^{+/-}$ mouse at 1 week post fracture. Scale bar = 1mm

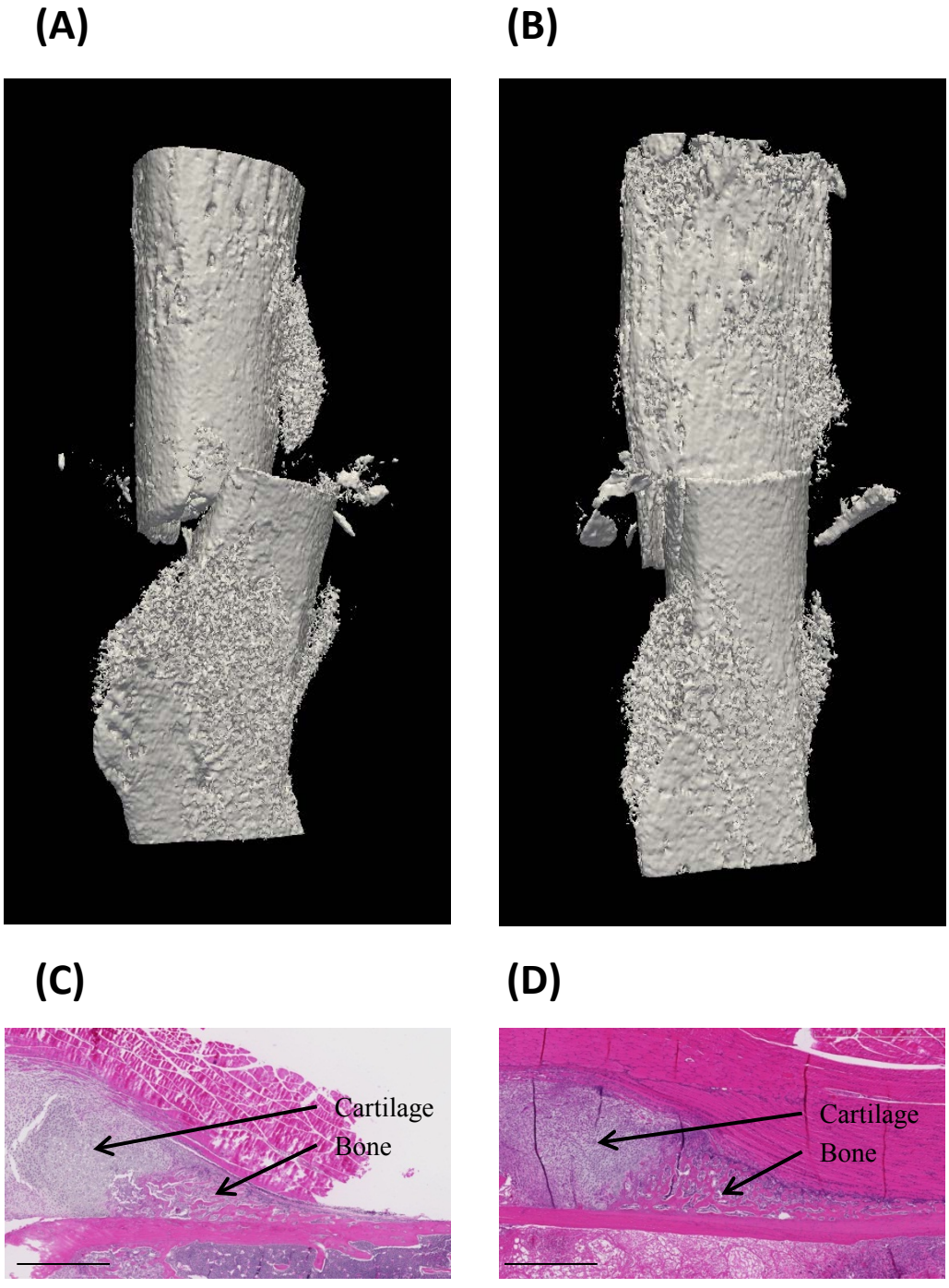
(A)
(B)
(C)
(D)
Cartilage
Bone
Cartilage
Bone

Figure 4.14 - *TWIST-1*$^{+/-}$ mice show complete bone bridging at 2 weeks post fracture. (A) Wild Type 3D reconstructed femur at 2 weeks post fracture (B) *TWIST-1*$^{+/-}$ 3D reconstructed femur at 2 weeks post fracture (C) Section of H&E stained callus from the fractured femur of a wild type mouse at 2 weeks post fracture. (D) Section of H&E stained callus from the fractured femur of a *TWIST-1*$^{+/-}$ mouse at 2 weeks post fracture. (E) Longitudinal section of von kossa stained fractured femur from wild type mouse showing incomplete bone bridging at 2 weeks post fracture (F) Longitudinal section of von kossa stained fractured femur from *TWIST-1*$^{+/-}$ mouse showing complete bone bridging at 2 weeks post fracture . Scale bar: 1mm

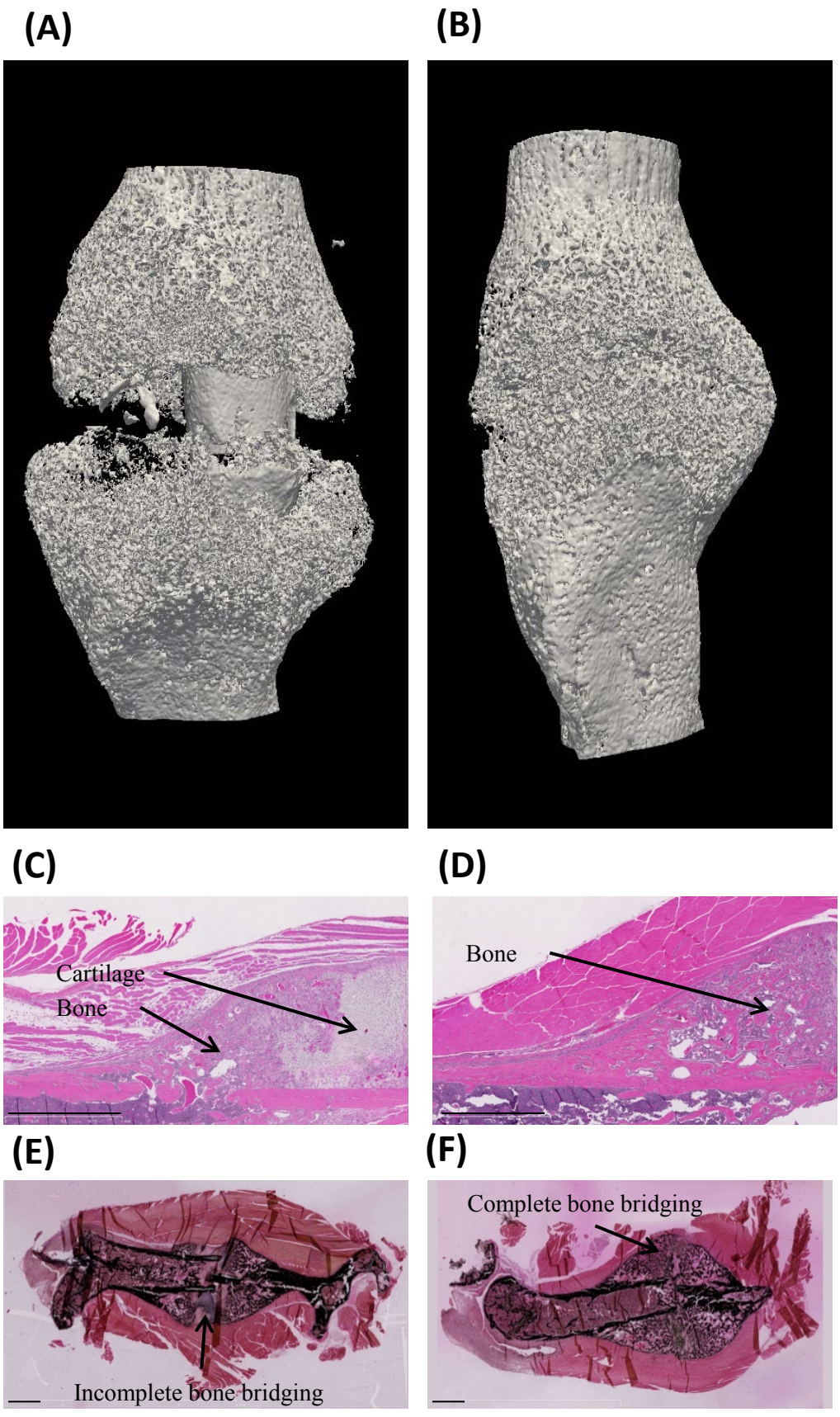
(A)
(B)
(C)
Cartilage
Bone
(D)
Bone
(E)
Incomplete bone bridging
(F)
Complete bone bridging

Figure 4.15 – No significant differences in cartilage area or fibrous area between WT and *TWIST-1*$^{+/-}$ animals . Histomorphometric analysis showing; **(A)** Cartilage area. **(B)** Fibrous area. **(C)** Section of safranin O stained callus from the fractured femur of a wild type mouse at 1 week post fracture. **(D)** Section of safranin O stained callus from the fractured femur of a *TWIST-1*$^{+/-}$ mouse at 1 week post fracture. **(E)** Section of safranin O stained callus from the fractured femur of a wild type mouse at 2 weeks post fracture. **(F)** Section of safranin O stained callus from the fractured femur of a *TWIST-1*$^{+/-}$ mouse at *2* weeks post fracture. Statistically significant (n = 5) (2 way ANOVA, Bonferroni test, $p < 0.05$) WT fracture vs *TWIST-1*$^{+/-}$ fracture denoted by (*). Scale bar: 1mm from

(A)

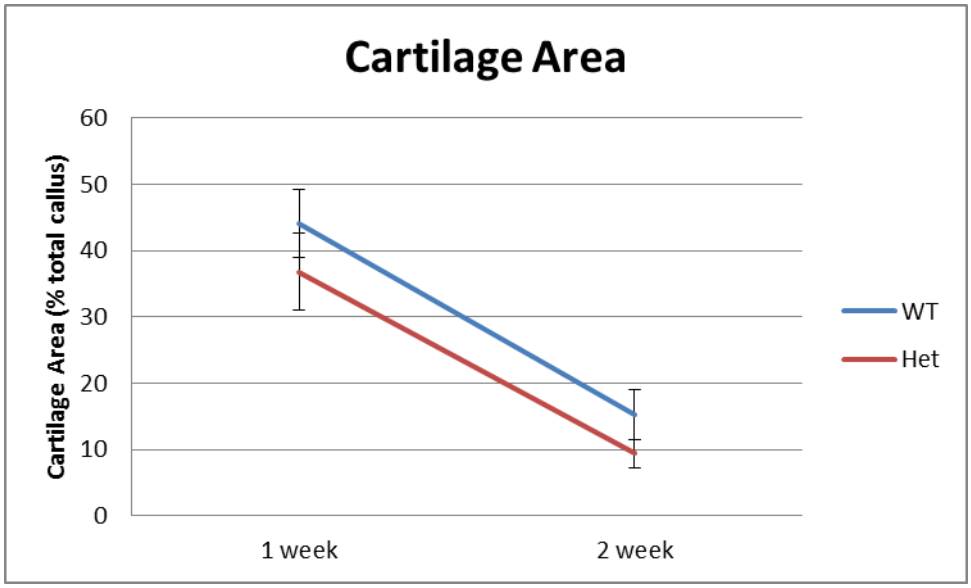
Cartilage Area
Cartilage Area (% total callus)
60
50
40
30
20
10
0
1 week
2 week
WT
Het

(B)

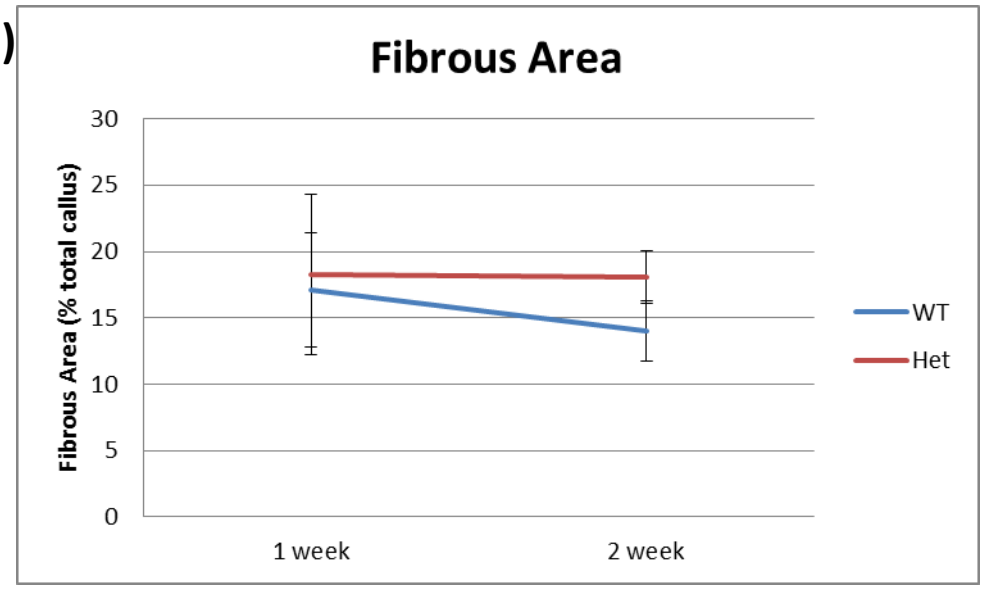
Fibrous Area
Fibrous Area (% total callus)
30
25
20
15
10
5
0
1 week
2 week
WT
Het

(C)

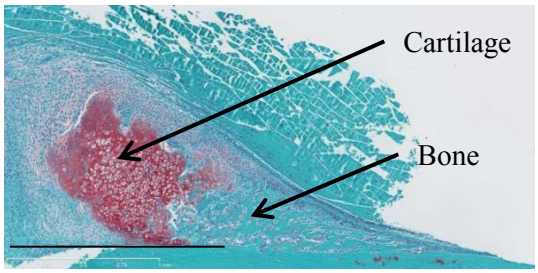
Cartilage
Bone

(D)

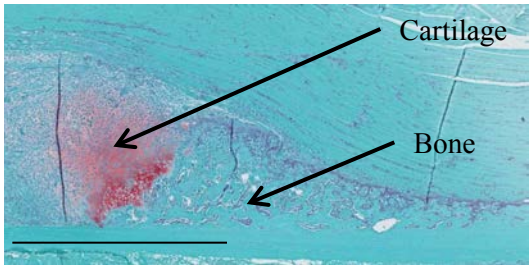
Cartilage
Bone

(E)

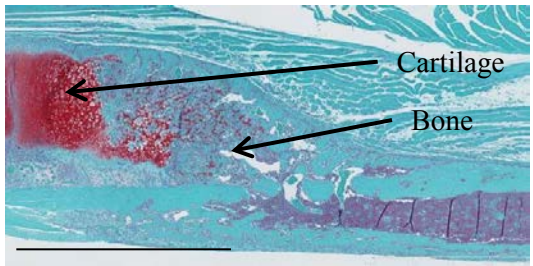
Cartilage
Bone

(F)

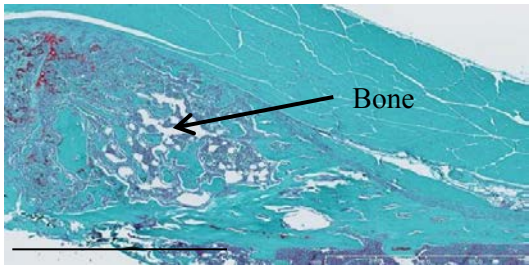
Bone

Figure 4.16 - *TWIST-1*$^{+/-}$ animals fractures are more remodelled at 8 weeks post fracture. Using four point testing, the ultimate load is a measure of the maximum load supported at failure. Statistically significant (n = 10) ($p < 0.5$, ANOVA, Tukey's post-test) results denoted by (*).

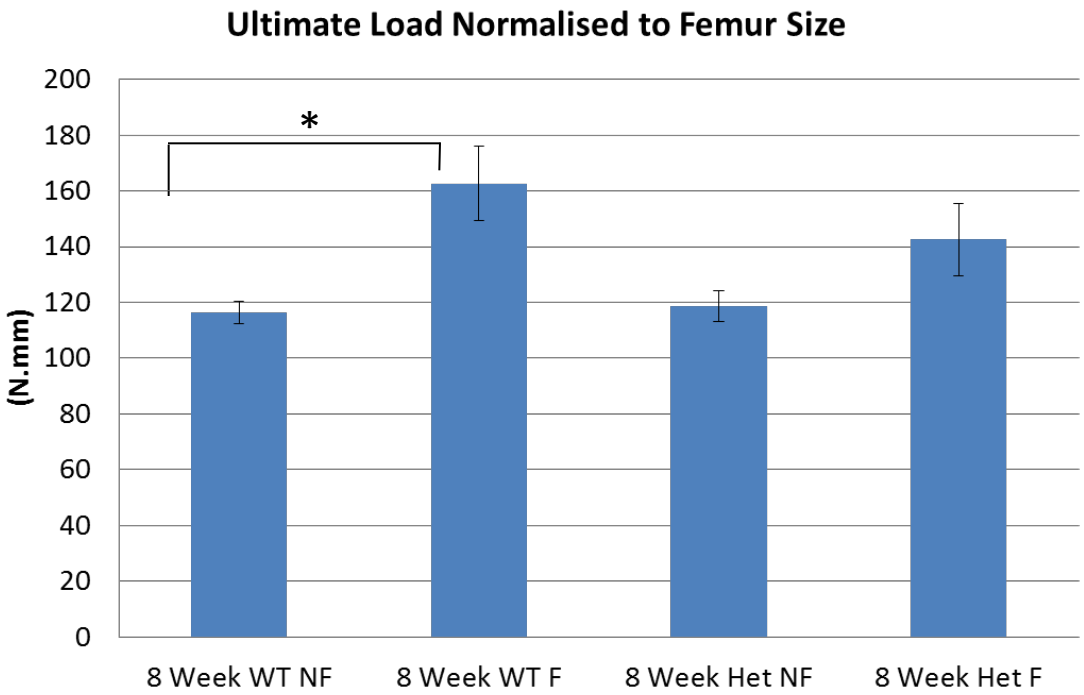
Ultimate Load Normalised to Femur Size
(N.mm)
200
180
160
140
120
100
80
60
40
20
0
*
8 Week WT NF
8 Week WT F
8 Week Het NF
8 Week Het F

statistically significant difference between the fractured and non-fractured limbs of *TWIST-1*$^{+/-}$ mice.

4.4.1 *TWIST-1*$^{+/-}$ mice display increased osteoblast numbers at eight weeks post fracture

A non-significant ($p < 0.05$, 2 way ANOVA with Bonferroni's post test) trend towards greater osteoblast numbers within the fractured limbs of *TWIST-1*$^{+/-}$ mice was shown at one, two and four weeks post fracture when compared to WT littermate controls using histomorphometric analysis (figure 4.17). At eight weeks post fracture a statistically significant ($p < 0.05$, 2 way ANOVA with Bonferroni's post test) increase in the number of osteoblasts and the osteoblast occupied bone surface was observed in *TWIST-1*$^{+/-}$ mice when compared to WT littermate controls.

4.4.2 *TWIST-1*$^{+/-}$ mice display increased osteoclast numbers at one week post fracture

A non-significant ($p < 0.05$, 2 way ANOVA with Bonferroni's post test) trend towards greater osteoclast numbers within the fractured limbs of *TWIST-1*$^{+/-}$ mice was observed at one week post fracture when compared to WT littermate controls using histomorphometric analysis (figure 4.18). Osteoclast numbers remained comparable between *TWIST-1*$^{+/-}$ mice and WT mice at two, four and eight weeks post fracture and no statistically significant ($p < 0.05$, 2 way ANOVA with Bonferroni's post test) differences were noted.

4.4.3 *TWIST-1*$^{+/-}$ mice exhibit a higher proportion of osteogenic committed CFU-F

Colony forming unit fibroblast assays were used to determine the relative numbers of MSC contained within the femora of fractured and non-fractured limbs of mice at one, four and eight

Figure 4.17 - *TWIST-1*$^{+/-}$ animals have increased relateive osteoblast numbers at all timepoints. Histomorphometric analysis showing **(A)** Osteoblast number **(B**) Osteoblast occupied bone surface. Statistically significant (n = 5) (2 way ANOVA, Bonferroni test, $p < 0.05$) WT fracture verses *TWIST-1*$^{+/-}$ fracture denoted by (*).

(A)

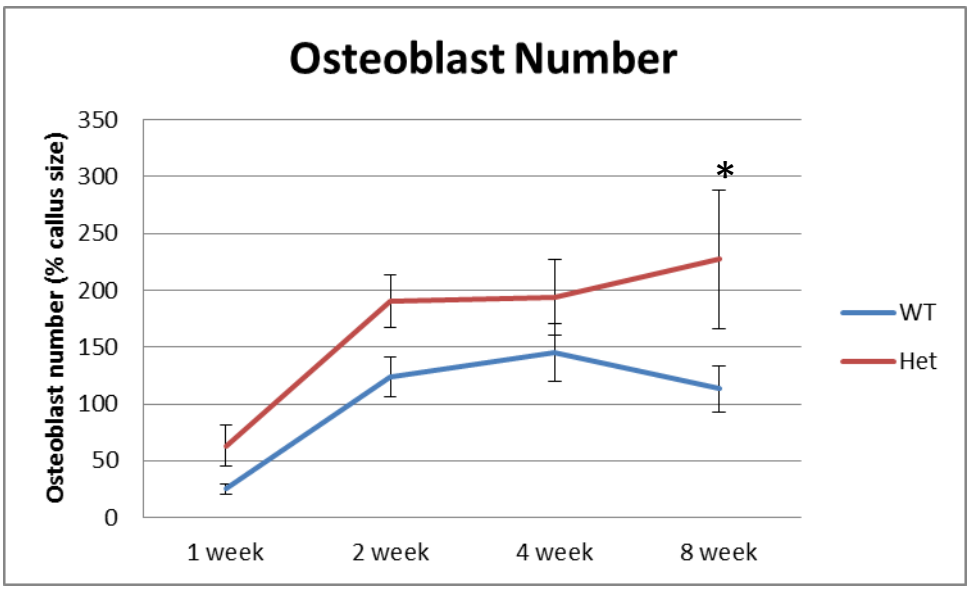
Osteoblast Number
Osteoblast number (% callus size)
350
300
250
200
150
100
50
0
1 week
2 week
4 week
8 week
*
WT
Het

(B)

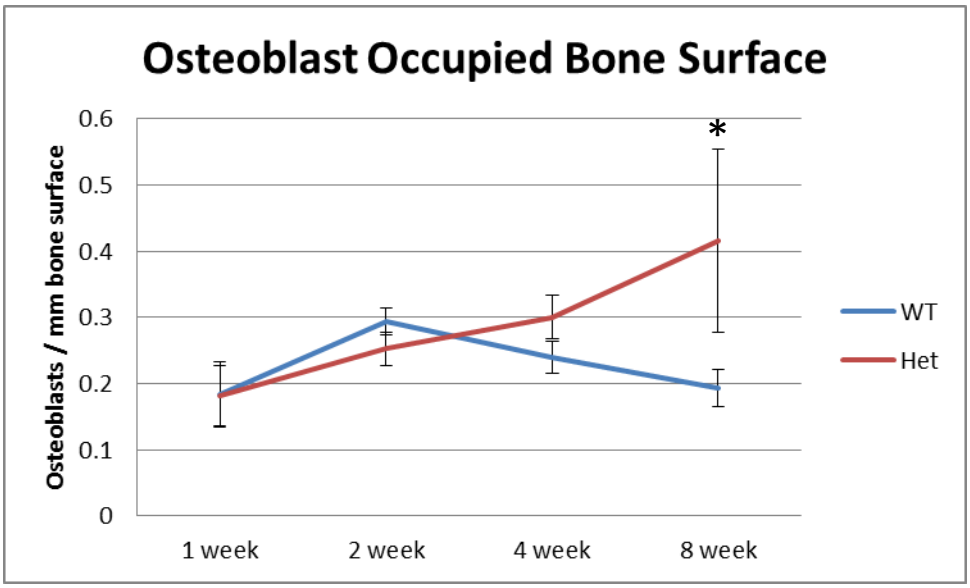
Osteoblast Occupied Bone Surface
Osteoblasts / mm bone surface
0.6
0.5
0.4
0.3
0.2
0.1
0
1 week
2 week
4 week
8 week
*
WT
Het

Figure 4.18 - *TWIST-1*$^{+/-}$ animals have increased relative osteoclast numbers at 1 week post fracture. Histomorphometric analysis showing **(A)** Osteoclast number **(B**) Osteoclast occupied bone surface. Statistically significant (n = 5) (2 way ANOVA, Bonferroni test, $p < 0.05$) WT fracture verses *TWIST-1*$^{+/-}$ fracture denoted by (*).

(A)

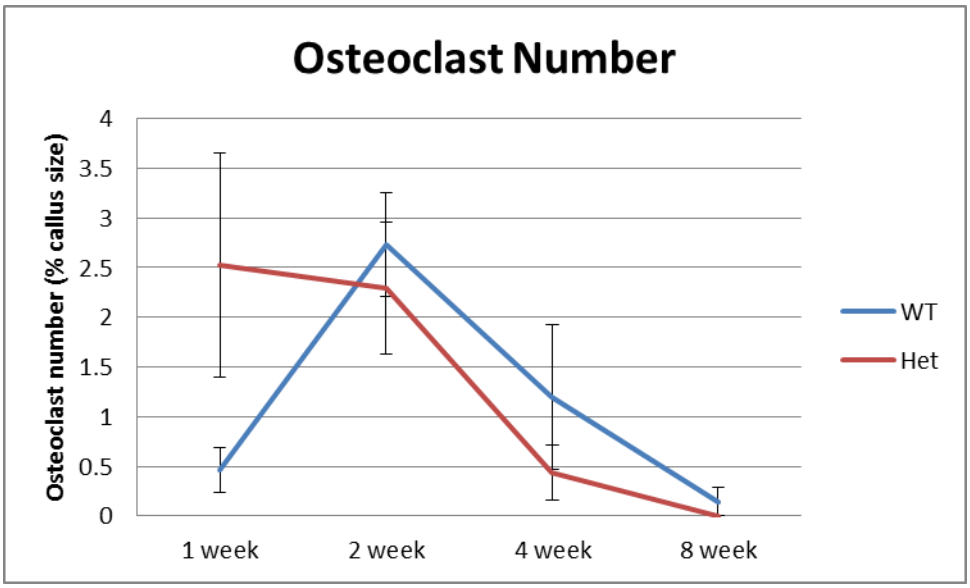
Osteoclast Number
Osteoclast number (% callus size)
4
3.5
3
2.5
2
1.5
1
0.5
0
1 week
2 week
4 week
8 week
WT
Het

(B)

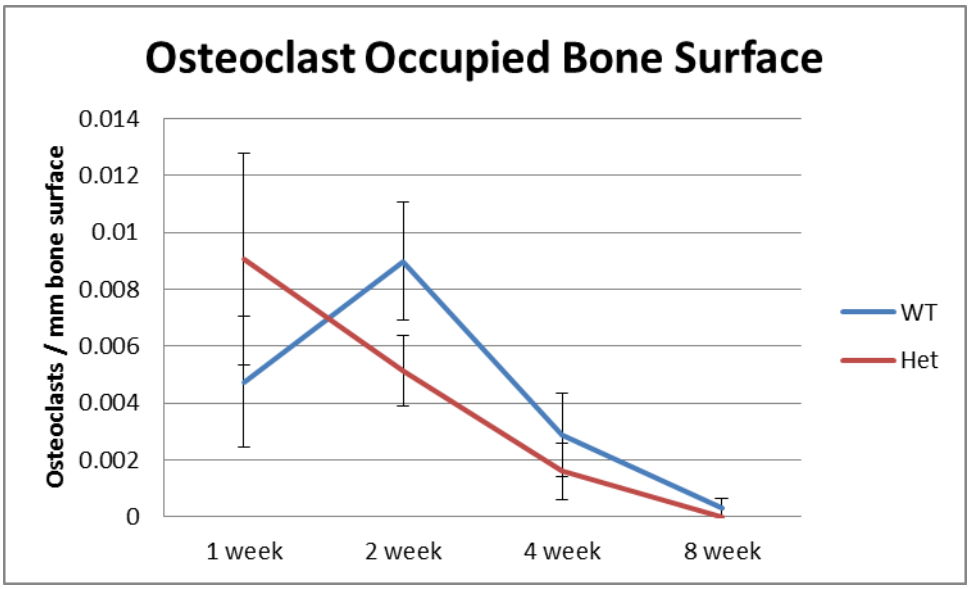
Osteoclast Occupied Bone Surface
Osteoclasts / mm bone surface
0.014
0.012
0.01
0.008
0.006
0.004
0.002
0
1 week
2 week
4 week
8 week
WT
Het

weeks post fracture. Alkaline phosphatase levels have previously been shown to be upregulated in human MSC cultured under osteogenic inductive conditions, correlating to a committed osteogenic population (Gronthos et al., 1994). To determine the relative proportions of committed verses non-committed cells within CFU-F assays, colonies were stained using a dual staining protocol utilising alkaline phosphatase and toluidine blue as described in (section 2.2.9 and figure 2.1).

At one week post fracture a statistically significant ($p < 0.05$, ANOVA with Tukey's post test) influx of cells was observed in the fractured limbs of WT mice compared to the corresponding contralateral non-fractured limbs (figure 4.19). An influx of cells was also observed in the fractured limbs of *TWIST-1*$^{+/-}$ mice although this was not statistically significant. Although not statistically significant, ($p < 0.05$, ANOVA with Tukey's post test), there were almost double the total number of CFU-F in the fractured limbs of WT mice when compared to the fractured limbs of *TWIST-1*$^{+/-}$ mice, ~11 per 10^3 cells plated verses ~6 per 10^3 cells plated, indicating greater total numbers of clonogenic MSC in WT mice. Of these cells, approximately 60% of the WT CFU-F population were comprised of immature non-committed MSC compared to approximately 35% of the MSC derived from *TWIST-1*$^{+/-}$ mice.

Both the WT and *TWIST-1*$^{+/-}$cohorts at four weeks post fracture displayed similar numbers of total CFU-F and no statistically significant ($p < 0.05$, ANOVA with Tukey's post test) differences were observed (figure 4.20). The CFU-F population from WT mice was comprised of approximately 50% mature cells, while the population from the *TWIST-1*$^{+/-}$ mice was comprised of around 75% mature cells.

Figure 4.19 - *TWIST-1*$^{+/-}$ animals have a more committed CFUF population at 1 week post fracture. (A) Total CFU-F colonies at 1 week post fracture. **(B)** Fractionated populations based on alkaline phosphatase staining ranging from immature non-committed cells (nill) to more committed pre-osteoblasts and osteoblast progenitors (25% - 100%). Statistically significant ($n = 4$) ($p < 0.5$, ANOVA, Tukey's post-test) results denoted by (*).

(A)

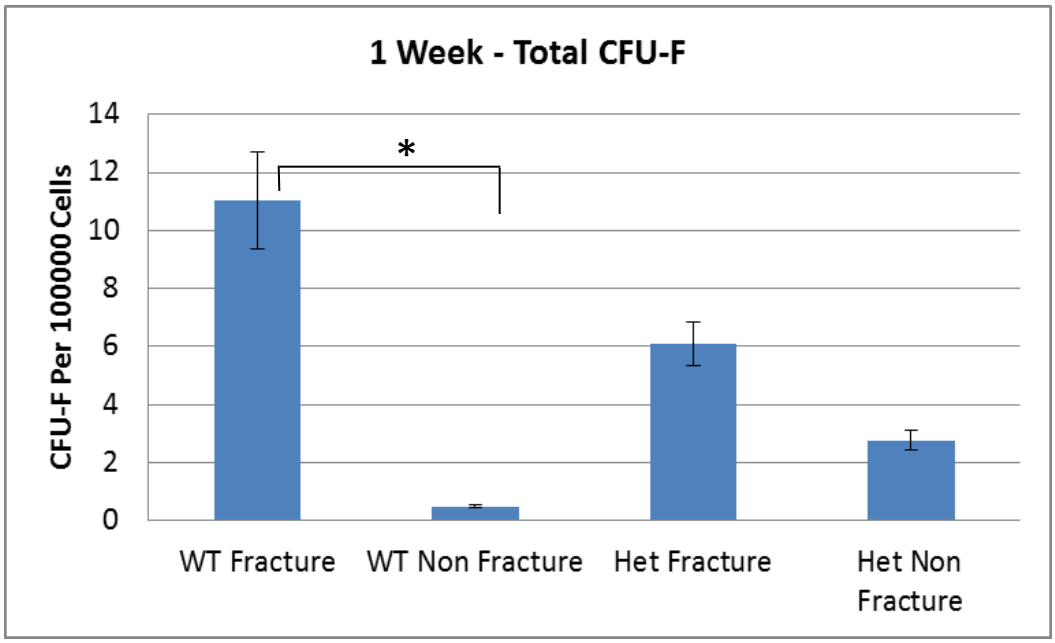
1 Week - Total CFU-F
CFU-F Per 100000 Cells
14
12
10
8
6
4
2
0
*
WT Fracture
WT Non Fracture
Het Fracture
Het Non Fracture

(B)

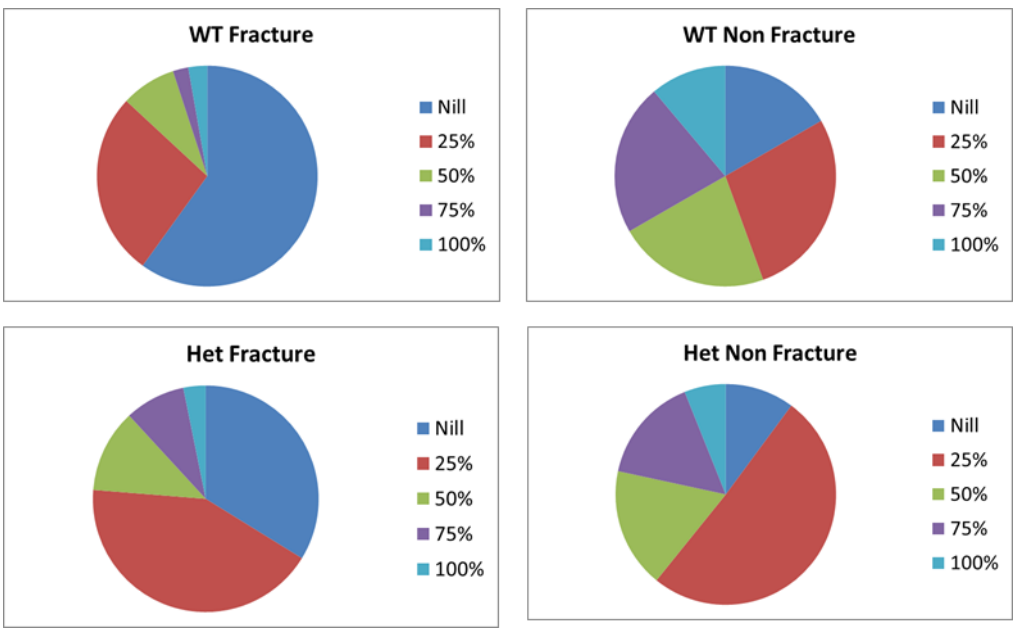
WT Fracture
Nill
25%
50%
75%
100%
WT Non Fracture
Nill
25%
50%
75%
100%
Het Fracture
Nill
25%
50%
75%
100%
Het Non Fracture
Nill
25%
50%
75%
100%

Figure 4.20 - *TWIST-1*$^{+/-}$ animals have a more committed CFUF population at 4 weeks. (A) Total CFU-F colonies at 4 weeks post fracture. (B) Fractionated populations based on alkaline phosphatase staining ranging from immature non-committed cells (nill) to more committed pre-osteoblasts and osteoblast progenitors (25% - 100%). Statistically significant ($n = 4$) ($p < 0.5$, ANOVA, Tukey's post-test) results denoted by (*).

(A)

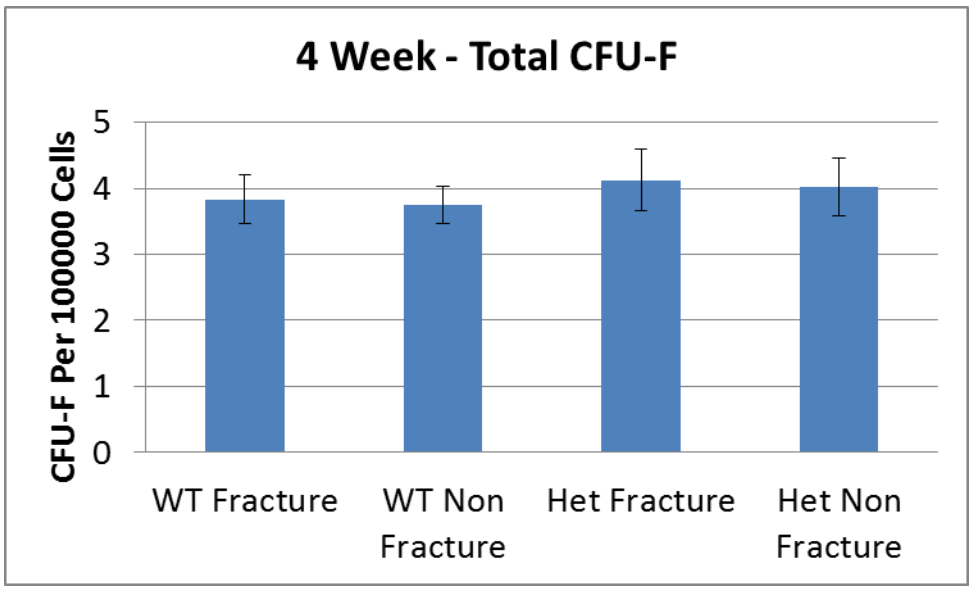
4 Week - Total CFU-F
CFU-F Per 100000 Cells
5
4
3
2
1
0
WT Fracture
WT Non Fracture
Het Fracture
Het Non Fracture

(B)

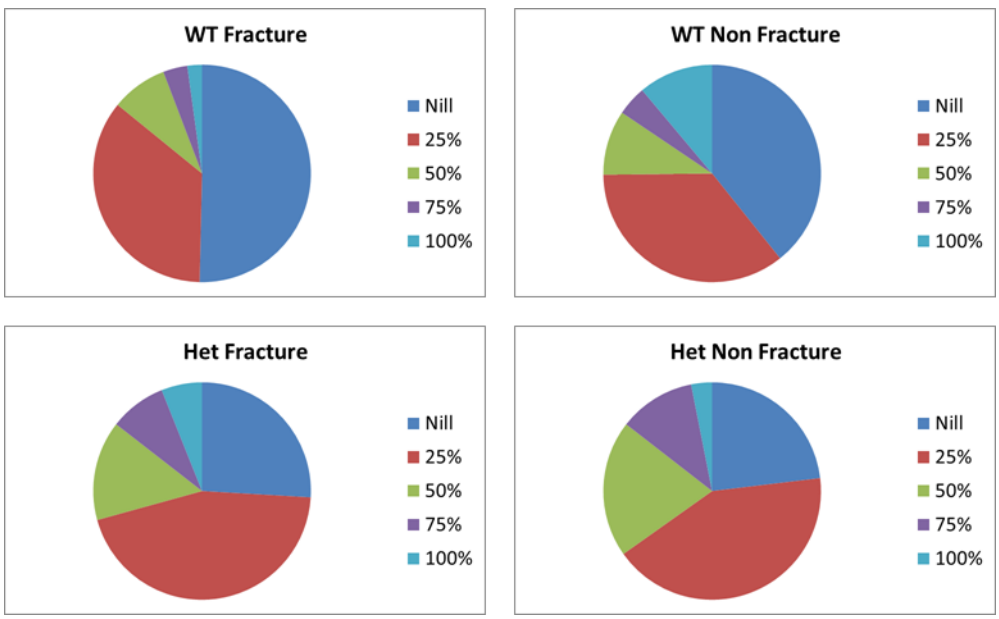
WT Fracture
Nill
25%
50%
75%
100%
WT Non Fracture
Nill
25%
50%
75%
100%
Het Fracture
Nill
25%
50%
75%
100%
Het Non Fracture
Nill
25%
50%
75%
100%

At eight weeks post fracture the total number of CFU-F remained comparable between WT and *TWIST-1*$^{+/-}$ mice and fractured and non-fractured limbs (figure 4.21), with no statistically significant ($p < 0.05$, ANOVA with Tukey's post test) differences observed. The fractured and non-fractured limbs of *TWIST-1*$^{+/-}$ mice contained almost identical percentages of committed verses immature cells while the CFU-F population isolated from the fractured limbs of WT mice contained a larger proportion of committed cells compared to the CFU-F population isolated from WT non-fractured contralateral limbs.

Figure 4.21 - *TWIST-1*$^{+/-}$ animals have a more committed CFUF population at 8 weeks post fracture. (A) Total CFU-F colonies at 8 weeks post fracture. (B) Fractionated populations based on alkaline phosphatase staining ranging from immature non-committed cells (nill) to more committed pre-osteoblasts and osteoblast progenitors (25% - 100%). Statistically significant (n = 4) ($p < 0.5$, ANOVA, Tukey's post-test) results denoted by (*).

(A)

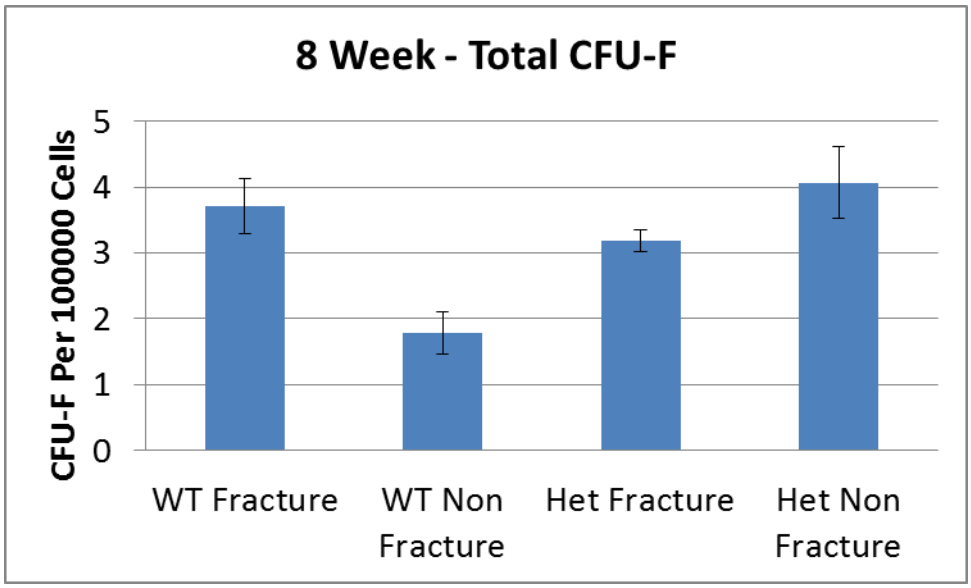
8 Week - Total CFU-F
CFU-F Per 100000 Cells
5
4
3
2
1
0
WT Fracture
WT Non Fracture
Het Fracture
Het Non Fracture

(B)

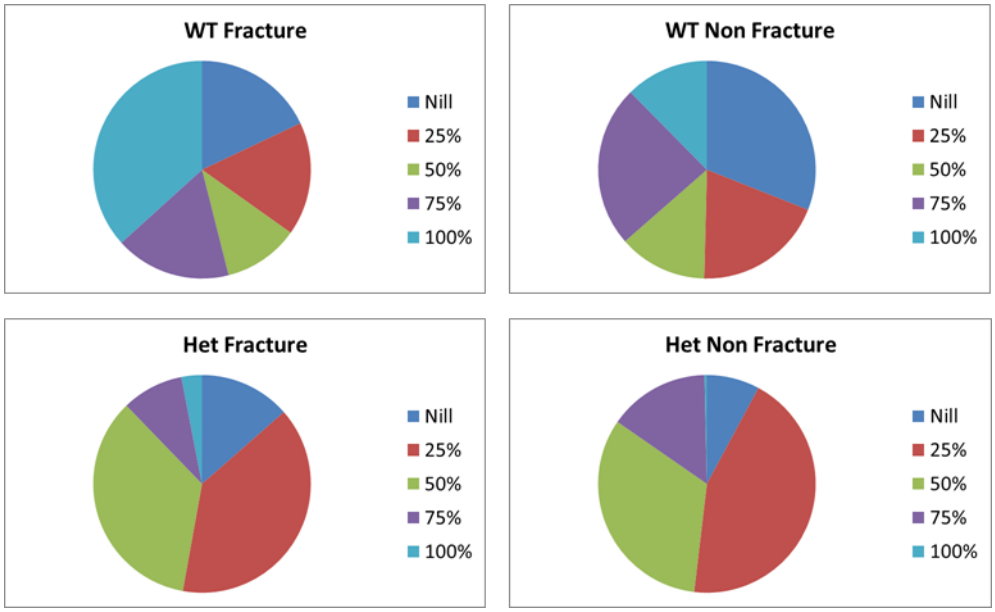
WT Fracture
WT Non Fracture
Het Fracture
Het Non Fracture
Nill
25%
50%
75%
100%

4.5 Discussion

Differential *TWIST-1* expression levels in MSC have previously been shown to regulate cellular proliferation, senescence and fate determination (Cakouros et al., 2012; Isenmann et al., 2009; Lee et al., 1999). In support of these findings, our laboratory has also provided evidence demonstrating accelerated senescence and decreased life span in stromal cells with a loss-of-function mutation within exon 1 of *TWIST-1* derived from a patient with Saethre-Chotzen syndrome (Cakouros et al., 2012). Consistent with these findings, the data presented in this chapter provide evidence for the role of *TWIST-1* in the proliferation and differentiation of the MSC populations of heterozygous *TWIST-1*$^{+/-}$ mice. Specifically, these studies showed that a reduction in the levels of *TWIST-1* expression induced a decrease in the proliferative potential while simultaneously increasing the capacity of *TWIST-1* mutant MSC to undergo osteogenic differentiation. We investigated the outcome of induced femoral fracture in *TWIST-1* deficient mice compared to WT littermate controls using histomorphometric analysis, μCT and CFU-F enumeration at one, four and eight week time points. Our results suggest that a reduction in *TWIST-1* expression enhances callus formation and remodelling resulting in accelerated fracture repair.

The results from this study show that at one and two weeks post fracture the callus of *TWIST-1*$^{+/-}$ mice contained a greater percentage of bone when compared to the callus of WT mice (Section 4.4.2). Furthermore, the number of osteoblasts relative to callus size was shown to be elevated in *TWIST-1*$^{+/-}$ mice compared to WT mice due to the presence of a smaller, more committed alkaline phosphatise positive CFU-F population (Sections 4.4.1 and 4.4.3). These results support previous studies that revealed pre-fusion of cranial sutures in mice with *TWIST-1* mutations and patients with Saethre-Chotzen syndrome (Bourgeois et al., 1998; Howard et al., 1997).

While the mechanism of action to explain these results has not been elucidated, studies conducted in our laboratory and described in chapter three have implicated *TWIST-1* in the regulation of genes involved in the Wnt/ β-catenin signalling pathway and the TGF-β superfamily of molecules including BMPs and SMADs. A role for *TGF-β* during fracture healing has been demonstrated by groups who have shown dose dependent increases in callus formation following injection of exogenous *TGF-β* (Lind et al., 1993; Nielsen et al., 1994). Elevated levels of *TGF-β*, BMPs and stimulatory SMADs as well as reduced levels of inhibitory *SMAD6* were detected 3 days post fracture induction in a rat model of bone fracture healing (Yu et al., 2002). The impact of BMPs on fracture healing has been investigated extensively and results show promising implications for the use of recombinant protein to enhance fracture union in both animal and human trials (Friedlaender et al., 2001; Garrison et al., 2010; Southwood et al., 2004; Tsuji et al., 2006). The largest study to date is a randomized, controlled single blind study involving 450 patients with an open tibial fracture treated with either standard treatment or the addition of an implant containing recombinant human *BMP2* (Govender et al., 2002). The results from this study demonstrate that patients treated with rh*BMP2* had reductions in the frequency of secondary interventions, accelerated fracture healing and a reduced infection rate. As described above (section 3.2.1) we demonstrated a reduction in the transcript levels of *BMP2* in human MSC with enforced *TWIST-1* expression suggesting that *TWIST-1*$^{+/-}$ mice would have elevated levels of *BMP2* expression. More recently, the effect of *BMP4* on skeletogenesis and fracture healing has been investigated using a mouse model with limb specific absence of *BMP4* (Tsuji et al., 2008). This group demonstrated that *BMP4* is not required for limb formation and that femoral fracture healing is unaffected by the absence of *BMP4*. In contrast to this, others have reported acute enhancement of *BMP4* mRNA at the early stages of fracture healing (Kawahata et al., 2003). This group also demonstrated enhanced *RUNX2* expression immediately following fracture. Collectively, these

studies data demonstrate that, during fracture repair, the expression profile of proteins known to be regulated by *TWIST-1* is converse to what is observed with enforced *TWIST-1* expression *in vitro,* revealing possible mechanisms for the observed heightened callus formation in *TWIST-1*$^{+/-}$ mice.

A role for the Wnt pathway is supported by studies which show upregulation of multiple Wnt pathway components within the injury site of fractures (Chen et al., 2007; Hadjiargyrou et al., 2002; Zhong et al., 2006). Results from chapter three (Section 3.2.2) showed that *WNT2B* and *WNT2* expression were upregulated in MSC with enforced *TWIST-1* expression suggesting that *WNT2B* expression may be reduced in *TWIST-1* deficient mice. It has been reported that *WNT2B* is upregulated at the defect site of injured tibiae in mice (Kim et al., 2007). Furthermore, *AXIN2* has been shown to act as a negative regulator of bone remodelling in adult mice and to regulate osteoblast differentiation (Yan et al., 2009). Using *LRP5*$^{-/-}$ mice Komatsu et al. demonstrated that Wnt signalling influences fracture repair showing that activation of Wnt signalling enhanced repair and inactivation impaired it (Komatsu et al., 2010). Supporting these findings, our results show that *AXIN2* is upregulated in MSC with enforced *TWIST-1* expression suggesting that *TWIST-1*$^{+/-}$ mice would have lower levels of *AXIN2* expression leading to enhanced bone remodelling and fracture repair. We demonstrated enhanced activated β-catenin protein levels in whole cell lysates generated from *TWIST-1* overexpressing MSC providing evidence of Wnt pathway stimulation with enforced *TWIST-1* expression. Other groups have shown that β-catenin signalling maintains the immature phenotype of osteoblast progenitors and prevents differentiation (Boland et al., 2004; Hill et al., 2005; Rodda and McMahon, 2006). Following from this work, Chen et al. proposed and provided evidence for the theory that β-catenin activation could be used to enhance fracture repair but only after MSC are committed to the osteoblastic lineage (Chen et al., 2007). These results provide validation for the investigation of

TWIST-1 mediated Wnt pathway regulation and could reveal the mechanism behind the pre-committed CFU-F populations observed in *TWIST-1*$^{+/-}$ mice.

Our data also show a reduction in the percentage bone volume at four and eight weeks post fracture in the callus of *TWIST-1*$^{+/-}$mice when compared to WT littermate controls. Furthermore, our data show an increase in the number of osteoclasts in the callus of *TWIST-1*$^{+/-}$ mice when compared to WT littermate controls at one week post fracture. The outcome of these differences is a remodelled femur with mechanical properties closer to that of its contralateral limb in *TWIST-1*$^{+/-}$mice at eight weeks post fracture in contrast to WT littermate controls. Together, these data show enhanced remodelling in the fractures of *TWIST-1*$^{+/-}$ mice. This result may be a secondary effect whereby the regulation of MSC by *TWIST-1* has led to the modulation of factors responsible for the recruitment of octeoclasts to the fracture site. The relative levels of these factors could be measured, by taking blood samples from *TWIST-1*$^{+/-}$ and WT mice that received a fracture, and compared using an ELISA assay.

This data shows clear evidence of a pre-committed population of MSC in *TWIST-1*$^{+/-}$ mice compared to WT mice. This pre-committed MSC population led to increased osteogenesis in *TWIST-1*$^{+/-}$ mice evidenced by increased bone volume and complete bone bridging at two weeks post fracture. Accelerated remodelling was shown in *TWIST-1*$^{+/-}$ mice by decreased callus bone volume compared to WT mice at four and eight weeks post fracture. Furthermore, the mechanical properties of *TWIST-1*$^{+/-}$ mice were shown to be closer to baseline providing further evidence for more complete remodelling in the callus of *TWIST-1*$^{+/-}$ mice compared to WT mice at 8 weeks post fracture. Although the mechanisms are not yet clear, our results suggest that *TWIST-1* plays a significant role in fracture repair. Finally, current literature supports the view that the

mechanism of *TWIST-1* in fracture repair could be due to the role of *TWIST-1* in the regulation of genes involved in the wnt/ β-catenin signalling pathway and the TGF-β superfamily of molecules.

5 Heterozygous *TWIST-1*$^{+/-}$ knockout mice exhibit reduced bone loss after ovariectomy

5.1 Introduction

Osteoporosis is defined as a disease characterised by a reduction of bone mineral density 2.5 or more standard deviations below the mean peak bone mass and micro-architectural deterioration (Dr N. Khaltaev, 2004; Kanis and Kanis, 1994). Osteoporotic bone loss is caused by either an increase in bone resorption or a decrease in bone formation leading to an increased fracture risk in affected individuals (Yamaza et al., 2008). It is known that MSC are capable of differentiation into osteoblasts that form new bone matrix to balance osteoclast-mediated bone resorption during the bone remodelling process (Tanaka Y, 2005). The disease is so prevalent that half of all women and one third of all men over 60 years of age in Australia will have a fracture due to osteoporosis (Australia, 2006). The goals of osteoporosis treatment are the prevention of fracture and this is achieved using bone resorption inhibitors, such as bisphosphonates to induce osteoclast apoptosis, or bone formation stimulants, such as active vitamin D_3 to increase the bioavailability of calcium (Orimo et al., 2012).

There are multiple pathways involved in osteoporosis including the Vitamin D endocrine system, the oestrogen endocrine pathway, the Wnt/β-catenin pathway, the *RANKL/RANK/OPG* pathway and the TGFβ superfamily of molecules (Li et al., 2010). The Vitamin D endocrine system has been shown to play important roles in bone metabolism and is mediated through the vitamin D receptor (Christakos et al., 2003; Morrison et al., 1994). The oestrogen endocrine pathway is critically important in regulating bone mass demonstrated by studies whereby oestrogen hormone replacement therapy has been shown to prevent bone loss and decrease fracture risk in treated patients (Cauley et al., 1995; Felson et al., 1993). The Wnt pathway has been implicated through

studies showing that loss of function of *LRP5* leads to early onset osteoporosis and gain of function mutations have the opposite effect leading to a high bone mass phenotype (Boyden, 2002; Gong et al., 2001; Little et al., 2002a). The *RANKL/RANK/OPG* pathway also plays a major roll as evidenced by studies investigating the *RANKL* decoy receptor osteoprotegrin (*OPG*) (Simonet et al., 1997). Mice deficient in *OPG* develop severe, early onset osteoporosis while mice with elevated levels of *OPG* present with an osteopetrosis phenotype (Boyce and Xing, 2007; Bucay et al., 1998). The TGFβ superfamily of molecules has been implicated in osteoporosis through a missense polymorphism in *BMP4,* which was associated with decreased BMD while other groups have demonstrated associations between *SMAD6* polymorphisms and reductions in BMD (Ramesh Babu et al., 2005; Urano et al., 2009). The master regulator *RUNX2* has also been implicated in osteoporosis through a study that identified an association between a polymorphism in *RUNX2* and elevated BMD in women (Vaughan et al., 2002).

The *TWIST-1* gene has been associated with bone mineral density in postmenopausal women (J.-Y. Hwang, 2010). This group demonstrated that *TWIST-1* mutations in postmenopausal women lead to increased bone mineral density of the femur, thus, indicating that a reduction in the amount of *TWIST-1* protein could have a protective effect in the osteoporosis condition. Further evidence to support this association comes from work by Balla et al who demonstrated that osteoporotic patients had significantly higher *TWIST-2* (*DERMO-1*) mRNA levels than their non-osteoporotic controls (Balla et al., 2008). As a close family member to *TWIST-1, TWIST-2* shares many functional roles including inhibition of the differentiation of osteoblasts (Isenmann et al., 2009; Lee et al., 2000).

Recent advances related to understanding key molecular processes involved in bone metabolism have highlighted the canonical Wnt pathway as a key regulator of bone formation (Baron and

Rawadi, 2007). The pathway is composed of multiple potential drug targets with known activators (Wnts, LRPs) and inhibitors (sclerostin, Dkk-1). However, when treating conditions on a molecular level it is important to identify targets that allow for a specific targeted therapy to minimise unwanted secondary effects (Kaufman et al.). In the case of the Wnt pathway, interference with Wnt inhibitory factor 1 (WIF1) has been reported to be associated with a potential risk of osteosarcoma (Kansara et al., 2009). If we can identify genes that, when targeted pharmaceutically, result only in the regulation of specific biological pathways then treatment outcomes can be improved.

The objective of this research chapter was to examine the effects of osteoporosis caused by oestrogen deficiency in the context of reduced levels of *TWIST-1* expression using an ovariectomy induced mouse model of osteoporosis. Heterozygous *TWIST-1*$^{+/-}$ knockout mice and WT littermate controls were subjected to an ovariectomy procedure whereby their ovaries were surgically removed. Heterozygous *TWIST-1*$^{+/-}$ mice were compared to WT littermate controls and ovariectomised mice were compared to equivalent Sham controls as described in section 2.6.4.

5.2 Results

5.2.1 Determination of optimal time point for analysis following ovariectomy

A small pilot study (3 WT and 3 *TWIST-1*$^{+/-}$ female mice) was conducted to determine the appropriate time-points required for assessment of osteoporosis in the *TWIST-1* model. Live μCT imaging was used at multiple time-points (1 week, 4 weeks and 8 weeks post-surgery) to examine changes in the trabecular structures within the femora of these mice. Based on the results obtained, the time-point selected for the final study was 8 weeks post ovariectomy. The main reason for selecting this time point was due to statistically significant ($p<0.05$, ANOVA with Tukey's post test) differences in a number of 3D histomorphometric parameters including; bone volume, percentage bone volume, bone surface, intersection surface, bone surface density and trabeculae number observed. The one week and 4 week time points followed the same trend but did not display statistically significant differences. The pilot study provided interesting preliminary results and enabled us to accurately predict time-point for analysis of the differences between *TWIST-1*$^{+/-}$ and WT mice with regards to the disease state of osteoporosis.

5.2.2 Ovariectomy experimental plan and analysis

The aim of the experiments, detailed below in figure 5.1, was to investigate the role played by *TWIST-1* in the development of osteoporosis caused by oestrogen deficiency, following ovariectomy. This process was assessed using quantitative histological analysis, analysis of CFU-F cultures, μCT analysis and mechanical load testing.

Figure 5.1 – Ovariectomy experimental plan.

Experimental Overview

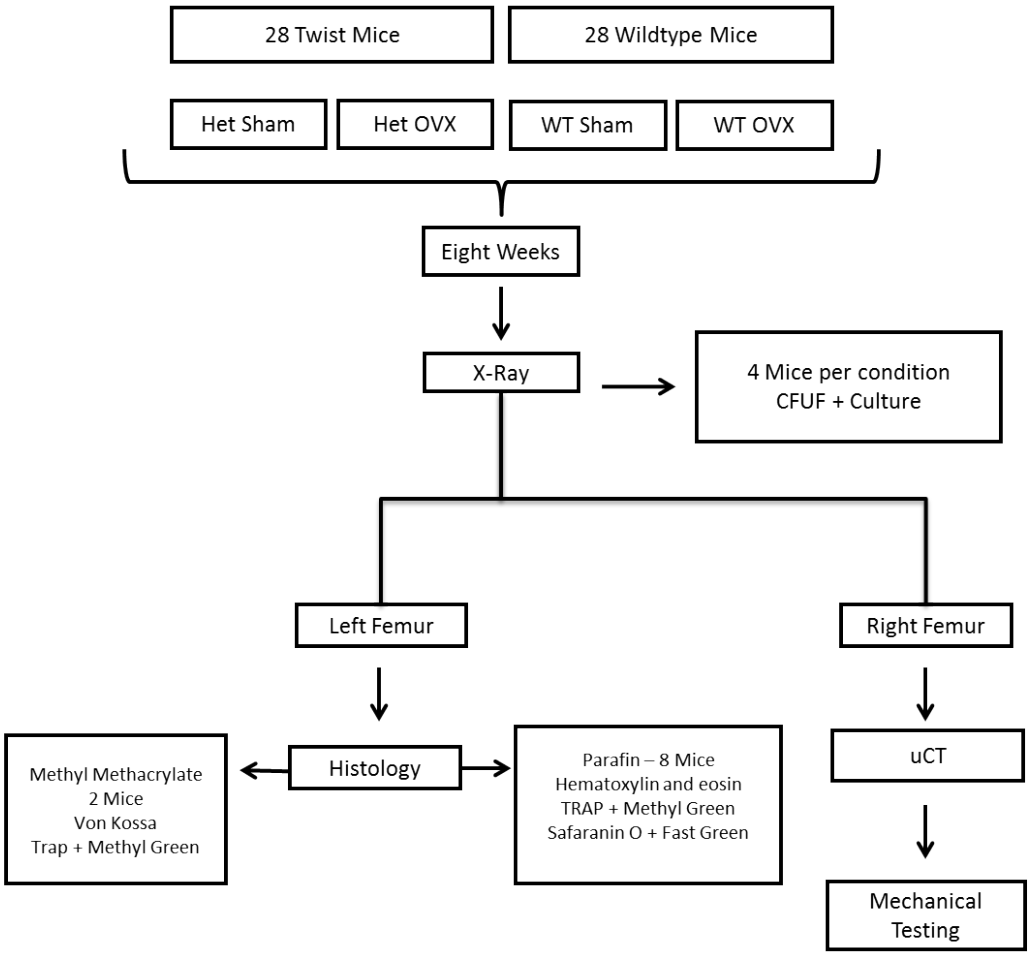

5.2.3 *TWIST-1*$^{+/-}$ mice maintain trabecular bone volume following ovariectomy

At eight weeks post ovariectomy, results showed statistically significant ($p<0.05$, ANOVA with Tukey's post test) trabecular bone loss in the WT cohort but not the *TWIST-1*$^{+/-}$ cohort by analysis of the trabecular region within the femora using μCT (figure 5.2). Reconstructed 3D μCT images of trabecular regions indicated that the starting bone volume percentage was lower in *TWIST-1*$^{+/-}$ mice compared to WT mice. Tissue volume was measured using μCT analysis and showed that, while no statistically significant ($p<0.05$, ANOVA with Tukey's post test) differences were observed between mice receiving sham surgery or ovariectomy, the tissue volume of *TWIST-1*$^{+/-}$ mice was lower than that of the WT mice due to the size differences between groups (figure 5.3). Furthermore, bone volume statistically significantly ($p<0.05$, ANOVA with Tukey's post test) decreased following ovariectomy in the WT group but not in the *TWIST-1*$^{+/-}$ group.

A non-significant ($p<0.05$, ANOVA with Tukey's post test) trend towards greater bone loss in WT mice compared *TWIST-1*$^{+/-}$ mice was observed using histomorphometric analysis of percentage bone volume (figure 5.4). Histomorphometric analysis also showed non-significant ($p<0.05$, ANOVA with Tukey's post test) reductions in bone surface following ovariectomy in WT mice and *TWIST-1*$^{+/-}$ mice. Statistically significant ($p<0.05$, ANOVA with Tukey's post test) reductions in intersection surface and trabeculae number were observed in WT mice following ovariectomy, while *TWIST-1*$^{+/-}$ mice maintained constant intersection surface and trabeculae number shown by μCT analysis (figures 5.5 and 5.6). There were no statistically significant ($p<0.05$, ANOVA with Tukey's post test) differences in bone surface, bone surface to volume ratio, bone surface density or trabecular thickness in WT mice or *TWIST-1*$^{+/-}$ mice measured by μCT analysis.

Figure 5.2 - *TWIST-1*$^{+/-}$ animals maintain trabecular bone volume following ovariectomy. μCT data (trabecular analysis) showing **(A)** Percent bone volume of trabecular region (BV/TV) **(B)** Reconstructed 3D μCT image of trabecular region WT Sham **(C)** Reconstructed 3D μCT image of trabecular region *TWIST-1*$^{+/-}$ Sham. **(D)** Reconstructed 3D μCT image of trabecular region WT OVX **(E)** Reconstructed 3D μCT image of trabecular region *TWIST-1*$^{+/-}$ OVX. Statistically significant (n = 10) ($p < 0.05$, ANOVA with Tukey's post test) results WT sham verses WT OVX denoted by (+) and *TWIST-1*$^{+/-}$ sham verses *TWIST-1*$^{+/-}$ OVX denoted by (*).

(A)

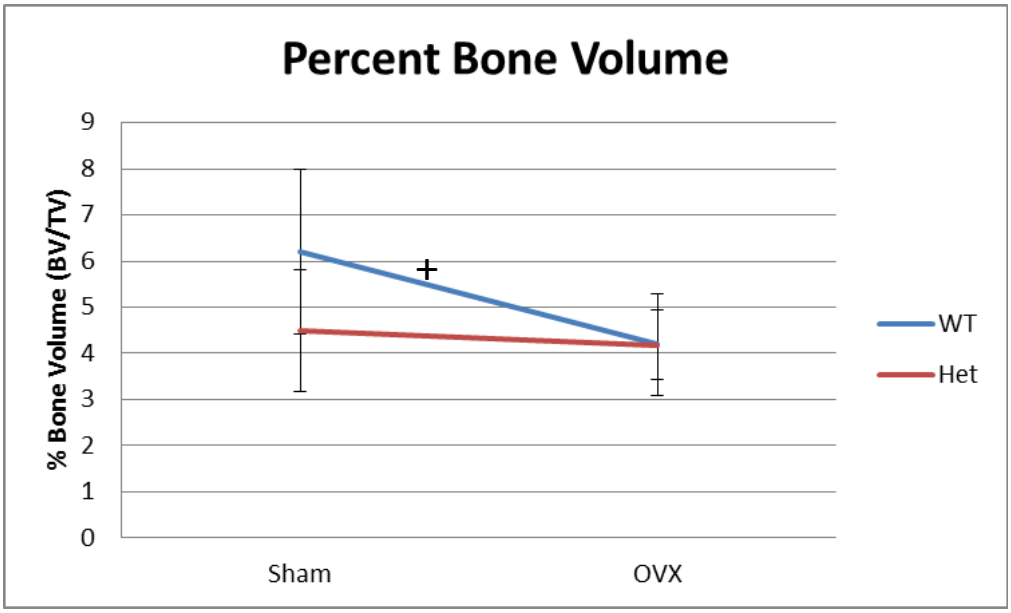
Percent Bone Volume
% Bone Volume (BV/TV)
9
8
7
6
5
4
3
2
1
0
Sham
OVX
WT
Het

(B)

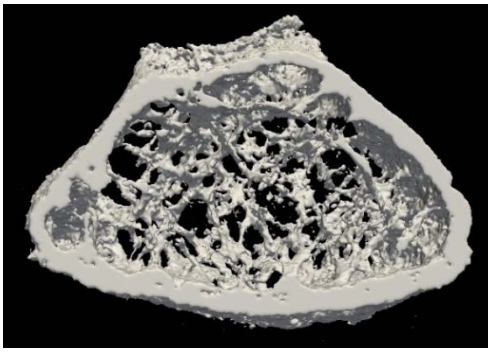

(C)

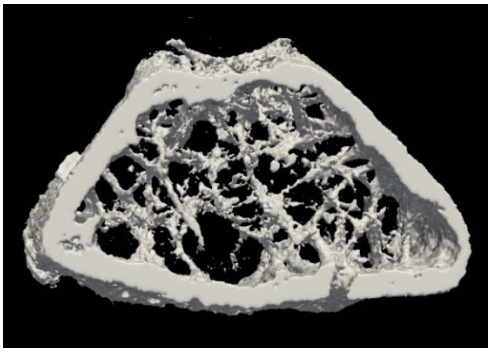

(D

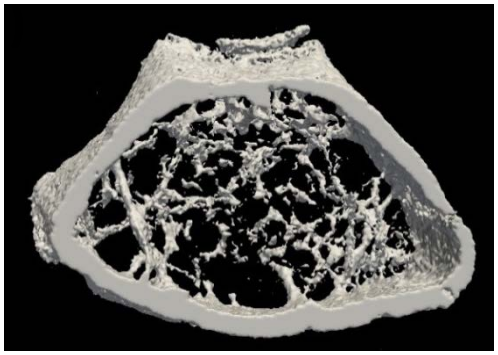

(E)

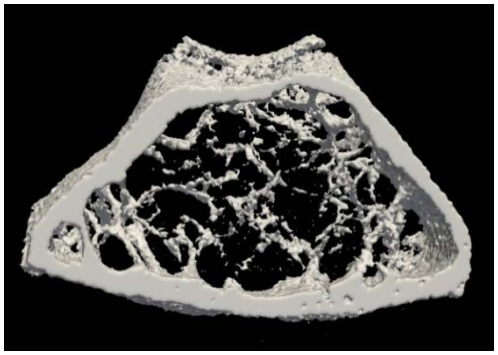

Figure 5.3 - *TWIST-1*$^{+/-}$ animals maintain trabecular bone volume following ovariectomy. μCT data (trabecular analysis) showing **(A)** Tissue volume **(B)** Bone volume. Statistically significant (n = 10) ($p < 0.05$, ANOVA with Tukey's post test) results WT sham verses WT OVX denoted by (+) and *TWIST-1*$^{+/-}$ sham verses *TWIST-1*$^{+/-}$ OVX denoted by (*).

(A)

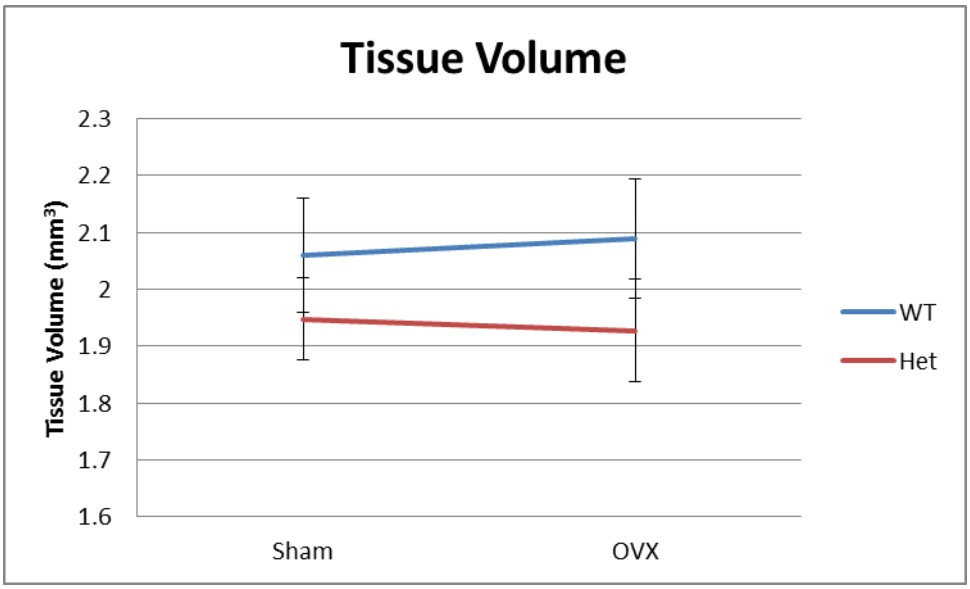
Tissue Volume
Tissue Volume (mm³)
2.3
2.2
2.1
2
1.9
1.8
1.7
1.6
Sham
OVX
WT
Het

(B)

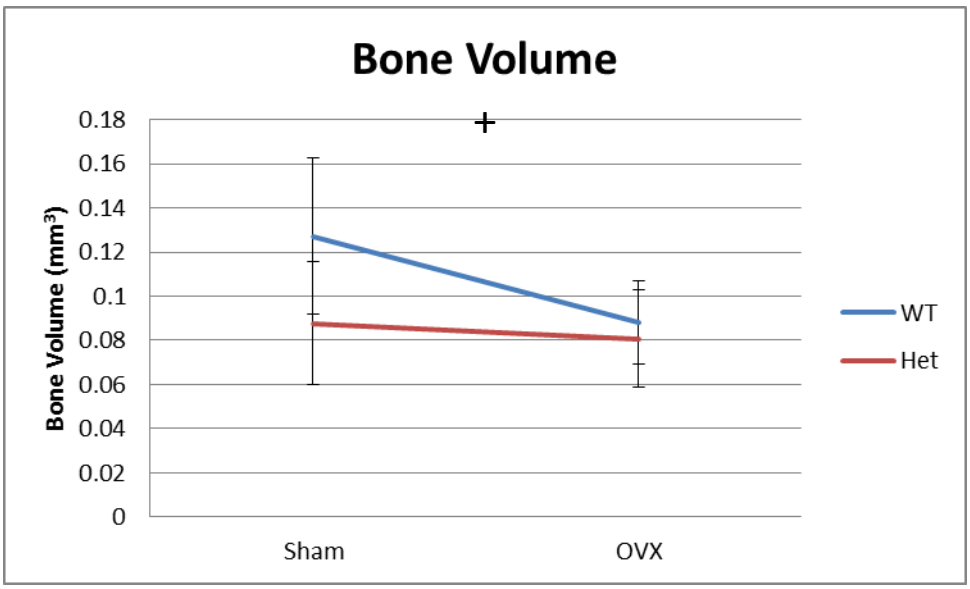
Bone Volume
Bone Volume (mm³)
0.18
0.16
0.14
0.12
0.1
0.08
0.06
0.04
0.02
0
Sham
OVX
WT
Het

Figure 5.4 – WT animals have significantly reduced bone surface following ovariectomy. Histomorphometric analysis showing **(A)** Per cent bone volume **(B**) Bone surface. Statistically significant (n = 4) ($p < 0.05$, ANOVA with Tukey's post test) results WT sham verses WT OVX denoted by (+) and *TWIST-1*$^{+/-}$ sham verses *TWIST-1*$^{+/-}$ OVX denoted by (*****).

(A)

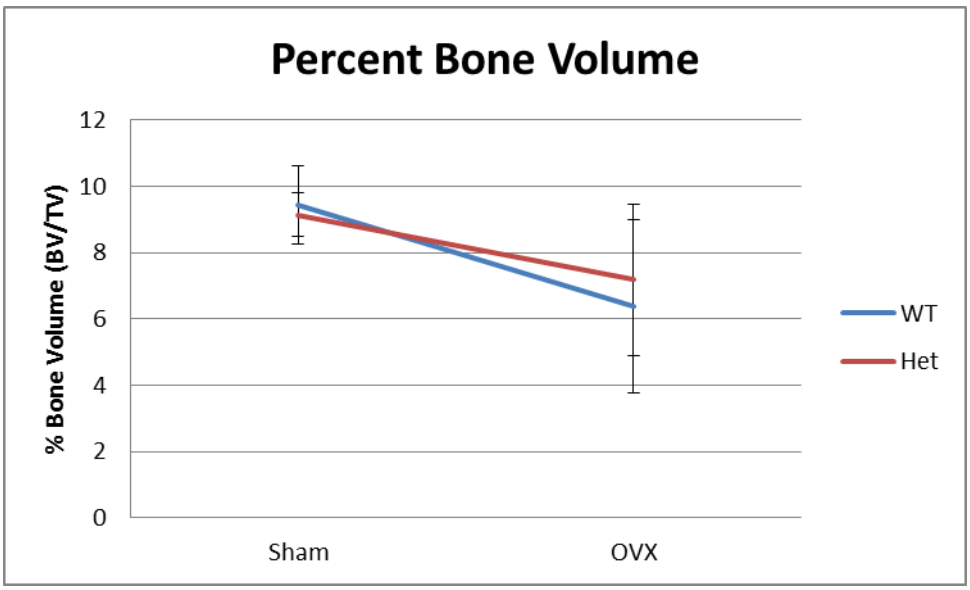
Percent Bone Volume
% Bone Volume (BV/TV)
12
10
8
6
4
2
0
Sham
OVX
WT
Het

(B)

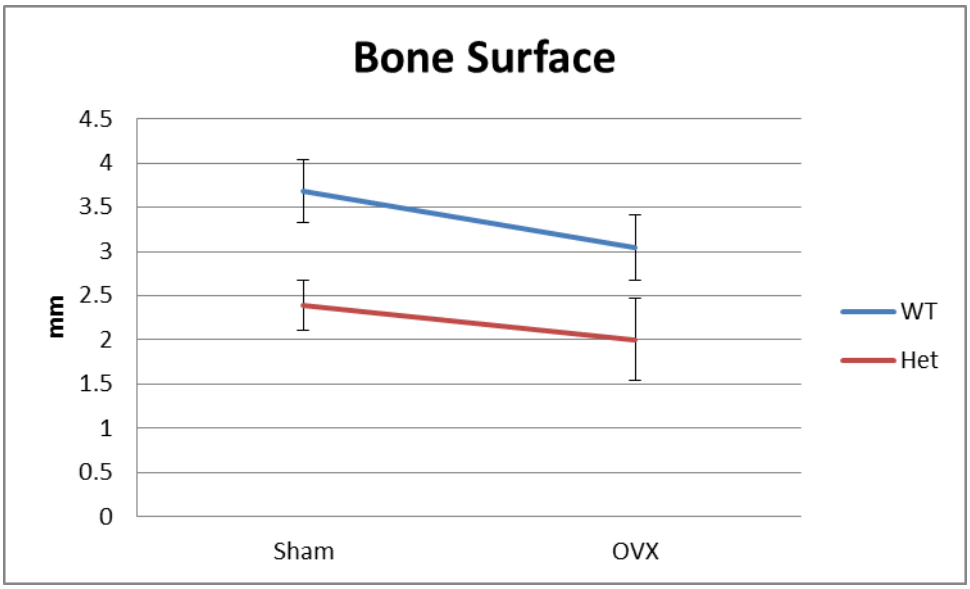
Bone Surface
mm
4.5
4
3.5
3
2.5
2
1.5
1
0.5
0
Sham
OVX
WT
Het

Figure 5.5 - *TWIST-1*$^{+/-}$ animals maintain bone surface and intersection surface following ovariectomy. μCT (trabecular analysis) data showing **(A)** Bone surface **(B)** Intersection surface **(C)** Bone surface to volume ratio. Statistically significant (n = 10) ($p < 0.05$, ANOVA with Tukey's post test) results WT sham verses WT OVX denoted by (+) and *TWIST-1*$^{+/-}$ sham verses *TWIST-1*$^{+/-}$ OVX denoted by (*).

(A)

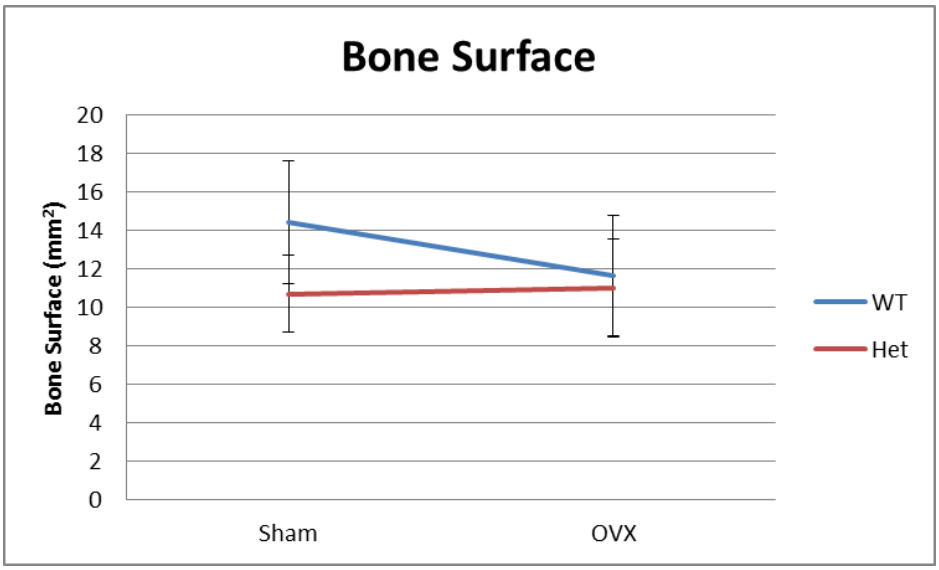
Bone Surface
Bone Surface (mm²)
20
18
16
14
12
10
8
6
4
2
0
Sham
OVX
WT
Het

(B)

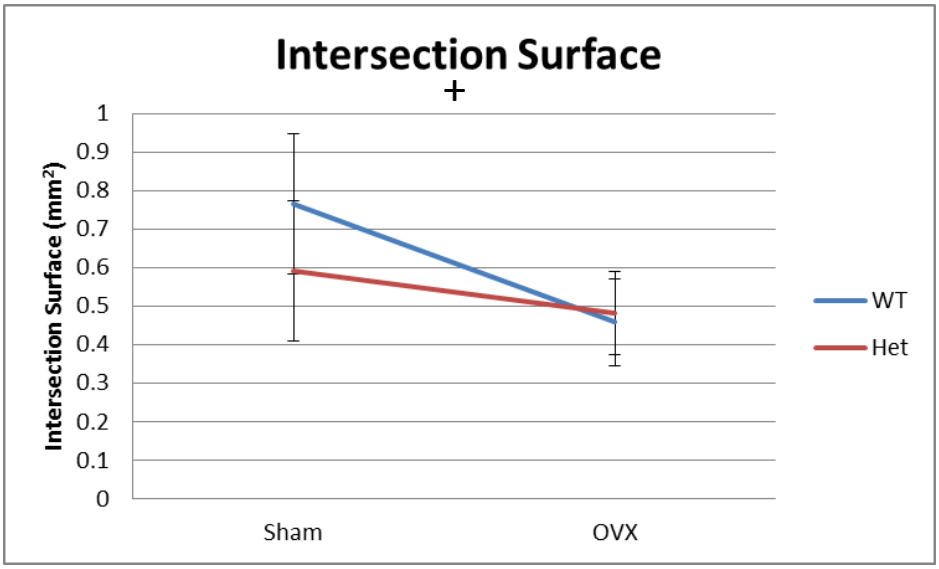
Intersection Surface
Intersection Surface (mm²)
1
0.9
0.8
0.7
0.6
0.5
0.4
0.3
0.2
0.1
0
Sham
OVX
WT
Het

(C)

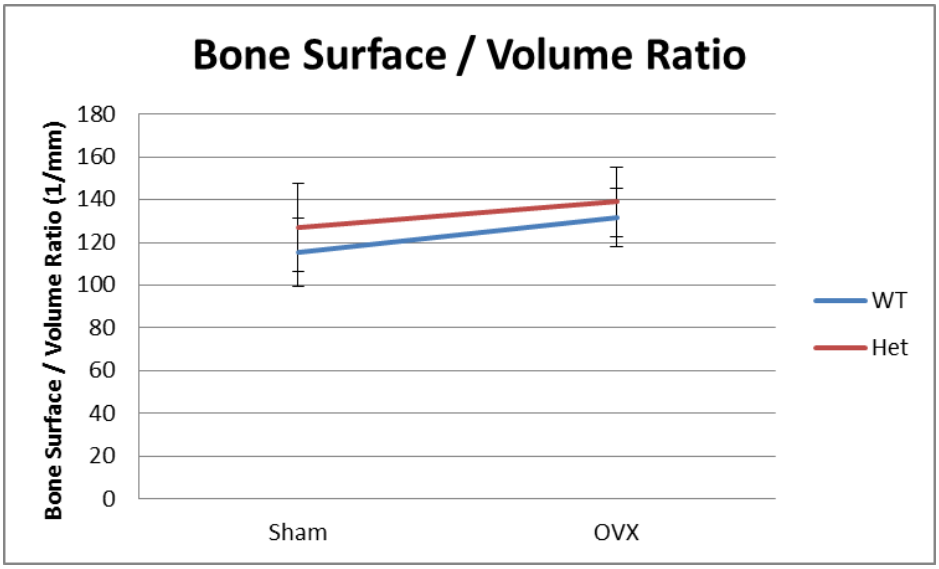
Bone Surface / Volume Ratio
Bone Surface / Volume Ratio (1/mm)
180
160
140
120
100
80
60
40
20
0
Sham
OVX
WT
Het

Figure 5.6 - *TWIST-1*$^{+/-}$ animals maintain bone surface density and trabecular number following ovariectomy. μCT data (trabecular analysis) showing **(A)** Bone surface density **(B)** Trabecular thickness **(C)** Trabecular number. Statistically significant (n = 10) ($p < 0.05$, ANOVA with Tukey's post test) results WT sham verses WT OVX denoted by (+) and *TWIST-1*$^{+/-}$ sham verses *TWIST-1*$^{+/-}$ OVX denoted by (*).

(A)

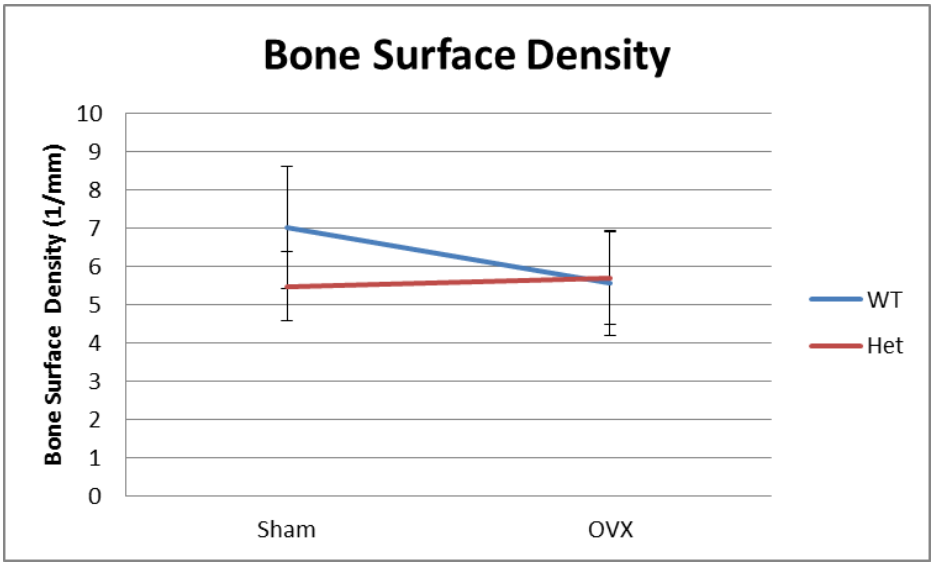
Bone Surface Density
Bone Surface Density (1/mm)
10
9
8
7
6
5
4
3
2
1
0
Sham
OVX
WT
Het

(B)

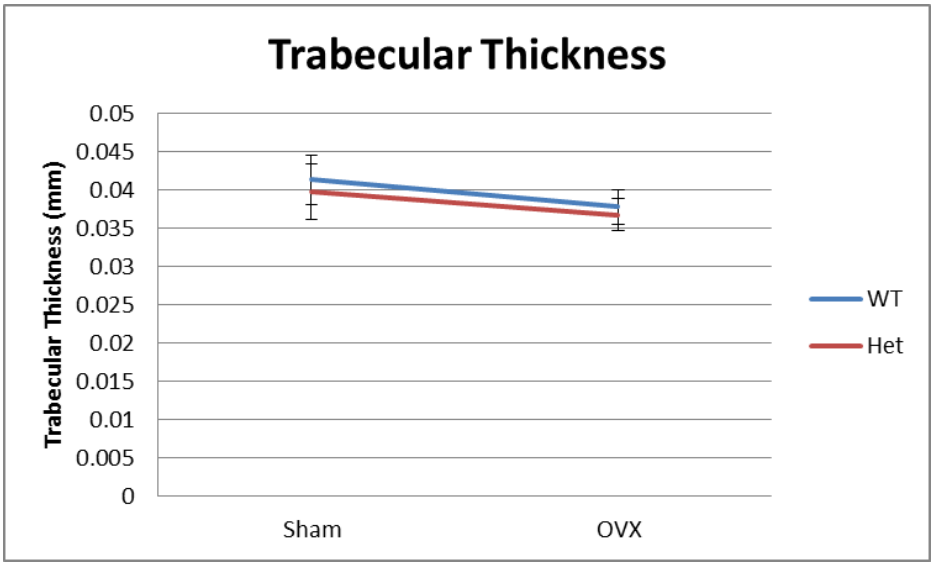
Trabecular Thickness
Trabecular Thickness (mm)
0.05
0.045
0.04
0.035
0.03
0.025
0.02
0.015
0.01
0.005
0
Sham
OVX
WT
Het

(C)

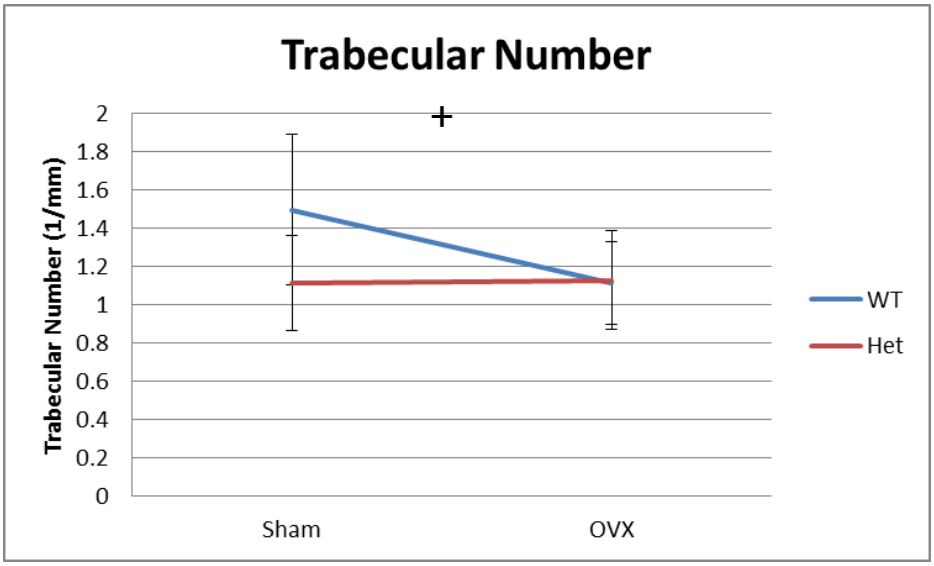
Trabecular Number
Trabecular Number (1/mm)
2
1.8
1.6
1.4
1.2
1
0.8
0.6
0.4
0.2
0
Sham
OVX
WT
Het

5.2.4 *TWIST-1*$^{+/-}$ mice maintain total CFU-F numbers following ovariectomy

Compact bone and marrow derived CFU-F were cultured to determine the effect of osteoporosis on bone marrow derived MSC populations in WT and *TWIST-1*$^{+/-}$ mice (figure 5.7). Following ovariectomy, WT mice experienced a statistically significant ($p<0.05$, ANOVA with Tukey's post test) reduction in the total number of CFU-F compared to relevant sham controls. In contrast, *TWIST-1*$^{+/-}$ mice exhibited no significant reduction in the total number of CFU-F following ovariectomy. Interestingly, there was a non-significant ($p<0.05$, ANOVA with Tukey's post test) trend toward a reduction in the relative number of CFU-F in *TWIST-1*$^{+/-}$ sham mice compared to WT sham mice.

5.2.5 *TWIST-1*$^{+/-}$ mice have decreased osteoblast numbers following ovariectomy

Histomorphometric analysis was used to determine the relative number of osteoblasts per mm^2 to determine the effect of osteoporosis on osteoblast numbers in WT and *TWIST-1*$^{+/-}$ mice (figure 5.8). Results showed a non-significant ($p<0.05$, ANOVA with Tukey's post test) trend towards a reduced osteoblast population present in the trabecular spaces of *TWIST-1*$^{+/-}$ mice following ovariectomy. Conversely, there was a non-significant ($p<0.05$, ANOVA with Tukey's post test) trend towards increased osteoblast numbers in the trabecular spaces of WT mice following ovariectomy.

5.2.6 *TWIST-1*$^{+/-}$ mice display no increase in osteoclast number following ovariectomy

Histomorphometric analysis was used to enumerate osteoclasts lining the growth plate to determine the effect of osteoporosis on osteoclast numbers in WT and *TWIST-1*$^{+/-}$ mice (figure 5.8). There was no change in the number of multi-nucleated osteoclasts per mm bone surface

Figure 5.7 – Wild type mice have a reduction in total CFU-F numbers following ovariectomy. Total CFU-F colonies at 8 weeks post ovariectomy. Statistically significant ($n = 4$) ($p < 0.05$, ANOVA with Tukey's post test) results denoted by (*).

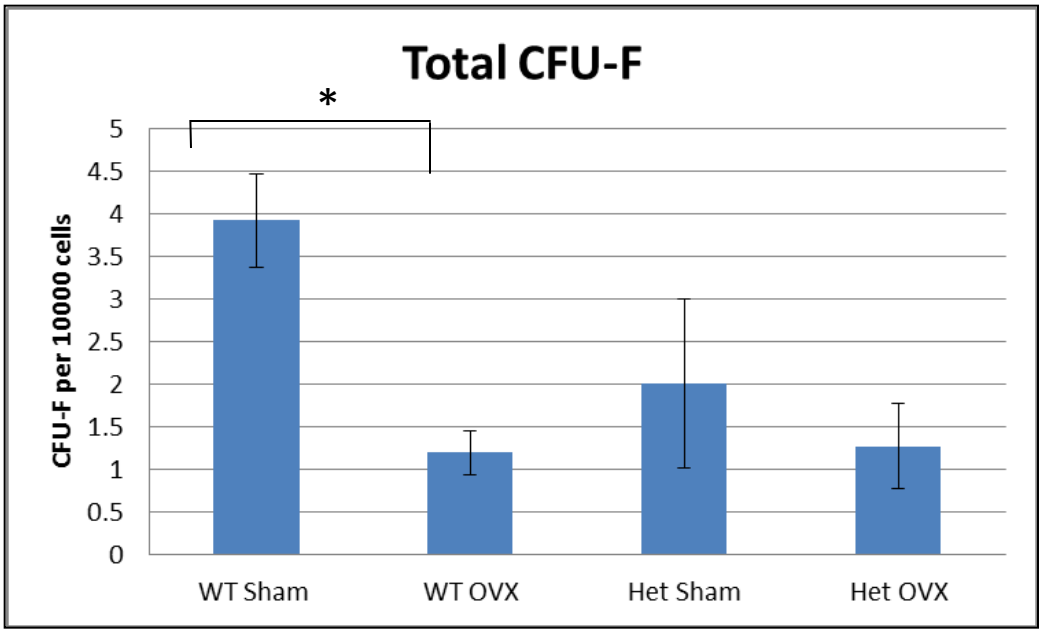
Total CFU-F
*
CFU-F per 10000 cells
5
4.5
4
3.5
3
2.5
2
1.5
1
0.5
0
WT Sham
WT OVX
Het Sham
Het OVX

Figure 5.8 - *TWIST-1*$^{+/-}$ animals have significantly reduced relative osteoblast numbers and maintain constant osteoclast numbers following ovariectomy. Histomorphometric analysis showing **(A)** Osteoblast number per mm^2 **(B**) Osteoclast number per mm bone surface. Statistically significant (n = 4) ($p < 0.05$, ANOVA with Tukey's post test) results WT sham verses WT OVX denoted by (+) and *TWIST-1*$^{+/-}$ sham verses *TWIST-1*$^{+/-}$ OVX denoted by (*).

(A)

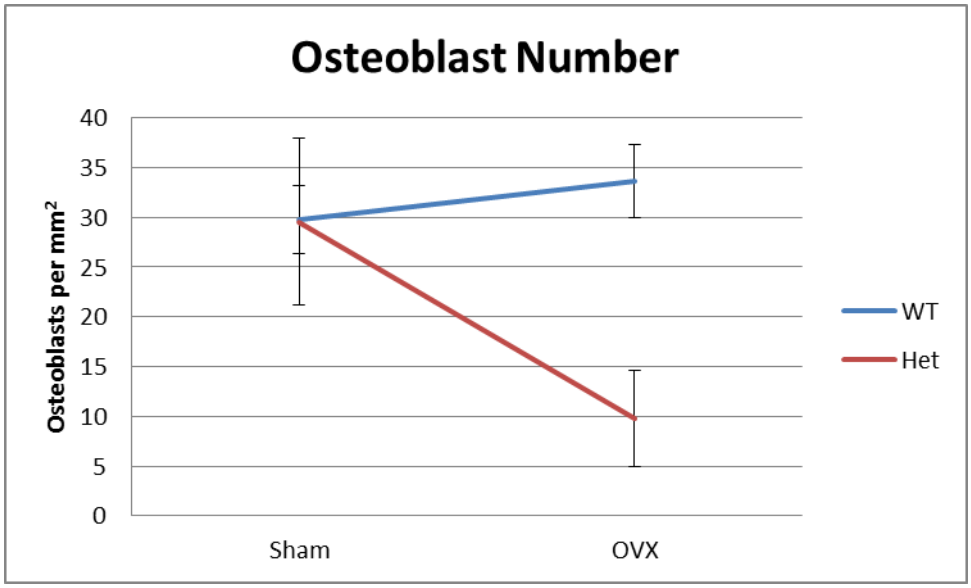
Osteoblast Number
Osteoblasts per mm²
40
35
30
25
20
15
10
5
0
Sham
OVX
WT
Het

(B)

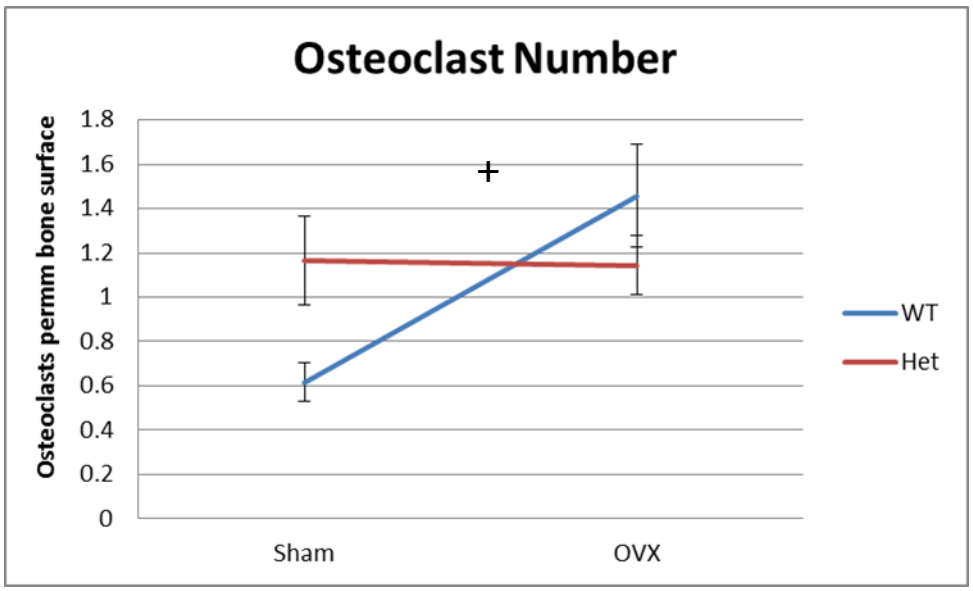
Osteoclast Number
Osteoclasts permm bone surface
1.8
1.6
1.4
1.2
1
0.8
0.6
0.4
0.2
0
Sham
OVX
WT
Het

following ovariectomy within the *TWIST-1*$^{+/-}$ mouse cohort. However, there was a statistically significant ($p<0.05$, ANOVA with Tukey's post test) increase in the relative number of osteoclasts within the WT mouse cohort following ovariectomy. When comparing the relative number of osteoclasts between WT and *TWIST-1*$^{+/-}$ mouse sham groups, there was a non-significant ($p<0.05$, ANOVA with Tukey's post test) trend towards a greater osteoclast number within the *TWIST-1*$^{+/-}$ mouse group.

5.2.7 Cortical bone strength is not affected at eight weeks post ovariectomy

Assessment of the mechanical properties of femora harvested from mice eight weeks post-surgery was conducted using three point bend testing as described in section 2.6.9. Results from these experiments showed that there were no statistically significant ($p<0.05$, ANOVA with Tukey's post test) differences following ovariectomy in the WT or *TWIST-1*$^{+/-}$ mouse cohort (figure 5.9). Analysis by μCT was used to determine the 3D histomorphometric differences in cortical bone following ovariectomy in WT and *TWIST-1*$^{+/-}$ mice (figure 5.10). Supporting the findings above, there were no statistically significant ($p<0.05$, ANOVA with Tukey's post test) differences in tissue volume, bone volume or percentage bone volume following ovariectomy in WT or *TWIST-1*$^{+/-}$ mice.

5.2.8 *TWIST-1*$^{+/-}$ mice display increased adipocyte number and area following ovariectomy

Histomorphometric analysis was used to show the effect of ovariectomy on adipogenesis by enumerating the relative number of adipocytes and adipose tissue area following ovariectomy in WT and *TWIST-1*$^{+/-}$ mice (figure 5.11). Relative adipocyte numbers were statistically

Figure 5.9 – No significant mechanical differences observed between Sham and OVX animals at 8 weeks post ovariectomy. Mechanical data using a three point bend test showing **(A)** Ultimate moment **(B)** Flexural rigidity. Statistically significant (n = 10) ($p < 0.05$, ANOVA with Tukey's post test) results WT sham verses WT OVX denoted by (+) and *TWIST-1*$^{+/-}$ sham verses *TWIST-1*$^{+/-}$ OVX denoted by (*).

(A)

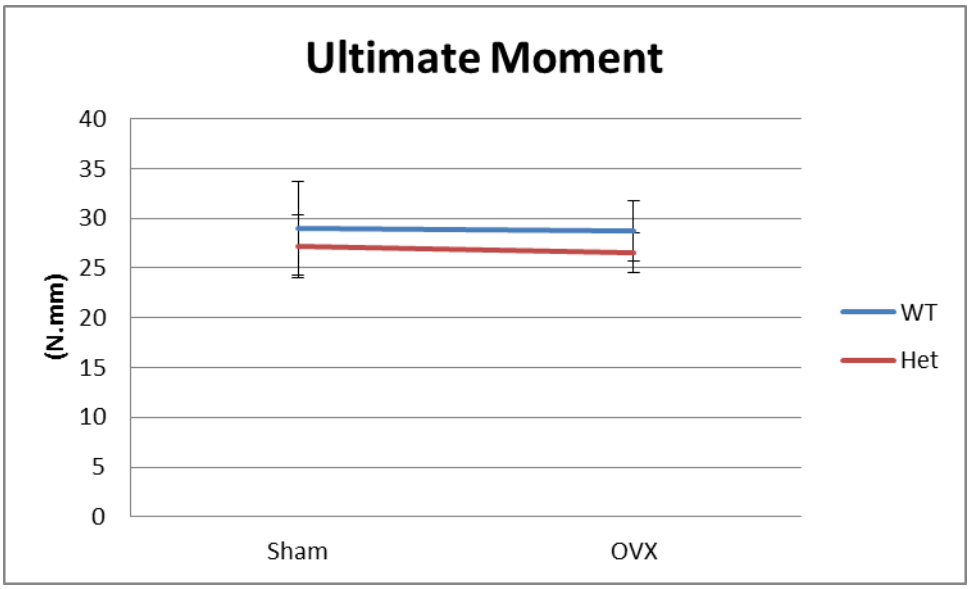
Ultimate Moment
40
35
30
25
20
15
10
5
0
(N.mm)
Sham
OVX
WT
Het

(B)

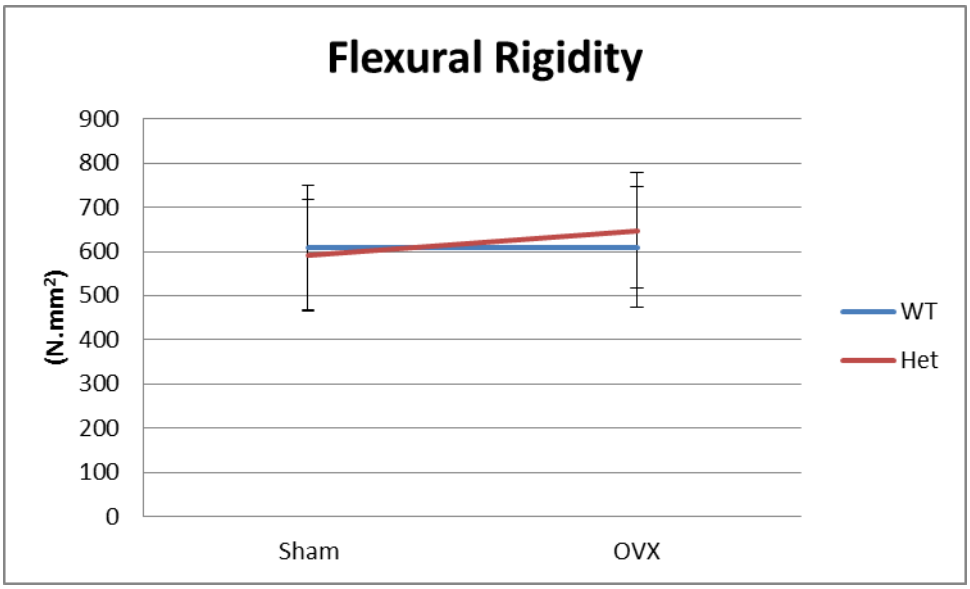
Flexural Rigidity
900
800
700
600
500
400
300
200
100
0
(N.mm²)
Sham
OVX
WT
Het

Figure 5.10 - *TWIST-1*$^{+/-}$ and WT animals maintain cortical bone volume following ovariectomy. μCT data (trabecular analysis) showing **(A)** Tissue volume **(B)** Bone volume **(C)** Per cent bone volume. Statistically significant (n = 10) ($p < 0.05$, ANOVA with Tukey's post test) results WT sham verses WT OVX denoted by (+) and *TWIST-1*$^{+/-}$ sham verses *TWIST-1*$^{+/-}$ OVX denoted by (*).

(A)

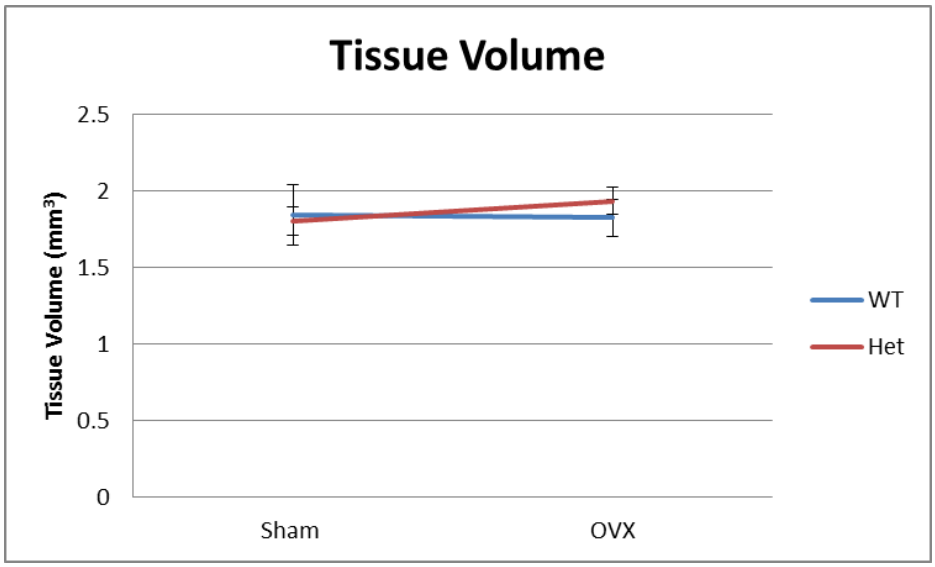
Tissue Volume
Tissue Volume (mm3)
2.5
2
1.5
1
0.5
0
Sham
OVX
WT
Het

(B)

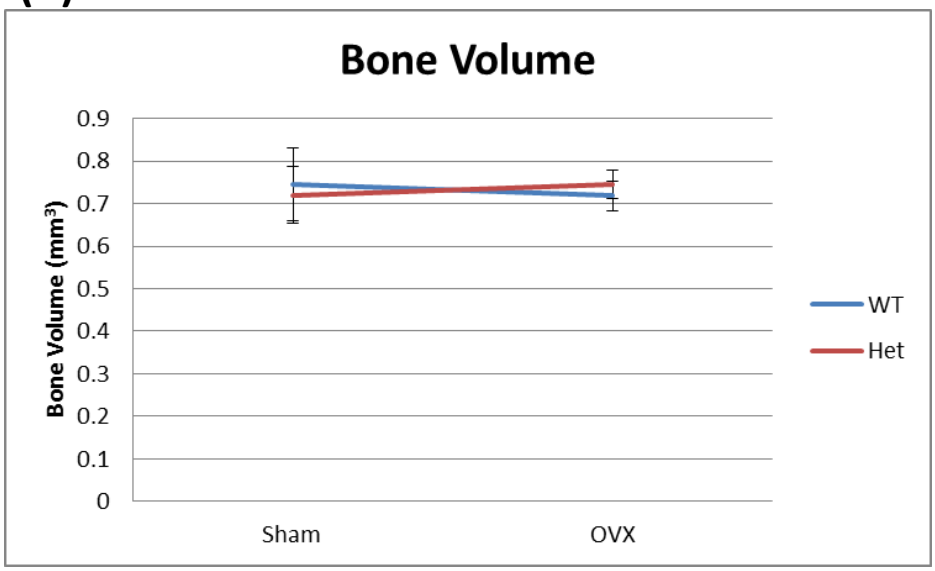
Bone Volume
Bone Volume (mm3)
0.9
0.8
0.7
0.6
0.5
0.4
0.3
0.2
0.1
0
Sham
OVX
WT
Het

(C)

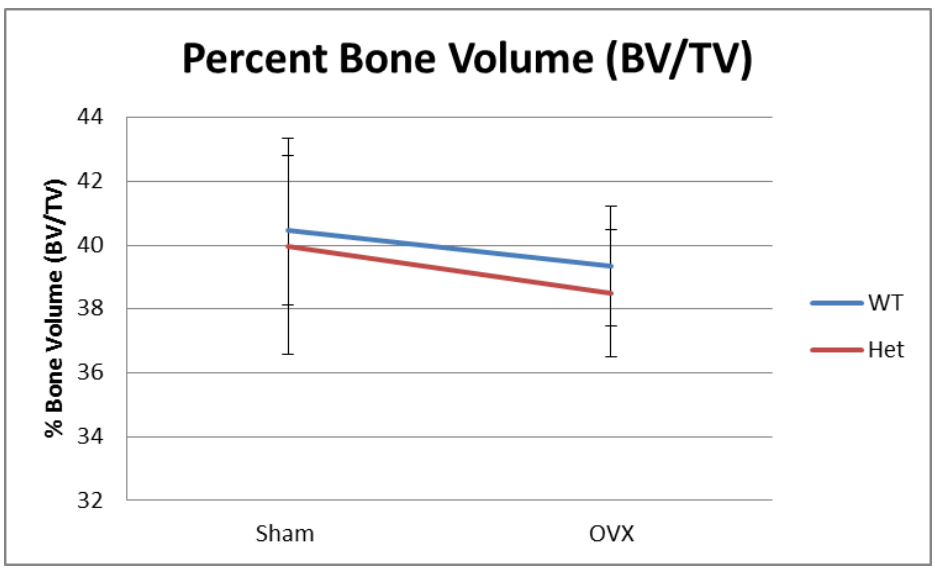
Percent Bone Volume (BV/TV)
% Bone Volume (BV/TV)
44
42
40
38
36
34
32
Sham
OVX
WT
Het

Figure 5.11 - *TWIST-1*$^{+/-}$ animals have significantly increased relative adipocyte numbers following ovariectomy. Histomorphometric analysis showing **(A)** Adipocyte number **(B**) Adipocyte area. **(C)** H&E section showing trabecular region of WT sham mouse at 8 weeks post ovariectomy **(D)** H&E section showing trabecular region of *TWIST-1*$^{+/-}$ sham mouse at 8 weeks post ovariectomy **(E)** H&E section showing trabecular region of WT OVX mouse at 8 weeks post ovariectomy **(F)** H&E section showing trabecular region of *TWIST-1*$^{+/-}$ OVX mouse at 8 weeks post ovariectomy. Statistically significant (n = 10) ($p < 0.05$, ANOVA with Tukey's post test) results WT sham verses WT OVX denoted by (+) and *TWIST-1*$^{+/-}$ sham verses *TWIST-1*$^{+/-}$ OVX denoted by (*). Scale bar: 1mm

(A)

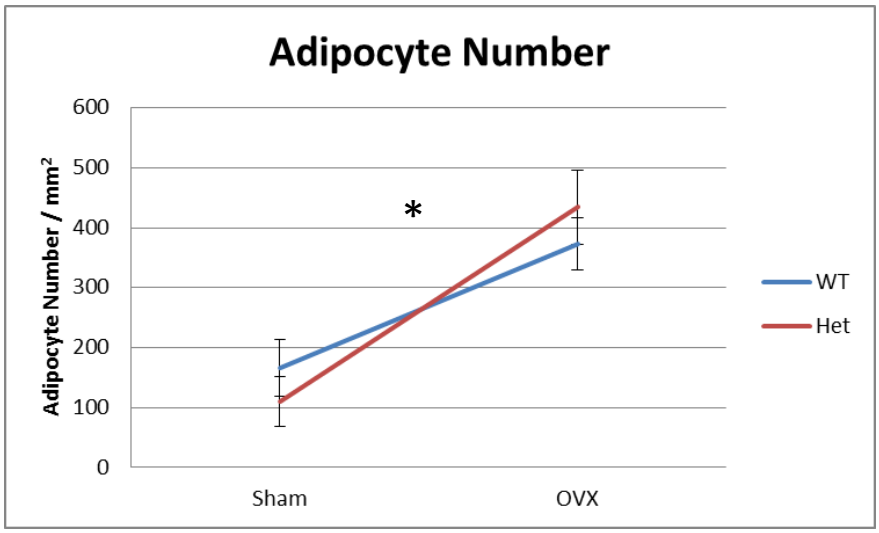
Adipocyte Number
Adipocyte Number / mm²
600
500
400
300
200
100
0
*
Sham
OVX
WT
Het

(B)

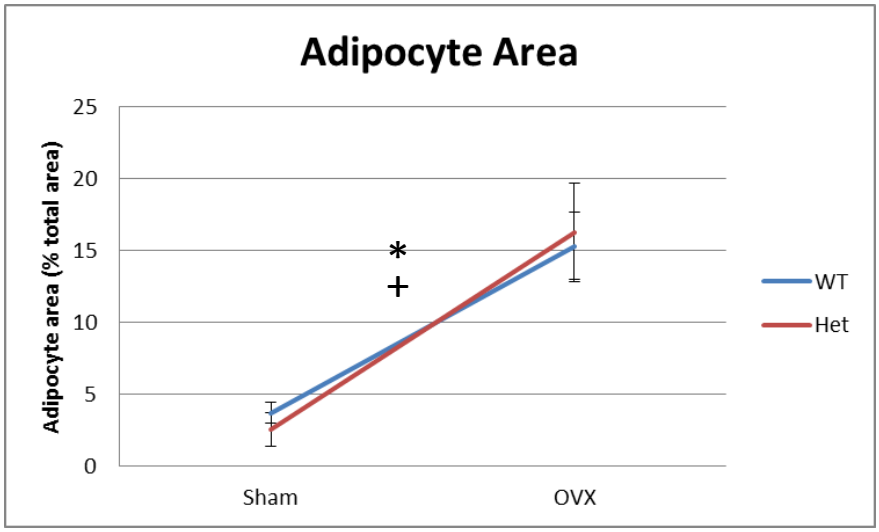
Adipocyte Area
Adipocyte area (% total area)
25
20
15
10
5
0
*
+
Sham
OVX
WT
Het

(C)


Growth Plate

(D)


Growth Plate

(E)


Growth Plate
Adipocytes

(F)

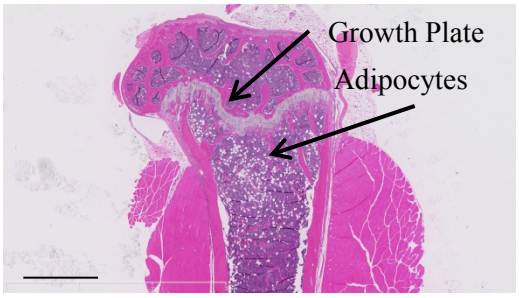
Growth Plate
Adipocytes

significantly ($p<0.05$, ANOVA with Tukey's post test) increased within the trabecular region of *TWIST-1*$^{+/-}$ mice following ovariectomy, while adipocyte area was increased in *TWIST-1*$^{+/-}$ mice and WT mice. These results show that there were a greater number of smaller adipocytes in *TWIST-1*$^{+/-}$ mice following ovariectomy.

5.3 Discussion

The present study focused on identifying the role of *TWIST-1* following ovariectomy induced osteopososis. Recently, reports by Balla et al have compared the bone tissue of aging postmenopausal osteoporotic and non-osteoporotic women and identified the Twist family member *TWIST-2* as being significantly upregulated in patients with osteoporosis (Balla et al., 2008). This group also identified the *TGFβ* signalling cascade as a possible molecular marker able to identify osteoporotic verses non-osteoporotic women prior to the currently accepted measurement of BMD as a diagnostic tool. These findings correlate with our data demonstrating downregulation of *TGF-β2* in MSC with enforced *TWIST-1* expression (section 3.2.1). Previous studies by Glackin et al. and more recent studies from our laboratory demonstrated that *TWIST-1* and *TWIST-2* share extensive homology and cause similar changes in the osteogenic properties of osteoblastic cells when overexpressed in human MSC (Isenmann et al., 2009; Lee et al., 2000). This early work into the functional role of *TWIST-1* and *TWIST-2* in MSC described *TWIST-1* as the upstream regulator of *TWIST-2* in osteogeneic development (Lee et al., 2000). Further to this, preliminary evidence supporting an association of *TWIST-1* with osteoporosis in postmenopausal women has recently been reported (J.-Y. Hwang, 2010). This group showed that human subjects with heterozygous *TWIST-1* mutations had higher BMD values in the femoral neck and proximal femora sites associated with a protective effect on osteoporosis risk in the postmenopausal general population. However, the authors did not discuss whether or not the *TWIST-1* mutation was functional. Therefore, identifying the functional nature of the mutation would help determine the role of the Twist family of genes in the development and progression of osteoporosis.

Genes in the Wnt pathway and the TGF-β superfamily of molecules, identified by microarray analysis of human MSC with enforced expression of *TWIST-1* in Chapter 3, have also been

implicated in ovariectomy induced bone loss. Overexpression of *TGF-β in vivo* has been demonstrated to prevent ovariectomy induced bone loss and *TGF-β* signalling in T-cells preserves bone homeostasis by blunting T cell activation (Gao et al., 2004). Supporting this data, *TGFβ-1* null mice and mutations in humans lead to reductions in bone mass (Geiser et al., 1998; Langdahl et al., 1997). More recently, it has been shown that *TGFβ-1* was downregulated six weeks post ovariectomy (Estai et al., 2011). Furthermore, *TGFβ-1* expression was recovered by administration of oestrogen resulting in improvements in fracture healing. Together these data support our findings as we demonstrated downregulation of TGFβ family members in MSC with enforced *TWIST-1* expression leading to reductions in the osteogenic capacity of MSC overexpression *TWIST-1*.

Bone morphogenetic proteins have been implicated in osteopososis since the 1980s when it was hyphothesised that osteoporosis was a BMP autoimmune disorder (Urist et al., 1985). BMPs, members of the TGF-β superfamily of molecules, and SMADs have been suggested as potential targets for the treatment of osteopososis (Li, 2008). The result of transduction of *BMP2* into human MSC from an aged person with osteoporosis demonstrated that these cells were able to produce ectopic mineral *in virto* to a similar degree as cells from a young, healthy individual (Turgeman et al., 2001). Interestingly, a common polymorphism in *BMP4* has been reported and associated with low BMD in postmenopausal women (Ramesh Babu et al., 2005). Our data show that enforced expression of *TWIST-1* results in the down regulation of *BMP4*, suggesting that *BMP4* would be upregulated in *TWIST-1*$^{+/-}$ mice leading to a reduction in the effects of osteoporosis in *TWIST-1*$^{+/-}$ mice. Further evidence supporting our findings comes from data suggesting that Twist family members control the onset of osteogenesis through interactions between the binding domain of *RUNX2* leading to inhibition of *RUNX2* activity and osteogenic gene activation (Bialek et al., 2004).

In contrast to our findings, the Wnt pathway, through loss of function or gain of function mutations in *LRP5,* has been implicated in early onset osteoporosis and conditions of increased bone mineral density respectively (Gong et al., 2001; Johnson et al., 1997; Korvala J, 2012; Levasseur et al., 2005). Analysis of the effects of *LRP5* knockout in mice has shown that the low bone mass is a result of decreases in the proliferation of osteoblasts and not from increased bone resorption (Kato et al., 2002). Studies investigating the role of Wnt signalling using *AXIN2* knockout mice demonstrated significant increases in trabecular bone mass compared to WT controls (Yan et al., 2009). This group were also able to show enhanced osteogenesis and a reduction in osteoclast formation *in vitro* suggesting a role for the Wnt pathway in osteoclastogenesis. In contrast, our findings show that enforced expression of *TWIST-1* stimulates the Wnt pathway suggesting Wnt pathway suppression in *TWIST-1* deficient mice does not lead to a reduction in osteoclast number.

The data generated in the present study found that during osteoporosis CFU-F numbers are diminished. However, no significant difference in the CFU-F population within *TWIST-1*$^{+/-}$ mice was observed following ovariectomy resulting in preservation of trabecular bone volume. Furthermore, osteoclast numbers were statistically significantly increased following ovariectomy in the WT group and not the *TWIST-1*$^{+/-}$ mouse group. A possible mechanism for the maintenance of bone volume of *TWIST-1*$^{+/-}$ mice following ovariectomy could be related to the relative amount of MSC producing fewer cytokines involved in the recruitment of bone resorbing osteoclasts as evidenced by a reduction in the relative osteoblast numbers of *TWIST-1*$^{+/-}$ mice coupled with no change in the relative numbers of osteoclasts, within this cohort, following ovariectomy.

In summary, our findings reveal a critical role for *TWIST-1* in osteoporosis. Inhibition of *TWIST-1* expression using a *TWIST-1*$^{+/-}$ mouse model allowed us to demonstrate a protective effect resulting in maintenance of bone mass following ovariectomy. The data support strong associations between *TWIST-1* and bone loss following ovariectomy and possible mechanisms relating to the Wnt/ β-catenin signalling pathway and the TGF-β superfamily of molecules including BMPs and SMADs have been outlined above with strong correlations between our *in vitro* data and multiple publications assessing *TWIST-1* target genes and pathways in the context of osteoporosis. Finally, the information provided gives rise to multiple lines of investigation relating to the regulation of various *TWIST-1* targets, or *TWIST-1* itself, with clinical applications for the maintenance of osteoporosis as patients treated would benefit from reductions in bone loss observed in the *TWIST-1*$^{+/-}$ mouse model.

6 General Discussion and Future Directions

Current literature provides strong support of the critical role of different stromal populations in skeletal tissue and blood cell development (Gronthos et al., 2006; Gronthos et al., 1994; Isenmann et al., 2007; Ramasamy et al., 2008; Shi et al., 2002). More recently, the genetic factors controlling MSC proliferation, differentiation and commitment are becoming clearer (Chang et al., 2007; de Boer et al., 2004; Gregory et al., 2005; Isenmann et al., 2009; Lin and Hankenson, 2011; Liu et al., 2011; Psaltis et al., 2008; Zhou, 2011; Zhou et al., 2004). The Twist family of proteins have been implicated in MSC proliferation, differentiation and commitment, where their association in the disease state of osteoporosis has been predicted by two groups (Balla et al., 2008; J.-Y. Hwang, 2010). Recent studies in our laboratory have shown that enforced expression of *TWIST-1* in MSC extends their lifespan *in vitro* and maintains the cells in an immature state by inhibiting cellular senescence (Cakouros et al., 2012; Isenmann et al., 2009). Preliminary studies have been performed regarding the effect of *TWIST-1* on osteogenesis using osteosarcoma cell lines and animal models (Bourgeois et al., 1998; Browning et al., 2001; Natacha Entz-Werlé, 2005). Although there are no papers directly assessing the role of *TWIST-1* in fracture, many *TWIST-1* target genes have been implicated in adult bone repair (Glatt et al., 2012; Jawad et al., 2013; Montjovent et al.; Regard et al., 2012; Schwabe et al., 2012). These data were an important factor in our line of investigation with regards to *TWIST-1* and osteoporosis and adult bone healing.

The aims of this thesis were to identify potential *TWIST-1* targets and examine the effects of these molecules on the process of proliferation, differentiation and commitment. In addition, this thesis examined the effects of *TWIST-1* deficiency during trauma and bone disease using a *TWIST-1*$^{+/-}$ mouse model of fracture healing and osteoporosis, respectively. The data generated

from these studies confirm interactions between *TWIST-1* and gene targets identified by microarray while also demonstrating their effect on the regulation of cell proliferation and differentiation *in vitro*, using genetically modified MSC lines. The data also demonstrated that lower levels of *TWIST-1 in vivo* resulted in enhanced bone fracture healing and reduced the impact of ovariectomy induced bone loss in mice. The *TWIST-1*$^{+/-}$ mice used in the fracture and ovariectomy experiments were deficient for *TWIST-1* globally. That is, there was only one functional *TWIST-1* allele in every cell type within the animal resulting in lower levels of *TWIST-1* expression in all cells that normally express *TWIST-1*. Therefore, the effects seen in the fracture and ovariectomy experiments may not be solely due to depleted levels of *TWIST-1* in the MSC/stromal population and could also be the result of a reduction in *TWIST-1* expression in other cell types.

Retroviral transduction was used to deliver *WNT2* and *WNT2B* expression constructs into human MSC that are normally refractory to conventional transfection. The expression vectors contained a GFP-reporter gene that indicated successful transduction and allowed the purification of infected MSC by FACS without the need for antibiotic selection which is often associated with cellular toxicity even for transduced primary cells. Confirmation of enforced *WNT2* and *WNT2B* expression at the mRNA was confirmed by real-time PCR analysis. The present study did not confirm increased protein expression of either *WNT2* or *WNT2B* due to the large number of cells required to obtain sufficient protein quantities for Western blot analysis, which has been a limiting factor to experiments using transformed human MSC in the past. The result of stimulation of the Wnt pathway by regulatory genes such as *WNT2* and *WNT2B* is the stabilization of activated β-catenin which translocates the nucleus to drive transcription and activate a negative feedback loop via *AXIN2* (Jho et al., 2002; Lustig et al., 2002). The present study confirmed elevated levels of the activated form of β-catenin in protein lysates of *TWIST-1*

overexpressing MSC and elevated levels of *AXIN2* at the mRNA level demonstrating stimulation of the Wnt pathway and adding credibility to the assessment of the functional role of *WNT2* and *WNT2B* in MSC. While retroviral transduction offers a relatively efficient mode of genetically modifying MSC, the initial infection efficiencies prior to selection by FACS varied between 10% and 82%. Therefore, it is difficult to determine which cells amongst a heterogeneous population are being infected, where the infection may preferentially favour a certain subpopulation of MSC. This may explain the differential properties between the donors analysed given that the transduction efficiency varied between populations. To investigate this inherent variation immunophenotypic analysis was performed to assess the relative maturation state of each donor population. The use of multiple, independent assays (such as BrdU, data not shown, and population doublings to measure proliferation) helped confirm observations and reduce the effects of variation between different *WNT2* and *WNT2B* overexpressing lines. In general, the observations made when multiple assays were used gave further confidence of low experimental error when similar results were generated using MSC derived from the same donor.

The Wnt pathway has been identified as an important regulator of MSC differentiation, however, the literature is divided as to the exact role as it is evident the levels of expression and microenvironment variation determine the cellular effect (Gaur et al., 2005; Hill et al., 2005; Liu et al., 2011; Maria P. Yavropoulou, 2007). The present study showed enhanced proliferation potential in MSC overexpressing *WNT2* and enhanced capacity of MSC overexpressing *WNT2B* to differentiate towards the adipogenic linage. These results are consistent with the effects of enforced *TWIST-1* expression on MSC *in vitro* and help to describe the mechanism of action of *TWIST-1* on MSC populations.

In Chapter 4, we employed a femoral fracture model to compare the bone healing in WT and *TWIST-1*$^{+/-}$ mice, utilising a carbon rod internal fixation system. The importance of *TWIST-1* in development and correct patterning of the skeleton of these mice was evident as a prominent phenotype with skeletal defects was observed consistently. We were able to demonstrate enhanced osteoblastic activity in the fractures of *TWIST-1*$^{+/-}$ mice due to a pre-committed alkaline phosphatise positive population of clonogenic MSC. This resulted in enhanced mineralization at early time-points as evidenced by increased percentage of bone volume and complete bone bridging in *TWIST-1*$^{+/-}$ mice at two weeks post fracture. Interestingly, at four and eight weeks post fracture, percent bone volume was reduced indicating enhanced remodelling in *TWIST-1*$^{+/-}$ mice. Together these results indicate enhanced fracture repair in *TWIST-1*$^{+/-}$ mice compared to WT controls. This highlights *TWIST-1* or *TWIST-1* regulated genes as possible therapeutic targets in fracture repair.

In Chapter 5, we used an ovariectomy induced osteoporosis model to compare the rate of bone loss between WT and *TWIST-1*$^{+/-}$ mice *in vivo*. Using μCT analysis we were able to demonstrate reduced bone volume and percentage bone volume in WT mice following ovariectomy but noted no changes to these values in the *TWIST-1*$^{+/-}$ cohort suggesting a protective effect due to reduced *TWIST-1* levels. However, there were no differences in the mechanical properties of these mice, where analyses of the cortical bone showed no differences between sham and ovariectomized mice. Further to this, trabecular thickness and intersection surface were both reduced significantly in the WT population following ovariectomy. These findings support the predictions of other groups relating to the role of *TWIST-1* in osteoporosis and may prove to reveal a promising target for the diagnosis and eventual treatment of osteopososis, through the discovery of *TWIST-1* target molecules involved in this disease that are receptive to drug therapies.

Mesenchymal stem cells and their progenitors are key cellular components of fracture repair and osteoporosis. Allogeneic human MSC are currently available as a treatment option for non-union fractures of long bones and genetic targets that regulate the properties of these cells have been suggested as potential targets for treatment of various conditions (Alden et al., 2000; Hayashi et al., 2009; Hoeppner et al., 2009; Rawadi and Roman-Roman, 2005). Continued studies determining the role of different factors regulated by *TWIST-1* may have clinical implications in the treatment of multiple conditions related to the maintenance and repair of bone. Further to this, determining the mechanisms by which *TWIST-1* is acting will identify possible targets that could be used to manipulate the properties of human MSC in an *in vivo* setting to enhance the reparative properties of these important cells.

6.1 Future Directions

6.1.1 Isolation and characterisation of mouse embryonic fibroblasts from homozygous Twist $^{-/-}$ embryos

The magnitude and duration of siRNA knockdown in human MSC has proven a limiting factor in our laboratory. Therefore, embryonic fibroblasts could be isolated from the breeding of two heterozygous *TWIST-1*$^{+/-}$ mice, and extraction before embryonic lethality at E11.5, resulting in primary cell lines with no functional *TWIST-1* allele (*TWIST-1*$^{-/-}$ embryos) as well as cells with one functional *TWIST-1* allele (*TWIST-1*$^{+/-}$ embryos*)* or normal *TWIST-1* expression (WT embryos). We could then use these cells *in vitro* to assess the proliferative potential and differentiation in the presence or absence of *TWIST-1*.

6.1.1 Isolation and characterisation of MSC from B6;129S7-*Twist1*^{tm2Bhr}/Mmnc mice

This strain of mouse has been genetically modified to have two loxP sites flanking the entire coding region of *TWIST-1*. Using mice homozygous for the mutation, MSC could be isolated from the bone marrow and cultured *in vitro*. Cultured MSC could be infected with a retroviral or lentiviral construct containing Cre recombinase. This would cause the *TWIST-1* gene to be excised and result in MSC with no *TWIST-1* expression. The resulting cells could be used to assess the proliferative potential and differentiation capacity in the presence or absence of *TWIST-1*. This would also enable us to examine the molecular mechanisms involved in bone formation *in vitro* in the complete absence of *TWIST-1* expression.

6.1.2 Isolation and genetic profiling of pure osteoclasts and osteoblasts from Twist$^{+/-}$ mice

Bone marrow and total bone isolates could be labelled and sorted using fluorescence activated cell sorting to select for specific populations of cells from *TWIST-1*$^{+/-}$ and WT mice. RNA could then be generated from these cells to assess the expression of key genes within specific cellular populations. Assays could also be performed to assess the activity of osteoclasts from *TWIST-1*$^{+/-}$ verses WT controls *in vitro.* Functional experiments of blood derived osteoclasts to test if they WT and *TWIST-1*$^{+/-}$ mice form similar multi-nuclear TRAP +ve cell numbers in vitro and whether they can form similar numbers and sizes of resorbtion pits *in vitro*.

7 References

Agna, J.W., H.C. Knowles, Jr., and G. Alverson. 1958. The mineral content of normal human bone. *J Clin Invest* 37:1357-1361.

Ahrens, M., T. Ankenbauer, D. Schroder, A. Hollnagel, H. Mayer, and G. Gross. 1993. Expression of human bone morphogenetic proteins-2 or -4 in murine mesenchymal progenitor C3H10T1/2 cells induces differentiation into distinct mesenchymal cell lineages. *DNA and cell biology* 12:871-880.

Akune, T., S. Ohba, S. Kamekura, M. Yamaguchi, U.I. Chung, N. Kubota, Y. Terauchi, Y. Harada, Y. Azuma, K. Nakamura, T. Kadowaki, and H. Kawaguchi. 2004. PPARgamma insufficiency enhances osteogenesis through osteoblast formation from bone marrow progenitors. *J Clin Invest* 113:846-855.

Alblowi, J., C. Tian, M.F. Siqueira, R. Kayal, E. McKenzie, Y. Behl, L. Gerstenfeld, T.A. Einhorn, and D.T. Graves. 2012. Chemokine expression is upregulated in chondrocytes in diabetic fracture healing. *Bone*

Alborzi, A., K. Mac, C.A. Glackin, S.S. Murray, and J.H. Zernik. 1996. Endochondral and intramembranous fetal bone development: osteoblastic cell proliferation, and expression of alkaline phosphatase, m-twist, and histone H4. *Journal of craniofacial genetics and developmental biology* 16:94-106.

Alden, T.D., E.J. Beres, J.S. Laurent, J.A. Engh, S. Das, S.D. London, J.A. Jane, Jr., S.B. Hudson, and G.A. Helm. 2000. The use of bone morphogenetic protein gene therapy in craniofacial bone repair. *The Journal of craniofacial surgery* 11:24-30.

Ali, A.A., R.S. Weinstein, S.A. Stewart, A.M. Parfitt, S.C. Manolagas, and R.L. Jilka. 2005. Rosiglitazone causes bone loss in mice by suppressing osteoblast differentiation and bone formation. *Endocrinology* 146:1226-1235.

An, J.H., H. Park, J.A. Song, K.H. Ki, J.Y. Yang, H.J. Choi, S.W. Cho, S.W. Kim, S.Y. Kim, J.J. Yoo, W.Y. Beak, J.E. Kim, S.J. Choi, W. Oh, and C.S. Shin. 2012. Transplantation of

Human Umbilical Cord Blood-Derived Mesenchymal Stem Cells or Their Conditioned Medium Prevents Bone Loss in Ovariectomized Nude Mice. *Tissue engineering. Part A*

Aranda, P., X. Agirre, E. Ballestar, E.J. Andreu, J. Roman-Gomez, I. Prieto, J.I. Martin-Subero, J.C. Cigudosa, R. Siebert, M. Esteller, and F. Prosper. 2009. Epigenetic signatures associated with different levels of differentiation potential in human stem cells. *PLoS ONE* 4:e7809.

Arthur, A., R.A. Panagopoulos, L. Cooper, D. Menicanin, I.H. Parkinson, J.D. Codrington, K. Vandyke, A.C.W. Zannettino, S.A. Koblar, N.A. Sims, K. Matsuo, and S. Gronthos. 2012. EphB4 enhances the process of endochondral ossification and inhibits remodelling during bone fracture repair. *Journal of Bone and Mineral Research* n/a-n/a.

Arthur, A., A. Zannettino, and S. Gronthos. 2009. The therapeutic applications of multipotential mesenchymal/stromal stem cells in skeletal tissue repair. *J Cell Physiol* 218:237-245.

Augello, A., and C. De Bari. 2010. The regulation of differentiation in mesenchymal stem cells. *Human gene therapy* 21:1226-1238.

Australia, O. 2006. Medications and Treatments for Osteoporosis. In NSW Multicultural Health Communication Service.

Baglio, S.R., D.M. Pegtel, and N. Baldini. 2012. Mesenchymal stem cell secreted vesicles provide novel opportunities in (stem) cell-free therapy. *Frontiers in physiology* 3:359.

Balla, B., J. Kósa, J. Kiss, A. Borsy, J. Podani, I. Takács, Á. Lazáry, Z. Nagy, K. Bácsi, G. Speer, L. Orosz, and P. Lakatos. 2008. Different Gene Expression Patterns in the Bone Tissue of Aging Postmenopausal Osteoporotic and Non-osteoporotic Women. *Calcified Tissue International* 82:12-26.

Barachini, S., L. Trombi, S. Danti, D. D'Alessandro, B. Battolla, A. Legitimo, C. Nesti, I. Mucci, M. D'Acunto, M.G. Cascone, L. Lazzeri, L. Mattii, R. Consolini, and M. Petrini. 2009. Morpho-functional characterization of human mesenchymal stem cells from umbilical cord blood for potential uses in regenerative medicine. *Stem Cells Dev* 18:293-305.

Baron, R., and G. Rawadi. 2007. Targeting the Wnt/β-Catenin Pathway to Regulate Bone Formation in the Adult Skeleton. *Endocrinology* 148:2635-2643.

Baron R, T.R., Vignery A. 1984. Evidence of sequential remodeling in rat trabecular bone: morphology, dynamic histomorphometry, and changes during skeletal maturation. *Anat Rec.* 137-145.

Barry, F., R.E. Boynton, B. Liu, and J.M. Murphy. 2001. Chondrogenic differentiation of mesenchymal stem cells from bone marrow: differentiation-dependent gene expression of matrix components. *Exp Cell Res* 268:189-200.

Behr, B., M.T. Longaker, and N. Quarto. 2010a. Differential activation of canonical Wnt signaling determines cranial sutures fate: a novel mechanism for sagittal suture craniosynostosis. *Dev Biol* 344:922-940.

Behr, B., M.T. Longaker, and N. Quarto. 2010b. Differential activation of canonical Wnt signaling determines cranial sutures fate: A novel mechanism for sagittal suture craniosynostosis. *Developmental Biology* 344:922-940.

Bialek, P., B. Kern, X. Yang, M. Schrock, D. Sosic, N. Hong, H. Wu, K. Yu, D.M. Ornitz, E.N. Olson, M.J. Justice, and G. Karsenty. 2004. A twist code determines the onset of osteoblast differentiation. *Dev Cell* 6:423-435.

Bodine, P., and B. Komm. 2006. Wnt signaling and osteoblastogenesis. *Reviews in Endocrine & Metabolic Disorders* 7:33-39.

Bodine, P., J. Robinson, R. Bhat, J. Billiard, F. Bex, and B. Komm. 2006. The role of Wnt signaling in bone and mineral metabolism. *Clinical Reviews in Bone and Mineral Metabolism* 4:73-96.

Boland, G.M., G. Perkins, D.J. Hall, and R.S. Tuan. 2004. Wnt 3a promotes proliferation and suppresses osteogenic differentiation of adult human mesenchymal stem cells. *J Cell Biochem* 93:1210-1230.

Bourgeois, P., A.L. Bolcato-Bellemin, J.M. Danse, A. Bloch-Zupan, K. Yoshiba, C. Stoetzel, and F. Perrin-Schmitt. 1998. The variable expressivity and incomplete penetrance of the twist-

null heterozygous mouse phenotype resemble those of human Saethre-Chotzen syndrome. *Hum. Mol. Genet.* 7:945-957.

Bourgeois, P., C. Stoetzel, A.L. Bolcato-Bellemin, M.G. Mattei, and F. Perrin-Schmitt. 1996. The human H-twist gene is located at 7p21 and encodes a B-HLH protein that is 96% similar to its murine M-twist counterpart. *Mamm Genome* 7:915-917.

Bowers, R.R., J.W. Kim, T.C. Otto, and M.D. Lane. 2006. Stable stem cell commitment to the adipocyte lineage by inhibition of DNA methylation: role of the BMP-4 gene. *Proc Natl Acad Sci U S A* 103:13022-13027.

Boyce, B.F., and L. Xing. 2007. Biology of RANK, RANKL, and osteoprotegerin. *Arthritis research & therapy* 9 Suppl 1:S1.

Boyden, L.M. 2002. High Bone Density Due to a Mutation in LDL-Receptor–Related Protein 5. *New England Journal of Medicine* 347:943-944.

Browning, V.L., S.S. Chaudhry, A. Planchart, M.J. Dixon, and J.C. Schimenti. 2001. Mutations of the Mouse Twist and sy (Fibrillin 2) Genes Induced by Chemical Mutagenesis of ES Cells. *Genomics* 73:291-298.

Bucay, N., I. Sarosi, C.R. Dunstan, S. Morony, J. Tarpley, C. Capparelli, S. Scully, H.L. Tan, W. Xu, D.L. Lacey, W.J. Boyle, and W.S. Simonet. 1998. osteoprotegerin-deficient mice develop early onset osteoporosis and arterial calcification. *Genes Dev* 12:1260-1268.

Cakouros, D., S. Isenmann, L. Cooper, A. Zannettino, P. Anderson, C. Glackin, and S. Gronthos. 2012. Twist-1 induces Ezh2 recruitment regulating histone methylation along the Ink4A/Arf locus in mesenchymal stem cells. *Mol Cell Biol* 32:1433-1441.

Cameron, D.A. 1963. The fine structure of bone and calcified cartilage. A critical review of the contribution of electron microscopy to the understading of osteogenesis. *Clinical orthopaedics and related research* 26:199-228.

Canalis, E., A.N. Economides, and E. Gazzerro. 2003. Bone Morphogenetic Proteins, Their Antagonists, and the Skeleton. *Endocrine Reviews* 24:218-235.

Castanon, I., and M.K. Baylies. 2002. A Twist in fate: evolutionary comparison of Twist structure and function. *Gene* 287:11-22.

Castanon, I., S. Von Stetina, J. Kass, and M.K. Baylies. 2001. Dimerization partners determine the activity of the Twist bHLH protein during Drosophila mesoderm development. *Development* 128:3145-3159.

Castro-Malaspina, H., R.E. Gay, G. Resnick, N. Kapoor, P. Meyers, D. Chiarieri, S. McKenzie, H.E. Broxmeyer, and M.A. Moore. 1980. Characterization of human bone marrow fibroblast colony-forming cells (CFU-F) and their progeny. *Blood* 56:289-301.

Cauley, J.A., D.G. Seeley, K. Ensrud, B. Ettinger, D. Black, and S.R. Cummings. 1995. Estrogen replacement therapy and fractures in older women. Study of Osteoporotic Fractures Research Group. *Annals of internal medicine* 122:9-16.

Chang, J., W. Sonoyama, Z. Wang, Q. Jin, C. Zhang, P.H. Krebsbach, W. Giannobile, S. Shi, and C.-Y. Wang. 2007. Noncanonical Wnt-4 Signaling Enhances Bone Regeneration of Mesenchymal Stem Cells in Craniofacial Defects through Activation of p38 MAPK. *Journal of Biological Chemistry* 282:30938-30948.

Chen, P.Y., D. Toroian, P.A. Price, and J. McKittrick. 2011. Minerals form a continuum phase in mature cancellous bone. *Calcif Tissue Int* 88:351-361.

Chen, Y., H.C. Whetstone, A.C. Lin, P. Nadesan, Q. Wei, R. Poon, and B.A. Alman. 2007. Beta-catenin signaling plays a disparate role in different phases of fracture repair: implications for therapy to improve bone healing. *PLoS medicine* 4:e249.

Chen, Z.F., and R.R. Behringer. 1995. twist is required in head mesenchyme for cranial neural tube morphogenesis. *Genes Dev* 9:686-699.

Christakos, S., P. Dhawan, Y. Liu, X. Peng, and A. Porta. 2003. New insights into the mechanisms of vitamin D action. *J Cell Biochem* 88:695-705.

Clarke, B. 2008. Normal Bone Anatomy and Physiology. *Clinical Journal of the American Society of Nephrology* 3:S131-S139.

Connerney, J., V. Andreeva, Y. Leshem, C. Muentener, M.A. Mercado, and D.B. Spicer. 2006. Twist1 dimer selection regulates cranial suture patterning and fusion. *Developmental dynamics : an official publication of the American Association of Anatomists* 235:1345-1357.

Cui, C.B., L.F. Cooper, X. Yang, G. Karsenty, and I. Aukhil. 2003. Transcriptional Coactivation of Bone-Specific Transcription Factor Cbfa1 by TAZ. *Molecular and Cellular Biology* 23:1004-1013.

Daadi, M.M., A.-L. Maag, and G.K. Steinberg. 2008. Adherent Self-Renewable Human Embryonic Stem Cell-Derived Neural Stem Cell Line: Functional Engraftment in Experimental Stroke Model. *PLoS ONE* 3:e1644.

Dao, D.Y., X.U.E. Yang, D.I. Chen, M. Zuscik, and R.J. O'Keefe. 2007. Axin1 and Axin2 Are Regulated by TGF-β and Mediate Cross-talk between TGF-β and Wnt Signaling Pathways. *Annals of the New York Academy of Sciences* 1116:82-99.

De Bari, C., F. Dell'Accio, P. Tylzanowski, and F.P. Luyten. 2001. Multipotent mesenchymal stem cells from adult human synovial membrane. *Arthritis and rheumatism* 44:1928-1942.

de Boer, J., R. Siddappa, C. Gaspar, A. van Apeldoorn, R. Fodde, and C. van Blitterswijk. 2004. Wnt signaling inhibits osteogenic differentiation of human mesenchymal stem cells. *Bone* 34:818-826.

De Ugarte, D.A., Z. Alfonso, P.A. Zuk, A. Elbarbary, M. Zhu, P. Ashjian, P. Benhaim, M.H. Hedrick, and J.K. Fraser. 2003. Differential expression of stem cell mobilization-associated molecules on multi-lineage cells from adipose tissue and bone marrow. *Immunology letters* 89:267-270.

Delaisse, J.M., T.L. Andersen, M.T. Engsig, K. Henriksen, T. Troen, and L. Blavier. 2003. Matrix metalloproteinases (MMP) and cathepsin K contribute differently to osteoclastic activities. *Microscopy research and technique* 61:504-513.

Dominici, M., K. Le Blanc, I. Mueller, I. Slaper-Cortenbach, F. Marini, D. Krause, R. Deans, A. Keating, D. Prockop, and E. Horwitz. 2006. Minimal criteria for defining multipotent

mesenchymal stromal cells. The International Society for Cellular Therapy position statement. *Cytotherapy* 8:315-317.

Dong, Y.F., Y. Soung do, Y. Chang, M. Enomoto-Iwamoto, M. Paris, R.J. O'Keefe, E.M. Schwarz, and H. Drissi. 2007. Transforming growth factor-beta and Wnt signals regulate chondrocyte differentiation through Twist1 in a stage-specific manner. *Molecular endocrinology* 21:2805-2820.

Dr N. Khaltaev, D.B.A.P. 2004. WHO SCIENTIFIC GROUP ON THE ASSESSMENT OF OSTEOPOROSIS AT PRIMARY HEALTH CARE LEVEL. In World Health Organization, Brussels, Belgium.

Ducy, P., R. Zhang, V. Geoffroy, A.L. Ridall, and G. Karsenty. 1997. Osf2/Cbfa1: a transcriptional activator of osteoblast differentiation. *Cell* 89:747-754.

Dwek, J.R. 2010. The periosteum: what is it, where is it, and what mimics it in its absence? *Skeletal radiology* 39:319-323.

Ebara, S., and K. Nakayama. 2002. Mechanism for the action of bone morphogenetic proteins and regulation of their activity. *Spine* 27:S10-15.

Einhorn, T.A., R.J. Majeska, E.B. Rush, P.M. Levine, and M.C. Horowitz. 1995. The expression of cytokine activity by fracture callus. *J Bone Miner Res* 10:1272-1281.

Einhorn, T.A.M. 1998. The Cell and Molecular Biology of Fracture Healing.[Miscellaneous Article]. *Clinical Orthopaedics & Related Research. Fracture Healing Enhancement.*

Estai, M.A., F. Suhaimi, S. Das, A.N. Shuid, Z. Mohamed, and I.N. Soelaiman. 2011. Expression of TGF-beta1 in the blood during fracture repair in an estrogen-deficient rat model. *Clinics* 66:2113-2119.

Etheridge, S.L., G.J. Spencer, D.J. Heath, and P.G. Genever. 2004. Expression Profiling and Functional Analysis of Wnt Signaling Mechanisms in Mesenchymal Stem Cells. *STEM CELLS* 22:849-860.

Fan, Q.M., B. Yue, Z.Y. Bian, W.T. Xu, B. Tu, K.R. Dai, G. Li, and T.T. Tang. 2012. The CREB-Smad6-Runx2 axis contributes to the impaired osteogenesis potential of bone marrow stromal cells in fibrous dysplasia of bone. *The Journal of pathology* 228:45-55.

Felson, D.T., Y. Zhang, M.T. Hannan, D.P. Kiel, P.W. Wilson, and J.J. Anderson. 1993. The effect of postmenopausal estrogen therapy on bone density in elderly women. *The New England journal of medicine* 329:1141-1146.

Feng, X.-H., and R. Derynck. 2005. SPECIFICITY AND VERSATILITY IN TGF-β SIGNALING THROUGH SMADS. *Annual Review of Cell and Developmental Biology* 21:659-693.

Field, J.R., M. McGee, R. Stanley, G. Ruthenbeck, T. Papadimitrakis, A. Zannettino, S. Gronthos, and S. Itescu. 2011. The efficacy of allogeneic mesenchymal precursor cells for the repair of an ovine tibial segmental defect. *Veterinary and comparative orthopaedics and traumatology : V.C.O.T* 24:113-121.

Filshie, R.J., A.C. Zannettino, V. Makrynikola, S. Gronthos, A.J. Henniker, L.J. Bendall, D.J. Gottlieb, P.J. Simmons, and K.F. Bradstock. 1998. MUC18, a member of the immunoglobulin superfamily, is expressed on bone marrow fibroblasts and a subset of hematological malignancies. *Leukemia* 12:414-421.

Franco, H.L., J. Casasnovas, J.R. Rodríguez-Medina, and C.L. Cadilla. 2011. Redundant or separate entities?—roles of Twist1 and Twist2 as molecular switches during gene transcription. *Nucleic Acids Research* 39:1177-1186.

Freemont, A.J. 1993. Basic bone cell biology. *International journal of experimental pathology* 74:411-416.

Friedenstein, A.J., R.K. Chailakhjan, and K.S. Lalykina. 1970. THE DEVELOPMENT OF FIBROBLAST COLONIES IN MONOLAYER CULTURES OF GUINEA-PIG BONE MARROW AND SPLEEN CELLS. *Cell Proliferation* 3:393-403.

Friedenstein, A.J., J.F. Gorskaja, and N.N. Kulagina. 1976. Fibroblast precursors in normal and irradiated mouse hematopoietic organs. *Exp Hematol* 4:267-274.

Friedenstein, A.J., A.A. Ivanov-Smolenski, R.K. Chajlakjan, U.F. Gorskaya, A.I. Kuralesova, N.W. Latzinik, and U.W. Gerasimow. 1978. Origin of bone marrow stromal mechanocytes in radiochimeras and heterotopic transplants. *Exp Hematol* 6:440-444.

Friedlaender, G.E., C.R. Perry, J.D. Cole, S.D. Cook, G. Cierny, G.F. Muschler, G.A. Zych, J.H. Calhoun, A.J. LaForte, and S. Yin. 2001. Osteogenic protein-1 (bone morphogenetic protein-7) in the treatment of tibial nonunions. *The Journal of bone and joint surgery. American volume* 83-A Suppl 1:S151-158.

Furumatsu, T., M. Tsuda, N. Taniguchi, Y. Tajima, and H. Asahara. 2005. Smad3 induces chondrogenesis through the activation of SOX9 via CREB-binding protein/p300 recruitment. *The Journal of biological chemistry* 280:8343-8350.

Gao, Y., W.P. Qian, K. Dark, G. Toraldo, A.S. Lin, R.E. Guldberg, R.A. Flavell, M.N. Weitzmann, and R. Pacifici. 2004. Estrogen prevents bone loss through transforming growth factor beta signaling in T cells. *Proc Natl Acad Sci U S A* 101:16618-16623.

Garrison, K.R., I. Shemilt, S. Donell, J.J. Ryder, M. Mugford, I. Harvey, F. Song, and V. Alt. 2010. Bone morphogenetic protein (BMP) for fracture healing in adults. *Cochrane database of systematic reviews* CD006950.

Gaur, T., C.J. Lengner, H. Hovhannisyan, R.A. Bhat, P.V.N. Bodine, B.S. Komm, A. Javed, A.J. van Wijnen, J.L. Stein, G.S. Stein, and J.B. Lian. 2005. Canonical WNT Signaling Promotes Osteogenesis by Directly Stimulating Runx2 Gene Expression. *Journal of Biological Chemistry* 280:33132-33140.

Geiser, A.G., Q.Q. Zeng, M. Sato, L.M. Helvering, T. Hirano, and C.H. Turner. 1998. Decreased bone mass and bone elasticity in mice lacking the transforming growth factor-beta1 gene. *Bone* 23:87-93.

Geoffroy, V., M. Kneissel, B. Fournier, A. Boyde, and P. Matthias. 2002. High bone resorption in adult aging transgenic mice overexpressing cbfa1/runx2 in cells of the osteoblastic lineage. *Mol Cell Biol* 22:6222-6233.

Glass, D.A., and G. Karsenty. 2007. In Vivo Analysis of Wnt Signaling in Bone. *Endocrinology* 148:2630-2634.

Glass Ii, D.A., and G. Karsenty. 2006. Molecular Bases of the Regulation of Bone Remodeling by the Canonical Wnt Signaling Pathway. In Current Topics in Developmental Biology. P.S. Gerald, editor Academic Press, 43-84.

Glatt, V., M. Miller, A. Ivkovic, F. Liu, N. Parry, D. Griffin, M. Vrahas, and C. Evans. 2012. Improved Healing of Large Segmental Defects in the Rat Femur by Reverse Dynamization in the Presence of Bone Morphogenetic Protein-2. *The Journal of Bone & Joint Surgery* 94:2063-2073.

Gong, Y., R.B. Slee, N. Fukai, G. Rawadi, S. Roman-Roman, A.M. Reginato, H. Wang, T. Cundy, F.H. Glorieux, D. Lev, M. Zacharin, K. Oexle, J. Marcelino, W. Suwairi, S. Heeger, G. Sabatakos, S. Apte, W.N. Adkins, J. Allgrove, M. Arslan-Kirchner, J.A. Batch, P. Beighton, G.C. Black, R.G. Boles, L.M. Boon, C. Borrone, H.G. Brunner, G.F. Carle, B. Dallapiccola, A. De Paepe, B. Floege, M.L. Halfhide, B. Hall, R.C. Hennekam, T. Hirose, A. Jans, H. Juppner, C.A. Kim, K. Keppler-Noreuil, A. Kohlschuetter, D. LaCombe, M. Lambert, E. Lemyre, T. Letteboer, L. Peltonen, R.S. Ramesar, M. Romanengo, H. Somer, E. Steichen-Gersdorf, B. Steinmann, B. Sullivan, A. Superti-Furga, W. Swoboda, M.J. van den Boogaard, W. Van Hul, M. Vikkula, M. Votruba, B. Zabel, T. Garcia, R. Baron, B.R. Olsen, M.L. Warman, and G. Osteoporosis-Pseudoglioma Syndrome Collaborative. 2001. LDL receptor-related protein 5 (LRP5) affects bone accrual and eye development. *Cell* 107:513-523.

Goss, A.M., Y. Tian, T. Tsukiyama, E.D. Cohen, D. Zhou, M.M. Lu, T.P. Yamaguchi, and E.E. Morrisey. 2009. Wnt2/2b and β-Catenin Signaling Are Necessary and Sufficient to Specify Lung Progenitors in the Foregut. *Developmental Cell* 17:290-298.

Govender, S., C. Csimma, H.K. Genant, A. Valentin-Opran, Y. Amit, R. Arbel, H. Aro, D. Atar, M. Bishay, M.G. Borner, P. Chiron, P. Choong, J. Cinats, B. Courtenay, R. Feibel, B. Geulette, C. Gravel, N. Haas, M. Raschke, E. Hammacher, D. van der Velde, P. Hardy, M. Holt, C. Josten, R.L. Ketterl, B. Lindeque, G. Lob, H. Mathevon, G. McCoy, D. Marsh, R. Miller, E. Munting, S. Oevre, L. Nordsletten, A. Patel, A. Pohl, W. Rennie, P. Reynders, P.M. Rommens, J. Rondia, W.C. Rossouw, P.J. Daneel, S. Ruff, A. Ruter, S. Santavirta, T.A. Schildhauer, C. Gekle, R. Schnettler, D. Segal, H. Seiler, R.B. Snowdowne, J. Stapert, G. Taglang, R. Verdonk, L. Vogels, A. Weckbach, A.

Wentzensen, T. Wisniewski, and B.M.P.E.i.S.f.T.T.S. Group. 2002. Recombinant human bone morphogenetic protein-2 for treatment of open tibial fractures: a prospective, controlled, randomized study of four hundred and fifty patients. *The Journal of bone and joint surgery. American volume* 84-A:2123-2134.

Grassel, S., and S. Anders. 2012. [Cell-based therapy options for osteochondral defects. Autologous mesenchymal stem cells compared to autologous chondrocytes]. *Orthopade* 41:415-428; quiz 429-430.

Grcevic, D., S. Pejda, B.G. Matthews, D. Repic, L. Wang, H. Li, M.S. Kronenberg, X. Jiang, P. Maye, D.J. Adams, D.W. Rowe, H.L. Aguila, and I. Kalajzic. 2012. In vivo fate mapping identifies mesenchymal progenitor cells. *STEM CELLS* 30:187-196.

Gregory, C.A., W.G. Gunn, E. Reyes, A.J. Smolarz, J. Munoz, J.L. Spees, and D.J. Prockop. 2005. How Wnt Signaling Affects Bone Repair by Mesenchymal Stem Cells from the Bone Marrow. *Annals of the New York Academy of Sciences* 1049:97-106.

Gronthos, S., S.O. Akintoye, C.-Y. Wang, and S. Shi. 2006. Bone marrow stromal stem cells for tissue engineering. *Periodontology 2000* 41:188-195.

Gronthos, S., S. Fitter, P. Diamond, P.J. Simmons, S. Itescu, and A.C. Zannettino. 2007. A novel monoclonal antibody (STRO-3) identifies an isoform of tissue nonspecific alkaline phosphatase expressed by multipotent bone marrow stromal stem cells. *Stem Cells Dev* 16:953-963.

Gronthos, S., S.E. Graves, S. Ohta, and P.J. Simmons. 1994. The STRO-1+ fraction of adult human bone marrow contains the osteogenic precursors. *Blood* 84:4164-4173.

Gronthos, S., M. Mankani, J. Brahim, P.G. Robey, and S. Shi. 2000. Postnatal human dental pulp stem cells (DPSCs) in vitro and in vivo. *Proc Natl Acad Sci U S A* 97:13625-13630.

Gronthos, S., R. McCarty, K. Mrozik, S. Fitter, S. Paton, D. Menicanin, S. Itescu, P.M. Bartold, C. Xian, and A.C. Zannettino. 2009. Heat Shock Protein-90 beta (Hsp90ss) is Expressed at the Surface of Multipotential Mesenchymal Precursor Cells (MPC): Generation of a Novel Monoclonal Antibody, STRO-4, with Specificity for MPC from Human and Ovine Tissues. *Stem Cells Dev*

Gronthos, S., and A.C. Zannettino. 2007. The role of the chemokine CXCL12 in osteoclastogenesis. *Trends Endocrinol Metab* 18:108-113.

Gronthos, S., and A.C. Zannettino. 2008a. A method to isolate and purify human bone marrow stromal stem cells. *Methods Mol Biol* 449:45-57.

Gronthos, S., A.C. Zannettino, S.J. Hay, S. Shi, S.E. Graves, A. Kortesidis, and P.J. Simmons. 2003a. Molecular and cellular characterisation of highly purified stromal stem cells derived from human bone marrow. *J Cell Sci* 116:1827-1835.

Gronthos, S., and A.C.W. Zannettino. 2008b. A Method to Isolate and Purify Human Bone Marrow Stromal Stem Cells. In Mesenchymal Stem Cells. 45-57.

Gronthos, S., A.C.W. Zannettino, S.J. Hay, S. Shi, S.E. Graves, A. Kortesidis, and P.J. Simmons. 2003b. Molecular and cellular characterisation of highly purified stromal stem cells derived from human bone marrow. *J Cell Sci* 116:1827-1835.

Gu, S., T.G. Boyer, and M.C. Naski. 2012. Basic helix-loop-helix transcription factor Twist1 inhibits transactivator function of master chondrogenic regulator Sox9. *The Journal of biological chemistry* 287:21082-21092.

Guiqian Chen1, Chuxia Deng2 Corresponding address, Yi-Ping Li1,3 Corresponding address. 2012. TGF-β and BMP Signaling in Osteoblast Differentiation and Bone Formation *International Journal of Biological Sciences* 8:272-288.

H. M. Frost, M.D.S. 1964. Bone remodeling dynamics. . *Arthritis & Rheumatism* 7:545-545.

Hadjiargyrou, M., F. Lombardo, S. Zhao, W. Ahrens, J. Joo, H. Ahn, M. Jurman, D.W. White, and C.T. Rubin. 2002. Transcriptional profiling of bone regeneration. Insight into the molecular complexity of wound repair. *The Journal of biological chemistry* 277:30177-30182.

Hartmann, C. 2006. A Wnt canon orchestrating osteoblastogenesis. *Trends in Cell Biology* 16:151-158.

Hayashi, K., T. Yamaguchi, S. Yano, I. Kanazawa, M. Yamauchi, M. Yamamoto, and T. Sugimoto. 2009. BMP/Wnt antagonists are upregulated by dexamethasone in osteoblasts

and reversed by alendronate and PTH: Potential therapeutic targets for glucocorticoid-induced osteoporosis. *Biochemical and Biophysical Research Communications* 379:261-266.

Hayashi, M., K. Nimura, K. Kashiwagi, T. Harada, K. Takaoka, H. Kato, K. Tamai, and Y. Kaneda. 2007. Comparative roles of Twist-1 and Id1 in transcriptional regulation by BMP signaling. *J Cell Sci* 120:1350-1357.

Hill, T.P., D. Später, M.M. Taketo, W. Birchmeier, and C. Hartmann. 2005. Canonical Wnt/β-Catenin Signaling Prevents Osteoblasts from Differentiating into Chondrocytes. *Developmental Cell* 8:727-738.

Hoeppner, L.H., F.J. Secreto, and J.J. Westendorf. 2009. Wnt signaling as a therapeutic target for bone diseases. *Expert Opinion on Therapeutic Targets* 13:485-496.

Hong, J.-H., E.S. Hwang, M.T. McManus, A. Amsterdam, Y. Tian, R. Kalmukova, E. Mueller, T. Benjamin, B.M. Spiegelman, P.A. Sharp, N. Hopkins, and M.B. Yaffe. 2005. TAZ, a Transcriptional Modulator of Mesenchymal Stem Cell Differentiation. *Science* 309:1074-1078.

Horwitz, E.M., K. Le Blanc, M. Dominici, I. Mueller, I. Slaper-Cortenbach, F.C. Marini, R.J. Deans, D.S. Krause, A. Keating, and T. International Society for Cellular. 2005. Clarification of the nomenclature for MSC: The International Society for Cellular Therapy position statement. *Cytotherapy* 7:393-395.

Horwitz, E.M., D.J. Prockop, L.A. Fitzpatrick, W.W.K. Koo, P.L. Gordon, M. Neel, M. Sussman, P. Orchard, J.C. Marx, R.E. Pyeritz, and M.K. Brenner. 1999. Transplantability and therapeutic effects of bone marrow-derived mesenchymal cells in children with osteogenesis imperfecta. *Nat Med* 5:309-313.

Howard, T.D., W.A. Paznekas, E.D. Green, L.C. Chiang, N. Ma, R.I.O.D. Luna, C.G. Delgado, M. Gonzalez-Ramos, A.D. Kline, and E.W. Jabs. 1997. Mutations in TWIST, a basic helix-loop-helix transcription factor, in Saethre-Chotzen syndrome. *Nat Genet* 15:36-41.

Howe, L.R., O. Watanabe, J. Leonard, and A.M.C. Brown. 2003. Twist Is Up-Regulated in Response to Wnt1 and Inhibits Mouse Mammary Cell Differentiation. *Cancer Research* 63:1906-1913.

Hu, H., M.J. Hilton, X. Tu, K. Yu, D.M. Ornitz, and F. Long. 2005. Sequential roles of Hedgehog and Wnt signaling in osteoblast development. *Development* 132:49-60.

Huang, D.W., B.T. Sherman, and R.A. Lempicki. 2008. Systematic and integrative analysis of large gene lists using DAVID bioinformatics resources. *Nat. Protocols* 4:44-57.

Huang, D.W., B.T. Sherman, and R.A. Lempicki. 2009. Bioinformatics enrichment tools: paths toward the comprehensive functional analysis of large gene lists. *Nucleic Acids Research* 37:1-13.

Ikeda, T., S. Kamekura, A. Mabuchi, I. Kou, S. Seki, T. Takato, K. Nakamura, H. Kawaguchi, S. Ikegawa, and U.I. Chung. 2004. The combination of SOX5, SOX6, and SOX9 (the SOX trio) provides signals sufficient for induction of permanent cartilage. *Arthritis and rheumatism* 50:3561-3573.

Inai, K., R.A. Norris, S. Hoffman, R.R. Markwald, and Y. Sugi. 2008. BMP-2 induces cell migration and periostin expression during atrioventricular valvulogenesis. *Dev Biol* 315:383-396.

Ip, Y.T., R.E. Park, D. Kosman, E. Bier, and M. Levine. 1992. The dorsal gradient morphogen regulates stripes of rhomboid expression in the presumptive neuroectoderm of the Drosophila embryo. *Genes & Development* 6:1728-1739.

Isenmann, S., A. Arthur, A.C. Zannettino, J.L. Turner, S. Shi, C.A. Glackin, and S. Gronthos. 2009. TWIST family of basic Helix-Loop-Helix Transcription Factors Mediate Human Mesenchymal Stromal/Stem Cell Growth and Commitment. *Stem Cells* 9999:N/A.

Isenmann, S., D. Cakouros, A. Zannettino, S. Shi, and S. Gronthos. 2007. hTERT transcription is repressed by Cbfa1 in human mesenchymal stem cell populations. *J Bone Miner Res* 22:897-906.

J.-Y. Hwang, S.-Y.K., S. H. Lee, G. S. Kim, M. J. Go, S. E. Kim, H.-C. Kim, H.-D. Shin, B. L. Park and T.-H. Kim, et al. 2010. Association of TWIST1 gene polymorphisms with bone mineral density in postmenopausal women *Osteoporosis International* 21:757-764.

Jabs, E.W. 2001. A TWIST in the fate of human osteoblasts identifies signaling molecules involved in skull development. *J Clin Invest* 107:1075-1077.

Jansen, B.J., C. Gilissen, H. Roelofs, A. Schaap-Oziemlak, J.A. Veltman, R.A. Raymakers, J.H. Jansen, G. Kogler, C.G. Figdor, R. Torensma, and G.J. Adema. 2010. Functional differences between mesenchymal stem cell populations are reflected by their transcriptome. *Stem Cells Dev* 19:481-490.

Jawad, M.U., K.E. Fritton, T. Ma, P.-G. Ren, S.B. Goodman, H.Z. Ke, P. Babij, and M.C. Genovese. 2013. Effects of sclerostin antibody on healing of a non-critical size femoral bone defect. *Journal of Orthopaedic Research* 31:155-163.

Jho, E.H., T. Zhang, C. Domon, C.K. Joo, J.N. Freund, and F. Costantini. 2002. Wnt/beta-catenin/Tcf signaling induces the transcription of Axin2, a negative regulator of the signaling pathway. *Mol Cell Biol* 22:1172-1183.

Jiang, Y., B.N. Jahagirdar, R.L. Reinhardt, R.E. Schwartz, C.D. Keene, X.R. Ortiz-Gonzalez, M. Reyes, T. Lenvik, T. Lund, M. Blackstad, J. Du, S. Aldrich, A. Lisberg, W.C. Low, D.A. Largaespada, and C.M. Verfaillie. 2002. Pluripotency of mesenchymal stem cells derived from adult marrow. *Nature* 418:41-49.

Johnson, M.L., G. Gong, W. Kimberling, S.M. Recker, D.B. Kimmel, and R.B. Recker. 1997. Linkage of a gene causing high bone mass to human chromosome 11 (11q12-13). *American journal of human genetics* 60:1326-1332.

Kalajzic, Z., H. Li, L.P. Wang, X. Jiang, K. Lamothe, D.J. Adams, H.L. Aguila, D.W. Rowe, and I. Kalajzic. 2008. Use of an alpha-smooth muscle actin GFP reporter to identify an osteoprogenitor population. *Bone* 43:501-510.

Kanis, J.A., and J.A. Kanis. 1994. Assessment of fracture risk and its application to screening for postmenopausal osteoporosis: Synopsis of a WHO report. *Osteoporosis International* 4:368-381.

Kansara, M., M. Tsang, L. Kodjabachian, N.A. Sims, M.K. Trivett, M. Ehrich, A. Dobrovic, J. Slavin, P.F. Choong, P.J. Simmons, I.B. Dawid, and D.M. Thomas. 2009. Wnt inhibitory factor 1 is epigenetically silenced in human osteosarcoma, and targeted disruption accelerates osteosarcomagenesis in mice. *J Clin Invest* 119:837-851.

Karsenty, G. 2000. Bone formation and factors affecting this process. *Matrix Biol* 19:85-89.

Kato, M., M.S. Patel, R. Levasseur, I. Lobov, B.H.-J. Chang, D.A. Glass, C. Hartmann, L. Li, T.-H. Hwang, C.F. Brayton, R.A. Lang, G. Karsenty, and L. Chan. 2002. Cbfa1-independent decrease in osteoblast proliferation, osteopenia, and persistent embryonic eye vascularization in mice deficient in Lrp5, a Wnt coreceptor. *The Journal of Cell Biology* 157:303-314.

Kaufman, J.M., J.Y. Reginster, S. Boonen, M.L. Brandi, C. Cooper, W. Dere, J.P. Devogelaer, A. Diez-Perez, J.A. Kanis, E. McCloskey, B. Mitlak, E. Orwoll, J.D. Ringe, G. Weryha, and R. Rizzoli. 2012. Treatment of osteoporosis in men. *Bone*

Kawahata, H., T. Kikkawa, Y. Higashibata, T. Sakuma, M. Huening, M. Sato, M. Sugimoto, K. Kuriyama, K. Terai, Y. Kitamura, and S. Nomura. 2003. Enhanced expression of Runx2/PEBP2alphaA/CBFA1/AML3 during fracture healing. *Journal of orthopaedic science : official journal of the Japanese Orthopaedic Association* 8:102-108.

Kawai, M., S. Mushiake, K. Bessho, M. Murakami, N. Namba, C. Kokubu, T. Michigami, and K. Ozono. 2007. Wnt/Lrp/beta-catenin signaling suppresses adipogenesis by inhibiting mutual activation of PPARgamma and C/EBPalpha. *Biochem Biophys Res Commun* 363:276-282.

Kawai, M., K.M. Sousa, O.A. MacDougald, and C.J. Rosen. 2010. The many facets of PPARgamma: novel insights for the skeleton. *American journal of physiology. Endocrinology and metabolism* 299:E3-9.

Keramaris, N.C., G.M. Calori, V.S. Nikolaou, E.H. Schemitsch, and P.V. Giannoudis. 2008. Fracture vascularity and bone healing: a systematic review of the role of VEGF. *Injury* 39 Suppl 2:S45-57.

Kern, S., H. Eichler, J. Stoeve, H. Kluter, and K. Bieback. 2006. Comparative analysis of mesenchymal stem cells from bone marrow, umbilical cord blood, or adipose tissue. *STEM CELLS* 24:1294-1301.

Kikuchi, A. 1999. Modulation of Wnt signaling by Axin and Axil. *Cytokine & growth factor reviews* 10:255-265.

Kim, J.-B., P. Leucht, K. Lam, C. Luppen, D. Ten Berge, R. Nusse, and J.A. Helms. 2007. Bone Regeneration Is Regulated by Wnt Signaling. *Journal of Bone and Mineral Research* 22:1913-1923.

Kitada, M., and M. Dezawa. 2012. Parkinson's disease and mesenchymal stem cells: potential for cell-based therapy. *Parkinson's disease* 2012:873706.

Komaki, M., T. Karakida, M. Abe, S. Oida, K. Mimori, K. Iwasaki, K. Noguchi, S. Oda, and I. Ishikawa. 2007. Twist negatively regulates osteoblastic differentiation in human periodontal ligament cells. *J Cell Biochem* 100:303-314.

Komatsu, D.E., M.N. Mary, R.J. Schroeder, A.G. Robling, C.H. Turner, and S.J. Warden. 2010. Modulation of Wnt signaling influences fracture repair. *Journal of orthopaedic research : official publication of the Orthopaedic Research Society* 28:928-936.

Komori, T. 2002. [Cbfa1/Runx2, an essential transcription factor for the regulation of osteoblast differentiation]. *Nihon rinsho. Japanese journal of clinical medicine* 60 Suppl 3:91-97.

Komori, T. 2006. Regulation of osteoblast differentiation by transcription factors. *Journal of Cellular Biochemistry* 99:1233-1239.

Komori, T., H. Yagi, S. Nomura, A. Yamaguchi, K. Sasaki, K. Deguchi, Y. Shimizu, R.T. Bronson, Y.H. Gao, M. Inada, M. Sato, R. Okamoto, Y. Kitamura, S. Yoshiki, and T. Kishimoto. 1997. Targeted disruption of Cbfa1 results in a complete lack of bone formation owing to maturational arrest of osteoblasts. *Cell* 89:755-764.

Kon, E., A. Muraglia, A. Corsi, P. Bianco, M. Marcacci, I. Martin, A. Boyde, I. Ruspantini, P. Chistolini, M. Rocca, R. Giardino, R. Cancedda, and R. Quarto. 2000. Autologous bone marrow stromal cells loaded onto porous hydroxyapatite ceramic accelerate bone repair in

critical-size defects of sheep long bones. *Journal of biomedical materials research* 49:328-337.

Korvala J, J.H., Mäkitie O, Sochett E, Schnabel D, Mora S, Bartels CF, Warman ML, Deraska D, Cole WG, Hartikka H, Ala-Kokko L, Männikkö M. 2012. Mutations in LRP5 cause primary osteoporosis without features of OI by reducing Wnt signaling activity. *BMC Med Genet.* 13:

Kress, W., C. Schropp, G. Lieb, B. Petersen, M. Busse-Ratzka, J. Kunz, E. Reinhart, W.-D. Schafer, J. Sold, F. Hoppe, J. Pahnke, A. Trusen, N. Sorensen, J. Krauss, and H. Collmann. 2005. Saethre-Chotzen syndrome caused by TWIST 1 gene mutations: functional differentiation from Muenke coronal synostosis syndrome. *Eur J Hum Genet* 14:39-48.

Krishnan, V., H.U. Bryant, and O.A. MacDougald. 2006. Regulation of bone mass by Wnt signaling. *The Journal of Clinical Investigation* 116:1202-1209.

Kulterer, B., G. Friedl, A. Jandrositz, F. Sanchez-Cabo, A. Prokesch, C. Paar, M. Scheideler, R. Windhager, K.H. Preisegger, and Z. Trajanoski. 2007. Gene expression profiling of human mesenchymal stem cells derived from bone marrow during expansion and osteoblast differentiation. *BMC genomics* 8:70.

Kuznetsov, S.A., P.H. Krebsbach, K. Satomura, J. Kerr, M. Riminucci, D. Benayahu, and P.G. Robey. 1997. Single-colony derived strains of human marrow stromal fibroblasts form bone after transplantation in vivo. *J Bone Miner Res* 12:1335-1347.

Kuznetsov, S.A., M.H. Mankani, S. Gronthos, K. Satomura, P. Bianco, and P.G. Robey. 2001. Circulating skeletal stem cells. *J Cell Biol* 153:1133-1140.

Langdahl, B.L., J.Y. Knudsen, H.K. Jensen, N. Gregersen, and E.F. Eriksen. 1997. A sequence variation: 713-8delC in the transforming growth factor-beta 1 gene has higher prevalence in osteoporotic women than in normal women and is associated with very low bone mass in osteoporotic women and increased bone turnover in both osteoporotic and normal women. *Bone* 20:289-294.

Lavery, K., P. Swain, D. Falb, and M.H. Alaoui-Ismaili. 2008. BMP-2/4 and BMP-6/7 differentially utilize cell surface receptors to induce osteoblastic differentiation of human bone marrow-derived mesenchymal stem cells. *The Journal of biological chemistry* 283:20948-20958.

Lee, M.-H., Y.-J. Kim, W.-J. Yoon, J.-I. Kim, B.-G. Kim, Y.-S. Hwang, J.M. Wozney, X.-Z. Chi, S.-C. Bae, K.-Y. Choi, J.-Y. Cho, J.-Y. Choi, and H.-M. Ryoo. 2005. Dlx5 Specifically Regulates Runx2 Type II Expression by Binding to Homeodomain-response Elements in the Runx2 Distal Promoter. *Journal of Biological Chemistry* 280:35579-35587.

Lee, M.S., G. Lowe, S. Flanagan, K. Kuchler, and C.A. Glackin. 2000. Human Dermo-1 has attributes similar to twist in early bone development. *Bone* 27:591-602.

Lee, M.S., G.N. Lowe, D.D. Strong, J.E. Wergedal, and C.A. Glackin. 1999. TWIST, a basic helix-loop-helix transcription factor, can regulate the human osteogenic lineage. *J Cell Biochem* 75:566-577.

Lee, R.H., B. Kim, I. Choi, H. Kim, H.S. Choi, K. Suh, Y.C. Bae, and J.S. Jung. 2004. Characterization and expression analysis of mesenchymal stem cells from human bone marrow and adipose tissue. *Cellular physiology and biochemistry : international journal of experimental cellular physiology, biochemistry, and pharmacology* 14:311-324.

Levasseur, R., D. Lacombe, and M.C. de Vernejoul. 2005. LRP5 mutations in osteoporosis-pseudoglioma syndrome and high-bone-mass disorders. *Joint, bone, spine : revue du rhumatisme* 72:207-214.

Li, B. 2008. Bone morphogenetic protein-Smad pathway as drug targets for osteoporosis and cancer therapy. *Endocrine, metabolic & immune disorders drug targets* 8:208-219.

Li, W.F., S.X. Hou, B. Yu, M.M. Li, C. Ferec, and J.M. Chen. 2010. Genetics of osteoporosis: accelerating pace in gene identification and validation. *Human genetics* 127:249-285.

Lin, G.L., and K.D. Hankenson. 2011. Integration of BMP, Wnt, and notch signaling pathways in osteoblast differentiation. *Journal of Cellular Biochemistry* 112:3491-3501.

Lind, M., B. Schumacker, K. Soballe, J. Keller, F. Melsen, and C. Bunger. 1993. Transforming growth factor-beta enhances fracture healing in rabbit tibiae. *Acta orthopaedica Scandinavica* 64:553-556.

Linda J. Vorvick, M. 2010. Bone fracture repair.

Little, R.D., J.P. Carulli, R.G. Del Mastro, J. Dupuis, M. Osborne, C. Folz, S.P. Manning, P.M. Swain, S.C. Zhao, B. Eustace, M.M. Lappe, L. Spitzer, S. Zweier, K. Braunschweiger, Y. Benchekroun, X. Hu, R. Adair, L. Chee, M.G. FitzGerald, C. Tulig, A. Caruso, N. Tzellas, A. Bawa, B. Franklin, S. McGuire, X. Nogues, G. Gong, K.M. Allen, A. Anisowicz, A.J. Morales, P.T. Lomedico, S.M. Recker, P. Van Eerdewegh, R.R. Recker, and M.L. Johnson. 2002a. A mutation in the LDL receptor-related protein 5 gene results in the autosomal dominant high-bone-mass trait. *American journal of human genetics* 70:11-19.

Little, R.D., C. Folz, S.P. Manning, P.M. Swain, S.-C. Zhao, B. Eustace, M.M. Lappe, L. Spitzer, S. Zweier, K. Braunschweiger, Y. Benchekroun, X. Hu, R. Adair, L. Chee, M.G. FitzGerald, C. Tulig, A. Caruso, N. Tzellas, A. Bawa, B. Franklin, S. McGuire, X. Nogues, G. Gong, K.M. Allen, A. Anisowicz, A.J. Morales, P.T. Lomedico, S.M. Recker, P. Van Eerdewegh, R.R. Recker, J.P. Carulli, R.G. Del Mastro, J. Dupuis, M. Osborne, and M.L. Johnson. 2002b. A Mutation in the LDL Receptor–Related Protein 5 Gene Results in the Autosomal Dominant High–Bone-Mass Trait. *The American Journal of Human Genetics* 70:11-19.

Liu, B., H.-M.I. Yu, and W. Hsu. 2007. Craniosynostosis caused by Axin2 deficiency is mediated through distinct functions of β-catenin in proliferation and differentiation. *Developmental Biology* 301:298-308.

Liu, F., S. Kohlmeier, and C.-Y. Wang. 2008. Wnt signaling and skeletal development. *Cellular Signalling* 20:999-1009.

Liu, G., S. Vijayakumar, L. Grumolato, R. Arroyave, H. Qiao, G. Akiri, and S.A. Aaronson. 2009. Canonical Wnts function as potent regulators of osteogenesis by human mesenchymal stem cells. *J Cell Biol* 185:67-75.

Liu, N., S. Shi, M. Deng, L. Tang, G. Zhang, N. Liu, B. Ding, W. Liu, Y. Liu, H. Shi, L. Liu, and Y. Jin. 2011. High levels of β-catenin signaling reduce osteogenic differentiation of stem cells in inflammatory microenvironments through inhibition of the noncanonical Wnt pathway. *Journal of Bone and Mineral Research* 26:2082-2095.

Liu, W., S. Toyosawa, T. Furuichi, N. Kanatani, C. Yoshida, Y. Liu, M. Himeno, S. Narai, A. Yamaguchi, and T. Komori. 2001. Overexpression of Cbfa1 in osteoblasts inhibits osteoblast maturation and causes osteopenia with multiple fractures. *J Cell Biol* 155:157-166.

Liu, Y.H., Z. Tang, R.K. Kundu, L. Wu, W. Luo, D. Zhu, F. Sangiorgi, M.L. Snead, and R.E. Maxson. 1999. Msx2 gene dosage influences the number of proliferative osteogenic cells in growth centers of the developing murine skull: a possible mechanism for MSX2-mediated craniosynostosis in humans. *Dev Biol* 205:260-274.

Logan, C.Y., and R. Nusse. 2004. THE WNT SIGNALING PATHWAY IN DEVELOPMENT AND DISEASE. *Annual Review of Cell and Developmental Biology* 20:781-810.

Lopez, M. 2009. Does the Use of Cyclooxygenase Inhibitors Delay Fracture Healing? *The Internet Journal of Academic Physician Assistants* 6:

Lustig, B., B. Jerchow, M. Sachs, S. Weiler, T. Pietsch, U. Karsten, M. van de Wetering, H. Clevers, P.M. Schlag, W. Birchmeier, and J. Behrens. 2002. Negative Feedback Loop of Wnt Signaling through Upregulation of Conductin/Axin2 in Colorectal and Liver Tumors. *Molecular and Cellular Biology* 22:1184-1193.

Ma, L., M.F. Lu, R.J. Schwartz, and J.F. Martin. 2005. Bmp2 is essential for cardiac cushion epithelial-mesenchymal transition and myocardial patterning. *Development* 132:5601-5611.

Mabed, M., and M. Shahin. 2012. Mesenchymal stem cell-based therapy for the treatment of type 1 diabetes mellitus. *Current stem cell research & therapy* 7:179-190.

Manolagas, S.C. 2000. Birth and Death of Bone Cells: Basic Regulatory Mechanisms and Implications for the Pathogenesis and Treatment of Osteoporosis. *Endocr Rev* 21:115-137.

Mao, J., J. Wang, B. Liu, W. Pan, G.H. Farr, 3rd, C. Flynn, H. Yuan, S. Takada, D. Kimelman, L. Li, and D. Wu. 2001. Low-density lipoprotein receptor-related protein-5 binds to Axin and regulates the canonical Wnt signaling pathway. *Mol Cell* 7:801-809.

Maria P. Yavropoulou, J.G.Y. 2007. The role of the Wnt signaling pathway in osteoblast commitment and differentiation. *Hormones* 6:279-294.

Marsh, D.M., FRCS. 1998. Concepts of Fracture Union, Delayed Union, and Nonunion.[Miscellaneous Article]. *Clinical Orthopaedics & Related Research. Fracture Healing Enhancement.*

Martin, I., A. Muraglia, G. Campanile, R. Cancedda, and R. Quarto. 1997. Fibroblast Growth Factor-2 Supports ex Vivo Expansion and Maintenance of Osteogenic Precursors from Human Bone Marrow. *Endocrinology* 138:4456-4462.

Martini, F.E.A. 2007. Anatomy and Physiology.

Matushansky, I., E. Hernando, N.D. Socci, J.E. Mills, T.A. Matos, M.A. Edgar, S. Singer, R.G. Maki, and C. Cordon-Cardo. 2007. Derivation of sarcomas from mesenchymal stem cells via inactivation of the Wnt pathway. *J Clin Invest* 117:3248-3257.

Mayhall, E.A., N. Paffett-Lugassy, and L.I. Zon. 2004. The clinical potential of stem cells. *Current Opinion in Cell Biology* 16:713-720.

McKibbin, B. 1978. The biology of fracture healing in long bones. *Journal of Bone & Joint Surgery, British Volume* 60-B:150-162.

Menicanin, D., P.M. Bartold, A.C. Zannettino, and S. Gronthos. 2010. Identification of a common gene expression signature associated with immature clonal mesenchymal cell populations derived from bone marrow and dental tissues. *Stem Cells Dev* 19:1501-1510.

Michael L. Voight, B.J.H., William E. Prentice. 2006. Musculoskeletal interventions: techniques for therapeutic exercise.

Millard, S.M., and N.M. Fisk. 2012. Mesenchymal stem cells for systemic therapy: Shotgun approach or magic bullets? *BioEssays*

Miraoui, H., and P.J. Marie. 2010. Pivotal role of Twist in skeletal biology and pathology. *Gene* 468:1-7.

Miura, M., S. Gronthos, M. Zhao, B. Lu, L.W. Fisher, P.G. Robey, and S. Shi. 2003. SHED: stem cells from human exfoliated deciduous teeth. *Proc Natl Acad Sci U S A* 100:5807-5812.

Montjovent, M.-O., M. Siegrist, F. Klenke, A. Wetterwald, S. Dolder, and W. Hofstetter. Expression of antagonists of WNT and BMP signaling after non-rigid fixation of osteotomies. *Bone*

Morrison, N.A., J.C. Qi, A. Tokita, P.J. Kelly, L. Crofts, T.V. Nguyen, P.N. Sambrook, and J.A. Eisman. 1994. Prediction of bone density from vitamin D receptor alleles. *Nature* 367:284-287.

Mrozik, K.M., P.S. Zilm, C.J. Bagley, S. Hack, P. Hoffmann, S. Gronthos, and P.M. Bartold. 2010. Proteomic characterization of mesenchymal stem cell-like populations derived from ovine periodontal ligament, dental pulp, and bone marrow: analysis of differentially expressed proteins. *Stem Cells Dev* 19:1485-1499.

Mundra, V., I.C. Gerling, and R.I. Mahato. 2012. Mesenchymal Stem Cell-Based Therapy. *Molecular pharmaceutics*

Mundy, G.R. 1999. Bone remodeling and its disorders. Martin Dunitz Ltd London. 263 pp.

Mundy GR, R.S., Majeska RJ, DeMartino S, Trimmier C, Martin TJ, Rodan GA. 1982. Unidirectional migration of osteosarcoma cells with osteoblast characteristics in response to products of bone resorption. *Calcified tissue international* 542-546.

Murre, C., P.S. McCaw, H. Vaessin, M. Caudy, L.Y. Jan, Y.N. Jan, C.V. Cabrera, J.N. Buskin, S.D. Hauschka, A.B. Lassar, and et al. 1989. Interactions between heterologous helix-loop-helix proteins generate complexes that bind specifically to a common DNA sequence. *Cell* 58:537-544.

Musina, R.A., E.S. Bekchanova, and G.T. Sukhikh. 2005. Comparison of mesenchymal stem cells obtained from different human tissues. *Bulletin of experimental biology and medicine* 139:504-509.

Nacamuli, R.P., K.D. Fong, S.M. Warren, T.D. Fang, H.M. Song, J.A. Helms, and M.T. Longaker. 2003. Markers of osteoblast differentiation in fusing and nonfusing cranial sutures. *Plast Reconstr Surg* 112:1328-1335.

Nakashima, K., X. Zhou, G. Kunkel, Z. Zhang, J.M. Deng, R.R. Behringer, and B. de Crombrugghe. 2002. The novel zinc finger-containing transcription factor osterix is required for osteoblast differentiation and bone formation. *Cell* 108:17-29.

Natacha Entz-Werlé, C.S.P.B.-M.C.K.L.B.H.P.C.S.M.-D.T.J.-C.G.R.Q.P.O.P.L.A.B.-B. 2005. Frequent genomic abnormalities at <I>TWIST</I> in human pediatric osteosarcomas. *International Journal of Cancer* 117:349-355.

Nielsen, H.M., T.T. Andreassen, T. Ledet, and H. Oxlund. 1994. Local injection of TGF-beta increases the strength of tibial fractures in the rat. *Acta orthopaedica Scandinavica* 65:37-41.

Nishikawa, K., T. Nakashima, S. Takeda, M. Isogai, M. Hamada, A. Kimura, T. Kodama, A. Yamaguchi, M.J. Owen, S. Takahashi, and H. Takayanagi. 2010. Maf promotes osteoblast differentiation in mice by mediating the age-related switch in mesenchymal cell differentiation. *The Journal of Clinical Investigation* 120:3455-3465.

Norton, J.D., and G.T. Atherton. 1998. Coupling of cell growth control and apoptosis functions of Id proteins. *Mol Cell Biol* 18:2371-2381.

Olszta, M.J., X. Cheng, S.S. Jee, R. Kumar, Y.-Y. Kim, M.J. Kaufman, E.P. Douglas, and L.B. Gower. 2007. Bone structure and formation: A new perspective. *Materials Science and Engineering* 58:77-116.

Onizuka, T., S. Yuasa, D. Kusumoto, K. Shimoji, T. Egashira, Y. Ohno, T. Kageyama, T. Tanaka, F. Hattori, J. Fujita, M. Ieda, K. Kimura, S. Makino, M. Sano, A. Kudo, and K. Fukuda. 2012. Wnt2 accelerates cardiac myocyte differentiation from ES-cell derived mesodermal cells via non-canonical pathway. *Journal of molecular and cellular cardiology* 52:650-659.

Orimo, H., T. Nakamura, T. Hosoi, M. Iki, K. Uenishi, N. Endo, H. Ohta, M. Shiraki, T. Sugimoto, T. Suzuki, S. Soen, Y. Nishizawa, H. Hagino, M. Fukunaga, and S. Fujiwara.

2012. Japanese 2011 guidelines for prevention and treatment of osteoporosis—executive summary. *Arch Osteoporos* 1-18.

Owen, M. 1980. The origin of bone cells in the postnatal organism. *Arthritis & Rheumatism* 23:1073-1080.

Owen, M., and A.J. Friedenstein. 1988. Stromal stem cells: marrow-derived osteogenic precursors. *Ciba Foundation symposium* 136:42-60.

Ozaki, A., M. Tsunoda, S. Kinoshita, and R. Saura. 2000. Role of fracture hematoma and periosteum during fracture healing in rats: interaction of fracture hematoma and the periosteum in the initial step of the healing process. *Journal of Orthopaedic Science* 5:64-70.

Pandur, P., D. Maurus, and M. Kühl. 2002. Increasingly complex: New players enter the Wnt signaling network. *BioEssays* 24:881-884.

Perrin-Schmitt, F., A.L. Bolcato-Bellemin, P. Bourgeois, C. Stoetzel, and J.M. Danse. 1997. The locations of the H-twist and H-dermo-1 genes are distinct on the human genome. *Biochim Biophys Acta* 1360:1-2.

Piek, E., L.S. Sleumer, E.P. van Someren, L. Heuver, J.R. de Haan, I. de Grijs, C. Gilissen, J.M. Hendriks, R.I. van Ravestein-van Os, S. Bauerschmidt, K.J. Dechering, and E.J. van Zoelen. 2010. Osteo-transcriptomics of human mesenchymal stem cells: Accelerated gene expression and osteoblast differentiation induced by vitamin D reveals c-MYC as an enhancer of BMP2-induced osteogenesis. *Bone* 46:613-627.

Pierro, M., L. Ionescu, T. Montemurro, A. Vadivel, G. Weissmann, G. Oudit, D. Emery, S. Bodiga, F. Eaton, B. Peault, F. Mosca, L. Lazzari, and B. Thebaud. 2012. Short-term, long-term and paracrine effect of human umbilical cord-derived stem cells in lung injury prevention and repair in experimental bronchopulmonary dysplasia. *Thorax*

Piters, E., E. Boudin, and W. Van Hul. 2008. Wnt signaling: A win for bone. *Archives of Biochemistry and Biophysics* 473:112-116.

Pittenger, M.F., A.M. Mackay, S.C. Beck, R.K. Jaiswal, R. Douglas, J.D. Mosca, M.A. Moorman, D.W. Simonetti, S. Craig, and D.R. Marshak. 1999. Multilineage Potential of Adult Human Mesenchymal Stem Cells. *Science* 284:143-147.

Psaltis, P.J., A.C. Zannettino, S.G. Worthley, and S. Gronthos. 2008. Concise review: mesenchymal stromal cells: potential for cardiovascular repair. *Stem Cells* 26:2201-2210.

Ramasamy, R., C.K. Tong, H.F. Seow, S. Vidyadaran, and F. Dazzi. 2008. The immunosuppressive effects of human bone marrow-derived mesenchymal stem cells target T cell proliferation but not its effector function. *Cellular Immunology* 251:131-136.

Ramesh Babu, L., S.G. Wilson, I.M. Dick, F.M. Islam, A. Devine, and R.L. Prince. 2005. Bone mass effects of a BMP4 gene polymorphism in postmenopausal women. *Bone* 36:555-561.

Rawadi, G., and S. Roman-Roman. 2005. Wnt signalling pathway: a new target for the treatment of osteoporosis. *Expert Opinion on Therapeutic Targets* 9:1063-1077.

Rebelatto, C.K., A.M. Aguiar, M.P. Moretao, A.C. Senegaglia, P. Hansen, F. Barchiki, J. Oliveira, J. Martins, C. Kuligovski, F. Mansur, A. Christofis, V.F. Amaral, P.S. Brofman, S. Goldenberg, L.S. Nakao, and A. Correa. 2008. Dissimilar differentiation of mesenchymal stem cells from bone marrow, umbilical cord blood, and adipose tissue. *Experimental biology and medicine* 233:901-913.

Regard, J.B., Z. Zhong, B.O. Williams, and Y. Yang. 2012. Wnt Signaling in Bone Development and Disease: Making Stronger Bone with Wnts. *Cold Spring Harbor Perspectives in Biology* 4:

Rice, D.P., T. Aberg, Y. Chan, Z. Tang, P.J. Kettunen, L. Pakarinen, R.E. Maxson, and I. Thesleff. 2000. Integration of FGF and TWIST in calvarial bone and suture development. *Development* 127:1845-1855.

Robertson, G., C. Xie, D. Chen, H. Awad, E.M. Schwarz, R.J. O'Keefe, R.E. Guldberg, and X. Zhang. 2006. Alteration of femoral bone morphology and density in COX-2-/- mice. *Bone* 39:767-772.

Robledo, R.F., L. Rajan, X. Li, and T. Lufkin. 2002. The Dlx5 and Dlx6 homeobox genes are essential for craniofacial, axial, and appendicular skeletal development. *Genes & Development* 16:1089-1101.

Rodda, S.J., and A.P. McMahon. 2006. Distinct roles for Hedgehog and canonical Wnt signaling in specification, differentiation and maintenance of osteoblast progenitors. *Development* 133:3231-3244.

Roodman, G.D. 1999. Cell biology of the osteoclast. *Exp Hematol* 27:1229-1241.

Ross, S.E., N. Hemati, K.A. Longo, C.N. Bennett, P.C. Lucas, R.L. Erickson, and O.A. MacDougald. 2000. Inhibition of adipogenesis by Wnt signaling. *Science* 289:950-953.

Sacchetti, B., A. Funari, S. Michienzi, S. Di Cesare, S. Piersanti, I. Saggio, E. Tagliafico, S. Ferrari, P.G. Robey, M. Riminucci, and P. Bianco. 2008. Self-renewing osteoprogenitors in bone marrow sinusoids can organize a hematopoietic microenvironment. *Cell* 131:324-336.

Salazar, K.D., S.M. Lankford, and A.R. Brody. 2009. Mesenchymal stem cells produce Wnt isoforms and TGF-beta1 that mediate proliferation and procollagen expression by lung fibroblasts. *American journal of physiology. Lung cellular and molecular physiology* 297:L1002-1011.

Salingcarnboriboon, R., H. Yoshitake, K. Tsuji, M. Obinata, T. Amagasa, A. Nifuji, and M. Noda. 2003. Establishment of tendon-derived cell lines exhibiting pluripotent mesenchymal stem cell-like property. *Exp Cell Res* 287:289-300.

Sanford, L.P., I. Ormsby, A.C. Gittenberger-de Groot, H. Sariola, R. Friedman, G.P. Boivin, E.L. Cardell, and T. Doetschman. 1997. TGFbeta2 knockout mice have multiple developmental defects that are non-overlapping with other TGFbeta knockout phenotypes. *Development* 124:2659-2670.

Satokata, I., L. Ma, H. Ohshima, M. Bei, I. Woo, K. Nishizawa, T. Maeda, Y. Takano, M. Uchiyama, S. Heaney, H. Peters, Z. Tang, R. Maxson, and R. Maas. 2000. Msx2 deficiency in mice causes pleiotropic defects in bone growth and ectodermal organ formation. *Nat Genet* 24:391-395.

Schriefer, J.L., A.G. Robling, S.J. Warden, A.J. Fournier, J.J. Mason, and C.H. Turner. 2005. A comparison of mechanical properties derived from multiple skeletal sites in mice. *Journal of biomechanics* 38:467-475.

Schwabe, P., S. Greiner, R. Ganzert, J. Eberhart, #xe4, K. hn, A. Stemberger, C. Plank, G. Schmidmaier, and B. Wildemann. 2012. Effect of a Novel Nonviral Gene Delivery of BMP-2 on Bone Healing. *The Scientific World Journal* 2012:9.

Schwarz, M.R. 1968. THE MIXED LYMPHOCYTE REACTION: AN IN VITRO TEST FOR TOLERANCE. *J. Exp. Med.* 127:879-890.

Segawa, Y., T. Muneta, H. Makino, A. Nimura, T. Mochizuki, Y.J. Ju, Y. Ezura, A. Umezawa, and I. Sekiya. 2009. Mesenchymal stem cells derived from synovium, meniscus, anterior cruciate ligament, and articular chondrocytes share similar gene expression profiles. *Journal of orthopaedic research : official publication of the Orthopaedic Research Society* 27:435-441.

Seo, B.M., M. Miura, S. Gronthos, P.M. Bartold, S. Batouli, J. Brahim, M. Young, P.G. Robey, C.Y. Wang, and S. Shi. 2004. Investigation of multipotent postnatal stem cells from human periodontal ligament. *Lancet* 364:149-155.

Shen, L., J. Glowacki, and S. Zhou. 2011. Inhibition of adipocytogenesis by canonical WNT signaling in human mesenchymal stem cells. *Exp Cell Res* 317:1796-1803.

Sherwood, L. 2004. Human Physiology, From Cells to Systems. Brooks/Cole, California. 802 pp.

Shi, S., and S. Gronthos. 2003. Perivascular niche of postnatal mesenchymal stem cells in human bone marrow and dental pulp. *J Bone Miner Res* 18:696-704.

Shi, S., S. Gronthos, S. Chen, A. Reddi, C.M. Counter, P.G. Robey, and C.Y. Wang. 2002. Bone formation by human postnatal bone marrow stromal stem cells is enhanced by telomerase expression. *Nat Biotechnol* 20:587-591.

Silva, M.J., M.D. Brodt, and S.L. Ettner. 2002. Long Bones From the Senescence Accelerated Mouse SAMP6 Have Increased Size But Reduced Whole-bone Strength and Resistance to Fracture. *Journal of Bone and Mineral Research* 17:1597-1603.

Silver, I.A., R.J. Murrills, and D.J. Etherington. 1988. Microelectrode studies on the acid microenvironment beneath adherent macrophages and osteoclasts. *Exp Cell Res* 175:266-276.

Simmons, P., and B. Torok-Storb. 1991. Identification of stromal cell precursors in human bone marrow by a novel monoclonal antibody, STRO-1. *Blood* 78:55-62.

Simonet, W.S., D.L. Lacey, C.R. Dunstan, M. Kelley, M.S. Chang, R. Luthy, H.Q. Nguyen, S. Wooden, L. Bennett, T. Boone, G. Shimamoto, M. DeRose, R. Elliott, A. Colombero, H.L. Tan, G. Trail, J. Sullivan, E. Davy, N. Bucay, L. Renshaw-Gegg, T.M. Hughes, D. Hill, W. Pattison, P. Campbell, S. Sander, G. Van, J. Tarpley, P. Derby, R. Lee, and W.J. Boyle. 1997. Osteoprotegerin: a novel secreted protein involved in the regulation of bone density. *Cell* 89:309-319.

SONG, L., and R.S. TUAN. 2004. Transdifferentiation potential of human mesenchymal stem cells derived from bone marrow. *FASEB J.* 18:980-982.

Sousa, K.M., J.C. Villaescusa, L. Cajanek, J.K. Ondr, G. Castelo-Branco, W. Hofstra, V. Bryja, C. Palmberg, T. Bergman, B. Wainwright, R.A. Lang, and E. Arenas. 2010. Wnt2 Regulates Progenitor Proliferation in the Developing Ventral Midbrain. *Journal of Biological Chemistry* 285:7246-7253.

Southwood, L.L., D.D. Frisbie, C.E. Kawcak, S.C. Ghivizzani, C.H. Evans, and C.W. McIlwraith. 2004. Evaluation of Ad-BMP-2 for enhancing fracture healing in an infected defect fracture rabbit model. *Journal of orthopaedic research : official publication of the Orthopaedic Research Society* 22:66-72.

Takahashi, K., K. Tanabe, M. Ohnuki, M. Narita, T. Ichisaka, K. Tomoda, and S. Yamanaka. 2007. Induction of Pluripotent Stem Cells from Adult Human Fibroblasts by Defined Factors. *Cell* 131:861-872.

Takahashi, K., and S. Yamanaka. 2006. Induction of Pluripotent Stem Cells from Mouse Embryonic and Adult Fibroblast Cultures by Defined Factors. *Cell* 126:663-676.

Tanaka-Douzono, M., S. Suzu, M. Yamada, N. Wakimoto, H. Hayasawa, K. Hatake, and K. Motoyoshi. 2001. Detection of murine adult bone marrow stroma-initiating cells in Lin−c-fms+c-kitlowVCAM-1+ cells. *Journal of Cellular Physiology* 189:45-53.

Tanaka Y, N.S., Okada Y. 2005. Osteoblasts and osteoclasts in bone remodeling and inflammation. *Curr Drug Targets Inflamm Allergy.* 4:325-328.

Tsuji, K., A. Bandyopadhyay, B.D. Harfe, K. Cox, S. Kakar, L. Gerstenfeld, T. Einhorn, C.J. Tabin, and V. Rosen. 2006. BMP2 activity, although dispensable for bone formation, is required for the initiation of fracture healing. *Nat Genet* 38:1424-1429.

Tsuji, K., K. Cox, A. Bandyopadhyay, B.D. Harfe, C.J. Tabin, and V. Rosen. 2008. BMP4 is dispensable for skeletogenesis and fracture-healing in the limb. *The Journal of bone and joint surgery. American volume* 90 Suppl 1:14-18.

Tsukiyama, T., and T.P. Yamaguchi. 2012. Mice lacking Wnt2b are viable and display a postnatal olfactory bulb phenotype. *Neuroscience Letters* 512:48-52.

Turgeman, G., D.D. Pittman, R. Muller, B.G. Kurkalli, S. Zhou, G. Pelled, A. Peyser, Y. Zilberman, I.K. Moutsatsos, and D. Gazit. 2001. Engineered human mesenchymal stem cells: a novel platform for skeletal cell mediated gene therapy. *The journal of gene medicine* 3:240-251.

Urano, T., M. Shiraki, T. Usui, N. Sasaki, Y. Ouchi, and S. Inoue. 2009. Bone mass effects of a Smad6 gene polymorphism in Japanese postmenopausal women. *J Bone Miner Metab* 27:562-566.

Urist, M.R., R.T. Hudak, Y.K. Huo, and J.K. Rasmussen. 1985. Osteoporosis: a bone morphogenetic protein auto-immune disorder. *Prog Clin Biol Res* 187:77-96.

Vaughan, T., J.A. Pasco, M.A. Kotowicz, G.C. Nicholson, and N.A. Morrison. 2002. Alleles of RUNX2/CBFA1 gene are associated with differences in bone mineral density and risk of fracture. *J Bone Miner Res* 17:1527-1534.

Wagner, W., F. Wein, A. Seckinger, M. Frankhauser, U. Wirkner, U. Krause, J. Blake, C. Schwager, V. Eckstein, W. Ansorge, and A.D. Ho. 2005. Comparative characteristics of

mesenchymal stem cells from human bone marrow, adipose tissue, and umbilical cord blood. *Exp Hematol* 33:1402-1416.

Wang, Q., X. Wei, T. Zhu, M. Zhang, R. Shen, L. Xing, R.J. O'Keefe, and D. Chen. 2007. Bone morphogenetic protein 2 activates Smad6 gene transcription through bone-specific transcription factor Runx2. *The Journal of biological chemistry* 282:10742-10748.

Webb, J.C.J., and J. Tricker. 2000. A review of fracture healing. *Current Orthopaedics* 14:457-463.

Weiss, S., T. Hennig, R. Bock, E. Steck, and W. Richter. 2010. Impact of growth factors and PTHrP on early and late chondrogenic differentiation of human mesenchymal stem cells. *J Cell Physiol* 223:84-93.

Westendorf, J.J., R.A. Kahler, and T.M. Schroeder. 2004. Wnt signaling in osteoblasts and bone diseases. *Gene* 341:19-39.

Williams, B.O., and K.L. Insogna. 2009. Where Wnts Went: The Exploding Field of Lrp5 and Lrp6 Signaling in Bone. *Journal of Bone and Mineral Research* 24:171-178.

Winter, A., S. Breit, D. Parsch, K. Benz, E. Steck, H. Hauner, R.M. Weber, V. Ewerbeck, and W. Richter. 2003. Cartilage-like gene expression in differentiated human stem cell spheroids: a comparison of bone marrow-derived and adipose tissue-derived stromal cells. *Arthritis and rheumatism* 48:418-429.

Wozney, J.M. 2002. Overview of bone morphogenetic proteins. *Spine* 27:S2-8.

Wuthier, R.E. 1982. A review of the primary mechanism of endochondral calcification with special emphasis on the role of cells, mitochondria and matrix vesicles. *Clinical orthopaedics and related research* 219-242.

Xue, G., D.F. Restuccia, Q. Lan, D. Hynx, S. Dirnhofer, D. Hess, C. Ruegg, and B.A. Hemmings. 2012. Akt/PKB-mediated phosphorylation of Twist1 promotes tumor metastasis via mediating cross-talk between PI3K/Akt and TGF-beta signaling axes. *Cancer discovery* 2:248-259.

Yamaza, T., Y. Miura, Y. Bi, Y. Liu, K. Akiyama, W. Sonoyama, V. Patel, S. Gutkind, M. Young, S. Gronthos, A. Le, C.-Y. Wang, W. Chen, and S. Shi. 2008. Pharmacologic Stem Cell Based Intervention as a New Approach to Osteoporosis Treatment in Rodents. *PLoS ONE* 3:e2615.

Yan, Y., D. Tang, M. Chen, J. Huang, R. Xie, J.H. Jonason, X. Tan, W. Hou, D. Reynolds, W. Hsu, S.E. Harris, J.E. Puzas, H. Awad, R.J. O'Keefe, B.F. Boyce, and D. Chen. 2009. Axin2 controls bone remodeling through the beta-catenin-BMP signaling pathway in adult mice. *J Cell Sci* 122:3566-3578.

Yang, X., L. Chen, X. Xu, C. Li, C. Huang, and C.X. Deng. 2001. TGF-beta/Smad3 signals repress chondrocyte hypertrophic differentiation and are required for maintaining articular cartilage. *J Cell Biol* 153:35-46.

Ying Zhang, M.Q.H., Zhao-Yong Li, Janet L. Stein, Jane B. Lian, Andre J. van Wijnen, Gary S. Stein,. 2008. Intricate gene regulatory networks of helix-loop-helix (HLH) proteins support regulation of bone-tissue related genes during osteoblast differentiation. *Journal of Cellular Biochemistry* 105:487-496.

Yongmin Yan, W.X., Hui Qian, Yuan Si, Wei Zhu, Huiling Cao, Hongxing Zhou, Fei Mao,. 2009. Mesenchymal stem cells from human umbilical cords ameliorate mouse hepatic injury in vivo. *Liver International* 29:356-365.

Young, D.W., J. Pratap, A. Javed, B. Weiner, Y. Ohkawa, A. van Wijnen, M. Montecino, G.S. Stein, J.L. Stein, A.N. Imbalzano, and J.B. Lian. 2005. SWI/SNF chromatin remodeling complex is obligatory for BMP2-induced, Runx2-dependent skeletal gene expression that controls osteoblast differentiation. *Journal of Cellular Biochemistry* 94:720-730.

Yu, H.M., B. Jerchow, T.J. Sheu, B. Liu, F. Costantini, J.E. Puzas, W. Birchmeier, and W. Hsu. 2005. The role of Axin2 in calvarial morphogenesis and craniosynostosis. *Development* 132:1995-2005.

Yu, Y., J.L. Yang, P.J. Chapman-Sheath, and W.R. Walsh. 2002. TGF-beta, BMPS, and their signal transducing mediators, Smads, in rat fracture healing. *Journal of biomedical materials research* 60:392-397.

Zaidi, M. 2007. Skeletal remodeling in health and disease. *Nat Med* 13:791-801.

Zannettino, A.C., A.N. Farrugia, A. Kortesidis, J. Manavis, L.B. To, S.K. Martin, P. Diamond, H. Tamamura, T. Lapidot, N. Fujii, and S. Gronthos. 2005. Elevated serum levels of stromal-derived factor-1alpha are associated with increased osteoclast activity and osteolytic bone disease in multiple myeloma patients. *Cancer Res* 65:1700-1709.

Zannettino, A.C., S. Paton, A. Arthur, F. Khor, S. Itescu, J.M. Gimble, and S. Gronthos. 2008. Multipotential human adipose-derived stromal stem cells exhibit a perivascular phenotype in vitro and in vivo. *J Cell Physiol* 214:413-421.

Zannettino, A.C., S. Paton, A. Kortesidis, F. Khor, S. Itescu, and S. Gronthos. 2007. Human mulipotential mesenchymal/stromal stem cells are derived from a discrete subpopulation of STRO-1bright/CD34 /CD45(-)/glycophorin-A-bone marrow cells. *Haematologica* 92:1707-1708.

Zannettino, S.G.a.A.C.W. 2006. Potential of Bone Marrow Stromal Cells to Repair Bone Defects and Fractures. Nova Science Publishers, Inc.,

Zhong, N., R.P. Gersch, and M. Hadjiargyrou. 2006. Wnt signaling activation during bone regeneration and the role of Dishevelled in chondrocyte proliferation and differentiation. *Bone* 39:5-16.

Zhou, H., W. Mak, Y. Zheng, C.R. Dunstan, and M.J. Seibel. 2008. Osteoblasts directly control lineage commitment of mesenchymal progenitor cells through Wnt signaling. *The Journal of biological chemistry* 283:1936-1945.

Zhou, S. 2011. TGF-β regulates β-catenin signaling and osteoblast differentiation in human mesenchymal stem cells. *Journal of Cellular Biochemistry* 112:1651-1660.

Zhou, S., K. Eid, and J. Glowacki. 2004. Cooperation Between TGF-β and Wnt Pathways During Chondrocyte and Adipocyte Differentiation of Human Marrow Stromal Cells. *Journal of Bone and Mineral Research* 19:463-470.

Zuk, P.A., M. Zhu, H. Mizuno, J. Huang, J.W. Futrell, A.J. Katz, P. Benhaim, H.P. Lorenz, and M.H. Hedrick. 2001. Multilineage cells from human adipose tissue: implications for cell-based therapies. *Tissue Eng* 7:211-228.